



Universiteit  
Leiden  
The Netherlands

## Fundamental studies focused on understanding of gold catalysis

Gluhoi, Andreea Catalina

### Citation

Gluhoi, A. C. (2005, October 19). *Fundamental studies focused on understanding of gold catalysis*. Retrieved from <https://hdl.handle.net/1887/4315>

Version: Corrected Publisher's Version

License: [Licence agreement concerning inclusion of doctoral thesis in the Institutional Repository of the University of Leiden](#)

Downloaded from: <https://hdl.handle.net/1887/4315>

**Note:** To cite this publication please use the final published version (if applicable).

**Fundamental studies focused on understanding of gold  
catalysis**

**Andreea Catalina Gluhoi**

**2005**



# **Fundamental studies focused on understanding of gold catalysis**

Proefschrift

ter verkrijging van  
de graad van Doctor aan de Universiteit Leiden,  
op gezag van de Rector Magnificus Dr. D. D. Breimer,  
hoogleraar in the faculteit der Wiskunde en  
Natuurwetenschappen en die der Geneeskunde,  
volgens besluit van het College voor Promoties  
te verdedigen op woensdag 19 oktober 2005  
te klokke 15:15 uur

door

Andreea Catalina Gluhoi

geboren te Cugir, Roemenië, in 1973



## Promotiecommissie

- Promotor: Prof. Dr. Bernard E. Nieuwenhuys
- Co-promotor: Dr. Nina Bogdanchikova (Centro de Ciencias de la Materia Condensada-UNAM, Mexico)
- Referent: Dr. Patricia J. Kooyman (DelftChemTech and National Centre for High Resolution Electron Microscopy, Delft)
- Overige leden: Prof. Dr. Johan Lugtenburg  
Prof. Dr. Eite Drent  
Prof. Dr. Bert Weckhuysen (Utrecht University)  
Prof. Dr. Jaap Brouwer

Andreea Catalina Gluhoi

Fundamental studies focused on understanding of gold catalysis/ A.C. Gluhoi  
Thesis Leiden University, The Netherlands, 2005. – With ref. – With summary in Dutch

The work described in this thesis has been supported financially by NWO (Netherlands Organization for Scientific Research), project number #700.99.037.

ISBN: 90-9019950-0

Copyright © 2005 by Andreea C. Gluhoi  
Printed by Wöhrmann Print Service

*"Rerum Cognoscere Causas"*

*Părinților mei*  
*To my parents*

## Abbreviations

<b>AAS</b>	<b>A</b> tomic <b>A</b> bsorption <b>S</b> pectroscopy
<b>BET</b>	<b>B</b> runauer- <b>E</b> mmett- <b>T</b> eller
<b>HDP</b>	<b>H</b> omogeneous <b>D</b> eposition <b>P</b> recipitation
<b>PVI</b>	<b>P</b> ore <b>V</b> olume <b>I</b> mpregnation
<b>STP</b>	<b>S</b> tandard <b>T</b> emperature and <b>P</b> ressure
<b>RT</b>	<b>R</b> oom <b>T</b> emperature
<b>MO<sub>x</sub></b>	<b>M</b> etal <b>O</b> xide
<b>TMO</b>	<b>T</b> ransition <b>M</b> etal <b>O</b> xide
<b>HC</b>	<b>H</b> ydrocarbon
<b>OSC</b>	<b>O</b> xygen <b>S</b> torage <b>C</b> apacity
<b>TWC</b>	<b>T</b> hree- <b>W</b> ay <b>C</b> atalyst
<b>XRD</b>	<b>X</b> - <b>R</b> ay <b>D</b> iffraction
<b>HRTEM</b>	<b>H</b> igh- <b>R</b> esolution <b>T</b> ransmission <b>E</b> lectron <b>M</b> icroscopy
<b>SEM</b>	<b>S</b> canning <b>E</b> lectron <b>M</b> icroscopy
<b>DR/UV-Vis</b>	<b>D</b> iffuse <b>R</b> eflectance <b>U</b> ltra <b>V</b> iolet <b>V</b> isible
<b>TPR</b>	<b>T</b> emperature <b>P</b> rogrammed <b>R</b> eduction
<b>EDX</b>	<b>E</b> nergy <b>D</b> ispersive <b>X</b> -ray <b>A</b> nalysis
<b>FTIR</b>	<b>F</b> ourier <b>T</b> ransform <b>I</b> nfra <b>R</b> ed
<b>XPS</b>	<b>X</b> - <b>R</b> ay <b>P</b> hotoelectron <b>S</b> pectroscopy
<b>TOF</b>	<b>T</b> urn <b>O</b> ver <b>F</b> requency
<b>E<sub>a</sub></b>	<b>A</b> ctivation <b>E</b> nergy
<b>r</b>	<b>S</b> pecific <b>R</b> eaction <b>R</b> ate
<b>GHSV</b>	<b>G</b> as <b>H</b> ourly <b>S</b> pace <b>V</b> elocity
<b>MS</b>	<b>M</b> ass <b>S</b> pectrometer
<b>GC</b>	<b>G</b> as <b>C</b> hromatograph

# Table of Contents

<b>Chapter1</b>	<b>Introduction</b>	<b>1</b>
1.1	Catalysis and catalysts	2
1.2	Green chemistry - Environmental-friendly catalysis	3
1.3	Gold as a catalyst	6
1.4	The aims of this thesis	10
1.5	References	11
<b>Chapter 2</b>	<b>Literature survey - Gold catalysis</b>	<b>15</b>
2.1	Alkanes combustion	16
2.2	Combustion of alkenes	19
2.3	Ammonia oxidation	20
2.4	NO and N <sub>2</sub> O reduction	23
2.5	CO oxidation in the absence and presence (PROX) of hydrogen	27
2.6	References	34
<b>Chapter 3</b>	<b>Sample preparation and experimental techniques</b>	<b>41</b>
3.1	Outline	42
3.2	Sample preparation	42
3.3	Experimental techniques	44
3.4	Catalytic activity experiments	49
3.5	References	53
<b>Chapter 4</b>	<b>Alumina-supported gold-based catalysts. Characterization results</b>	<b>55</b>
4.1	Outline	56
4.2	Gold loading (AAS), BET surface area, XRD, HRTEM and SEM results	56
4.3	Diffuse-reflectance ultra-violet measurements, DR/UV-Vis	69
4.4	Temperature-programmed reduction, TPR	75
4.5	X-ray photoelectron spectroscopy, XPS	78
4.6	General discussion	80
4.7	Conclusions	81
4.8	References	82
<b>Chapter 5</b>	<b>Oxidation of unsaturated hydrocarbons: total oxidation of propene</b>	<b>83</b>
5.1	Outline	84
5.2	Experimental	84
5.3	Catalytic performance in C <sub>3</sub> H <sub>6</sub> oxidation	84

5.4 Discussion	91
5.5 Conclusions	97
5.6 References	98

**Chapter 6 Oxidation of saturated hydrocarbons: total oxidation of methane and propane 101**

6.1 Outline	102
6.2 Experimental	102
6.3 Catalytic activity measurements	103
6.4 Discussion	112
6.5 Conclusions	115
6.6 References	115

**Chapter 7 Ammonia oxidation over mono- and multi- component gold-based catalysts 117**

7.1 Outline	118
7.2 Experimental	118
7.3 Ammonia oxidation, reactant ratio $\text{NH}_3:\text{O}_2 = 1:1$	119
7.4 Ammonia oxidation, reactant ratio $\text{NH}_3:\text{O}_2 = 1:10$	127
7.5 FTIR spectroscopy measurements	130
7.6 Discussion	134
7.7 Conclusions	136
7.8 References	137

**Chapter 8 Reduction reactions involving nitrogen oxides (NO and  $\text{N}_2\text{O}$ ) over gold-based catalysts 139**

8.1 Outline	140
8.2 Experimental	140
8.3 Catalytic performance in NO reduction by $\text{H}_2$	140
8.4 Catalytic performance in $\text{N}_2\text{O}$ reduction by $\text{H}_2$	147
8.5 Discussion	149
8.6 Conclusions	156
8.7 References	156

**Chapter 9 CO oxidation in the presence (PROX) and absence of hydrogen over Au-based catalysts 159**

9.1 Outline	160
9.2 Experimental	160
9.3 Catalytic activity measurements	161
9.4 Discussion	174

9.5 Conclusions	182
9.6 References	183
<b>Chapter 10 General discussion</b>	<b>185</b>
10.1 Introduction	186
10.2 Unpromoted Au/Al <sub>2</sub> O <sub>3</sub> . Preparation, activation and working state	186
10.3 Multicomponent Au-based catalysts. Promoter vs. cocatalyst	188
10.4 Mechanistic considerations	190
10.5 Future prospects and recommendations	190
10.6 References	191
<b>Summary</b>	<b>193</b>
<b>Samenvatting</b>	<b>197</b>
<b>Acknowledgements</b>	<b>201</b>
<b>List of publications and patents related to this thesis</b>	<b>203</b>
<b>Curriculum Vitae</b>	<b>205</b>



# Chapter 1

## Introduction

*This chapter describes the aim of the research presented in this thesis. Some background information regarding catalysis/catalyst concepts is outlined. In addition, the role of catalysis for “environmental-friendly” applications is emphasized, in particular in automotive catalysis and hydrogen fuel cells. Finally gold is presented as a potential catalyst for a number of “environmental-friendly” reactions.*



## 1.1 Catalysis and catalysts

*Catalysis* bridges chemistry, chemical engineering, materials science and biology. However, what is *catalysis*?

The first valid modern definition of *catalysis* was given around 1895 by W. Ostwald, whose work in catalysis, chemical equilibrium and reaction rates was recognized with a Nobel Prize for chemistry. Sixty years before, J. Berzelius had coined the term “catalysis”, recognizing that a single concept could account for changes in compositions of numerous substances resulting from their mere contact with liquids, solids or “ferments”. Berzelius’s insight bears on phenomena that had earlier puzzled the alchemists, who, aware of the mysterious actions of these “ferments” and other substances (“contacts”), sought unsuccessfully for a philosopher’s stone to change base metals into gold. Ostwald’s definition of catalysis rests on reaction kinetics and, indeed, at about the time he stated it, the beginnings of physical chemistry were emerging in the quantitative representation of thermodynamics and kinetics of chemical reactions. Catalysis at an interface (usually a solid surface) is called *heterogeneous catalysis*; it means that more than one phase is present in the reactor, i.e. a gas or liquid in contact with a solid.

The application of a *catalyst* is one of the most fascinating and significant concepts in science and the world, and is one of the few words that have carried over broadly outside scientific language. Catalysts have always been used in the production of wine, beer and cheese. A catalyst speeds up a chemical reaction without being consumed substantially during the reaction. In other words, a catalyst works by forming chemical bonds with reactants, generating intermediates that react more readily to give products than the reactants would alone - and giving back the catalyst. In this way it affects the rate of approach to equilibrium of a reaction but not the position of the equilibrium. It also provides subtle control of chemical conversions, increasing the rate of a desired reaction but not the rates of undesired side reactions (i.e. it affects the selectivity of a chemical process). Only an increase in temperature provides a comparable means for increasing reaction rates, but high temperatures are often unacceptable.

An important issue in a chemical process is the *selectivity* to one of the products. Unfortunately, each chemical process has its specific needs, including catalyst, and there is not one universal catalyst composition for all reactions. For example, Pd/Cu catalyzes the oxidation of ethene to vinyl acetate, whereas Ag is used to obtain ethene oxide.

The *stability* of a catalyst accounts for how fast it loses its activity or selectivity during operation; the ideal catalyst is infinitely stable, but real catalysts undergo changes causing loss of activity and selectivity, and must be replaced or regenerated (at intervals ranging from seconds to years).

Most catalysts used in heterogeneous catalysis are solids. The catalytically active components (i.e. metals, metal oxides or metal sulphides), typically in a low concentration,

are deposited, preferably in a highly dispersed state, on a support or carrier (i.e.  $\gamma$ -Al<sub>2</sub>O<sub>3</sub>, SiO<sub>2</sub>, carbon or zeolites). This support often lacks catalytic activity. Additionally, other components, including those with catalytic activity, are added. They are named promoters or additives. **Chemical promoters**, although not active themselves, improve the effectiveness of the catalyst by chemical means. This is, for example, the role of alkali metal oxides (K<sub>2</sub>O, Cs<sub>2</sub>O) on Fe- and Ru-based catalysts in ammonia synthesis [1-4]. It is well established that these promoters help by lowering the N<sub>2</sub> dissociation barrier. **Cocatalysts** have an active role during the process and act along with the main catalyst (for example by supplying active oxygen). **Textural (structural) promoters**, on the other hand, play a role in stabilization of the catalyst, or increasing the number of “active sites”. For instance, they can influence (reduce) the tendency of a porous material to collapse or sinter and lose internal surface area, which is a mechanism of deactivation.

## 1.2 Green chemistry - Environmental-friendly catalysis

The chemical industry fulfils a large number of human needs already for more than 150 years. However, particularly since about 50 years ago, it has become obvious that the practice of industrial chemistry has, apart from the desired products, some strong drawbacks. These are the environmental “costs”, directly related to human health. In recognition of the environmental effects of the chemical industry and related enterprises, many laws have been passed and implemented throughout the world to regulate chemical processes and products. Two aspects directly related to environmental pollution control will be briefly introduced below: automotive catalysts (in particular three-way catalysts, TWC) and hydrogen fuel cells.

### *Automotive catalysis*

The development of catalytic reactors for cleaning the exhaust gases of motor vehicles has been stimulated enormously in the past 50 years. The only aim was to achieve a reduction of emission of harmful exhaust gases. Later, because of the more strict legislation rules, the use of a catalytic converter became a fundamental issue. The catalytic converter was initially aimed to reduce the emission of CO and unburned hydrocarbons (HC), thus performing only oxidation reactions. Later, also the emission of NO<sub>x</sub> was regulated and a catalytic converter was introduced that simultaneously performs oxidation of CO and HCs and reduction of NO<sub>x</sub>. This is a difficult task for any catalytic process. Typical concentrations in the exhaust gases of a gasoline engine are given in Fig. 1.1. For  $\lambda < 1$  (i.e. substoichiometric conditions, known also as “rich burning”), the emission of CO and HCs is high. At  $\lambda > 1$  (known also as “lean burning”), the combustion is more efficient; however, due to an increase in the temperature and the excess of oxygen, more NO<sub>x</sub> is emitted. At still higher values of  $\lambda$ , because of the large excess of air, the temperature drops and less NO<sub>x</sub> is formed. The window of  $\lambda$  where both the oxidation and reduction reactions take place is very narrow. Recently, attempts have been made to develop and manufacture engines working at larger  $\lambda$  values.

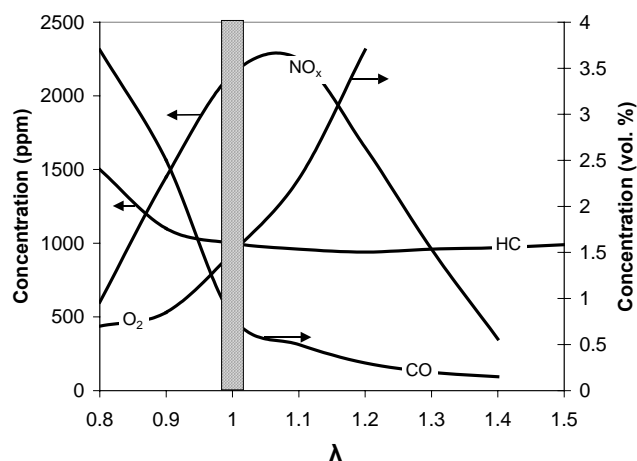
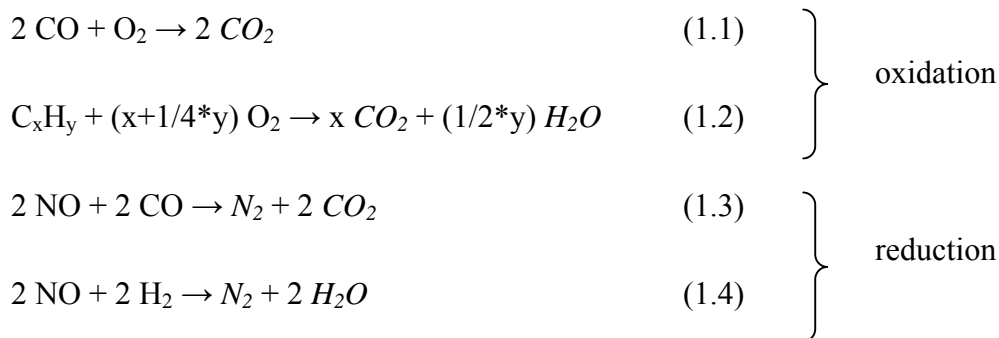
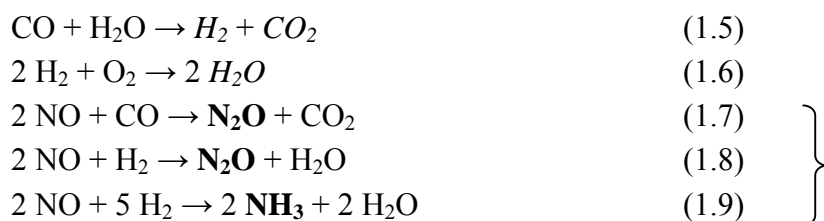


**Figure 1.1:** The concentrations of CO, HCs, NO<sub>x</sub> and O<sub>2</sub> emitted by a gasoline engine in the absence of a three-way catalyst as a function of air/fuel ratio,  $\lambda$ .  $\lambda = 1$  corresponds to stoichiometric combustion.

The main reactions that occur in a catalytic converter are:



In addition, there are also some side-reactions that may take place, part of them unwanted because of their harmful products such as NH<sub>3</sub> or N<sub>2</sub>O:



Catalysts used to solve the problems of air pollution consist of Pt/Rh, Pd or Pd/Rh supported on La-stabilized alumina (Otto engines). Pt is used as an efficient oxidation catalyst. The main role of Rh is the reduction of NO<sub>x</sub> because it has a superior selectivity to N<sub>2</sub>, compared with Pt and Pd. Also some promoters are present, i.e. CeO<sub>2</sub>. The role of ceria is more than a stabilizer of the alumina carrier [5]. Ceria alone is able to oxidize CO and HCs and to reduce NO<sub>x</sub> emission, although it requires higher temperatures than the noble metals

Pt, Pd or Rh [6]. More important, however, is the ability of ceria to store and release oxygen under various reaction conditions (i.e. oxygen storage capacity, OSC), due to the facile redox cycle existing between  $\text{Ce}^{4+}$  and  $\text{Ce}^{3+}$  [7]. It should be mentioned that the exhaust gases from Diesel engines additionally contain  $\text{SO}_2$  and soot particles as pollutants.

### **Hydrogen fuel cells**

As mentioned above, the emission of vehicles is one of the major pollution sources nowadays. An alternative method to produce energy and at the same time to reduce the emission and increase the overall efficiency is to use fuel cells [8-10]. A variety of fuel cells for different applications is under development [11]: solid polymer fuel cells (SPFC), also known as proton-exchange membrane (PEM) fuel cells operating at  $\sim 80^\circ\text{C}$ , alkaline fuel cells (AFC), operating at  $\sim 100^\circ\text{C}$ , phosphoric acid fuel cells (PAFC) for  $\sim 200^\circ\text{C}$  operation, molten carbonate fuel cells (MCFC) at  $\sim 650^\circ\text{C}$ , solid oxide fuel cells (SOFC) for high temperature operation,  $> 800^\circ\text{C}$  [12]. PEM fuel cells have a series of advantageous features that make them leading candidates for mobile power applications (vehicles) or for small stationary power units: low operating temperature, sustained operation at high current density, low weight, compactness, potential for low cost and volume, etc.

Except for the case of direct methanol fuel cells (DMFC), the ideal fuel for PEM fuel cells is pure hydrogen, with less than 50 ppm CO, as dictated by the poisoning limit of the Pt fuel cell catalyst. By using PEM fuel cells, the energy obtained from the reaction of a fuel stream comprising hydrogen and oxygen (air) is converted into electrical energy. Various technical limitations make it difficult to store  $\text{H}_2$  "on-board". Therefore, "on-board"  $\text{H}_2$  production is preferred. Thus,  $\text{H}_2$  is generated by steam reforming or partial oxidation of fuels such as natural gas, gasoline, propane (LPG), and methanol. The resulting gas mixture, which usually comprises  $\sim 75\%$   $\text{H}_2$  and  $\sim 25\%$   $\text{CO}_2$ , is contaminated with at least 1-2vol % CO which acts as a poison for the anode catalyst (generally Pt-based). One of the most promising processes used to decrease the CO concentration in the reformer gas below 100ppm is to selectively oxidize CO to  $\text{CO}_2$  in the presence of hydrogen (SCO), also known as preferential CO oxidation (PROX). Hence, the catalyst should be highly active in CO oxidation at low temperature (below  $100^\circ\text{C}$ ) and very selective towards  $\text{CO}_2$ . The oxidation of hydrogen should be avoided. These requirements are relatively hard to meet, since at low temperatures noble metals (Pt or Pd) are poisoned by CO and the unwanted reaction proceeds faster than the desired one. Besides the problems caused by CO production, water may also be detrimental by decreasing the efficiency of PEM fuel cells. New catalytic systems with an increased resistance towards CO and  $\text{H}_2\text{O}$  are under development [12].

Thus, it is evident that the pollution level must decrease and there is an urgent need for new catalytic systems that can be successfully employed to achieve this goal. In the next section gold will be introduced as a *relatively* new catalyst, with a real potential as an active catalyst in reactions relevant to air pollution control.

## 1.3 Gold as a catalyst

### *Brief review. Short history of Au catalysis*

It was long believed that Au failed as a catalyst because its chemisorption ability was too small, compared with, for example, the platinum group metals (PGM). The Tanaka-Tamaru Rule [13] had shown that initial enthalpies of chemisorption of oxygen and any related molecules are linearly related to the enthalpies of formation of the most stable oxides. This implies that chemisorbed oxygen atoms are energetically similar to atoms or ions in bulk oxides, and the nobility of gold, which is due to the instability of its oxide  $\text{Au}_2\text{O}_3$  ( $\Delta H_f = 19.3 \text{ kJ mol}^{-1}$ ), also determines its inability to chemisorb oxygen.

The differences between the *4d* and *5d* elements and their compounds have been ascribed to the large stability of the  $6s^2$  electron pair. Due to the large size of its nucleus the relativistic effects become very important for Au [14-16]. Because of the increased mass of the nucleus, the *s* orbitals and to a lesser extent the *p* orbitals are contracted, whereas the *d* and *f* orbitals are in fact expanded [17]. As a result, the  $6s^2$  pair is contracted and stabilized and much of the chemistry (including the catalytic properties [18, 19]) is due to the *5d* band. The yellow colour of Au, similar to that of Cu, but different from that of silver, caused by optical absorption in the visible region, is due to the relativistic lowering gap between the *5d* band and the Fermi level [15, 20]. In the absence of this effect, gold would be white like Ag and have the same propensity to tarnish and corrode [15].

First attempts to use Au as a catalyst were carried out as early as 1906 and Au gauzes were reported as catalysts for  $\text{H}_2$  oxidation [21]. This result was later confirmed [22, 23]. The earliest reference to Au as a catalyst for CO oxidation dates from 1925 [24]. In the next 40 years the reports about Au as a catalyst were rather scarce and were reviewed in 1971 [25]. An interesting paper reported in the same period that Au acts as a hydrogenation catalyst [26]. There were also reports that Au deposited on silica and alumina is active in alkene hydrogenation at  $100^\circ\text{C}$  [27, 28]. It should also be mentioned that a significant contribution in the field of Au catalysis was made by Hutchings who realised that the very high standard electrode potential of Au (+1.4 V) would make  $\text{AuCl}_3$  a very effective catalyst for the hydrochlorination of ethyne [29]. However, the most important breakthrough came in 1987, thanks to the work of Haruta, who showed that Au-based catalysts prepared in a suitable manner are very active in oxidation of CO even at sub-ambient temperature [30]. Since then, a lot of research has been carried out, mostly in the field of CO oxidation [31-33]. Comprehensive reviews may be found (for example [17, 34, 35]). Au-based catalysts were tested for other reactions as well, i.e.  $\text{NO}_x$  reduction [36-38], hydrogenation of unsaturated hydrocarbons [39], WGS reaction [40-42],  $\text{NH}_3$  oxidation [43], total oxidation of volatile organic compounds (VOCs) [44-47], and preferential oxidation of CO in the presence of  $\text{H}_2$  (PROX) [48-50].

### *Gold as a working catalyst*

Explanations for the high activity of gold nanoparticles in various reactions can broadly be classified into four groups, namely, the influence of the preparation method (including the

pretreatment conditions), the particle size effect, the separate catalytic role of the support/additive and the presence of ionic gold. These factors will be briefly discussed below.

### *The preparation technique*

Traditionally, noble metal-based catalysts are prepared by impregnation. However, this method is not suitable for Au for at least two reasons. The first reason is that Au has a relatively low affinity for metal oxides and, thus, the interaction with the support is weak. Secondly, during calcination of  $\text{HAuCl}_4$ , because of the presence of chloride ions, the coagulation of Au particles is greatly enhanced and the result is an inactive Au-based catalyst, due to the formation of large, inactive Au ensembles. However, recently, a modified impregnation method was reported by Datye *et al.* [51]. According to their method, it is possible to obtain Au-based catalysts with an average particle size around 2.4 nm. Most important, however, was that the activity at room temperature of these catalysts in CO oxidation was comparable to catalysts prepared by deposition-precipitation.

The most widely used method to prepare active Au-based catalysts is deposition-precipitation [35, 52, 53]. There are different ways to deposit Au onto the support: either by adjusting the pH of  $\text{HAuCl}_4$  with  $\text{Na}_2\text{CO}_3$  or  $\text{NaOH}$  [35, 52] and then adding the support, or by slowly increasing the pH of the  $\text{HAuCl}_4$  solution in the presence of the support [38, 49, 53]. In each of these approaches, the pH is very important. A detailed discussion of the role of the pH during deposition of Au can be found in *Chapter 3* of this thesis. By using any of these approaches it is claimed that very small Au particles are obtained, highly dispersed over the support. However, this method is only applicable for a basic support. If the support has an acidic character, gas phase grafting (GG) is more suitable [54].

Another preparation method often used for its simplicity is coprecipitation [35]. Also in this case the pH at which Au precipitates is very important. Besides the pH, the identity of the basic reagent used to precipitate Au was reported to be important [35]:  $\text{Na}_2\text{CO}_3$  or  $\text{K}_2\text{CO}_3$  are more efficient to obtain small gold particles than  $\text{NaOH}$  or  $\text{NH}_4\text{OH}$ .

In order to avoid any contamination of chloride ions originating from the Au precursor ( $\text{HAuCl}_4$  or  $\text{AuCl}_3$ ), GG using monodispersed Au colloids stabilized by organic ligands or polymer compounds can be used [55, 56]. This method may be used to deposit Au on carbon, but the size of the Au particles is relatively large ( $\sim 10$  nm). A more precise control of the dispersion and size of Au nanoparticles may be obtained by using Au sols stabilized by polyvinyl pyrrolidone, or other organic compounds [56].

The thermal treatment (i.e. calcination if air/oxygen is employed) of the catalyst precursor has also been reported to have a great influence on the final catalytic properties of Au. It was reported that for Au/ $\text{TiO}_2$  [57, 58], Au/ $\text{Fe}_2\text{O}_3$  [58-60], and Au/ $\text{MnO}_x$  [61] catalysts, calcination at mild temperatures (100-200 $^\circ\text{C}$ ) results in more active catalysts than if they were calcined at higher temperatures. There are also reports that uncalcined Au/ $\text{Al}_2\text{O}_3$  [62] or Au/Y [63] can be very active. In addition, a higher calcination temperature may cause a severe sintering of the gold crystallites [49, 64]. On the other hand, it has been reported that a higher calcination temperature may positively influence the catalytic activity of Au/ $\text{TiO}_2$  in the sense that a stronger interaction between Au and support is created and this phenomenon

leads to a higher catalytic efficiency, even though the gold particles sinter [64]. Regarding the effect of the treatment prior to the reaction, viz. heating in hydrogen or in oxygen, Dekkers found that for Au/Al<sub>2</sub>O<sub>3</sub>, a reductive pretreatment gives better results than an oxidative one (300°C) [65]. Later, Grisel confirmed this [49]. In addition, he found, in line with previous results [64], that larger Au particles (~ 10 nm), obtained by calcination at only 400°C, are less active than smaller gold particles, obtained by calcination at 300°C [49].

### *Particle size effect*

Another origin of very high activities for Au-based catalysts resides in the size of the Au particles. Except for H<sub>2</sub> oxidation and hydrocarbon hydrogenation, most reactions are remarkably structure-sensitive over supported Au catalysts [52]. Thus, for all the other reactions the average size of the gold particles should be below 5 nm [34]. As the size of a metal particle decreases, a number of effects occur:

- (i) The fraction of surface atoms increases, and because these vibrate more freely the melting temperature falls and surface mobility rises;
- (ii) Because the overlap of electron orbitals decreases as the average number of bonds between atoms becomes less, the band structure is weakened, and in particular the surface atoms start to behave more as individuals;
- (iii) A larger fraction of the atoms comes into contact with the support, and the length of the periphery per unit mass of metals rises;
- (iv) More steps, edge and kink sites are formed on the particles.

There are many reports that highlight the role of the Au particle size in various reactions [34, 35, 47, 49, 52, 65]. Theoretical calculations tried to explain this “particle size effect”. It was proposed that the high activity results from a quantum size effect with respect to the thickness of the gold, based on the onset of a metal-to-nonmetal transition that was observed to occur for very small Au particles (below 5 nm) [66]. Low coordinated Au atoms found on small particles have also been suggested to play an important role in the activity of supported Au [67, 68], i.e. see (iv) in the list above. The size of the Au particles may also affect the shape of the Au particles [69]. It was reported that the relative amount of corner and edge atoms is larger on flat particles than on round particles with the same diameter [69]. Because the shape of a gold particle depends on the interaction between the gold and the support, different supports induce gold particle shapes with a varying amount of edge and corner atoms.

However, not all differences in catalytic activity of various Au-based catalysts can be explained by a particle size effect [31, 70]. For example, Schubert *et al.* proposed that the metal oxide support may serve as oxygen supplier [71]. They distinguished active support materials, which can supply oxygen to Au particles (i.e. TiO<sub>2</sub> and Fe<sub>2</sub>O<sub>3</sub>), and inert support materials such as Al<sub>2</sub>O<sub>3</sub>. For the former it was proposed that the size of the gold particles is not very important.

---

*The role of the support/additive*

There are different ways to explain the influence of the support/promoter on the catalytic activity of Au catalysts. One model suggests that the role of additives such as MgO, Li<sub>2</sub>O, Rb<sub>2</sub>O or BaO is to stabilize small gold particles during the preparation and further thermal treatments [47, 49, 50].

Regarding the direct role of the support, some theoretical studies suggested that it can influence the electronic structure of Au at the interface [72]. The authors suggested a charge transfer between the support, particularly negatively charged defects (F centres) and Au particles. Other theoretical calculations showed that defects on a support such as TiO<sub>2</sub> are crucial for adhesion of Au and in this way both the size and the shape of the Au particles are affected [73]. However, it was further suggested that these defects are not necessary oxygen vacancies, since similar results were obtained for nonreducible metal oxides such as Al<sub>2</sub>O<sub>3</sub>, MgO or SiO<sub>2</sub> [74, 75]. Of course, the reducible supports have a larger number of oxygen vacancies, useful for anchoring of Au. Moreover, it was suggested that for this type of easily reducible metal oxides, an additional reaction path is valid, i.e. the metal oxide may be the supplier of the active oxygen during the reaction [46, 71].

From a practical point of view, the choice of the support/additive is directly connected with the reaction that should be catalysed by Au. For instance, CO oxidation is successfully catalysed by Au supported on any material except acidic ones, such as SiO<sub>2</sub>-Al<sub>2</sub>O<sub>3</sub> and activated carbon. It was reported for example that Mg(OH)<sub>2</sub> is the best support for Au in CO oxidation at sub-ambient temperatures [76], but that deactivation occurs after 3 months. The effect of the support was explained on the basis of the structure of the as-prepared catalyst.

If the desired reaction is the combustion of hydrocarbons, Co<sub>3</sub>O<sub>4</sub> is the best support, based on the fact that this support is by itself highly active in complete oxidation reactions [77-80]. If the goal is the partial oxidation of hydrocarbons, then the choice is more restricted. Thus, it was reported that only TiO<sub>2</sub> and Ti-silicates act as efficient supports, especially if H<sub>2</sub> and O<sub>2</sub> are present in the feed [81-83]. For nitrogen-containing compounds, ferric oxide and nickel ferrites were reported to lead to the highest activity owing to their high affinity to nitrogen [52]. There are also reports of methanol synthesis over supported Au catalysts and according to [84], ZnO is the best support also for Au, not only for the commercial Cu catalyst.

*The nature of the Au active sites*

The nature of the active sites was mostly a matter of debate in CO oxidation, the most frequently studied reaction over Au-based catalysts. However, until now there is no general consensus about this. As already mentioned in the previous paragraph, for some systems it is clear that the *size of the Au crystallites* is not sufficient to explain the high activity. Therefore, it has been proposed that the *perimeter or gold-support interface* [33, 49, 57, 70, 85, 86], or small Au clusters that have nonmetallic electronic properties due to a *quantum-size effect* [66], or *step sites on the surface and strain defects* [87] are more important than only Au nanoparticles with a size between 2 and 5 nm. On the other hand, other groups are convinced that *Au<sup>3+</sup>* is responsible for the high activity in either CO oxidation [59], hydrogenation of



ethene [88, 89], ethyne hydrochlorination [90-92], or water-gas shift [93]. An intermediate model was proposed: an *ensemble of metallic Au atoms and Au cations* with hydroxyl ligands [94, 95]. This model suggests that the Au cations must be stable in a reducing environment and also in the neighbourhood of metallic gold. It was further concluded that  $\text{Au}^+$  would be able to satisfy these requirements, rather than  $\text{Au}^{3+}$  and  $[\text{Au}^+-\text{OH}]$  has been proposed as the cationic component. It has also been suggested that the active site for gold catalysis is *anionic gold*,  $\text{Au}^-$ . These species are mainly formed if Au is deposited on a defect-rich support, i.e. with an increased concentration of F-centres [72, 96-98].

The last factor that is believed by some authors to have a great influence during the catalytic reactions is *water*. According to some studies, the moisture effect is directly connected with CO activation *and* the nature of the support [99]. More water is required to promote CO oxidation over Au/ $\text{Al}_2\text{O}_3$  or Au/ $\text{SiO}_2$ , compared to Au/ $\text{TiO}_2$ .  $\text{H}_2\text{O}$  was also found to be responsible for the stabilization of  $\text{Au}^+$  [30, 70], as well as for the deactivation of the catalyst, viz. a detrimental role of  $\text{H}_2\text{O}$  [55, 85, 100, 101]. It was, for example, suggested that in the presence of water the dissociation of oxygen on gold particles may be activated and that the oxygen reacts with water to produce an oxygen radical available for reaction and two surface hydroxyl groups [102]. A beneficial effect of water on the activation of  $\text{O}_2$  was also proposed by Bond and Thompson [94]. Their reaction mechanism proceeds via a reaction between an OH group that spilled over from the support to  $\text{Au}^{3+}$  and the CO adsorbed on the gold particle, via a carboxylate group. The existence of the OH groups was used to explain the negative activation energy found for Au/ $\text{Mg}(\text{OH})_2$  tested under ultra-dry reaction conditions in CO oxidation [103]. Water was even proposed as an easy way to regenerate the Au/ $\text{Al}_2\text{O}_3$  catalyst [104]. For other reactions reports on the effect of water on the catalytic activity of Au-based catalysts are rather scarce. However, Haruta reported that some Au-based catalysts were tolerant against moisture in NO reduction by CO [105, 106], and in reduction of NO with  $\text{C}_3\text{H}_6$  in the presence of oxygen [107].

#### 1.4 The aims of this thesis

One important conclusion that can be drawn based on the results presented above is that Au *is* an active catalyst with real potential mainly in processes relevant to air pollution control. It is also evident that, in spite of the many papers that inundated the scientific community in the past 25 years, many aspects that underlie the Au reactivity are still uncertain.

Aiming for commercial applications of some very active gold-based catalysts, fundamental studies concerning various aspects of Au catalysis have been carried out throughout this thesis. The investigations have been performed using supported Au-based catalysts, alumina being the common used carrier. Two main types of Au-based catalysts were prepared, viz. Au/ $\text{MO}_x/\text{Al}_2\text{O}_3$  and Au/ $\text{M}^{\text{I}}\text{O}_x/\text{M}^{\text{II}}\text{O}_x/\text{Al}_2\text{O}_3$  (M,  $\text{M}^{\text{I}}$ ,  $\text{M}^{\text{II}}$ : alkali (earth), transition, rare-earth, and group IB metals) and their catalytic performance has been compared to the reference Au/ $\text{Al}_2\text{O}_3$ . Various reactions with direct relevance to air-pollution control were studied, viz. oxidation of CO in the presence or absence of hydrogen,  $\text{NH}_3$  oxidation to  $\text{N}_2/\text{N}_2\text{O}/\text{NO}$ , combustion of alkanes ( $\text{CH}_4$  and  $\text{C}_3\text{H}_8$ ) and alkenes ( $\text{C}_3\text{H}_6$ ), and

reduction of NO and N<sub>2</sub>O by hydrogen. Different aspects of these reactions were studied: (i) the effect of the Au particle size on the catalytic activity, (ii) the role of the additives on both the activity and selectivity, and (iii) the nature of the active sites of (un)promoted Au/Al<sub>2</sub>O<sub>3</sub>. In addition, particularly for CO oxidation and PROX, the influence of the pretreatment on the catalytic performance of Au-based catalysts was considered as a case study.

The structure of the thesis is as follows: **chapter 2** briefly presents an overview of the most relevant data published in the field of the above-mentioned reactions; **chapter 3** presents a detailed description of all the experimental techniques (i.e. preparation of the catalysts, characterization and catalytic tests) performed throughout this thesis; **chapter 4** deals with a comprehensive presentation and discussion of all the results obtained in the field of sample characterization (AAS, BET, XRD, HRTEM, SEM, DR-UV/Vis, TPR, XPS). **Chapter 5** presents the catalytic results of various Au-based catalysts tested in total oxidation of propene; **chapter 6** compares the catalytic activity of various Au-based catalysts in CH<sub>4</sub> and C<sub>3</sub>H<sub>8</sub> total oxidation. **Chapter 7** deals with ammonia abatement using Au-based catalysts and production of N<sub>2</sub>, N<sub>2</sub>O and NO; **chapter 8** is devoted to the reduction of NO and N<sub>2</sub>O by H<sub>2</sub>, and **chapter 9** is focused on a study concerning CO oxidation in the presence and absence of H<sub>2</sub>. The final **Chapter 10**, gives a general discussion and the conclusions of the most relevant results of the previous chapters. Most of the results presented in this thesis have been published in the form of journal articles or proceedings of (international) conferences.

## 1.5 References

- [1] Z. Kowalczyk, J. Sentek, S. Jodzis, M. Muhler, O. Hinrichsen, J. Catal. 169 (1997) 407.
- [2] Z. Kowalczyk, M. Krukowski, W. Rarog-Pilecka, D. Szmigiel, J. Zielinski, Appl. Catal. A 248 (2003) 67.
- [3] D. Szmigiel, H. Bielawa, M. Kurtz, O. Hinrichsen, M. Muhler, W. Rarog, S. Jodzis, Z. Kowalczyk, L. Znak, J. Zielinski, J. Catal. 205 (2002) 205.
- [4] R. A. van Santen, J. W. Niemantsverdriet, Chemical Kinetics and Catalysis, Plenum Press, New York 1995.
- [5] M. Ozawa, M. Kimura, Mater. Sci. Lett. 9 (1990) 291.
- [6] J. Stubenrauch, J. M. Vohs, J. Catal. 159 (1996) 50.
- [7] H. C. Yao, Y. F. Y. Yau, J. Catal. 89 (1984) 254.
- [8] S. E. Golunski, Plat. Met. Rev. 42 (1998) 2.
- [9] P. G. Gray, M. I. Petch, Plat. Met. Rev. 44 (2000) 108.
- [10] N. Edwards, S. R. Ellis, J. C. Frost, S. E. Golunski, A. N. J. van Keulen, N. G. Lindewald, J. Power Sources 71 (1998) 123.
- [11] G. J. K. Acres, J. C. Frost, G. A. Hards, R. J. Potter, T. R. Ralph, D. Thompsett, Catal. Today 38 (1997) 393.
- [12] F. Ghenciu, Current Opinion Solid State Mat. Sci. 6 (2002) 389.
- [13] K. Tanaka, K. Tamaru, J. Catal. 2 (1963) 366.
- [14] G. C. Bond, Catal. Today 72 (2002) 5.
- [15] G. C. Bond, J. Mol. Catal. A 156 (2000) 1.
- [16] P. Pyykko, Angew. Chem. Int. Ed. 41 (2002) 3573.
- [17] R. Meyer, C. Lemire, S. K. Shaikhutdinov, H.-J. Freund, Gold Bull. 37 (2004) 72.
- [18] G. C. Bond, Plat. Met. Rev. 44 (2000) 146.
- [19] P. Pyykko, Chem. Rev. 88 (1988) 563.
- [20] A. H. Guerrero, H. J. Fasoli, J. L. Costa, J. Chem. Educ. 76 (1999) 200.
- [21] W. A. Bone, R. V. Wheeler, Philos. Trans. 206A (1906) 1.
- [22] D. L. Chapman, J. E. Ramsbottom, C. G. Trotman, Proc. Roy. Soc. A 107 (1925) 92.
- [23] A. F. Benton, J. C. Elgin, J. Am. Chem. Soc. 49 (1927) 2426.
- [24] W. A. Bone, G. W. Andrew, Proc. Roy. Soc. A 109 (1925) 409.

- [25] G. C. Bond, *Gold Bull.* 5 (1971) 11.
- [26] R. S. Yolles, B. J. Wood, H. Wise, *J. Catal.* 21 (1971) 66.
- [27] G. C. Bond, P. A. Sermon, *Gold Bull.* 6 (1973) 102.
- [28] P. A. Sermon, G. C. Bond, P. B. Wells, *J. Chem. Soc. Farad. Trans. I* 75 (1979) 385.
- [29] G. J. Hutchings, *Gold Bull.* 29 (1996) 123.
- [30] M. Haruta, T. Kobayashi, N. Yamada, *Chem. Lett.* 2 (1987) 405.
- [31] M. Haruta, N. Yamada, T. Kobayashi, S. Iijima, *J. Catal.* 115 (1989) 301.
- [32] S. D. Gardner, G. B. Hoflund, B. T. Upchurch, D. R. Schryer, E. J. Kielin, J. Schryer, *J. Catal.* 129 (1991) 114.
- [33] S. D. Lin, M. Bollinger, M. A. Vannice, *Catal. Lett.* 17 (1993) 245.
- [34] G. C. Bond, D. T. Thompson, *Catal. Rev. Sci. Eng.* 41 (1999) 319.
- [35] M. Haruta, *Gold Bull.* 37 (2004) 27.
- [36] A. Ueda, T. Oshima, M. Haruta, *Appl. Catal. B* 12 (1997) 81.
- [37] M. A. P. Dekkers, M. J. Lippits, B. E. Nieuwenhuys, *Catal. Today* 54 (1999) 381.
- [38] A. C. Gluhoi, M. A. P. Dekkers, B. E. Nieuwenhuys, *J. Catal.* 219 (2003) 197.
- [39] P. Claus, A. Bruckner, C. Mohr, H. Hofmeister, *J. Am. Chem. Soc.* 122 (2000) 11430 and refs. therein.
- [40] D. Andreeva, V. Idakiev, T. Tabakova, A. Andreev, *J. Catal.* 158 (1996) 354.
- [41] D. Andreeva, *Gold Bull.* 35 (2002) 82.
- [42] D. Andreeva, V. Idakiev, T. Tabakova, L. Ilieva, P. Falaras, A. Bourlinos, A. Travlos, *Catal. Today* 72 (2002) 51.
- [43] S. D. Lin, A. C. Gluhoi, B. E. Nieuwenhuys, *Catal. Today* 90 (2004) 3.
- [44] S. Minico, S. Scire, C. Crisafulli, R. Maggiore, S. Galvagno, *Appl. Catal. B* 28 (2000) 245.
- [45] S. Scire, S. Minico, C. Crisafulli, C. Satriano, A. Pistone, *Appl. Catal. B* 40 (2003) 43.
- [46] A. C. Gluhoi, N. Bogdanchikova, B. E. Nieuwenhuys, *J. Catal.* 229 (2005) 154.
- [47] A. C. Gluhoi, N. Bogdanchikova, B. E. Nieuwenhuys, *J. Catal.* 232 (2005) 96.
- [48] M. Haruta, A. Ueda, S. Tsubota, R. M. Torres Sanchez, *Catal. Today* 29 (1996) 443.
- [49] R. J. H. Grisel, *Supported gold catalysts for environmental applications*, PhD thesis, Leiden University (2002).
- [50] R. J. H. Grisel, B. E. Nieuwenhuys, *J. Catal.* 199 (2001) 48.
- [51] Q. Xu, K. C. C. Kharas, A. K. Datye, *Catal. Lett.* 85 (2003) 229.
- [52] M. Haruta, *CATTECH* 6 (2002) 102.
- [53] R. J. H. Grisel, P. J. Kooyman, B. E. Nieuwenhuys, *J. Catal.* 191 (2000) 430.
- [54] M. Okumura, K. Tanaka, A. Ueda, M. Haruta, *Solid State Ionics* 95 (1997) 143.
- [55] J. D. Grunwaldt, C. Kiener, C. Wogerbauer, A. Baiker, *J. Catal.* 181 (1999) 223.
- [56] L. Prati, M. Rossi, *Green Chemistry: Challenging Perspectives*, P. Tundo, P. Anastas eds., Oxford 2000, p.183.
- [57] F. Boccuzzi, A. Chiorino, M. Manzoli, P. Lu, T. Akita, S. Ichikawa, M. Haruta, *J. Catal.* 202 (2001) 256.
- [58] E. D. Park, J. S. Lee, *J. Catal.* 186 (1999) 1.
- [59] N. A. Hodge, C. J. Kiely, R. Whyman, M. R. H. Siddiqui, G. J. Hutchings, Q. A. Pankhurst, F. E. Wagner, R. R. Rajaram, S. E. Golunski, *Catal. Today* 72 (2002) 133.
- [60] S. Minico, S. Scire, C. Crisafulli, S. Galvagno, *Appl. Catal. B* 34 (2001) 277.
- [61] S.-J. Lee, A. Gavriilidis, Q. A. Pankhurst, A. Kyek, F. E. Wagner, P. C. L. Wong, K. L. Yeung, *J. Catal.* 200 (2001) 298.
- [62] A. Wolf, F. Schuth, *Appl. Catal. A* 226 (2002) 1.
- [63] J.-N. Lin, J.-H. Chen, C.-Y. Hsiao, Y.-M. Kang, B.-Z. Wan, *Appl. Catal. B* 36 (2002) 19.
- [64] S. Tsubota, T. Nakamura, K. Tanaka, M. Haruta, *Catal. Lett.* 56 (1998) 131.
- [65] M. A. P. Dekkers, *Supported gold catalysts for automotive catalysis reactions*, PhD thesis, Leiden University (2000).
- [66] M. Valden, X. Lai, D. W. Goodman, *Science* 281 (1998) 1647.
- [67] N. Lopez, J. K. Norskov, *J. Am. Chem. Soc.* 124 (2002) 11262.
- [68] Z.-P. Liu, P. Hu, A. Alavi, *J. Am. Chem. Soc.* 124 (2002) 14770.
- [69] J. D. Grunwaldt, M. Maciejewski, O. S. Becker, P. Fabrizioli, A. Baiker, *J. Catal.* 186 (1999) 458.
- [70] M. Haruta, S. Tsubota, T. Kobayashi, H. Kageyama, M. J. Genet, B. Delmon, *J. Catal.* 144 (1993) 175.
- [71] M. M. Schubert, S. Hackenberg, A. C. van Veen, M. Muhler, V. Plzak, R. J. Behm, *J. Catal.* 197 (2001) 113.
- [72] A. Sanchez, S. Abbet, U. Heiz, W.-D. Schneider, H. Hakkinen, R. N. Barnett, U. Landman, *J. Phys. Chem. A* 103 (1999) 9573.
- [73] N. Lopez, J. K. Norskov, T. V. W. Janssens, A. Carlsson, A. Puig-Molina, B. S. Clausen, J. D. Grunwaldt, *J. Catal.* 225 (2004) 86.

- 
- [74] A. M. Ferrari, G. Pacchioni, *J. Phys. Chem.* 100 (1996) 9032.  
[75] Z. Lodziana, J. K. Norskov, *Surf. Sci.* 518 (2002) L577.  
[76] D. A. H. Cunningham, W. Vogel, H. Kageyama, S. Tsubota, M. Haruta, *J. Catal.* 177 (1998) 1.  
[77] R. D. Walters, J. J. Weimer, J. E. Smith, *Catal. Lett.* 30 (1995) 181.  
[78] J. E. Germain, *Catalytic Conversion of Hydrocarbons*, Academic Press 1967.  
[79] G. K. Boreskov, *Catalysis Science and Technology*, Vol. 3, Springer-Verlag, Berlin 1985.  
[80] E. Garbowski, M. Guenin, M. C. Marion, M. Primet, *Appl. Catal.* 64 (1990) 209.  
[81] B. S. Uphade, M. Okumura, S. Tsubota, M. Haruta, *Appl. Catal. A* 190 (2000) 43.  
[82] Y. A. Kalvachev, T. Hayashi, S. Tsubota, M. Haruta, *J. Catal.* 186 (1999) 228.  
[83] B. S. Uphade, S. Tsubota, T. Hayashi, M. Haruta, *Chem. Lett.* (1998) 1277.  
[84] H. Sakurai, M. Haruta, *Appl. Catal. A* 127 (1995) 93.  
[85] M. Bollinger, M. A. Vannice, *Appl. Catal. B* 8 (1996) 417.  
[86] R. J. H. Grisel, C. J. Weststrate, A. Goossens, M. W. J. Craje, A. M. van der Kraan, B. E. Nieuwenhuys, *Catal. Today* 72 (2002) 123.  
[87] M. Mavrikakis, P. Stoltze, J. K. Norskov, *Catal. Lett.* 64 (2000) 101.  
[88] J. Guzman, B. C. Gates, *Angew. Chem. Int. Ed.* 42 (2003) 690.  
[89] J. Guzman, B. C. Gates, *J. Phys. Chem. B* 106 (2002) 7659.  
[90] B. Nkosi, N. J. Coville, G. J. Hutchings, M. D. Adams, J. Friedl, F. E. Wagner, *J. Catal.* 128 (1991) 366.  
[91] B. Nkosi, M. D. Adams, N. J. Coville, G. J. Hutchings, *J. Catal.* 128 (1991) 378.  
[92] G. J. Hutchings, *J. Catal.* 96 (1985) 292.  
[93] Q. Fu, H. Saltsburg, M. Flytzani-Stephanopoulos, *Science* 301 (2003) 935.  
[94] G. C. Bond, D. T. Thompson, *Gold Bull.* 33 (2000) 41.  
[95] C. K. Costello, M. C. Kung, S.-O. Oh, Y. Wang, H. H. Kung, *Appl. Catal. A* 232 (2002) 159.  
[96] W. T. Wallace, R. L. Whetten, *J. Am. Chem. Soc.* 124 (2002) 7499.  
[97] L. D. Socaciu, J. Hagen, T. M. Bernhardt, L. Woste, U. Heiz, H. Hakkinen, U. Landman, *J. Am. Chem. Soc.* 125 (2003) 10437.  
[98] H. Hakkinen, U. Landman, *J. Am. Chem. Soc.* 123 (2001) 9704.  
[99] M. Date, M. Haruta, *J. Catal.* 201 (2001) 221.  
[100] G. B. Hoflund, S. D. Gardner, D. R. Schryer, B. T. Upchurch, E. J. Kielin, *Langmuir* 11 (1995) 3431.  
[101] S. J. Lee, A. Gavriilidis, *J. Catal.* 206 (2002) 305.  
[102] F. Boccuzzi, A. Chiorino, *J. Phys. Chem. B* 104 (2000) 5414.  
[103] D. A. H. Cunningham, W. Vogel, M. Haruta, *Catal. Lett.* 63 (1999) 43.  
[104] H. H. Kung, M. C. Kung, C. K. Costello, *J. Catal.* 216 (2003) 425.  
[105] M. Haruta, *Catal. Today* 36 (1997) 153.  
[106] M. Haruta, *Catal. Surv. Jpn.* 1 (1997) 61.  
[107] A. Ueda, M. Haruta, *Gold Bull.* 32 (1999) 3.



# Chapter 2

## Literature survey - Gold catalysis

*This chapter presents a brief overview of the most relevant results published in the field of alkane (methane and propane) and alkene (propene) combustion, ammonia oxidation and CO oxidation in the presence or absence of hydrogen. The most significant results concerning NO and N<sub>2</sub>O reduction by H<sub>2</sub> are also reviewed. Catalysis by gold is reviewed in more detail.*

## 2.1 Alkane combustion

### *Methane combustion*

Combustion of hydrocarbons, especially methane, the main component of natural gas requires high temperatures, leading to undesired NO<sub>x</sub> formation. Catalytic combustion can lower the temperature and thus the emission of NO<sub>x</sub> [1-4]. The key to this process is a highly efficient catalyst. Many materials show interesting activity, but very few sustain operation at high temperatures. This is because the activation of C-H bond requires, besides an active catalyst, relatively high operating temperatures. The sensitivity of the combustion catalysts to high temperatures, or their thermal stability, is related to the stability of the active component and the loss of active sites by sintering. Although all catalysts lose their activity on exposure to high operation temperatures, the onset, the rate and the degree of this activity loss vary significantly [2, 3].

The catalysts that are used can be roughly divided into three groups: noble metal-based catalysts, binary oxides, and mixed oxides with a spinel-like or perovskite-like structure. Among the noble metal-based catalysts, the activity of Pd and Pt catalysts is generally considered to be significantly higher than that of Rh, with palladium (oxide) being the most active. However, it appears that the rate of combustion of methane on Pt or Pd catalysts depends on the state of the catalyst surface [5]. It was suggested that the optimum activity occurs when the Pt is partly oxidized, whereas Pd is fully oxidized to PdO [5]. The difference between the two metals can be rationalized by the fact that the Pt surface, fully covered with adsorbed oxygen, cannot readily activate the almost non-polar C-H bonds in methane (by a homolytic mechanism), whereas the Pd<sup>2+</sup>O<sup>2-</sup> ions at the surface of the PdO can more easily activate the C-H bonds by a heterolytic mechanism [5]. However, if the oxygen concentration in the reaction mixture is low, Pt can be a more effective catalyst than Pd [5]. For Pd/Al<sub>2</sub>O<sub>3</sub> an apparent activation energy lying between 70 and 95 kJ mol<sup>-1</sup> was reported [6-9], whereas for PdO/Al<sub>2</sub>O<sub>3</sub> a significantly smaller  $E_a$  was found, i.e. between 51 and 87 kJ mol<sup>-1</sup> [10, 11]. For Pt/Al<sub>2</sub>O<sub>3</sub> much larger values for  $E_a$  were reported: between 98 and 125 kJ mol<sup>-1</sup> [12, 13]. The activity of Pd-based catalysts was also studied for various supports [14], and mixed SnO<sub>2</sub>-MO<sub>x</sub> supports [15]. For the latter, no improvement was reported, whatever the MO<sub>x</sub> used as additive (M: Al, Ce, Fe, Mn, Ni, and Zr) [15]. On the other hand, for Pd/Al<sub>2</sub>O<sub>3</sub>, NiO was reported as a good promoter [16]. Other reports have shown that active Pd/Al<sub>2</sub>O<sub>3</sub> catalysts are obtained using additives of the type CeO<sub>x</sub>-MO<sub>x</sub> (M: Zr, La, Ca, and Mg) [17]. However, due to the operation at high temperatures, PdO loses its activity mainly due to its decomposition, while Pt suffers from sintering and volatilisation [2, 3, 18, 19].

On the other hand, a variety of transition metal oxides are known to catalyze the oxidation of methane, the best results being obtained with Co<sub>3</sub>O<sub>4</sub> [20, 21]. However, Co<sub>3</sub>O<sub>4</sub> is not stable at high temperatures [22]. On the other hand, a variety of perovskites may withstand substantially elevated temperatures and with an activity comparable with Pt [2-4, 23-25]. The loss in the catalytic activity due to a collapse of the surface area is partly compensated by the fast oxygen mobility in oxygen nonstoichiometric compositions [4]. Zr- or Sm-doped ceria have also been reported as active catalysts in high-temperature CH<sub>4</sub> oxidation [26, 27].

Concerning the reaction mechanism of methane combustion, there are still disputes regarding the elementary steps, although it is generally accepted that the activation of the C-H bond is the most difficult step. This can be done homolytic, if Pt-based catalysts and maybe some transition metal oxides are used [4, 5], or heterolytic, over PdO [5]. It was also suggested that the acid-base character of the additives (for Pt and Pd), or of the transition metal oxide-based catalysts may directly influence the overall catalytic activity [5, 28, 29]. Moreover, based on the H<sub>2</sub>O inhibition especially for PdO, it was also proposed that the breaking of the O-H bond may be slower than that of C-H and then the rate determining step would not be the activation of the C-H bond, but rather that of O-H [5]. On the other hand, there is a more general consensus regarding the oxygen activation step and it involves lattice oxygen, viz. nucleophilic oxygen, via a Mars and van Krevelen mechanism [4, 28, 30]. This mechanism is valid when transition metal oxides, spinel or perovskites-based catalysts are employed.

#### *Gold as a catalyst in methane combustion*

Gold-based catalysts attracted less interest for CH<sub>4</sub> oxidation, probably because of the high temperature needed to activate this hydrocarbon. However, it was reported that 5 wt-% Au/Co<sub>3</sub>O<sub>4</sub> was active at very low temperatures, viz. 200-250<sup>o</sup>C [31]. Based on the light-off temperatures for 5 wt-% Au catalysts and with a reaction mixture CH<sub>4</sub>:O<sub>2</sub> = 1:15, the reported activities were as follows: Au/Co<sub>3</sub>O<sub>4</sub> > Au/NiO > Au/MnO<sub>x</sub> > Au/Fe<sub>2</sub>O<sub>3</sub> > Au/CeO<sub>x</sub>. Analysis of the used catalysts using XPS evidenced the co-existence of at least two oxidation states of Au, and the increased activity was correlated with a higher oxidation state. According to a study of Haruta [32], the temperature of 50% CH<sub>4</sub> conversion decreases in the following order: Au/Co<sub>3</sub>O<sub>4</sub> > Au/NiFe<sub>2</sub>O<sub>4</sub> > Au/ZnFe<sub>2</sub>O<sub>4</sub> > Au/Fe<sub>2</sub>O<sub>3</sub> [32, 33]. In these papers Pt/Al<sub>2</sub>O<sub>3</sub> was reported to be a poor catalyst, even inferior to Au/Fe<sub>2</sub>O<sub>3</sub>. Interestingly, Au/Co<sub>3</sub>O<sub>4</sub> was reported to have an activity similar to Pt/Al<sub>2</sub>O<sub>3</sub>. However, it was not considered that the effective loading of Au was 10 times larger than that of Pt. More recently, Grisel *et al.* studied methane oxidation over unpromoted and MO<sub>x</sub>-promoted Au/Al<sub>2</sub>O<sub>3</sub> and concluded that MnO<sub>x</sub>, FeO<sub>x</sub> or CoO<sub>x</sub> are efficient additives for Au/Al<sub>2</sub>O<sub>3</sub> [34-36]. A combination of Au with CuO resembles more the performance of CuO, rather than that of Au [36]. This is expected, since CuO is well-known for its intrinsic activity in (total) oxidation reactions [28, 37].

#### *Propane combustion*

Studies of catalytic oxidation reactions showed that short-chain hydrocarbons are amongst the most difficult to oxidize [38]. However, for longer C-C chains, the activation of hydrocarbons becomes easier. As mentioned in the previous paragraph, except for palladium in the case of methane, platinum is recognized to be the most active metal for hydrocarbon oxidation [8, 39]. However, there are also some reports that describe the good catalytic performance of Pd-based catalysts [40-44], Pd-Rh [45], and perovskite-type catalysts [27, 46]. The effect of additives on the performance of Pt/Al<sub>2</sub>O<sub>3</sub> in propane combustion was investigated by Yazawa *et al.* by incorporating into the support several additives, such as Na,



Cs, Ca, Mg, and Mo [47]. The catalytic activity of platinum increased with the increase of the electronegativity of the additives and this was explained by assuming that the oxidation resistance of platinum under oxidizing conditions is enhanced by an increase of the electronegativity of the additive. Similarly, the same authors reported that the propane oxidation activity of platinum is enhanced when the metal is supported on more acidic supports. These results were ascribed to a higher resistance of Pt against oxidation [48, 49]. In contrast, Hubbard *et al.* [50] claimed that the strength of the acidic support does not significantly influence the activity in propane oxidation. It is worth noting that in all these previous studies regarding the effect of support acidity on the activity of Pt in propane oxidation, platinum supported on zeolitic materials was not studied. When the catalytic performance of Pt-supported catalysts was followed as a function of the support (i.e. MgO, Al<sub>2</sub>O<sub>3</sub>, and various types of zeolites), the authors found that propane oxidation is structure insensitive in the case of Pt/Al<sub>2</sub>O<sub>3</sub> and that the TOF values of Pt/acidic zeolites were more than two orders of magnitude higher than for Pt/Al<sub>2</sub>O<sub>3</sub> [51]. The reported apparent activation energy varies between 121 kJ mol<sup>-1</sup> (Pt/Beta) and 37 kJ mol<sup>-1</sup> (Pt/MgO) [51]. Although there is a rather general consensus regarding the active state of Pt, i.e. metallic, an additional oxidation pathway has also been proposed in terms of propane adsorbed on the metal-oxide interface region and reacting with oxygen spilled-over from the metal surface [51]. Finally, it was also shown by other authors that the activity of Pt/Al<sub>2</sub>O<sub>3</sub> may be substantially increased by alumina sulphation [50, 52-54], or by the addition of electrophilic additives to the support [47, 55]. In the case of the promotion of propane oxidation over Pt/Al<sub>2</sub>O<sub>3</sub> by SO<sub>2</sub>, it is believed that the formation of stable sulphate species at the Pt/support interface facilitates the dissociative chemisorption of propane and thereby enhances the intrinsic oxidation activity of platinum [52, 53].

#### *Gold as a catalyst for propane combustion*

Results concerning the use of supported Au catalysts for C<sub>3</sub>H<sub>8</sub> (total) oxidation are scarce. The first report of Au-based catalysts for C<sub>3</sub>H<sub>8</sub> oxidation was published by Haruta in 1992 [32] and included in a comprehensive review published by Bond and Thompson [33]. Haruta concluded that, similar to methane oxidation, Au/Co<sub>3</sub>O<sub>4</sub> is more active than Pd or Pt supported on Al<sub>2</sub>O<sub>3</sub> for the oxidation of propane. However, those results should be considered with care because the author did not estimate the specific reaction rate for various samples, especially where different loadings of the active metal had been used (10 wt-% Au vs. 1 wt-% Pt). Later, by comparing the activity of Au/Al<sub>2</sub>O<sub>3</sub> and Pt/Al<sub>2</sub>O<sub>3</sub> in C<sub>3</sub>H<sub>8</sub> total oxidation, Haruta admitted that Au is inferior to Pt [56]. Surprisingly, the authors reported a relatively low apparent activation energy (i.e. 43 kJ mol<sup>-1</sup>) for the Au catalyst, although Au-based catalysts are considerably less active than Pt-based catalysts. This value cannot correspond to the very low activity found in their experiments [56]. The same paper also presents the influence of the sulphation on the catalytic performance of supported Pt and Au catalysts. It was found that sulphation promotes the oxidation of propane on Pt/TiO<sub>2</sub>, whereas for Au/TiO<sub>2</sub> it acts as a poison. The same poisonous effect of SO<sub>2</sub> was found for CO oxidation on Au/TiO<sub>2</sub> [56]. Au deposited on Al<sub>2</sub>O<sub>3</sub> and CeO<sub>2</sub> was studied in C<sub>3</sub>H<sub>8</sub> oxidation

reaction, but the results were not very encouraging [57]. However, the authors claimed that the co-existence of  $\text{Au}^{3+}$  and  $\text{Ce}^{4+}$ , obtained by thermal treatment at  $800^\circ\text{C}$ , are essential for high activity. More recently, Au deposited on  $\text{V}_2\text{O}_5/\text{SiO}_2$  and  $\text{MoO}_3/\text{SiO}_2$  was tested for partial oxidation of propane [58]. However, due to the relatively low conversion of propane, these results are not very encouraging for practical applications.

## 2.2 Combustion of alkenes

### *Propene oxidation*

As already mentioned in the previous section, most common catalysts for total oxidation of hydrocarbons, including propene, are based on Pt or Pd [59]. Most of the papers concerning combustion of hydrocarbons, including propene, have already been reviewed in the previous section. However, a comparative study of Pt and Pd-based catalysts, supported on  $\text{Al}_2\text{O}_3$  and  $\text{ZrO}_2$  is presented in [55]. The authors reported rather different behaviour in  $\text{C}_3\text{H}_6$  oxidation for the two catalytic systems studied [55]. The catalytic activities of both Pt- and Pd-based catalysts were improved by increasing the basic strength of the support and Pt/ $\text{Al}_2\text{O}_3$  performed better than Pt/ $\text{ZrO}_2$ . Opposite results were obtained for Pd-based catalysts, although there the differences were not significant.

The effect of promoters ( $\text{Co}_3\text{O}_4$  and  $\text{CeO}_2$ ) on the catalytic performance of Pt and Pd was studied. Positive results were found for both metals, and the catalytic activity could be further enhanced upon applying a reductive pretreatment [60]. However, attention has also been paid to base metals. Cobalt oxide, chromium oxide, copper oxide, manganese oxide and iron oxide are reported to be among the most active oxides in catalytic combustion [20, 22, 61-63]. The effect of Zr addition to copper oxide-based catalysts has also been investigated [64]. The same authors compared the catalytic performance of  $\text{ZrO}_2$ ,  $\text{Y}_2\text{O}_3$ , and  $\text{ZrO}_2$  doped with  $\text{Y}_2\text{O}_3$  in the presence and absence of copper and found significant synergistic effects by combining the above-mentioned oxides [65]. The authors explained their results on the basis of the co-existence of anionic vacancies and CuO as the active site for the reaction. Spinel-like materials, i.e.  $\text{CoCr}_2\text{O}_4$ ,  $\text{CuCr}_2\text{O}_4$ ,  $\text{ZnCr}_2\text{O}_4$  [66, 67], or perovskite-like compounds,  $\text{LaMO}_3$  [68, 69] are reported to be promising due to their high activity and stability at high temperatures. The mechanism of the total combustion of propene was established to be of the Mars and van Krevelen type, and proceeds through nucleophilic attack of the lattice oxygen of the above mentioned oxides [37, 70].

### *Gold as a catalyst in propene combustion*

Gold has attracted more interest for potential applications in partial oxidation of propene, than in total oxidation. It has been found that gold nanoparticles show extraordinary selectivity to propylene oxide (> 99%), although at a very low conversion (< 2%) on a Au/ $\text{TiO}_2$  catalyst [71]. However, it was reported that the yield of propene oxide can be increased by optimising the support composition [71-73]. Catalysts based on Au were also tested for the reduction of NO with propene over Au/ $\text{Al}_2\text{O}_3$  and Au/ $\text{ZnO}$  [74, 75], Au/ $\text{Al}_2\text{O}_3$  mixed mechanically with  $\text{Mn}_2\text{O}_3$  [76, 77], and Au/ $\text{Co}_3\text{O}_4$  [78]. Interesting results were reported by Kung *et al.* concerning the oxidation of  $\text{C}_3\text{H}_6$  in the absence of  $\text{NO}_x$ : very large

Au particles (~15 nm) were found to be more active than smaller Au particles (~2 nm) [75]. The suggested mechanism includes the reaction between NO and O<sub>2</sub> to form NO<sub>2</sub>, which then reacts with propene to form N<sub>2</sub> [76]. Surprisingly, these authors claimed that Au is able to adsorb propene above room temperature [76], although surface science studies point to a relatively weak interaction/adsorption of propene with the Au surface and the adsorption of propene on Au was found to proceed at much lower temperatures [79, 80], possibly at the perimeter of gold islands on TiO<sub>2</sub> (110).

For total oxidation of propene, Au/Co<sub>3</sub>O<sub>4</sub> was reported to be more active than Au deposited on NiFe<sub>2</sub>O<sub>4</sub> or Fe<sub>2</sub>O<sub>3</sub>, but not as active as Pt/Al<sub>2</sub>O<sub>3</sub> [32, 33]. Later, Kim *et al.* found some synergism between Pt/Al<sub>2</sub>O<sub>3</sub> and Au/TiO<sub>2</sub> in low temperature oxidation of propene [81]. The authors observed that the addition of Au/TiO<sub>2</sub> to Pt/Al<sub>2</sub>O<sub>3</sub> prevents CO formation and lowers the light-off temperature for C<sub>3</sub>H<sub>6</sub> oxidation by ~54<sup>0</sup>C. However, too many parameters have been varied by changing from Pt/Al<sub>2</sub>O<sub>3</sub> to Au/TiO<sub>2</sub> and finally to the multicomponent catalyst, and no information regarding the specific reaction rate or the apparent activation energy were provided. A recent contribution in this field presents the influence of additives such as transition metal oxides (TMO), ceria, and alkali (earth) metal oxides on the catalytic performance of Au/Al<sub>2</sub>O<sub>3</sub> [82, 83]. The authors found that the role of TMO and ceria is twofold: that of a structural promoter by stabilizing small Au particles against sintering, and that of a co-catalyst by providing the active oxygen via a Mars and van Krevelen mechanism [82]. On the other hand the alkali (earth) metal oxides are solely structural promoters [83].

### 2.3 Ammonia oxidation

There are a lot of chemical processes that use ammonia as a reactant or produce ammonia as a by-product. All these processes are affected by ammonia slip problems. Low temperature selective oxidation of ammonia with oxygen (NH<sub>3</sub>-SCO) to nitrogen and water is a potentially efficient method for removal of ammonia from oxygen-containing flue gases, via reaction:

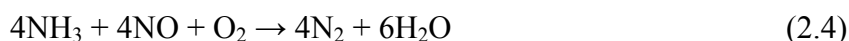


Such a SCO reaction may also be used for the control of other ammonia emission sources, e.g. agricultural sources and nitric acid production plants. There are two important issues about this SCO reaction: one is the selectivity and the other is the application temperature. The oxidation of ammonia can also produce NO<sub>x</sub> via reactions (2.2) and (2.3), which makes the selectivity of SCO reaction critical:



Potentially, N<sub>2</sub>O may be used for SCO of hydrocarbons [84-86]. Therefore, it would be interesting to develop a catalyst with a high selectivity to N<sub>2</sub>O (reaction (2.2)). Operation at

high temperatures (800-900<sup>0</sup>C) selectively produces NO and this Ostwald process has been used for many years for the industrial production of nitric acid [87]. Noble-metal catalysts (Pt with Rh) are used for this purpose. Therefore, a lower SCO reaction temperature (< 300<sup>0</sup>C) would be better for NH<sub>3</sub> abatement. NH<sub>3</sub> is also used as an effective NO<sub>x</sub> (NO+NO<sub>2</sub>) reducer in power plants, via reaction:



The commercial catalysts of this process are based on V<sub>2</sub>O<sub>5</sub>-TiO<sub>2</sub> [88]. Many systems have been tested for these processes, but apparently a high selectivity to N<sub>2</sub> is not always in line with a high conversion of ammonia. For example, Pt-based catalysts were reported to produce N<sub>2</sub> rather than NO [89], but the selectivity is comparatively low since high levels of N<sub>2</sub>O are co-produced [90]. However, the most important drawback of the platinum-based catalysts is their fast deactivation. High NH<sub>3</sub> conversion and selectivity to N<sub>2</sub> even under wet conditions were found by combining Pt with CuO/Al<sub>2</sub>O<sub>3</sub> (20 wt% CuO) [91]. However, the authors did not compare the performance of Pt/CuO/Al<sub>2</sub>O<sub>3</sub> with CuO/Al<sub>2</sub>O<sub>3</sub>, although it is well known that CuO itself is an outstanding catalyst in NH<sub>3</sub> oxidation with high selectivity to N<sub>2</sub> (see below).

Other catalysts consisting of a precious metal supported on an oxidic system include Pd-V<sub>2</sub>O<sub>5</sub>-WO<sub>3</sub>/TiO<sub>2</sub>-SiO<sub>2</sub> [92], Ir-V<sub>2</sub>O<sub>5</sub>-WO<sub>3</sub>/TiO<sub>2</sub>-SiO<sub>2</sub> [92, 93], Ag/CuO/Al<sub>2</sub>O<sub>3</sub> [93, 94], and Ag powder [95]. Catalysts based on metal oxides have been studied as well: MoO<sub>3</sub>/SiO<sub>2</sub> [96, 97], V<sub>2</sub>O<sub>5</sub>/TiO<sub>2</sub> [90, 98], CuO/TiO<sub>2</sub> [98], CuO/Al<sub>2</sub>O<sub>3</sub> [99, 100], NiO/Al<sub>2</sub>O<sub>3</sub> [101], Fe<sub>2</sub>O<sub>3</sub>/TiO<sub>2</sub> [102]. Topsøe (Denmark) patented a process for NH<sub>3</sub> oxidation between 200 and 500<sup>0</sup>C [103]. The catalysts used contain Cu, Co and Ni oxides doped with small amounts of noble metals (100-200 ppm) and are supported on SiO<sub>2</sub>. The authors claimed that the selectivity and activity of the catalysts were improved when the catalysts were sulphated either during, or prior to the contact with the reactant gas. Moreover, sulphation improved the selectivity to N<sub>2</sub> from 53 to 99%.

The ion-exchange zeolite systems Cu-ZSM-5 [98, 104], Cu-Y [99], Pd-ZSM-5 [90] and Fe-ZSM-5 [104, 105] have attracted attention as well. The activity of a Cu-Y catalyst was reported to increase after treating the sample with NaOH [99]. The authors speculated that the treatment with NaOH increased the amount of low temperature active centres. More recently, a comparison of various catalytic systems comprising 5% Fe/Al<sub>2</sub>O<sub>3</sub>, 5% Mn/Al<sub>2</sub>O<sub>3</sub>, 20% CuO/Al<sub>2</sub>O<sub>3</sub>, 1% Pt/20%CuO/Al<sub>2</sub>O<sub>3</sub>, 2% Rh/Al<sub>2</sub>O<sub>3</sub> and Fe zeolite (Fe-SH-27) has been reported under fuel-lean and fuel-rich conditions [106]. The authors claimed that a Fe-zeolite catalyst exhibits the lowest NO<sub>x</sub> yield under fuel-lean conditions, whereas under fuel-rich conditions the 20% CuO/Al<sub>2</sub>O<sub>3</sub> was superior with close to zero NO<sub>x</sub> formation [106], in line with previously reported data. However, the authors compared the catalytic performance of their samples without considering the large difference in the loading of each active material.

Catalytic studies using the surface science approach revealed that the formation of NO, N<sub>2</sub> and H<sub>2</sub>O is possible on Pt single crystal surfaces under very low pressure [89, 107, 108]. It was concluded that the selectivity mainly depends on the temperature and the NH<sub>3</sub>/O<sub>2</sub> ratio.

Other studies devoted to  $\text{NH}_3$  oxidation over various Ir surfaces showed that on Ir(510) and Ir(110) the reaction products are  $\text{N}_2$  and  $\text{H}_2\text{O}$ ; NO and  $\text{N}_2\text{O}$  are not observed (reaction temperature 300-800 K) [109]. However, on Ir(100)  $\text{N}_2\text{O}$  was also formed [110]. A study concerning the decomposition and oxidation of  $\text{NH}_3$  on Ru(0001) showed that ammonia was dissociatively adsorbed between 150 and 300 K, and that the products of the oxidation were  $\text{H}_2\text{O}$ ,  $\text{N}_2$  and  $\text{N}_2\text{O}$  [111].

The majority of the mechanistic studies concerning  $\text{NH}_3$  oxidation have been done on platinum-based catalysts. Early studies proposed three reaction mechanisms. Thus, it was suggested that the first step in  $\text{NH}_3$  oxidation is the formation of a nitroxyl species (HNO), that further reacts to produce  $\text{N}_2$ ,  $\text{N}_2\text{O}$ , and NO (the nitroxyl mechanism) [112]. This mechanism has been extended by suggesting that the formation of hydroxylamine ( $\text{NH}_2\text{OH}$ ) was the first step [113, 114]. In the next reaction step the  $\text{NH}_2\text{OH}$  is converted to HNO. In another mechanism it was proposed that the first step yields imide (NH) (the imide mechanism) [115, 116]. The formation of  $\text{N}_2$  was proposed to be the reaction product between NO and  $\text{NH}_3$ . According to other authors, the first step in  $\text{NH}_3$  oxidation would be the formation of  $\text{NH}_x$  species through oxydehydrogenation of  $\text{NH}_3$ , and NO and  $\text{N}_2$  would be formed by the combination of  $\text{N}_{\text{ads}}$  with  $\text{O}_{\text{ads}}$  or with  $\text{N}_{\text{ads}}$ , respectively [108]. On the other hand it was suggested that NO is the reaction product between  $\text{NH}_{\text{ads}}$  and  $\text{O}_{\text{ads}}$  and  $\text{N}_2$  resulted from the consecutive dissociation of NO [89]. Since only NO and  $\text{N}_2$  were produced under the reaction conditions used in these studies, the formation of  $\text{N}_2\text{O}$  was not discussed. Later, it was shown that on Pt and Ir sponge, NH and OH fragments were the main adsorbed species [117]. The reaction between NH and OH was speculated to be the rate-determining step and  $\text{N}_2\text{O}$  was proposed to be produced by NO reacting with  $\text{N}_{\text{ads}}$ . More recently, a model for the oxidation of  $\text{NH}_3$  has been proposed for Pt(533) and Pt(433) [118]. In this model  $\text{NH}_x$  species were not relevant in the mechanism. This theoretical model is in good agreement with the experimental results and consists of direct H abstraction from  $\text{NH}_3$  by adsorbed oxygen as the essential step. The model works quantitatively in excess of oxygen.

Over Ag catalysts, NO was found to be the main reaction intermediate that produced  $\text{N}_2\text{O}$  and  $\text{N}_2$  [93, 95]. NO could even be formed at room temperature. Its subsequent oxidation to  $\text{NO}_x$  leads to adsorption on the Ag surface, blocking the active sites for oxygen adsorption [93]. The pathway for  $\text{NH}_3$  oxidation was proposed to consist of two-step consecutive reactions. In the first step NO was formed. This reaction step was very fast on Ag. At intermediate temperatures (below 300°C), NO could then be removed either as  $\text{N}_2\text{O}$  or as  $\text{N}_2$ , through a selective reduction reaction (the second step). At higher temperatures NO could directly desorb as one of the products [95]. For catalysts containing both Cu and Ag, the authors proposed a bifunctional mechanism in which the Ag component mainly catalyses  $\text{NH}_3$  oxidation to NO (the first step of the reaction) and Cu is active for the selective reduction of NO to  $\text{N}_2$  [93].

Finally it should be mentioned that a mechanism based on the recombination of two  $\text{NH}_x$  species giving rise to a hydrazinium intermediate was also proposed for some metal oxide catalysts [119-121].

*Gold as a catalyst for ammonia oxidation*

To the best of my knowledge ammonia oxidation over Au based-catalysts has not been reported in the literature until our work [122, 123]. Various Au-based catalysts have been tested in NH<sub>3</sub> oxidation (reactant ratio NH<sub>3</sub>/O<sub>2</sub> = 1) and it was found that the catalytic activity/selectivity are less correlated with the average gold particle size, and more influenced by the nature of the additive. In addition to a structural role of the additives in stabilization of gold particles, some of the additives are active participants in the reaction process (CuO and FeO<sub>x</sub>). Concerning the reaction mechanism, FT-IR results indicated that the presence of Au increases the surface concentration of the imido-species [122, 123]. It was suggested that possible steps in the reaction mechanism include, at low temperature, a direct participation of OH groups and in the higher temperature range the formation of HNO as an intermediate may play a role. Finally, N<sub>2</sub>O and/or NO are formed at higher temperatures.

**2.4 NO and N<sub>2</sub>O reduction***NO reduction*

The environmental effects caused by NO<sub>x</sub> (NO + NO<sub>2</sub>) release from both mobile and stationary sources are well-known [124, 125] and have resulted in increasingly stringent legislation [126]. Whilst three-way catalysts (TWCs) have been successfully used for several decades with engines that operate close to stoichiometry, current technology cannot remove NO<sub>x</sub> at low temperatures or under lean conditions [127-129]. As a result there is a need to find catalytic systems able to operate under these reaction conditions. Hydrogen may offer a practical solution for reduction of NO to N<sub>2</sub> since it can be generated on-board from the fuel and is active at low temperatures.

The reduction of NO by hydrogen may proceed via the following reactions:



According to the reactions 2.5-2.7, other products than N<sub>2</sub>, i.e. N<sub>2</sub>O and NH<sub>3</sub>, may also be formed.

The NO/H<sub>2</sub> reaction has been well investigated over the past few decades using various catalytic systems [130-136]. It has long been recognized that Ru-based catalysts would be very attractive for this reaction, with a high selectivity to N<sub>2</sub> and only traces of NH<sub>3</sub> [130, 137-140]. The problem with Ru is, however, that under the reaction conditions running in automotive catalysis, a volatile and toxic ruthenium oxide is formed. Thus, catalysts based on other (noble) metals are required. In the 1970s a number of supported noble metals were screened for activity in NO reduction and it was found that both Pt and Pd are particularly active [138]. Furthermore, the authors also reported that N<sub>2</sub> and NH<sub>3</sub> were the main reaction products. The effect of various additives on the catalytic activity of both Pt and Pd has also been investigated and it was reported that MoO<sub>3</sub> and WO<sub>3</sub> increase the catalytic performance of Pt-based catalysts in NO reduction by CO [141-145]. An extensive study concerning the

effect of various additives on the catalytic performance of Pt-based catalysts in NO reduction reported that Pt/CoO<sub>x</sub>/SiO<sub>2</sub> catalysts show a superior N<sub>2</sub> selectivity, compared to the commercial PtRh/Al<sub>2</sub>O<sub>3</sub> catalysts, if a reductive pretreatment is applied [146]. However, the latter becomes more active following an oxidative pretreatment. The production of N<sub>2</sub>O could not be significantly diminished by addition of Co<sub>3</sub>O<sub>4</sub> or MnO<sub>2</sub> to Pt/SiO<sub>2</sub> [146]. More recently, other authors have reported that Na can be used to increase the NO conversion and N<sub>2</sub> selectivity over Pt-based catalysts [147, 148]. These authors proposed that the results could be explained by considering that since sodium is electropositive the chemisorption strength of an electron acceptor adsorbate (i.e. NO) would be increased. It was further speculated that the increased strength of the Pt-NO interaction caused a weakening of the N-O bond, leading to increased dissociation. Sodium addition has also been found to promote the reaction characteristics over catalysts based on Pt, Pd, and Rh using both CO and hydrocarbon reductants [149-152]. However, it should be emphasized that under realistic conditions Na is oxidized to Na<sup>+</sup> and, consequently, the Na additive loses its ability to donate electrons.

Also in the field of surface chemistry many papers reported on the interaction of NO with Pt surfaces. NO was found to dissociate differently on Pt, as a function of the surface structure. Most of the studies showed that Pt(111) and Pt(110) are inactive for NO dissociation [153, 154], whereas NO readily dissociates at room temperature on Pt(100), Pt(210), Pt(310), Pt(410) [155-158]. On polycrystalline Pt, NO dissociation occurs at temperatures above 400K, whereas at lower temperatures NO is molecularly adsorbed [159]. The molecularly adsorbed NO is an inhibitor for the NO-H<sub>2</sub> reaction. It should also be mentioned that over Pt-group metals, under certain reaction conditions, the reactions NO-H<sub>2</sub> and NO-CO may exhibit nonlinear phenomena, such as rate oscillations [160, 161].

Extensive reviews have been published by Nieuwenhuys concerning the reduction of NO by CO and H<sub>2</sub> over Group VIII metals [135, 136]. Most of the results point to dissociation of NO as an essential step. In order to obtain N<sub>2</sub> as the main product during NO reduction, the dissociation rate of NO should be rather high.

An efficient alternative to reduce the emission of NO in automotive catalysis is Rh [162], because the selectivity to N<sub>2</sub> of Rh-based catalysts was reported to be superior to Pt and Pd [162]. It was proposed that under reaction conditions, the concentration of N<sub>ads</sub> is higher on Rh, compared with Pt [163]. This is most probable because Rh is more active in NO dissociation than Pt. An interesting paper dealing with the effect of preadsorbed potassium on pattern formation observed during the NO+H<sub>2</sub> reaction on Rh(110) has been published by Imbihl *et al.* [164]. The reduction reaction has been studied in the 10<sup>-7</sup> mbar range using photoelectron emission microscopy (PEEM) and scanning photoelectron microscopy (SPEM) as spatially resolved methods. It has been shown that potassium is concentrated in the oxygen covered part of the pattern whereas the nitrogen covered parts are largely free of potassium. Most probably this is due to K diffusion on the Rh surface as a function of oxygen coverage.

Compounds such as nitrides have also been reported to catalyze the reduction of NO by H<sub>2</sub> [165]. It was found that NO dissociation proceeds over all three nitrides used as catalysts, viz. VN, Mo<sub>2</sub>N and W<sub>2</sub>N [165]. Moreover, the VN catalyst acts more as a reactant, rather

than as a catalyst, by capturing all oxygen generated during the NO dissociation. The deactivation of the catalysts has been explained on the basis of gradual oxidation of the nitrides.

Perovskite-like mixed oxides have also been used as catalysts in NO reduction by H<sub>2</sub> [166-168] or CO [169-171]. It was suggested that the catalytic performance of these materials depends on structural defects.

Regarding the reaction mechanism of NO reduction by hydrogen over Pt-group metals, it is generally accepted that at low temperatures NO is molecularly adsorbed on the catalytic surface. At low temperature the concentration of the vacant sites where NO would dissociate is rather low. For this reason the main reaction products are N<sub>2</sub>O and eventually N<sub>2</sub>. By increasing the temperature, NO desorption may proceed and the result is a decrease of NO<sub>ads</sub> and an increase of vacancy concentration. Then NO dissociation starts and the main product is most likely N<sub>2</sub>, formed by the reaction of two N<sub>ads</sub> fragments. The formation of NH<sub>3</sub> is favoured at higher temperatures and if more hydrogen is present.

#### *Gold as a catalyst for NO reduction by H<sub>2</sub>*

Some reports concerning the reduction of NO over Au-based catalysts exist in literature. Most of the papers are devoted to the reduction of NO by hydrocarbons, eventually in the presence of O<sub>2</sub> and H<sub>2</sub>O. Galvagno and Parravano have published the first study concerning the reduction of NO by H<sub>2</sub> as early as in 1978 [172]. The authors reported on the reduction of NO by hydrogen over Au/SiO<sub>2</sub>, Au/MgO and Au/Al<sub>2</sub>O<sub>3</sub> at 350°C. It was found that, depending on the support, more N<sub>2</sub> or more NH<sub>3</sub> is formed. The authors considered that the amount of N<sub>2</sub> strongly depends on the size of the gold particles, as well as on the Au-support interaction. Two reaction mechanisms were proposed, depending on the support identity. The associative path, which gives rise to more ammonia, was considered to be valid for Au/SiO<sub>2</sub>. The dissociative path, which results in more N<sub>2</sub>, would be valid for Au/Al<sub>2</sub>O<sub>3</sub> and Au/MgO. However, no direct evidence for NO adsorption and/or dissociation was presented.

Later, in an infrared spectroscopic study carried out on Au/SiO<sub>2</sub> and Au/MgO, Lee and Schwank [173] claimed that NO does not adsorb on either catalyst. Moreover, they detected N<sub>2</sub>O formation at very low temperature (338K), which is probably an intermediate, along with HNO, another possible reaction intermediate. Finally they assumed that the reduction of NO by hydrogen proceeds via associative adsorption of NO. A very weak or even absent NO adsorption was also reported by Dekkers on supported gold catalysts [174, 175].

In a recent paper Haruta *et al.* compared the catalytic performance of various noble metal-based catalysts in NO reduction by H<sub>2</sub> in the presence of H<sub>2</sub>O and O<sub>2</sub> and found the following sequence: Pt > Rh > Pd > Au, Ru > Ir [77]. The authors explained this order by the fact that Au exhibits an intermediate activity for both NO decomposition and H<sub>2</sub> + O<sub>2</sub> reactions [77]. The effect of various additives on the catalytic performance of Au/Al<sub>2</sub>O<sub>3</sub> and Au/SiO<sub>2</sub> in the NO-H<sub>2</sub> reaction was extensively studied by Dekkers [174, 175]. The results showed that the addition of CoO<sub>x</sub>, LaO<sub>x</sub> and CeO<sub>x</sub> results in an enhanced activity for Au/SiO<sub>2</sub>, but these additives were detrimental for the catalytic performance of Au/Al<sub>2</sub>O<sub>3</sub>. The results have been explained by assuming that MO<sub>x</sub> (M: Co, La, Ce) could block some of the active sites for NO



reduction. The presence of  $\text{LaO}_x$  and  $\text{CoO}_x$  has been reported to be beneficial concerning the selectivity to  $\text{N}_2$ , at the expense of  $\text{NH}_3$  production [174].

Reduction of  $\text{NO}$  by  $\text{H}_2$  was also studied over  $\text{Au/zeolites}$ . It was found that over  $\text{Au/NaY}$  and  $\text{Au/ZSM-5}$  catalysts, the presence of  $\text{O}_2$  is beneficial for the formation of  $\text{N}_2$  and suppression of  $\text{NH}_3$  [176]. The authors explained these results by assuming that  $\text{O}_2$  in the gas stream suppresses the dissociation of  $\text{NO}$  on  $\text{Au/NaY}$ , while promoting the formation of oxygenated intermediates such as  $\text{NO}_2$  and  $\text{N}_2\text{O}_4$ , which are readily and selectively reduced by hydrogen to  $\text{N}_2$ .

As already mentioned, there are also reports concerning the reduction of  $\text{NO}$  by hydrocarbons to  $\text{N}_2$ , even in excess  $\text{O}_2$  [77, 177]. According to these publications, there is a strong relationship between the catalytic performance of the  $\text{Au}$ -based catalysts and the identity of the metal oxide used as support, with  $\text{ZnO}$  being a good choice. The same authors claimed that a mechanical mixture of  $\text{Au/Al}_2\text{O}_3$  and  $\text{MnO}_x$  results in an increased activity in  $\text{NO}$  reduction by hydrocarbons because the latter is particularly active in  $\text{NO}$  oxidation to  $\text{NO}_2$ , being a crucial step in the reaction [76].

There are a few reports based on surface science studies relevant for understanding  $\text{NO}$  reduction on  $\text{Au}$  surfaces. McClure *et al.* reported that  $\text{NO}$  adsorption on  $\text{Au}(111)$  is very weak or even absent [178]. It was also reported that nitric oxide decomposition/adsorption does not proceed on gold-based catalysts [174, 175]. On the other hand, recent theoretical studies have shown that  $\text{NO}$  can adsorb on cationic, anionic and neutral  $\text{Au}_n$  clusters ( $n = 1-6$ ) [179], or on  $\text{Au}(310)$  [180]. It was also shown that  $\text{NO}$  induced lifting of the surface reconstruction of  $\text{Au}(100)$  [181].

Regarding the intermediates that are likely to be formed during  $\text{NO}$  reduction,  $\text{HNO}$  [173] and  $\text{NO}_2$  were suggested [176]. However, there is not a general consensus regarding this reaction. Very recently, it was found that during  $\text{NO}$  adsorption at 300 K on  $\text{Au}$  3D hemispherical crystals ("field emitter tips"),  $(\text{NO})_2$  and  $\text{N}_2\text{O}$  are formed [182]. The dimer  $(\text{NO})_2$  was proposed as the intermediate in  $\text{N}_2\text{O}$  formation. However, other authors claim that dimer formation is unlikely on  $\text{Au}(310)$  [180]. These authors reported that on the  $\text{Au}(310)$  surface  $\text{NO}$  decomposes even at 80 K and forms  $\text{N}_2\text{O}_{\text{ads}}$  and  $\text{O}_{\text{ads}}$ .

### ***N<sub>2</sub>O reduction***

$\text{N}_2\text{O}$  coexists with  $\text{NO}_x$  in flue gases of many industrial processes [125, 183, 184]. Although  $\text{N}_2\text{O}$  is not an abundant component of exhaust gases, it is a known intermediate of  $\text{NO}$  reduction, being produced as a by-product in some  $\text{NO}_x$  abatement processes [125]. The most widespread technology for the abatement of nitrogen oxide emissions from stationary combustion sources is its selective catalytic reduction with ammonia ( $\text{NH}_3\text{-SCR}$ ) [125, 185]. However, this method presents several drawbacks such as the production of  $\text{N}_2\text{O}$  as a by-product and the use of an expensive and polluting reductant [185]. The selective catalytic reduction with hydrocarbons ( $\text{HC-SCR}$ ) is a promising technology for the abatement of both  $\text{NO}_x$  [125, 185-187] and  $\text{N}_2\text{O}$  [125, 188, 189]. Other reducing agents that can be used include  $\text{CO}$  and  $\text{H}_2$  [185]. An extensive review concerning  $\text{N}_2\text{O}$  decomposition on supported metal and oxides can be found in [190].

N<sub>2</sub>O reduction by H<sub>2</sub> has been studied in detail on Rh catalysts [136]. McCabe and Wong studied the reduction of N<sub>2</sub>O by CO on Rh/Al<sub>2</sub>O<sub>3</sub> and the authors proposed a reaction mechanism that involves the dissociative adsorption of N<sub>2</sub>O [191]. They suggested that the observed lower activity for the CO/N<sub>2</sub>O reaction compared to the CO/O<sub>2</sub> or CO/NO reactions is caused by slower dissociative adsorption of N<sub>2</sub>O relative to O<sub>2</sub> and NO. N<sub>2</sub>O dissociation might be the rate determining step, as was also concluded by other authors [192].

N<sub>2</sub>O reduction on Ni/K or Pt/K catalysts supported on carbon revealed a considerable synergy between Ni/Pt and K [193]. Systems comprising Fe-FMI have also been studied extensively [194-196]. More recently, a study of N<sub>2</sub>O reduction and decomposition on Ni-Pt/SiO<sub>2</sub> catalysts showed that the bimetallic catalyst Ni-Pt is more active than the monocomponent catalysts, viz. Ni/SiO<sub>2</sub> and Pt/SiO<sub>2</sub> [197].

Investigations concerning adsorption and decomposition of N<sub>2</sub>O on well defined fcc surfaces have shown that Pt(111) does not dissociate N<sub>2</sub>O [198] whereas Ni(100) [199], Ni(110) [200], polycrystalline surfaces of Pt [201] and supported Pt [202] are able to dissociate N<sub>2</sub>O. On systems such as Ir (110) [203], Pd(110) [204], or Rh supported on zirconia-based catalysts [205], oscillatory behaviour was found for N<sub>2</sub>O reduction.

#### *Gold as a catalyst for N<sub>2</sub>O reduction*

There are not many papers dealing with N<sub>2</sub>O decomposition and reduction over gold based-catalysts. Early results showed that gold wires [206] and films [207] were able to decompose N<sub>2</sub>O to N<sub>2</sub> and O<sub>2</sub>. More recently, Au/Co<sub>3</sub>O<sub>4</sub> has been reported to be active for N<sub>2</sub>O decomposition at relatively low temperature (523 K) in the presence of 10 vol% O<sub>2</sub> and 5 vol% H<sub>2</sub>O [208].

Au/TiO<sub>2</sub> and Au/CoO<sub>x</sub>/TiO<sub>2</sub> were reported to be promising catalysts for CO/N<sub>2</sub>O reaction [209]. Dekkers found that Au/Al<sub>2</sub>O<sub>3</sub> and Au/TiO<sub>2</sub> were also highly active in N<sub>2</sub>O reduction by H<sub>2</sub> at low temperatures and that the decomposition of N<sub>2</sub>O in the absence of H<sub>2</sub> did not proceed [174]. It was proposed that the mechanism of N<sub>2</sub>O reduction might include N<sub>2</sub>O decomposition, possibly assisted by H<sub>2</sub> or CO. More recently, the effect of various additives on the catalytic activity of Au/Al<sub>2</sub>O<sub>3</sub> has been reported and large synergistic effects have been found by combining two different additives (i.e. Li<sub>2</sub>O and CeO<sub>x</sub>) [210].

## **2.5 CO oxidation in the absence and presence (PROX) of hydrogen**

### *CO oxidation*

The catalytic oxidation of CO with O<sub>2</sub> has been investigated extensively and intensively in heterogeneous catalysis [211]. Because of the simplicity that the only product is CO<sub>2</sub>, which is gaseous and it hardly sticks on metal surfaces, CO oxidation is now rather well understood at the atomic scale as the result of the application of a variety of surface science methods using single crystal metal surfaces [212, 213].

Figure 2.1 shows schematically the interaction of CO with a metal surface. The CO bonding to the metal surface is visualized by the so-called Blyholder model [214]. An empty

metal orbital of proper symmetry overlaps with the occupied  $5\sigma$  orbitals of CO and a  $\sigma$  bond is formed. In that situation CO donates electrons to the metal.

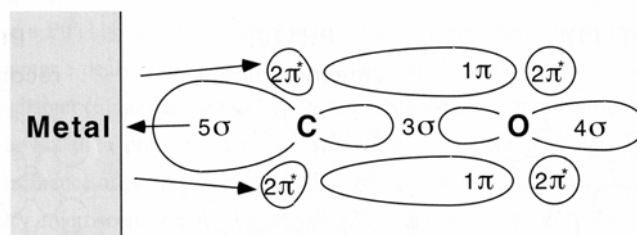


**Figure 2.1:** Blyholder model of CO bonding on transition metals.

In addition, back-donation, from the metal to CO, by overlap of the antibonding  $2\pi^*$  orbitals of CO with partly filled  $d$  orbitals with the right symmetry is important for the metal-CO bond. The presence of electrons in the  $2\pi^*$  orbitals of CO causes C-O bond weakening.

Whereas during CO interaction with Pt and Pd, both direct and back-donation are important, for Au it has been reported that the bond with CO is almost entirely due to electron donation from CO to Au [215].

A lot of materials have been reported to be active in CO oxidation at low temperature and this section briefly reviews *some* of the aspects related to CO oxidation. For example, it was reported that transition metal oxides are more active at low temperatures than supported noble metals [216]. However, a serious constraint is that base metal oxide catalysts are heavily deactivated by moisture [217]. Over the Pt-group metals supported on  $\text{Al}_2\text{O}_3$  and  $\text{SiO}_2$ , CO oxidation takes place only at temperatures above  $150^\circ\text{C}$ , because CO is relatively strongly adsorbed, blocking the adsorption of  $\text{O}_2$ . The advantage of Pt-group metal catalysts is, however, that the moisture enhances their catalytic activity, which can even be further increased by using easily reducible metal oxides as supports [218].

Good catalytic results have been reported for Pt-group metals deposited on  $\text{SnO}_2$ ,  $\text{TiO}_2$  and  $\text{CeO}_2$  [219-222]. These metal oxides make Pt-group metals active in CO oxidation even at room temperature. Especially  $\text{SnO}_2$  was reported as a good carrier for Pt and Pd and these catalysts are commercially used for sealed  $\text{CO}_2$  lasers and semiconductor-type gas leak detectors [223-225].

The oxidation of CO was found to depend on several factors such as partial pressure of CO,  $\text{CO}/\text{O}_2$  molar ratio, and catalyst temperature. Under CO-rich reaction conditions it was found that the reactivity decreases in the following order [216]:



Under excess  $\text{O}_2$ , metal oxide layers that are less reactive are formed on the metal surface and the catalytic activity order changes, compared to CO-rich conditions. In particular Ru is deactivated appreciably with time-on-stream [216].

It was also reported that Ru, Rh, Pd, Ir and Pt supported on Al<sub>2</sub>O<sub>3</sub> or SiO<sub>2</sub> give almost identical turnover frequency (TOF), specific rate of reaction per surface exposed atoms [216]. However, the TOF for Pt/Al<sub>2</sub>O<sub>3</sub> increases with a decrease in diameter of Pt particles at 245<sup>0</sup>C, while it remains unchanged at 160<sup>0</sup>C [226], indicating that the structure sensitivity of CO oxidation depends on the reaction temperature. The structure-insensitive character of CO oxidation over Pt group metals surfaces was also reported in [227]. The results showed that the CO oxidation rate is similar for different planes of single crystals of the Pt group metals. Theoretical calculations showed that CO oxidation is strongly coverage-sensitive on Pt(111), whereas it is less sensitive on Pt(100) [228].

Other catalytic systems have also been tested in CO oxidation: Cu<sub>2</sub>Ag<sub>2</sub>O<sub>3</sub> [229], Co<sub>3</sub>O<sub>4</sub> [230], CuO/CeO<sub>2</sub> and Cu/CeO<sub>2</sub> [231, 232], perovskite-like materials [23], and Ag-based catalyst [233]. However, at low temperatures the activity of Au exceeds the activity of catalysts based on Pt group metals by a factor of about 5 [234]. Therefore, recently a large number of the papers dealing with CO oxidation has been devoted to gold-based catalysts.

#### *Gold as a catalyst in CO oxidation*

Because of its well-known nobility, gold is inactive in its massive form. However, gold nano-particles exhibit high catalytic activity even at sub-ambient temperatures [235]. It was shown for the first time that if prepared according to specific recipes, a surprisingly high activity is found [235]. Since then a lot of research has been carried out and it is generally (but not universally [236]) accepted that the property of catalytically active gold is related to the presence of discrete, nano-scale gold particles in a very narrow and particular size range, either 2 to 3 nm [237, 238], or 3 to 5 nm [234, 239].

Since there are a lot of well-written and documented reviews on this topic [33, 237, 239-246], and because many aspects concerning catalysis by Au were already briefly discussed in *Chapter 1*, such as *the influence of the preparation method*, (including *the pretreatment*), *the particle size effect*, *the role of the support/additive*, *the nature of the active sites*, this section will only mention a few aspects concerning mechanistic aspects.

Both CO and O<sub>2</sub> have a negligible affinity for bulk gold surfaces [238, 239], at least for temperatures above 150 K [236], thereby explaining the absence of catalytic activity for this reaction on bulk gold. However, very small nano-particles are certainly different, and direct evidence that both oxygen and CO can adsorb on neutral [247] or negatively-charged [248] gold nano-particles is available. Therefore, at least three mechanisms have been postulated: (i) CO and O<sub>2</sub> are both adsorbed onto the catalyst where they subsequently react (via a Langmuir-Hinshelwood mechanism) [249], (ii) only one of the reacting species adsorbs, with the other coming into contact with it from the gas phase (via a Eley-Rideal reaction pathway) [249], (iii) on certain supported Au catalysts, the reaction mechanism involves the direct participation of the support lattice oxygen, which reacts with adsorbed CO [36, 250-252].

The apparent activation energy for CO oxidation over gold-based catalysts has been reported to vary between 20 and 40 kJ mol<sup>-1</sup> below 300 K, whereas a value close to zero was reported at temperatures above 300 K [242]. On the other hand, the Pt- group metals, which are more active than Au-based catalysts in CO oxidation but only at temperatures above 500

K, display a value of  $E_a$  ranging from 50 kJ mol<sup>-1</sup> to 170 kJ mol<sup>-1</sup> [242]. It was further reported by Haruta that the rate of CO oxidation over Au/TiO<sub>2</sub>, Au/Fe<sub>2</sub>O<sub>3</sub> and Au/Co<sub>3</sub>O<sub>4</sub> is independent of the concentration of CO and slightly dependent on the concentration of O<sub>2</sub> (of the order of 0 to 0.25) [253]. This is, somehow, in contradiction with the general belief that the adsorption of oxygen, either dissociatively or molecularly, is the rate determining step due to the extreme difficulty of oxygen adsorption on Au [246]. The results of Haruta suggested that CO and O<sub>2</sub> are adsorbed on the catalyst surface nearly to saturation and that the reaction between CO and O<sub>2</sub> is the rate-determining step [242]. However, the catalytic activity data of various Au-based catalysts, as summarized by Kung *et al.* [254] revealed that for the same type of catalyst, viz. Au/Al<sub>2</sub>O<sub>3</sub>, more oxygen in the gas stream produced a significant increase in the reaction rate, compared to the value obtained under stoichiometric conditions. More recently, using isotopic transient analysis, it was found that on Au/Al<sub>2</sub>O<sub>3</sub>, a CO coverage of only 4.9 % is attained, in spite of the very high Au dispersion of 80 % [255]. This low coverage corresponds to a CO concentration far below the saturation limit and may also explain why it is so difficult to identify the active sites. For this catalyst the apparent activation energy was estimated to be as low as 10 kJ mol<sup>-1</sup>.

A reaction mechanism which brings together the role of both metallic and ionic Au, as well as OH groups and the periphery, was proposed by Bond and Thompson [240] and Kung and co-workers [254, 256]. According to Bond and Thompson, the (Au<sup>0</sup>...CO) ensemble is attacked by an OH group either on a support cation or on a peripheral Au<sup>3+</sup>, forming a carboxylate group attached to the latter. This is in turn attacked by a superoxide ion, which must be responsible for oxidizing two carboxylate ions. In the next step the hydroxyl group may again be actively involved in the catalytic cycle. The role of Au<sup>3+</sup> is very important because it acts as a “chemical glue” which binds the Au<sup>0</sup> to the support. In this mechanistic view, the oxygen molecule is adsorbed to an anion vacancy. However, if the support has no vacancies, the oxygen molecule would simply be weakly bound to a support cation. In the absence of OH groups, the reaction would proceed between the chemisorbed CO and an oxygen molecule or a superoxide ion. These alternatives may be valid as a function of the identity of the catalyst [240].

The mechanism proposed by Kung and co-workers [254, 256] is similar to the above-described mechanism. However, their mechanism considers that the ionic form of Au is Au<sup>+</sup> and that the deactivation of the catalyst is due to the transformation of the bicarbonate intermediate into a relatively inactive carbonate.

Haruta suggested another reaction mechanism, valid for Au/TiO<sub>2</sub>, which takes into account the temperature regime of the reaction [241]. According to this mechanism, at very low temperatures (below 200 K), the only active sites are the steps, kinks, edges and corners on the Au particles. Neither the support nor the perimeter interface between Au and TiO<sub>2</sub> participate because they are covered with carbonate species produced by surface reaction between CO and TiO<sub>2</sub>. At temperatures between 200 and 300 K, the reaction proceeds at the perimeter interface. By increasing the temperature, the amount of carbonate decreases. The reaction continues to proceed at the perimeter interface with an activation energy of nearly zero as the temperature is increased further.

All the published data agree that CO is most probably adsorbed on the Au particles, probably on the edge or step sites [241, 257]. The adsorption of oxygen is not clear, although there are indications that either the support or the interface is involved. Most of the scientists agree that the Au-support interface is the place where the reaction proceeds. There is no doubt that the size of the Au particles is important, particularly because the size is associated with the concentration of highly uncoordinated atoms. Some particular shapes, viz. hemispherical, are believed to be more active than the spherical one [235]. The possible roles of ionic gold and water remain to be clarified.

### CO oxidation in the presence of hydrogen (PROX)

Application of fuel cell powered systems for transportation recently received increasing attention because of their theoretical high fuel efficiency and low environmental impact [258]. Among the numerous types of fuel cells that have already been developed, the proton exchange membrane fuel cell (PEMFC) is one of the most promising ones. However, trace amounts of CO in the H<sub>2</sub>-PEMFC poison the efficiency of the fuel cell Pt catalyst. Several approaches are currently applied: CO preferential oxidation, catalytic methanation, Pd-membrane separation. Among these, the preferential oxidation (PROX) is the least expensive method to reduce CO to the desired level without excessive hydrogen consumption [259, 260].

PROX catalysts need to be active and selective; the catalyst should oxidize 0.5-1 % CO to less than 50 ppm without oxidizing a large amount of hydrogen at the temperature of the fuel cell (~ 80°C).



The amount of oxygen with respect to the minimum amount of oxygen required for CO oxidation to CO<sub>2</sub> in the absence of side reactions is characterized by the process parameter  $\lambda$  (equation 2.11). Therefore, the value of  $\lambda$  in the PROX process should be as close as possible to 1 (i.e. stoichiometric), not to oxidize excessive amounts of hydrogen.

$$\lambda = \frac{C_{\text{O}_2,i}}{2 \cdot C_{\text{CO},i}} \quad (2.11)$$

The unwanted reaction (2.10) leads to a loss in fuel efficiency.

Depending on the nature of the catalyst, the water produced through hydrogen oxidation may affect the catalyst's activity. The lower the selectivity of the process, the higher the required ratio O<sub>2</sub>/CO is in order to completely oxidize CO to CO<sub>2</sub>. In addition, secondary reactions such as reverse water gas-shift (WGS) and methanation of CO can occur, depending on the temperature, O<sub>2</sub>/CO ratio and contact time. Based on the high activity required to remove CO while maintaining a high CO oxidation selectivity, catalyst formulations used for

PROX involve, in general, a high Pt group metal (PGM) loading and high surface area supports, and are operated at temperatures between 70-200<sup>0</sup>C.

Oh and Sinkevitch studied a large variety of materials for the PROX reaction, among which Pt, Pd, Rh, and Ru on alumina support, as well as other possible oxidation catalysts, such as Co/Cu, Ni/Co/Fe, Ag, Cr, Fe and Mn [261]. The reaction conditions consisted of SV= 20,000 h<sup>-1</sup> and a very diluted CO and H<sub>2</sub> feed. Improved selectivities were found for Ru and Rh only at very low H<sub>2</sub> concentrations compared to Pt/Al<sub>2</sub>O<sub>3</sub>. An optimum reaction temperature was 100<sup>0</sup>C for Rh and Ru [261] and around 170<sup>0</sup>C for Pt [261, 262]. Co/Cu/Al<sub>2</sub>O<sub>3</sub> and Ni/Cu/Al<sub>2</sub>O<sub>3</sub> were active in the reaction only above 250<sup>0</sup>C, with a 40-50 % selectivity at  $\lambda = 2$ .

The most extensively studied system so far remains the Pt-based catalysts [263-265]. It was reported that at low temperatures and a stoichiometric ratio O<sub>2</sub>/CO, the CO conversion was improved for Ce-promoted Pt/Al<sub>2</sub>O<sub>3</sub> [266]. No improvement in conversion was observed in the presence of Ce at high temperature. The combination Ce-ZrO<sub>2</sub> was reported to act as an efficient promoter for Pt/Al<sub>2</sub>O<sub>3</sub>, both in CO oxidation and selectivity to CO<sub>2</sub>, under stoichiometric [267], or excess O<sub>2</sub> [258]. The high catalytic activity exhibited by the promoted Pt/Al<sub>2</sub>O<sub>3</sub> was explained on the basis of the high oxygen storage capacity of Ce-ZrO<sub>2</sub> and the nano-crystalline nature of cubic Ce<sub>0.8</sub>Zr<sub>0.2</sub>O<sub>2</sub> [267]. Among various base metals used as additives for Pt-based catalysts, the combination Pt-Co turned out to be the most active catalyst [268] for PROX. Also the beneficial effect of Fe on the catalytic performance of Pt/Al<sub>2</sub>O<sub>3</sub> was reported [263, 269]. A 6 wt-% Pt /zeolite showed superior selectivity, compared to Pt/Al<sub>2</sub>O<sub>3</sub> [264]. Depending on the temperature and water content in the feed, water adsorption may, however, be an issue for these materials [264]. Other formulations have also been tested and include Pt-Sn alloy, Pt, Ru and Rh containing Al<sub>2</sub>O<sub>3</sub>-SiO<sub>2</sub> microporous membranes [270].

A short communication presented the beneficial effect of K on the catalytic performance of Rh/SiO<sub>2</sub> and Rh/USY [271]. It was suggested that the role of K is different on SiO<sub>2</sub> and USY. In the case of Rh/SiO<sub>2</sub> it was proposed that K addition enhances the Rh dispersion, whereas in the case of Rh/USY, the TOF increased. There are also a few reports concerning the use of Ag as a catalyst for PROX reaction [272, 273]. The results were explained on the basis of subsurface oxygen, assumed to play an important role [272]. Moreover, by means of FTIR (Fourier Transform Infrared Spectroscopy), these authors proposed that over Ag/SiO<sub>2</sub> PROX proceeds via a non-competitive Langmuir-Hinshelwood mechanism, which occurs in the high rate branch on a surface covered with CO below saturation [273]. CuO-CeO<sub>2</sub> mixed oxides have also been reported as promising candidates for PROX [274]. In a comparative study of Pt/Al<sub>2</sub>O<sub>3</sub>, Au/Fe<sub>2</sub>O<sub>3</sub> and CuO-CeO<sub>2</sub>, the Au catalyst was the most active at low temperature, while the selectivity of CuO-CeO<sub>2</sub> was remarkably higher than that of both Au and Pt catalysts. Pt/Al<sub>2</sub>O<sub>3</sub> was the most resistant towards H<sub>2</sub>O and CO<sub>2</sub> in the feed.

The kinetics of CO oxidation on Pt/Al<sub>2</sub>O<sub>3</sub> under integral and differential conditions have been investigated by Kahlich *et al.* [262]. It was reported that on 0.5 % Pt/Al<sub>2</sub>O<sub>3</sub>, the presence of hydrogen actually increases the rate of CO oxidation. Trying to find a correlation between CO surface coverage and selectivity, the authors proposed a mechanism similar to that of CO

oxidation in the absence of hydrogen, “low rate branch” vs. “high rate branch” [262]. According to this mechanism, the decrease in CO conversion at temperatures higher than 250°C is a consequence of the loss in the selectivity due to the decrease in the “protective” CO coverage. In a later study, the same group confirmed that the reaction kinetics depend on the steady-state coverage of the metal with CO in the presence of H<sub>2</sub>, and were able to explain the differences between Pt/Al<sub>2</sub>O<sub>3</sub> and Au/Fe<sub>2</sub>O<sub>3</sub> catalysts [275]. The decrease in the selectivity of Au/Fe<sub>2</sub>O<sub>3</sub> with temperature compared to that of Pt/Al<sub>2</sub>O<sub>3</sub> was interpreted on the basis of differences in CO surface coverage as a function of temperature [275]. This behaviour explains the larger range of operation temperature for Pt catalysts in multistage PROX reactors, whereas Au remains attractive for low temperature operation. Mechanistic studies using *in-situ* DRIFTS (Diffuse Reflectance Infrared Fourier Transform Spectroscopy) on Pt/Al<sub>2</sub>O<sub>3</sub> indicate the existence of formate surface species. Its formation is enhanced by hydroxylated surfaces [265]. The results obtained for a sol-gel Pt/Al<sub>2</sub>O<sub>3</sub> having 1-2 % metal incorporated in the oxide lattice indicated that for this type of catalyst, water has a beneficial effect [276].

#### *Gold as a catalyst for PROX reaction*

As already mentioned, a number of laboratories reported Au as a potential catalyst for PROX. This is mainly because Au-based catalysts are intrinsically more active for CO oxidation than for oxidation of hydrogen and, also, because the catalytic activity of Au-based catalysts is enhanced by water and almost insensitive to CO<sub>2</sub> [36, 251, 277-282].

DFT calculations performed on Au(111), Cu(111) and Pt(111) have demonstrated that the barrier for CO oxidation on Au is 0.18 eV; the corresponding barrier for OH formation is much higher, 0.9 eV (at low temperatures) [283]. Similarly, Cu(111) shows a lower barrier for CO oxidation (0.82 eV) than for H<sub>2</sub> oxidation (1.28 eV), whereas Pt(111) shows a higher barrier for CO oxidation (0.96 eV) than for H<sub>2</sub> oxidation (0.83 eV). These calculations explain why Au and Cu are more selective than Pt for PROX at low temperatures and are consistent with experimental data [274].

In a research note Haruta and co-workers showed that Au/MnO<sub>x</sub> converts more than 95% CO at temperatures between 323 and 353 K under H<sub>2</sub>-rich conditions and O<sub>2</sub>/CO = 1 [284]. Moreover, the authors reported a rather good stability of the catalyst with time on stream and a good resistivity to both CO<sub>2</sub> and H<sub>2</sub>O. Bethke and Kung found improved selectivity of Au/Al<sub>2</sub>O<sub>3</sub> when Mg citrate is added during preparation and rationalized the results based on increased Au dispersion [278]. Grisel *et al.* further ascribed to the effect of MgO and MnO<sub>x</sub> through the stabilization of Au particles, and the supply of active oxygen, respectively [36, 251]. Schumacher and co-workers studied the kinetics of the PROX process and the reaction mechanism over Au/TiO<sub>2</sub> [282] and found that H<sub>2</sub> affects the CO oxidation, most probably by competing hydrogen adsorption on the Au nanoparticles. Formate and carbonate species formed during the reaction represent side products/inhibitors, but they do not take part in the reaction as reaction intermediates. A H<sub>2</sub>-rich atmosphere inhibits the formation of formates. A variety of Au-based catalysts such as Au/Co<sub>3</sub>O<sub>4</sub>, Au/SnO<sub>2</sub>, Au/Al<sub>2</sub>O<sub>3</sub>, Au/Fe<sub>2</sub>O<sub>3</sub>, Au/CeO<sub>2</sub>, Au/NiO<sub>x</sub>, Au/MnO<sub>x</sub>, Au/Mg(OH)<sub>2</sub> and Au/TiO<sub>2</sub> has been studied by the same group and the



results showed that the presence of hydrogen does not have an important effect on the oxidation of CO [285]. Moreover, the authors considered that an additional reaction path is created if a reducible support is present, by supplying oxygen, and that deactivation is caused by build-up of surface carbonate species. The most active samples comprise CeO<sub>2</sub>, TiO<sub>2</sub> or Fe<sub>2</sub>O<sub>3</sub> as supports. Other published results are in line with these data, i.e. that Au/CeO<sub>2</sub> [286] and Au/FeO<sub>x</sub>/C [287] are promising catalysts for the PROX process.

Recently a paper presented the performance of model gold-based catalysts, viz. Au/Al<sub>2</sub>O<sub>3</sub>, Au/ZrO<sub>2</sub> and Au/TiO<sub>2</sub> [288] in PROX. Under H<sub>2</sub>-rich conditions and  $\lambda = 2$ , a boost in CO conversion was reported, and the extent of this boost depends on the support identity. The reactivity order found for CO oxidation (Au/Al<sub>2</sub>O<sub>3</sub> << Au/ZrO<sub>2</sub> < Au/TiO<sub>2</sub>) was changed after adding H<sub>2</sub> to the gas feed. A mechanism was proposed, which includes H<sub>2</sub> dissociation on the gold particles and reaction between an adsorbed CO molecule and an adsorbed H-O-O species (or any H<sub>x</sub>O<sub>y</sub> species).

## 2.6 References

- [1] R. Prasad, L. A. Kennedy, E. Ruckenstein, *Catal. Rev. Sci. Eng.* 26 (1984) 1.
- [2] M. F. M. Zwinkels, S. G. Jaras, P. G. Menon, T. A. Griffin, *Catal. Rev. Sci. Eng.* 35 (1993) 319.
- [3] R. A. Dalla Betta, *Catal. Today* 35 (1997) 129.
- [4] M. Alifanti, J. Kirchnerova, B. Delmon, D. Klvana, *Appl. Catal. A* 262 (2004) 167.
- [5] R. Burch, D. J. Crittle, M. J. Hayes, *Catal. Today* 47 (1999) 229.
- [6] C. F. Cullis, D. E. Keene, D. Trimm, *Trans. Faraday Soc.* 67 (1971) 864.
- [7] T. R. Baldwin, R. Burch, *Appl. Catal.* 66 (1990) 337.
- [8] F. H. Ribeiro, M. Chow, R. A. Dalla Betta, *J. Catal.* 146 (1994) 537.
- [9] C. F. Cullis, D. E. Keene, D. Trimm, *J. Catal.* 19 (1970) 378.
- [10] R. B. Anderson, K. C. Stein, J. J. Feenan, L. J. E. Hofer, *Ind. Eng. Chem.* 53 (1961) 809.
- [11] S. H. Oh, P. J. Mitchell, R. M. Siewert, *J. Catal.* 132 (1991) 287.
- [12] Y.-F. Yao, *Ind. Eng. Chem. Prod. Res. Dev.* 19 (1980) 293.
- [13] D. Trimm, C. W. Lam, *Chem. Eng. Sci.* 35 (1980) 1405.
- [14] H. Widjaja, K. Sekizawa, K. Eguchi, *Chem. Lett.* (1998) 481.
- [15] H. Widjaja, K. Sekizawa, K. Eguchi, *Bull. Chem. Soc. Jpn.* 72 (1999) 313.
- [16] T. Ishihara, H. Shigematsu, Y. Abe, Y. Takita, *Chem. Lett.* (1993) 407.
- [17] L. Xiao, K. Sun, Y. Yang, X. Xu, *Catal. Lett.* 95 (2004) 151.
- [18] J. Lee, D. Trimm, *Fuel Process Technol.* 42 (1995) 339.
- [19] P. Gelin, M. Primet, *Appl. Catal. B* 39 (2002) 1.
- [20] J. E. Germain, *Catalytic Conversion of Hydrocarbons*, Academic Press 1967.
- [21] G. K. Boreskov, *Catalysis, Science and Technology*, J.R. Anderson and M. Boudart Editors, Vol. 3, Springer Verlag, New York 1982, p. 39.
- [22] E. Garbowski, M. Guenin, M. C. Marion, M. Primet, *Appl. Catal.* 64 (1990) 209.
- [23] S. Royer, F. Berube, S. Kaliaguine, *Appl. Catal. A* 282 (2005) 273.
- [24] N. Yi, Y. Cao, Y. Su, W. L. Dai, H. Y. He, K. N. Fan, *J. Catal.* 230 (2005) 249.
- [25] V. V. Kharton, A. A. Yaremchenko, A. A. Valente, V. A. Sobyenin, V. D. Belyaev, G. L. Semin, S. A. Veniaminov, E. V. Tsipis, A. L. Shaula, J. R. Frade, J. Rocha, *Solid State Ionics* 176 (2005) 781.
- [26] S. Pengpanich, V. Meeyoo, T. Rirksomboon, *J. Chem. Eng. Japan* 38 (2005) 49.
- [27] S. Zhao, R. J. Gorte, *Appl. Catal. A* 277 (2004) 129.
- [28] G. Busca, E. Finocchio, G. Ramis, G. Ricchiardi, *Catal. Today* 32 (1996) 133.
- [29] V. R. Choudhary, V. H. Rane, *J. Catal.* 130 (1991) 411.
- [30] G. Busca, M. Daturi, E. Finocchio, V. Lorenzelli, G. Ramis, R. J. Wiley, *Catal. Today* 33 (1997) 239.
- [31] R. D. Waters, J. J. Weimer, J. E. Smith, *Catal. Lett.* 30 (1995) 181.
- [32] M. Haruta, *Now and Future* 7 (1992) 13.
- [33] G. C. Bond, D. T. Thompson, *Catal. Rev. Sci. Eng.* 41 (1999) 319.
- [34] R. J. H. Grisel, P. J. Kooyman, B. E. Nieuwenhuys, *J. Catal.* 191 (2000) 430.
- [35] R. J. H. Grisel, B. E. Nieuwenhuys, *Catal. Today* 64 (2001) 69.

- [36] R. J. H. Grisel, *Supported gold catalysts for environmental applications*, PhD thesis, Leiden University (2002).
- [37] E. Finocchio, R. J. Willey, G. Busca, V. Lorenzelli, *J. Chem. Soc.-Farad. Trans.* 93 (1997) 175.
- [38] T. V. Choudhary, S. Banerjee, V. R. Choudhary, *Appl. Catal. A* 234 (2002) 1.
- [39] R. F. Hicks, H. H. Qi, M. L. Young, R. G. Lee, *J. Catal.* 122 (1990) 280.
- [40] T. Garcia, B. Solsona, D. M. Murphy, K. L. Antcliff, S. H. Taylor, *J. Catal.* 229 (2005) 1.
- [41] I. Yuranov, L. Kiwi-Minsker, A. Renken, *Appl. Catal. B* 43 (2003) 217.
- [42] L. Kiwi-Minsker, I. Yuranov, E. Slavinskaia, V. Zaikovskii, A. Renken, *Catal. Today* 59 (2000) 61.
- [43] T. Maillot, C. Solleau, J. Barbier, D. Duprez, *Appl. Catal. B* 14 (1997) 85.
- [44] T. Maillot, J. Barbier, D. Duprez, *Appl. Catal. B* 9 (1996) 251.
- [45] T. Maillot, J. Barbier, P. Gelin, H. Praliaud, D. Duprez, *J. Catal.* 202 (2001) 367.
- [46] N. A. Merino, B. P. Barbero, P. Grange, L. E. Cadus, *J. Catal.* 231 (2005) 232.
- [47] Y. Yazawa, H. Yoshida, S. Komai, T. Hattori, *Appl. Catal. A* 233 (2002) 113.
- [48] Y. Yazawa, N. Kagi, S. Komai, A. Satsuma, Y. Murakami, T. Hattori, *Catal. Lett.* 72 (2001) 157.
- [49] Y. Yazawa, H. Yoshida, T. Hattori, *Appl. Catal. A* 237 (2002) 139.
- [50] C. P. Hubbard, K. Otto, H. S. Gandhi, K. Y. S. Ng, *J. Catal.* 144 (1993) 484.
- [51] T. F. Garetto, E. Rincon, C. R. Apesteguia, *Appl. Catal. B* 48 (2004) 167.
- [52] R. Burch, E. Halpin, M. Hayes, K. Ruth, J. A. Sullivan, *Appl. Catal. B* 19 (1998) 199.
- [53] A. F. Lee, K. Wilson, R. M. Lambert, C. P. Hubbard, R. G. Hurley, R. W. McCabe, H. S. Gandhi, *J. Catal.* 184 (1999) 491.
- [54] A. Hinz, M. Skoglundh, E. Fridell, A. Andersson, *J. Catal.* 201 (2001) 247.
- [55] H. C. Wu, L. C. Liu, S. M. Yang, *Appl. Catal. A* 211 (2001) 159.
- [56] K. Ruth, M. Hayes, R. Burch, S. Tsubota, M. Haruta, *Appl. Catal. B* 24 (2000) L133.
- [57] P. Bera, M. S. Hegde, *Catal. Lett.* 79 (2002) 75.
- [58] M. Ruszel, B. Grzybowska, M. Gasior, K. Samson, I. Gressel, J. Stoch, *Catal. Today* 99 (2005) 151.
- [59] D. L. Trimm, *Appl. Catal.* 7 (1983) 249.
- [60] A. Tornocrona, M. Skoglundh, P. Thormahlen, E. Fridell, E. Jobson, *Appl. Catal. B* 14 (1997) 131.
- [61] G. K. Boreskov, *Catalysis Science and Technology*, Vol. 3, Springer-Verlag, Berlin 1985.
- [62] M. Baldi, V. S. Escribano, J. M. G. Amores, F. Milella, G. Busca, *Appl. Catal. B* 17 (1998) L175.
- [63] M. Baldi, E. Finocchio, F. Milella, G. Busca, *Appl. Catal. B* 16 (1998) 43.
- [64] M. Labaki, J. F. Lamonier, S. Siffert, E. A. Zhilinskaya, A. Aboukais, *Coll. and Surf. A* 227 (2003) 63.
- [65] M. Labaki, J. F. Lamonier, S. Siffert, E. A. Zhilinskaya, A. Aboukais, *Kinet. and Catal.* 45 (2004) 227.
- [66] L. Y. Margolis, *Adv. Catal.* 14 (1963) 429.
- [67] A. Terleckibaricevic, B. Grbic, D. Jovanovic, S. Angelov, D. Mehandziev, C. Marinova, P. Kirilovstefanov, *Appl. Catal.* 47 (1989) 145.
- [68] K. Tabata, M. Misono, *Catal. Today* 8 (1990) 249.
- [69] T. Seiyama, *Catal. Rev. Sci. Eng.* 34 (1992) 281.
- [70] E. Finocchio, G. Busca, V. Lorenzelli, V. S. Escribano, *J. Chem. Soc.-Farad. Trans.* 92 (1996) 1587.
- [71] T. Hayashi, L. B. Han, S. Tsubota, M. Haruta, *Ind. Eng. Chem. Res.* 34 (1995) 2298.
- [72] M. Haruta, *Proc. CatGold 2003*, Vancouver, Canada (2003).
- [73] G. Mul, A. Zwijnenburg, B. van der Linden, M. Makkee, J. A. Moulijn, *J. Catal.* 201 (2001) 128.
- [74] A. Ueda, T. Oshima, M. Haruta, *Appl. Catal. B* 12 (1997) 81.
- [75] M. C. Kung, K. A. Bethke, J. Yang, J. Lee, H. H. Kung, *Appl. Surf. Sci.* 121/122 (1997) 261.
- [76] A. Ueda, M. Haruta, *Appl. Catal. B* 18 (1998) 115.
- [77] A. Ueda, M. Haruta, *Gold Bull.* 32 (1999) 3.
- [78] B. W. L. Yang, J. J. Spivey, M. C. Kung, H. H. Kung, *Energy & Fuels* 11 (1997) 299.
- [79] H. M. Ajo, V. A. Bondzie, C. T. Campbell, *Catal. Lett.* 78 (2002) 359.
- [80] K. A. Davis, D. W. Goodman, *J. Phys. Chem. B* 104 (2000) 8557.
- [81] D. H. Kim, M. C. Kung, A. Kozlova, S. D. Yuan, H. H. Kung, *Catal. Lett.* 98 (2004) 11.
- [82] A. C. Gluhoi, N. Bogdanchikova, B. E. Nieuwenhuys, *J. Catal.* 229 (2005) 154.
- [83] A. C. Gluhoi, N. Bogdanchikova, B. E. Nieuwenhuys, *J. Catal.* 232 (2005) 96.
- [84] A. A. Ivanov, V. S. Chernyavsky, M. J. Gross, A. S. Kharitonov, A. K. Uriarte, G. I. Panov, *Appl. Catal. A* 249 (2003) 327.
- [85] H. Orita, H. Kondoh, H. Nozoye, *J. Catal.* 177 (1998) 217.
- [86] V. N. Parmon, G. I. Panov, A. K. Uriarte, A. S. Noskov, *Catal. Today* 100 (2005) 115.
- [87] Kirk-Othmer, *Encyclopedia of Chemical Technology*, Vol. 15, Wiley 1981, p. 856.
- [88] L. Chmielarz, P. Kustrowski, A. Rafalska-Lasocha, R. Dziembaj, *Appl. Catal. B* 58 (2005) 237.
- [89] J. M. Bradley, A. Hopkinson, D. A. King, *J. Phys. Chem.* 99 (1995) 17032.
- [90] Y. Li, J. N. Armor, *Appl. Catal. B* 13 (1997) 131.
- [91] G. Olofsson, L. R. Wallenberg, A. Andersson, *J. Catal.* 230 (2005) 1.

- [92] M. Ueshima, K. Sano, M. Ikeda, K. Yoshino, J. Okamura, Res. Chem. Intermed. 24 (1998) 133.
- [93] L. Gang, B. G. Anderson, J. van Grondelle, R. A. van Santen, W. J. H. van Gennip, J. W. Niemantsverdriet, P. J. Kooyman, A. Knoester, H. H. Brongersma, J. Catal. 206 (2002) 60.
- [94] M. Yang, C. Wu, C. Zhang, H. He, Catal. Today 90 (2004) 263.
- [95] L. Gang, B. G. Anderson, J. van Grondelle, R. A. van Santen, J. Catal. 199 (2001) 107.
- [96] J. J. P. Biermann, F. J. J. G. Janssen, M. de Boer, A. J. van Dillen, J. W. Geus, E. T. C. Vogt, J. Mol. Catal. 60 (1990) 229.
- [97] L. Lietti, G. Ramis, G. Busca, F. Bregani, P. Forzatti, Catal. Today 61 (2000) 187.
- [98] N. N. Sazanova, A. V. Simakov, T. A. Nikoro, G. B. Barannik, V. F. Lyakhova, V. I. Zheivot, Z. R. Ismagilov, H. Veringa, React. Kinet. Catal. Lett. 57 (1996) 71.
- [99] L. Gang, J. van Grondelle, B. G. Anderson, R. A. van Santen, J. Catal. 186 (1999) 100.
- [100] T. Curtin, F. O' Regan, C. Deconinck, N. Knuttel, B. K. Hodnett, Catal. Today 55 (2000) 189.
- [101] M. Amblard, R. Burch, B. W. L. Southward, Appl. Catal. B 22 (1999) L159.
- [102] R. Q. Long, R. T. Yang, J. Catal. 207 (2002) 158.
- [103] F. Dannevang, US patent 5, 587 (1996) 134.
- [104] R. Q. Long, R. T. Yang, Chem. Commun. 1651 (2000).
- [105] R. Q. Long, R. T. Yang, J. Catal. 201 (2001) 145.
- [106] H. M. J. Kusar, A. G. Ersson, M. Vosecky, S. G. Jaras, Appl. Catal. B 58 (2005) 25.
- [107] J. L. Gland, V. N. Korchak, J. Catal. 53 (1978) 9.
- [108] W. D. Miehler, W. Ho, Surf. Sci. 322 (1995) 151.
- [109] S. A. C. Carabineiro, B. E. Nieuwenhuys, Surf. Sci. 532 (2003) 87.
- [110] S. A. C. Carabineiro, B. E. Nieuwenhuys, Surf. Sci. 505 (2002) 163.
- [111] S. A. C. Carabineiro, A. V. Matveev, V. V. Gorodetskii, B. E. Nieuwenhuys, Surf. Sci. 555 (2004) 83.
- [112] L. Andrussov, Z. Angew. Chem. 39 (1926) 321.
- [113] M. Bodenstein, Z. Elektrochem. 41 (1935) 466.
- [114] M. Bodenstein, Z. Elektrochem. 47 (1935) 501.
- [115] F. Raschig, Z. Angew. Chem. 40 (1927) 1183.
- [116] M. Fogel, M. Ya, B. T. Nadykto, V. F. Rybalco, V. I. Shvachko, I. E. Korobchanskaya, Kinet. Catal. 8 (1964) 431.
- [117] A. C. M. van den Broek, J. van Grondelle, R. A. van Santen, J. Catal. 185 (1999) 297.
- [118] A. Scheibe, M. Hinz, R. Imbihl, Surf. Sci. 576 (2005) 131.
- [119] J. M. G. Amores, V. S. Escibano, G. Ramis, G. Busca, Appl. Catal. B 13 (1997) 45.
- [120] M. Trombetta, G. Ramis, G. Busca, B. Montanari, A. Vaccari, Langmuir 13 (1997) 4628.
- [121] G. Ramis, L. Yi, G. Busca, Catal. Today 28 (1996) 373.
- [122] S. D. Lin, A. C. Gluhoi, B. E. Nieuwenhuys, Catal. Today 90 (2004) 3.
- [123] A. C. Gluhoi, S. D. Lin, B. E. Nieuwenhuys, Catal. Today 90 (2004) 175.
- [124] M. Chiron, Stud. Surf. Sci. Catal. 30 (1987) 1.
- [125] J. N. Armor, Appl. Catal. B 1 (1992) 221.
- [126] K. M. Adams, J. V. Cavataio, R. H. Hammerle, Appl. Catal. B 10 (1996) 157.
- [127] G. C. Bond, *Heterogeneous Catalysis, Principles and Applications*, Oxford University Press, Oxford, 2nd edn. 1987.
- [128] A. Fritz, V. Pitchon, Appl. Catal. B 13 (1997) 1.
- [129] Z. Hu, F. M. Allen, C. Z. Wan, R. M. Heck, J. J. Steger, R. E. Lakis, C. E. Lyman, J. Catal. 174 (1998) 13.
- [130] K. C. Taylor, R. L. Klimisch, J. Catal. 30 (1973) 478.
- [131] H. C. Yao, Y. Yao, K. Otto, J. Catal. 56 (1979) 21.
- [132] K. Otto, H. C. Yao, J. Catal. 66 (1980) 229.
- [133] R. G. Sharpe, M. Bowker, Surf. Sci. 360 (1996) 21.
- [134] R. Burch, A. A. Shestov, J. A. Sullivan, J. Catal. 186 (1999) 353.
- [135] B. E. Nieuwenhuys, *Elementary reaction steps in heterogeneous catalysis*, R.W. Joyner, R.A. van Santen (eds.), Kluwer 1993.
- [136] B. E. Nieuwenhuys, *Adv. Catal.*, 44 (1999).
- [137] R. J. H. Voorhoeve, L. E. Trimble, J. Catal. 38 (1975) 80.
- [138] T. P. Kobylinski, B. W. Taylor, J. Catal. 33 (1974) 376.
- [139] A. A. Davydov, A. T. Bell, J. Catal. 49 (1977) 345.
- [140] M. Uchida, A. T. Bell, J. Catal. 60 (1979) 204.
- [141] J. R. Regalbuto, T. H. Fleisch, E. E. Wolf, J. Catal. 107 (1987) 115.
- [142] J. R. Regalbuto, C. W. Allen, E. E. Wolf, J. Catal. 108 (1987) 305.
- [143] J. R. Regalbuto, E. E. Wolf, J. Catal. 109 (1988) 13.
- [144] H. S. Gandhi, H. C. Yao, H. K. Stepien, ASC Symp. Series 178 (1982) 143.

- [145] H. S. Gandhi, M. Shelef, *Stud. Surf. Sci. Catal.* 30 (1987) 199.
- [146] Y. Mergler, *Rh-free automotive catalysts*, PhD thesis, Leiden University (1995).
- [147] I. R. Harkness, R. M. Lambert, *J. Chem. Soc. Farad. Trans.* 93 (1997) 1425.
- [148] O. A. Marina, I. V. Yentekakis, C. G. Vayenas, A. Palermo, R. M. Lambert, *J. Catal.* 166 (1997) 218.
- [149] A. Palermo, R. M. Lambert, I. R. Harkness, I. V. Yentekakis, O. Marina, C. G. Vayenas, *J. Catal.* 161 (1996) 471.
- [150] I. V. Yentekakis, M. Konsolakis, R. M. Lambert, N. Macleod, L. Nalbantian, *Appl. Catal. B* 22 (1999) 123.
- [151] I. V. Yentekakis, A. Palermo, N. C. Filkin, M. S. Tikhov, R. M. Lambert, *J. Phys. Chem. B* 101 (1997) 3759.
- [152] I. V. Yentekakis, M. Konsolakis, R. M. Lambert, A. Palermo, M. S. Tikhov, *Solid State Ionics* 136 (2000) 783.
- [153] R. J. Gorte, J. L. Gland, *Surf. Sci.* 102 (1981) 348.
- [154] M. E. Lesley, L. D. Schmidt, *Surf. Sci.* 155 (1985) 215.
- [155] E. D. L. Rienks, J. W. Bakker, A. Baraldi, S. A. C. Carabineiro, S. Lizzit, C. J. Weststrate, B. E. Nieuwenhuys, *Surf. Sci.* 516 (2002) 109.
- [156] R. J. Mukerji, A. S. Bolina, W. A. Brown, *J. Chem. Phys.* 119 (2003) 10844.
- [157] Y. O. Park, W. F. Banholzer, R. I. Masel, *Surf. Sci.* 155 (1985) 57.
- [158] S. Sugai, K. Takeuchi, T. Ban, H. Miki, K. Kawasaki, *Surf. Sci.* 282 (1993) 67.
- [159] G. Pirug, H. P. Bonzel, *J. Catal.* 5 (1977) 77.
- [160] N. M. H. Janssen, B. E. Nieuwenhuys, M. Ikai, K. Tanaka, A. R. Cholach, *Surf. Sci.* 319 (1994) L29.
- [161] P. D. Cobden, N. M. H. Janssen, Y. van Breugel, B. E. Nieuwenhuys, *Surf. Sci.* 366 (1996) 432.
- [162] B. W. Taylor, *Automotive Catalytic Converters*, Springer, Berlin 1984.
- [163] H. Hirano, T. Yamada, K. I. Tanaka, J. Siera, P. Cobden, B. E. Nieuwenhuys, *Surf. Sci.* 262 (1992) 97.
- [164] H. Marbach, S. Gunther, T. Neubrand, R. Imbihl, *Chem. Phys. Lett.* 395 (2004) 64.
- [165] C. Shi, A. M. Zhu, X. F. Yang, C. T. Au, *Appl. Catal. B* 276 (2004) 223.
- [166] A. Lindstedt, D. Stromberg, M. Abul Milh, *Appl. Catal.* 116 (1994) 109.
- [167] R. J. H. Voorhoeve, J. P. Remeika, L. E. Trimble, A. S. Cooper, F. J. Disalvo, P. K. Gallagher, *J. Sol. State Chem.* 14 (1975) 395.
- [168] D. Ferri, L. Forni, M. A. P. Dekkers, B. E. Nieuwenhuys, *Appl. Catal. B* 16 (1998) 339.
- [169] N. Mizuno, M. Yamato, M. Tanaka, M. Misono, *Chem. Mater.* 1 (1989) 232.
- [170] N. Mizuno, M. Tanaka, M. Misono, *J. Chem. Soc. Farad. Trans.* 88 (1992) 91.
- [171] L. Simonot, F. Garin, G. Maire, *Appl. Catal. B* 11 (1997) 181.
- [172] S. Galvagno, G. Parravano, *J. Catal.* 55 (1978) 178.
- [173] J. Y. Lee, J. Schwank, *J. Catal.* 102 (1986) 207.
- [174] M. A. P. Dekkers, *Supported gold catalysts for automotive catalysis reactions*, PhD thesis, Leiden University (2000).
- [175] M. A. P. Dekkers, M. J. Lippits, B. E. Nieuwenhuys, *Catal. Today* 54 (1999) 381.
- [176] T. M. Salama, R. Ohnishi, M. Ichikawa, *Chem. Commun.* (1997) 105.
- [177] A. Ueda, M. Haruta, *Appl. Catal. B* 285 (1996) 81.
- [178] S. M. McClure, T. S. Kim, J. D. Stiehl, P. L. Tanaka, C. B. Mullins, *J. Phys. Chem. B* 108 (2004) 17952.
- [179] X. Ding, Z. Li, J. Yang, K. G. Hou, Q. Zhu, *J. Chem. Phys.* 121 (2004) 2558.
- [180] C. P. Vinod, J. W. Niemantsverdriet, B. E. Nieuwenhuys, *Appl. Catal. A* 291 (2005) 93.
- [181] E. D. L. Rienks, G. P. van Berkel, J. W. Bakker, B. E. Nieuwenhuys, *Surf. Sci.* 571 (2004) 187.
- [182] T.-D. Chau, T. Visart de Bocarme, N. Kruse, *Catal. Lett.* 98 (2004) 85.
- [183] J. Perez-Ramirez, F. Kapteijn, K. Scoffel, J. A. Moulijn, *Appl. Catal. B* 44 (2003) 117.
- [184] K. M. Thomas, *Fuel* 76 (1997) 457.
- [185] V. I. Parvulescu, P. Grange, B. Delmon, *Catal. Today* 46 (1998) 233.
- [186] T. Tabata, M. Kokitsu, O. Okada, *Catal. Today* 22 (1994) 147.
- [187] G. Ferraris, G. Fierro, M. L. Jacono, M. Inversi, R. Dragone, *Appl. Catal. B* 36 (2002) 251.
- [188] J. Perez Ramirez, J. M. Garcia-Cortez, F. Kapteijn, M. J. Illan-Gomez, A. Ribeiro, C. S. M. d. Lecea, J. A. Moulijn, *Appl. Catal. B* 25 (2000) 191.
- [189] U. Li, J. N. Armor, *Appl. Catal. B* 3 (1993) 55.
- [190] F. Kapteijn, J. Rodriguez-Mirasol, J. A. Moulijn, *Appl. Catal. B* 9 (1996) 25.
- [191] R. W. McCabe, C. Wong, *J. Catal.* 121 (1990) 422.
- [192] D. N. Belton, S. J. Schmeig, *J. Catal.* 144 (1993) 9.
- [193] F. Goncalves, J. L. Figueiredo, *Appl. Catal. B* 50 (2004) 271.
- [194] J. Perez Ramirez, F. Kapteijn, A. Bruckner, *J. Catal.* 21/ (2003) 234.
- [195] J. Perez Ramirez, F. Kapteijn, *Catal. Commun.* 4 (2003) 333.

- [196] T. Nobukawa, M. Yoshida, K. Okumura, K. Tomishige, K. Kunimori, *J. Catal.* 229 (2005) 374 and refs. therein.
- [197] J. Arenas-Alatorre, A. Gomez-Cortes, M. Avalos-Borja, G. Diaz, *J. Phys. Chem. B* 109 (2005) 2371.
- [198] N. R. Avery, *Surf. Sci.* 131 (1983) 304.
- [199] D. A. Hoffman, J. B. Hudson, *Surf. Sci.* (1987).
- [200] R. Sau, J. B. Hudson, *J. Vac. Sci. Technol.* 18 (1981) 607.
- [201] J. P. Redmond, *J. Phys. Chem.* 67 (1993) 267.
- [202] M. H. Kim, J. R. Ebner, R. M. Friedman, M. A. Vannice, *J. Catal.* 204 (2001) 348.
- [203] S. A. C. Carabineiro, W. D. van Noort, B. E. Nieuwenhuys, *Surf. Sci.* 532 (2003) 96.
- [204] H. Horino, S. Liu, M. Sano, S. Wako, A. Hiratsuka, Y. Ohno, I. Kobal, T. Matsushima, *Topics Catal.* 18 (2002) 21.
- [205] G. Centi, L. Dall'Olio, S. Perathoner, *J. Catal.* 192 (2000) 224.
- [206] C. N. Hinshelwood, C. R. Prichard, *Proc. Roy. Soc. London A* 108 (1925) 211.
- [207] V. M. Stepanov, V. D. Yagodovskii, H. Agilar, *Russ. J. Phys. Chem.* 49 (1975) 1335.
- [208] L. Yan, X. Zhang, T. Ren, H. Zhang, X. Wang, *J. Suo, Chem. Commun.* (2002) 860.
- [209] N. W. Cant, N. Ossipoff, *Catal. Today* 36 (1997) 125.
- [210] A. C. Gluhoi, M. A. P. Dekkers, B. E. Nieuwenhuys, *J. Catal.* 219 (2003) 197.
- [211] A. Bielanski, J. Haber, *Oxygen in catalysis*, Marcel Dekker, New York 1991, p. 211-276.
- [212] G. Ertl, *Chem. Record* (2000) 33.
- [213] G. A. Somorjai, *CATTECH* 3 (1999) 84.
- [214] G. Blyholder, *J. Phys. Chem.* 68 (1964) 2772.
- [215] J. France, P. Hollins, *J. Electron. Spectros. Relat. Phenom.* 64-64 (1993) 251.
- [216] A. Wieckowski, E. R. Savinova, C. G. Vayenas (eds.), *Catalysis and Electrocatalysis at Nanoparticle Surface*, Marcel Dekker, New York 2003, p. 645-665.
- [217] D. A. H. Cunningham, T. Kobayashi, N. Kamijo, M. Haruta, *Catal. Lett.* 25 (1994) 257.
- [218] G. Croft, M. J. Fuller, *Nature* 269 (1977) 585.
- [219] T. Bunluesin, H. Cordatos, P. J. Gorte, *J. Catal.* 157 (1995) 222.
- [220] A. D. Logan, M. T. Paffett, *J. Catal.* 133 (1992) 179.
- [221] A. V. Kalinkin, V. I. Savchenko, A. V. Pashis, *Catal. Lett.* 59 (1999) 115.
- [222] Y. Mergler, A. van Aalst, J. van Delft, B. E. Nieuwenhuys, *Appl. Catal. B* 10 (1996) 245.
- [223] R. K. Hertz, D. R. Badlani, D. R. Schryer, B. T. Upchurch, *J. Catal.* 141 (1993) 219.
- [224] D. R. Schryer, B. T. Upchurch, B. D. Sidney, K. G. Brown, G. B. Hoflund, R. K. Hertz, *J. Catal.* 130 (1991) 314.
- [225] S. D. Gardner, G. B. Hoflund, D. R. Schryer, B. T. Upchurch, *J. Phys. Chem.* 95 (1991) 835.
- [226] S. Ladas, H. Poppa, M. Boudart, *Surf. Sci.* 102 (1981) 151.
- [227] C. H. F. Peden, *Surface Science of Catalysis-In Situ Probes and Reaction Kinetics*, ACS Symp. Ser. 482, D.J. Dwyer, F.M. Hoffmann (eds.), AM. Chem. Soc., Washington D.C. 1992, p. 143-159.
- [228] C. J. Zhang, P. Hu, *J. Am. Chem. Soc.* 123 (2001) 1166.
- [229] S. H. Taylor, C. Rhodes, *Catal. Lett.* 101 (2005) 31.
- [230] C. B. Wang, C. W. Tang, S. Gan, S. H. Chien, *Catal. Lett.* 101 (2005) 59.
- [231] X. C. Zheng, D. Z. Han, S. P. Wang, S. M. Zhang, S. R. Wang, W. P. Huang, S. H. Wu, *J. Rare Earths* 23 (2005) 47.
- [232] X. C. Zheng, S. H. Wu, S. P. Wang, S. R. Wang, S. M. Zhang, W. P. Huang, *Appl. Catal. A* 283 (2005) 217.
- [233] K.-S. Song, S.-K. Kang, S. D. Kim, *Catal. Lett.* 49 (1997) 65.
- [234] D. T. Thompson, *Gold Bull.* 31 (1998) 111.
- [235] M. Haruta, T. Kobayashi, N. Yamada, *Chem. Lett.* 2 (1987) 405.
- [236] M. M. Schubert, S. Hackenberg, A. C. van Veen, M. Muhler, V. Plzak, R. J. Behm, *J. Catal.* 197 (2001) 113.
- [237] D. T. Thompson, *Gold Bull.* 32 (1999) 12.
- [238] M. Valden, X. Lai, D. W. Goodman, *Science* 281 (1998) 1647.
- [239] G. C. Bond, *Gold Bull.* 34 (2001) 117.
- [240] G. C. Bond, D. T. Thompson, *Gold Bull.* 33 (2000) 41.
- [241] M. Haruta, *CATTECH* 6 (2002) 102.
- [242] M. Haruta, *Gold Bull.* 37 (2004) 27.
- [243] M. Haruta, M. Date, *Appl. Catal. A* 222 (2001) 427.
- [244] G. J. Hutchings, *Gold Bull.* 37 (2004) 3.
- [245] G. Patrick, E. van der Lingen, C. W. Corti, R. J. Holliday, D. T. Thompson, *Topics Catal.* 30/31 (2004) 273.
- [246] R. Meyer, C. Lemire, S. K. Shaikhutdinov, H.-J. Freund, *Gold Bull.* 37 (2004) 72.

- [247] U. Heiz, A. Sanchez, S. Abbet, W.-D. Schneider, *Chem. Phys.* 262 (2000) 189.
- [248] B. E. Salisbury, W. T. Wallace, R. L. Whetten, *Chem. Phys.* 262 (2000) 131.
- [249] G. Mills, M. S. Gordon, H. Metiu, *Chem. Phys. Lett.* 359 (2002) 493.
- [250] A. C. Gluhoi, H. S. Vreeburg, J. W. Bakker, B. E. Nieuwenhuys, *Appl. Catal. A* 291 (2005) 145.
- [251] R. J. H. Grisel, B. E. Nieuwenhuys, *J. Catal.* 199 (2001) 48.
- [252] N. M. Gupta, A. K. Tripathi, *Gold Bull.* 34 (2001) 120.
- [253] M. Haruta, S. Tsubota, T. Kobayashi, H. Kageyama, M. J. Genet, B. Delmon, *J. Catal.* 144 (1993) 175.
- [254] H. H. Kung, M. C. Kung, C. K. Costello, *J. Catal.* 216 (2003) 425.
- [255] J. T. Calla, R. J. Davis, *J. Phys. Chem. B* 109 (2005) 2307.
- [256] C. K. Costello, M. C. Kung, S.-O. Oh, Y. Wang, H. H. Kung, *Appl. Catal. A* 232 (2002) 159.
- [257] N. Lopez, J. K. Norskov, *J. Am. Chem. Soc.* 124 (2002) 11262.
- [258] A. Wootsch, C. Descorme, D. Duprez, *J. Catal.* 225 (2004) 259.
- [259] S. E. Golunski, *Plat. Met. Rev.* 42 (1998) 2.
- [260] P. G. Gray, M. I. Petch, *Plat. Met. Rev.* 44 (2000) 108.
- [261] S. H. Oh, R. Sinkevitch, *J. Catal.* 142 (1993) 254.
- [262] M. J. Kahlich, H. A. Gasteiger, R. J. Behm, *J. Catal.* 171 (1997) 93.
- [263] O. Korotkikh, R. Farrauto, *Catal. Today* 62 (2000) 249.
- [264] H. Igarashi, M. Uchida, Y. Suzuki, M. Sasaki, M. Watanabe, *Appl. Catal. A* 159 (1997) 159.
- [265] M. M. Schubert, H. A. Gasteiger, R. J. Behm, *J. Catal.* 172 (1997) 256.
- [266] H. Son, A. M. Lane, *Catal. Lett.* 76 (2001) 151.
- [267] H.-S. Roh, H. S. Potdar, K.-W. Jun, S. Y. Han, J. W. Kim, *Catal. Lett.* 93 (2004) 203.
- [268] D. J. Suh, C. Kwak, J. H. Kim, S. M. Kwon, T. J. Park, *J. Power Sources* 142 (2005) 70.
- [269] X. Liu, O. Korotkikh, R. Farrauto, *Appl. Catal. A* 226 (2002) 293.
- [270] Y. Hasegawa, A. Ueda, K. Kusakabe, S. Morooka, *Appl. Catal. A* 225 (2002) 109.
- [271] H. Tanaka, S.-I. Ito, S. Kameoka, K. Tomishige, K. Kunimori, *Catal. Commun.* 4 (2003) 1.
- [272] Z. Qu, M. Cheng, X. Dong, X. Bao, *Catal. Today* 93-95 (2004) 247.
- [273] Z. Qu, S. Zhou, W. Wu, C. Li, X. Bao, *Catal. Lett.* 101 (2005) 21.
- [274] G. Avgouropoulos, T. Ioanides, C. Papadopoulou, J. Batista, S. Hocevar, H. K. Matralis, *Catal. Today* 75 (2002) 157.
- [275] M. M. Schubert, M. J. Kahlich, H. A. Gasteiger, R. J. Behm, *J. Power Sources* 84 (1999) 175.
- [276] A. Manasilp, E. Gulari, *Appl. Catal. B* 37 (2002) 17.
- [277] R. J. H. Grisel, C. J. Weststrate, A. C. Gluhoi, B. E. Nieuwenhuys, *Gold Bull.* 35 (2002) 39.
- [278] G. K. Bethke, H. H. Kung, *Appl. Catal. A* 194 (2000) 43.
- [279] M. Haruta, A. Ueda, S. Tsubota, R. M. Torres Sanchez, *Catal. Today* 29 (1996) 443.
- [280] M. Okumura, S. Nakamura, S. Tsubota, T. Nakamura, M. Azuma, M. Haruta, *Catal. Lett.* 51 (1998) 53.
- [281] T. V. Choudhary, D. W. Goodman, *Catal. Today* 77 (2002) 65.
- [282] B. Schumacher, Y. Denkwitz, V. Plzaak, M. Kinne, R. J. Behm, *J. Catal.* 224 (2004) 449.
- [283] S. Kandoi, A. A. Gokhale, L. C. Grabow, J. A. Dumesic, M. Mavrikakis, *Catal. Lett.* 93 (2004) 93.
- [284] R. M. T. Sanchez, A. Ueda, K. Tanaka, M. Haruta, *J. Catal.* 168 (1997) 125.
- [285] M. M. Schubert, V. Plzak, J. Garche, R. J. Behm, *Catal. Lett.* 76 (2001) 143.
- [286] A. Luengnaruemitchai, S. Osuwan, E. Gulari, *Int. J. Hydrogen Energy* 29 (2004) 429.
- [287] D. A. Bulushev, L. Kiwi-Minsker, I. Yuranov, E. I. Suvorova, P. A. Buffat, A. Renken, *J. Catal.* 210 (2002) 149.
- [288] C. Rossignol, S. Arrii, F. Morfin, L. Piccolo, V. Caps, J.-L. Rousset, *J. Catal.* 230 (2005) 476.



# Chapter 3

## Sample preparation and experimental techniques

*This chapter describes the preparation procedures of various gold-based catalysts and the experimental techniques employed for their physico-chemical characterization. In addition, the experimental set-ups used for the catalytic activity and the Fourier Transform Infrared Spectroscopy measurements are described. The procedure used for evaluation of the catalytic performance is also presented.*



### 3.1 Outline

This chapter provides a detailed description of all the experimental techniques that have been used in order to acquire the data. Section 3.2 describes various preparation methods employed in order to manufacture the gold-based catalysts. Section 3.3 deals with a detailed description of each technique used to characterize the catalysts (i.e. AAS, BET, XRD, HRTEM, SEM, DR/UV-Vis, XPS and TPR). Section 3.4 describes the manner of performing catalytic tests (i.e. experimental set-up for various reactions, data evaluation and FTIR).

### 3.2 Sample preparation

#### 3.2.1 Unpromoted gold-based catalysts

Previously reported results proved that one of the most suitable preparation methods to obtain nanosized Au/Al<sub>2</sub>O<sub>3</sub> catalysts is homogeneous deposition-precipitation (HDP) using excess urea as precipitating agent [1, 2]. The materials used for the preparation of the catalysts were:

- gold precursor: HAuCl<sub>4</sub>·3H<sub>2</sub>O, Aldrich, 99.999% purity,
- urea, (NH<sub>2</sub>)<sub>2</sub>CO, Acros, p.a.,
- γ-Al<sub>2</sub>O<sub>3</sub>, Engelhard, Al-4172P, S<sub>BET</sub> = 275 m<sup>2</sup> g<sup>-1</sup>, pore volume, V<sub>p</sub> = 3 ml g<sup>-1</sup>.

The atomic ratio Au:Al was 1:75. This ratio corresponds to approximately 5 wt-% Au.

The chemical process occurring during the preparation procedure involves a reactant that transforms the gold precursor into an insoluble form that is generated slowly in the solution, and its concentration is raised homogeneously. If urea is present in the solution and the temperature is raised to 70-75<sup>0</sup>C, a slow hydrolysis occurs according to:



which leads to a slow increase in pH.

The hydroxyl ions are produced homogeneously throughout the solution, thus strong mixing is needed to prevent agglomeration of Au particles. Since, in the presence of a strong precursor-support interaction, nucleation of the catalyst precursor at the surface of the support proceeds at lower concentration than that needed for precipitation in the solution, precipitation exclusively on the support surface can be achieved.

At the beginning (room temperature, RT), the pH of the solution that contains HAuCl<sub>4</sub>·3H<sub>2</sub>O, γ-Al<sub>2</sub>O<sub>3</sub> and urea is around 2.5. This pH corresponds to [AuCl<sub>4</sub>]<sup>-</sup>, which forms [AuCl<sub>3</sub>(OH)]<sup>-</sup> by hydrolysis. By increasing the pH and heating up the solution to 70-75<sup>0</sup>C, different gold complexes are formed: [AuCl<sub>2</sub>(OH)<sub>2</sub>]<sup>-</sup>, [AuCl(OH)<sub>3</sub>]<sup>-</sup> and finally [Au(OH)<sub>4</sub>]<sup>-</sup>, at a pH above 7. The anion exchange with the support (γ-Al<sub>2</sub>O<sub>3</sub>) proceeds via protonation of OH groups of alumina and a subsequent release of water with vacancy formation and interaction with the OH groups of the gold complex. Thus, the mechanism of the exchange depends upon the pH, i.e. the concentration of the OH groups. At low pH, when only [AuCl<sub>4</sub>]<sup>-</sup> is present in the solution, there is no exchange with OH of γ-Al<sub>2</sub>O<sub>3</sub>, thus no gold deposition will occur. By increasing the pH, the gold precursor, progressively transformed in the final form of [Au(OH)<sub>4</sub>]<sup>-</sup>, will be deposited onto the support. However, another aspect is also important:

the isoelectric point of the support. The solid oxide particles in aqueous suspensions are often electrically charged. Charged particles are formed when there is an imbalance between the densities of adsorbed  $H^+$ ,  $OH^-$  and ionised surface OH groups. There exists a pH at which there is no net surface charge. This pH is called the isoelectric point (IEP), also known as point of zero charge (PZC). Below IEP, the support surface is positively charged and it will interact with the negatively charged ions. Above IEP, the support surface becomes negatively charged and it will interact with positive ions. The IEP of  $\gamma\text{-Al}_2\text{O}_3$  is 8-9 [3, 4] and this implies that below pH=9, gold is successfully deposited on the  $\gamma\text{-Al}_2\text{O}_3$ . As the pH approaches 8-9, the gold precursor, in the form of  $[\text{Au}(\text{OH})_4]^-$  is free of  $\text{Cl}^-$  ions, thus the final catalyst will be free of poisonous  $\text{Cl}^-$ . However, if the solution pH exceeds 9, there will be no gold deposition, since the alumina surface will be positively charged. Of course, the IEP of different oxides varies. This is the reason why gold cannot be deposited via this preparation route onto  $\text{SiO}_2$  (IEP = 2),  $\text{SiO}_2\text{-Al}_2\text{O}_3$  (IEP = 1),  $\text{WO}_3$  (IEP = 1) and  $\text{MgO}$  (IEP = 12) [3, 5], but it is successfully deposited on  $\text{Al}_2\text{O}_3$  (IEP = 8-9),  $\text{CeO}_2$  (IEP = 7) [6],  $\text{ZrO}_2$  (IEP = 6.7) [7] and  $\text{Fe}_2\text{O}_3$  (IEP = 7) [5].

The final pH of the precursor solution for Au/ $\text{Al}_2\text{O}_3$  catalysts prepared in this thesis was ~ 8.5. After the pH was reached, the solution was filtered and thoroughly washed several times with hot water, until no  $\text{Cl}^-$  was detected ( $\text{AgNO}_3$  test<sup>1</sup>). The obtained catalyst precursor (yellow) was dried for 16 hours in static air at  $80^\circ\text{C}$ . After drying, the color had not changed, implying no change in the chemical state of gold. Subsequent treatment consisted of calcination of the precursor in a pure  $\text{O}_2$  flow at  $300^\circ\text{C}$  (heating ramp  $5^\circ\text{C min}^{-1}$ ) and keeping the catalyst at that temperature for 2 hours. After the calcination, the color of the catalyst changed to mauve, dark red or brownish, depending on the gold loading and particle size. At this stage, the catalyst was ready to use. It has to be mentioned that the catalysts were stored at low temperature ( $\sim 4^\circ\text{C}$ ) to avoid growing of the gold particles during time. Very small Au particles have a melting point around  $327^\circ\text{C}$  due to the quantum size effect [8]. This implies that the Tamman temperature of nanosized gold particles is around  $27^\circ\text{C}$  and storage of the gold-based catalysts at room temperature may cause growth of the particles.

### 3.2.2 Multicomponent gold-based catalysts

Multicomponent gold-based catalysts prepared and studied in this thesis comprise two types: Au/ $\text{MO}_x/\text{Al}_2\text{O}_3$  and Au/ $\text{M}^{\text{I}}\text{O}_x/\text{M}^{\text{II}}\text{O}_x/\text{Al}_2\text{O}_3$ , where  $\text{MO}_x$  and  $\text{M}^{\text{I}}\text{O}_x/\text{M}^{\text{II}}\text{O}_x$  correspond to different types of metal oxides. First, the preparation procedure of the mixed supports  $\text{MO}_x/\text{Al}_2\text{O}_3$  and  $\text{M}^{\text{I}}\text{O}_x/\text{M}^{\text{II}}\text{O}_x/\text{Al}_2\text{O}_3$  is described.

#### 3.2.2.1 Mixed metal oxides as supports for gold-based catalysts

The metal oxides catalysts used in further experiments as mixed supports for gold-based catalysts have been prepared by vacuum impregnation. For this purpose, dried  $\gamma\text{-Al}_2\text{O}_3$  was always used and it was impregnated under vacuum conditions with the corresponding

<sup>1</sup> A solution that still contains  $\text{Cl}^-$  gives after mixing with  $\text{AgNO}_3$  a precipitate,  $\text{AgCl}$ . The test with  $\text{AgNO}_3$  is successful when no precipitate is formed, implying that the solution is free of  $\text{Cl}^-$ .

aqueous solution of a metal nitrate to yield catalysts with an intended M:Al atomic ratio of 1:15. When two different metal oxides were used, the atomic ratio was  $M^I:M^{II}:Al=1:1:15$ . The samples were subsequently dried in static air at 80°C overnight and subjected to calcination in a pure oxygen flow at 350°C, for two hours. The heating ramp was 5°C min<sup>-1</sup>. The M, M<sup>I</sup> and M<sup>II</sup> include Li, Rb, Ba, Mg, Cr, Mn, Fe, Co, Ni, Cu, Zn, Zr, Ti, Ce, La, V and Y. The metal nitrates precursors were high purity Aldrich or Acros products (>99.99%).

### 3.2.2.2 Multicomponent gold-based catalysts

The multicomponent Au/MO<sub>x</sub>/Al<sub>2</sub>O<sub>3</sub> and Au/M<sup>I</sup>O<sub>x</sub>/M<sup>II</sup>O<sub>x</sub>/Al<sub>2</sub>O<sub>3</sub> catalysts have been prepared by using the same route as previously described for Au/Al<sub>2</sub>O<sub>3</sub> catalyst (HDP with urea). Alternatively, for some of the samples, the metal oxide MO<sub>x</sub> was added to Au/Al<sub>2</sub>O<sub>3</sub> via vacuum-impregnation, thus, the final form of the catalyst was MO<sub>x</sub>/Au/Al<sub>2</sub>O<sub>3</sub>. All the samples were dried overnight in static air (80°C) and then subjected to calcination in pure oxygen, for two hours at 300°C (heating ramp 5°C min<sup>-1</sup>). The theoretical gold loading was 5 wt-%.

## 3.3 Experimental techniques

### 3.3.1 Atomic absorption spectroscopy, AAS

It has been already mentioned that the intended gold loading for the as-prepared samples was 5 wt-%. However, an incomplete gold deposition during the preparation step could occur, thus the exact gold loading has been determined by means of atomic absorption spectroscopy, AAS. For this purpose, a *Perkin Elmer 3100* apparatus with an air/acetylene flame was used. A known amount of the gold-based catalyst was dissolved in *aqua regia* (3HCl:HNO<sub>3</sub>), followed by filtration of undissolved alumina and dilution with demineralised water. In addition, if possible, the concentration of the MO<sub>x</sub> was also determined (CuO). The Cl<sup>-</sup> contamination was confirmed to be very low.

### 3.3.2 BET total surface area

The total surface area of the catalysts has been determined on the basis of the Brunauer, Emmet and Teller (BET) theory. The amount of a certain gas, physically adsorbed on the whole surface at very low temperature (-196°C), is measured, and the total surface area can be estimated according to:

$$S = x_m \cdot N \cdot A_m \cdot 10^{-20} \quad (\text{m}^2 \text{ g}^{-1}) \quad (3.1)$$

where  $x_m$  is the monolayer capacity (moles per gram of solid),  $N$  is Avogadro's constant (=  $6.023 \cdot 10^{23}$  molecules per mole) and  $A_m$  is the molecular cross-sectional area of the adsorbate, i.e. the area which an adsorbed molecule occupies on the surface of the solid in a complete monolayer (Å<sup>2</sup>). For nitrogen at -196°C the value of  $A_m$  is 16.2 Å<sup>2</sup> [9].

The monolayer capacity was determined by applying the BET equation to the experimental data. The BET equation is given by:

$$\frac{P}{x \cdot (P_0 - P)} = \frac{1}{x_m \cdot c} + \frac{(c-1) \cdot P}{x_m \cdot c \cdot P_0} \quad (3.2)$$

where  $P$  is the equilibrium pressure,  $P_0$  is the saturation vapour pressure of the adsorbate ( $N_2$  in the present case),  $x$  is the amount of gas adsorbed at the pressure  $P$ ,  $c$  is a constant and  $x_m$  is the amount of the gas adsorbed at saturation (monolayer capacity). According to this equation, when  $\frac{P}{x \cdot (P_0 - P)}$  is plotted against  $\frac{P}{P_0}$ , a straight line results with slope  $s = \frac{c-1}{x_m \cdot c}$

and intercept  $i = \frac{1}{x_m \cdot c}$ . Finally, the monolayer capacity  $x_m$  can be determined and by applying equation 3.1, the total surface area of the catalyst is found. It has to be mentioned that the BET theory is valid in the pressure range  $0.05 < P/P_0 < 0.3$ .

The experiments have been performed using an automated Qsurf M1 analyser (*Thermo Finnigan*). Before each measurement the catalyst was degassed for two hours in helium at  $200^\circ\text{C}$  in order to remove any adsorbed impurities. For each measurement at least three points have been taken in order to calculate the total surface area of the samples.

### 3.3.3 X-ray powder diffraction, XRD

X-ray diffraction is generally used to identify bulk crystalline phases and to estimate particle sizes. The diffraction method is based on Bragg's law which is the condition for the constructive interference of scattering from a set of planes with a  $d$ -spacing ( $d_{(hkl)}$ ) at an angle ( $2\theta$ ), with a wavelength ( $\lambda$ ) according to the equation (3.3)-see figure 3.1:

$$\lambda = 2 \cdot d_{(hkl)} \cdot \sin \theta \quad (3.3)$$

where  $\lambda$  is the wavelength of the incident beam,  $\theta$  is the diffraction angle and  $d_{(hkl)}$  is the distance between two successive planes characterized by Miller indices ( $h,k,l$ ). Bragg reflection according to the above equation is illustrated in fig. 3.1.

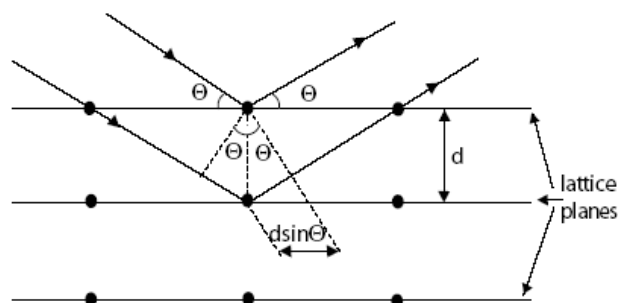


**Fig. 3.1:** Bragg reflection from a set of lattice planes.

For  $\text{Cu } K_\alpha$  radiation, the corresponding  $\lambda$  wavelength is  $1.54 \text{ \AA}$ .

The particle size may be estimated by using the Scherrer formula:

$$d = \frac{K \cdot \lambda}{\beta \cdot \cos \theta} \quad (3.4)$$

where  $d$  is the average metal particle size (Å),  $K$  is the Scherrer constant (0.9) and  $\beta$  is the full width at the half-maximum (radians) of the peak [10]. This method, although widely used in characterization of powders, has some disadvantages. First, it estimates an average size of the metallic particles and gives no information about the size distribution of the metallic particles. Second, the sensitivity ranges between 3 nm and 50 nm. Thus, very small particles, below 3 nm are not detected by X-ray diffraction.

The X-ray diffractograms have been recorded using a *Philips Goniometer (PW 1050/25)* diffractometer equipped with a Cu PW2253 X-ray tube. The source provided Cu  $K_{\alpha}$  radiation and was operated at 50 kV and 40 mA. The diffractograms were recorded at room temperature, using air-exposed samples. All the gold-containing samples were subjected to XRD analysis, both in an as-prepared form and after the reaction, as used catalyst. In addition, the support-only was also investigated by means of XRD analysis. The fast scan analysis was made in the range of  $30^{\circ} < 2\theta < 50^{\circ}$ , with a scan rate of  $0.01^{\circ} \text{ s}^{-1}$ . Extended XRD analysis was conducted in the range of  $20^{\circ} < 2\theta < 60^{\circ}$ , with a scan rate of  $0.02^{\circ} \text{ s}^{-1}$ .

The results obtained from XRD have also been used to estimate the metallic surface area of gold. The calculations have been made by assuming that the gold particles are hemispherical in shape with the flat side on the support, according to the following formula:

$$S_{\text{Au}} = \frac{50000 \cdot W}{\rho \cdot d} \quad (3.5)$$

where  $W$  corresponds to the gold loading,  $\rho$  is the density of gold ( $19.3 \text{ cm}^3 \text{ g}^{-1}$ ) and  $d$  is the diameter of gold particles as determined by XRD (Å).

### 3.3.4 High-resolution transmission electron microscopy, HRTEM

Some selected gold based-catalysts were subjected to detailed structural analysis by means of high-resolution transmission electron microscopy, HRTEM. This approach is especially useful when very small particles are involved since their detection is not possible using XRD. The HRTEM powder analysis was performed using two different microscopes. One of the microscopes was a *Philips CM30T* equipped with a  $\text{LaB}_6$  filament as the source of electrons and operated at 300 kV. In addition, elemental quantitative analysis could be performed with energy dispersive analysis (EDX) by means of a built-in *LINK EDX* system to detect possible contaminations in the catalyst. The maximum resolution was  $\sim 5 \text{ \AA}$  at 500 k magnification. Alternatively, a *JEOL 2010* microscope operated at 200 kV with a point-to-point resolution better than  $1.9 \text{ \AA}$  was used. The source of electrons was a  $\text{LaB}_6$  filament. The sample was mounted on a carbon polymer supported copper micro-grid. A few droplets of a

suspension of the ground catalyst in ethanol or isopropyl alcohol were placed on the grid, followed by drying at ambient conditions. The average gold particle size and their distribution were determined by counting at least 250-300 particles.

The equations used for the estimation of different parameters based on HRTEM analysis are as follows [11, 12]:

$$\text{- the average diameter} \quad D_n = \frac{\sum n_i \cdot d_i}{\sum n_i} \quad (3.6)$$

$$\text{- the surface average diameter} \quad D_s = \frac{\sum n_i \cdot d_i^3}{\sum n_i \cdot d_i^2} \quad (3.7)$$

$$\text{- the volume average diameter} \quad D_v = \frac{\sum n_i \cdot d_i^4}{\sum n_i \cdot d_i^3} \quad (3.8)$$

$$\text{- the dispersion} \quad D\% = \frac{100}{D_s} \quad (3.9)$$

$$\text{- the perimeter average (defined as the sum of the squares of the diameter divided by the sum of diameters):} \quad D_p = \frac{D_n^2 + D_s^2}{D_n + D_s} \quad (3.10)$$

To compare the catalytic activity based on the HRTEM measurement, also the following parameters are defined:

$$\text{- perimeter sites:} \quad \frac{1}{D_p^2} \quad (3.11)$$

$$\text{- surface sites:} \quad \frac{1}{D_s} \quad (3.12)$$

### 3.3.5 Scanning electron microscopy, SEM

Scanning electron microscopy (SEM) has been performed in order to visualize possible macroscopic changes of the alumina structure after gold deposition. The measurements were performed by using a JEOL (*JSM 5300*) microscope coupled with facilities for quantitative analysis by means of energy dispersive spectroscopy (*EDS*). The electron source was a tungsten filament operated at 35 kV.

### 3.3.6 Diffuse reflectance ultra-violet and visible spectroscopy, DR/UV-Vis

The absorption of ultraviolet or visible radiation (UV = 200 – 400 nm, Visible = 400 – 800 nm) corresponds to the excitation of outer-shell electrons. When an atom or molecule absorbs energy, electrons jump from their ground state to an excited state. There are three types of electronic transitions that can be considered: transitions involving  $\sigma$  and  $\pi$  electrons, transitions involving charge-transfer electrons and transitions involving  $d$  and  $f$  electrons.

The surface plasmon absorption in the metal nanoparticles arises from the collective oscillations of the free conduction band electrons that are induced by the incident electromagnetic radiation. Such resonances are seen when the wavelength of the incident light far exceeds the particle diameter. Metallic gold shows distinct and well-defined plasmon

absorption in the visible region of the spectra (wavelength  $\lambda \sim 550$  nm). In addition, the plasmon absorption of gold nanoparticles is sensitive to the surrounding environment and the interaction between gold and support [13].

The experiments were performed on two different commercial units: a *Perkin-Elmer Spectrometer (Lambda 900)* and a *CARY 300 SCAN (Varian)*, using air-exposed samples. The scans were made between 200 nm and 850 nm with a band pass of 1 nm. In addition, optical spectra of the support-only were also acquired.

### 3.3.7 X-ray photoelectron spectroscopy, XPS

X-ray photoelectron spectroscopy is an electron spectroscopic method that uses X-rays to eject electrons from inner-shell orbitals. The kinetic energy,  $E_k$ , of these photoelectrons is determined by the energy of the X-ray radiation,  $h\nu$ , and the electron binding energy,  $E_b$ , as given by:

$$E_k = h\nu - E_b \quad (3.13)$$

The experimentally measured energies of the photoelectrons are given by:

$$E_k = h\nu - E_b - E_w \quad (3.14)$$

where  $E_w$  is the work function of the spectrometer.

The electron binding energies are dependent on the chemical environment of the atom, making XPS useful to identify the oxidation state and ligands of an atom. Ejected electrons can escape only from a depth of approximately 3 nm or less, making electron spectroscopy most useful to study surfaces of solid materials.

The XPS measurements have been performed using a *Riber-Cameka Mac-3* photoelectron spectrometer with  $AlK\alpha$  radiation (1486.6 eV). As an internal reference the C 1s peak at 284.6 eV was used and the positions of other peaks were corrected according to the position of the C 1s signal. The samples (calcined) were analysed by XPS without any pretreatment.

### 3.3.8 Temperature programmed reduction spectroscopy, TPR

Temperature programmed reduction (TPR) is a useful technique for the characterization of metal oxide catalysts. During a TPR experiment, the catalyst is exposed to a reducing mixture while the temperature is increased according to a linear temperature program. The difference between the inlet and outlet concentration of the gas mixture is measured as function of time using a thermal conductivity detector (TCD). The resulting TPR profile contains information on the oxidation state of the reducible species present. The reducing gas might be, for example, hydrogen or carbon monoxide.

The measurements were performed by using two different apparatuses. One was a laboratory set-up specially designed for this purpose, with a thermal conductivity detector (TCD) for gas analysis. The gas flow passing through the catalyst bed consisted of 5.5 %  $H_2$  in Ar, at a total flow of  $25 \text{ ml min}^{-1}$ . The reduction degree of gold was estimated by

calibrating using the hydrogen needed to completely reduce a known amount of CuO. The second one was an *AMI 1 Altamira-Instrument*. The reducing gas, 5 % H<sub>2</sub> in Ar, passed with a flow rate of 30 ml min<sup>-1</sup> through the catalyst bed at a heating ramp of 5<sup>0</sup>C min<sup>-1</sup>. Prior to each experiment the sample was heated in an Ar flow at 100<sup>0</sup>C in order to eliminate the physically adsorbed water. The water produced during the thermal treatment and reduction processes was trapped before the gas mixture reached the TCD, used to monitor the rate of hydrogen consumption.

### 3.4 Catalytic activity experiments

#### 3.4.1 Experimental set-up

The catalytic activity studies were carried out with two different lab-scale flow systems. A schematic design of the two integrated systems is presented in Figure 3.2. Typically 0.2 g catalyst was loaded for each catalytic test. Prior to the measurement, the catalyst was pretreated in a flow of 4 vol % H<sub>2</sub>/He. Alternatively, for some measurements, an oxidative pretreatment was performed by using 4 vol % O<sub>2</sub>/He. The pretreatment temperature was 300<sup>0</sup>C, reached by a heating ramp of 10<sup>0</sup>C min<sup>-1</sup>. After cooling to room temperature, the reactor was purged with helium to remove the previous gas used in the pretreatment step. All the reactant gases were 4 vol % in He and separate lines were used for each gas. The reactant flow rates were adjusted by means of mass flow controllers (*Bronkhorst*). Both the thermocouple and the oven were connected to a temperature controller (*Shimaden*), allowing the reaction to be temperature-programmed.

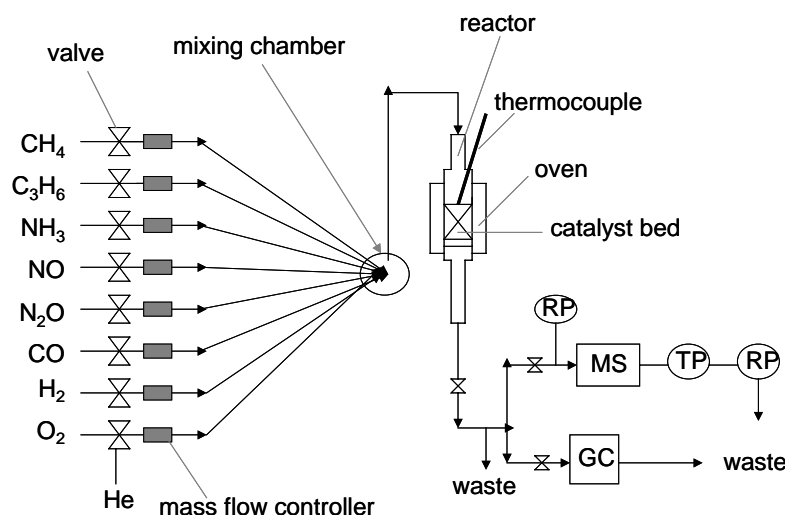


**Figure 3.2:** Schematic picture of the flow system used for catalytic activity measurements. MS = mass spectrometer, GC = gas chromatograph, RP = rotary pump, TP = turbo pump.

Every reaction test consisted of at least two heating-cooling cycles in order to monitor possible catalyst deactivation and hysteresis processes. The outlet gas composition was



analysed on-line by means of either a gas chromatograph or a mass spectrometer. The experiments were carried out under atmospheric pressure.

The turnover frequency (TOF), defined as the number of molecules converted per second and per surface metal atom, is a realistic parameter to compare the performance of catalysts. In general, CO and H<sub>2</sub> titration are used to determine the number of exposed metal atoms. For gold-based catalysts, this titration method is not applicable due to the weak adsorption of these molecules on the Au surface. Therefore, to compare the catalytic performance of various catalysts tested in this study, the light-off temperature, defined as the temperature where a conversion of 50% is attained, is considered as the measure of the catalytic performance. However, for CO oxidation it was not possible to express the catalytic activity in a similar manner, since some of the gold-based catalysts were highly active already at room temperature. Thus, for this reaction the catalytic activity is expressed as the temperature where 95% conversion of CO is obtained. Alternatively, the CO conversion at 70°C is considered.

### 3.4.2 Carbon monoxide oxidation in the absence or presence (PROX) of hydrogen

CO oxidation over gold-based catalysts has been performed by using the set-up shown in Fig. 3.2 and a glass reactor with  $\phi = 20$  mm. The reactant ratio was CO: O<sub>2</sub> = 2:1. The gases were passing through the catalyst bed with a total flow of 40 ml min<sup>-1</sup> STP (standard temperature and pressure), resulting in a gas hourly space velocity (GHSV) of ~2500 h<sup>-1</sup>. The catalytic test consisted of at least two heating-cooling cycles between room temperature (RT) and 300°C. The outlet gas concentration was analysed by a gas chromatograph (*Chrompack CP-2002*) equipped with two columns: a Molsieve 5Å column for detection of CO and O<sub>2</sub> and a Hayesep A column for CO<sub>2</sub> detection.

Preferential oxidation of CO in the presence of hydrogen (PROX process) was studied with the same experimental set-up, using a mixture of H<sub>2</sub> (70 vol %) and CO+O<sub>2</sub> (1.2 vol %) in helium (~29 vol %). All the experimental conditions were exactly the same as in the case of CO oxidation in the absence of hydrogen.

### 3.4.3 Hydrocarbon oxidation reactions: methane (CH<sub>4</sub>), propene (C<sub>3</sub>H<sub>6</sub>) and propane (C<sub>3</sub>H<sub>8</sub>) oxidation

The reactor (quartz) used to study the hydrocarbon oxidation reactions had a diameter of 10 mm. A reactant ratio of CH<sub>4</sub>:O<sub>2</sub> = 1:4 was passed through the catalyst bed with a total flow of 30 ml min<sup>-1</sup> STP, GHSV ~1800 h<sup>-1</sup>. The reaction was stabilized at room temperature for 30 minutes, followed by a temperature increase to 200°C. Starting from that temperature, a programmed reaction was employed between 200°C and 740°C for at least two consecutive heating-cooling cycles. The effluent gas stream was analysed by a gas chromatograph (*Chrompack CP-9001*) equipped with a flame ionisation detector (FID), a Hayesep N column and a methanizer.

The total oxidation of propene (C<sub>3</sub>H<sub>6</sub>) has been studied using the same system as the previous one. The reactant ratio was C<sub>3</sub>H<sub>6</sub>:O<sub>2</sub> = 1:9. The total flow rate was 30 ml min<sup>-1</sup> STP. The outlet gas composition was analysed by means of either a gas chromatograph

(Chrompack CP-9001), or a mass spectrometer (*Balzers or Spectra*). The reaction was first stabilized for 30 minutes at room temperature (RT) and then temperature programmed between RT and 400<sup>0</sup>C, with at least two heating-cooling cycles.

The total oxidation of propane (C<sub>3</sub>H<sub>8</sub>) was studied using a reactant ratio C<sub>3</sub>H<sub>8</sub>:O<sub>2</sub> = 1:16. The experimental procedure was similar to the one employed for propene oxidation.

### 3.4.4 Reactions of N-containing molecules

The reactions of N-containing molecules include NO and N<sub>2</sub>O reduction by H<sub>2</sub> and NH<sub>3</sub> oxidation. The experiments were performed with the same experimental set-up as that described in Section 3.4.3. NO reduction by H<sub>2</sub> was performed by using two different ratios: NO/H<sub>2</sub> = 0.4 and NO/H<sub>2</sub> = 1. The reduction of N<sub>2</sub>O by H<sub>2</sub> was followed with a N<sub>2</sub>O/H<sub>2</sub> ratio of 0.5. For ammonia oxidation, the reactant mixture used was NH<sub>3</sub>:H<sub>2</sub> = 1. In addition, several experiments were also carried out in excess of oxygen (NH<sub>3</sub>:O<sub>2</sub> = 1:10). The concentration of the outlet gases was analysed by means of a mass spectrometer (*Balzer or Spectra*). For all the reactions, a period of at least 30 minutes was used for stabilization. The reactions were temperature programmed between RT and 300<sup>0</sup>C (NO + H<sub>2</sub> and N<sub>2</sub>O + H<sub>2</sub>), or 400<sup>0</sup>C (NH<sub>3</sub> + O<sub>2</sub>). The masses followed by MS were corrected when needed for the corresponding fragmentation factors, as well as for the MS sensitivity [14].

### 3.4.5 Data evaluation

The conversion of a reactant A at the temperature T, X<sub>A(T)</sub> is defined as the amount of the reactant A (mol ml<sup>-1</sup>) transformed at the temperature T divided by the total amount of A in the gas feed (mol ml<sup>-1</sup>). The corresponding equation is defined as follows:

$$X_{A(T)} = \frac{C_{A,i} - C_{A,T}}{C_{A,i}} \quad (3.15)$$

where  $C_{A,i}$  represents the initial concentration of the reactant A (mol min<sup>-1</sup>) and  $C_{A,T}$  the concentration of A (mol min<sup>-1</sup>) at a temperature T.

The selectivity for various products was calculated according to the following formulas:

- selectivity to CO<sub>2</sub> in CO+O<sub>2</sub>+H<sub>2</sub> reaction:

$$S_{CO_2,T} = \frac{C_{CO_2,T}}{2 \cdot (C_{O_2,i} - C_{O_2,T})} \quad (3.16)$$

- selectivity to N<sub>2</sub>O, N<sub>2</sub>, NH<sub>3</sub> in NO+H<sub>2</sub> reaction:

$$S_{N_2O} = \frac{2 \cdot C_{N_2O}}{2 \cdot C_{N_2O} + 2 \cdot C_{N_2} + C_{NH_3}} \quad (3.17)$$

$$S_{N_2} = \frac{2 \cdot C_{N_2}}{2 \cdot C_{N_2O} + 2 \cdot C_{N_2} + C_{NH_3}} \quad (3.18)$$

$$S_{NH_3} = \frac{C_{NH_3}}{2 \cdot C_{N_2O} + 2 \cdot C_{N_2} + C_{NH_3}} \quad (3.19)$$

- selectivity to  $N_2$ ,  $N_2O$ ,  $NO$  and  $NO_2$  in  $NH_3+O_2$  reaction:

$$S_{N_2} = \frac{2 \cdot C_{N_2}}{2 \cdot C_{N_2} + C_{NO} + 2 \cdot C_{N_2O} + C_{NO_2}} \quad (3.20)$$

$$S_{NO} = \frac{C_{NO}}{2 \cdot C_{N_2} + C_{NO} + 2 \cdot C_{N_2O} + C_{NO_2}} \quad (3.21)$$

$$S_{N_2O} = \frac{2 \cdot C_{N_2O}}{2 \cdot C_{N_2} + C_{NO} + 2 \cdot C_{N_2O} + C_{NO_2}} \quad (3.22)$$

$$S_{NO_2} = \frac{C_{NO_2}}{2 \cdot C_{N_2} + C_{NO} + 2 \cdot C_{N_2O} + C_{NO_2}} \quad (3.23)$$

### 3.4.6 Infrared spectroscopy, IR

Fourier Transform Infrared Spectroscopy (FTIR) measurements were employed to study ammonia oxidation in more detail. For this purpose, a *Mattson Galaxy 2020* spectrometer was used. The IR spectrum was measured in the transmission mode at a resolution of  $2 \text{ cm}^{-1}$  and corrected for the background spectrum that was averaged from 50 scans of the empty cell (at pressures lower than  $1 \cdot 10^{-5}$  mbar).

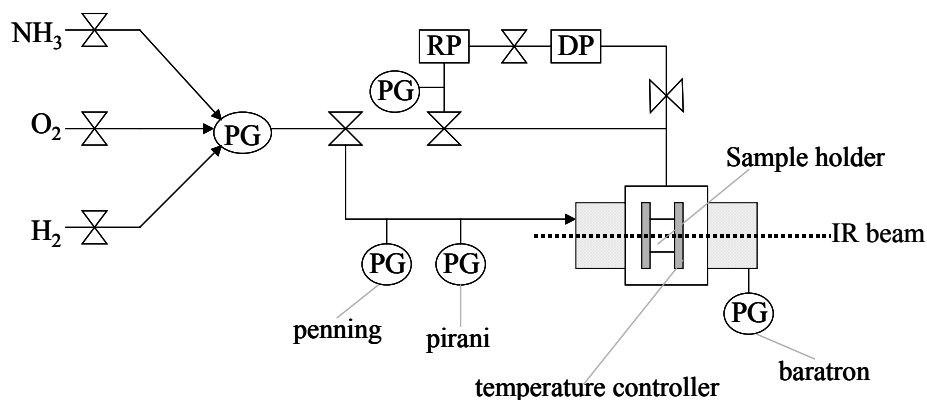


**Figure 3.3:** Schematic representation of the vacuum cell used for FTIR measurements. PG: pressure gauge, RP: rotary pump, DP: diffusion pump.

The pressure of the admitted gases was measured by using a MKS baratron. A self-supporting wafer was made from catalyst powders (with  $\sim 1.5 \text{ tons cm}^{-1}$ ). After mounting, the wafer was evacuated to  $1 \cdot 10^{-3}$  mbar, then subjected to a heat-treatment to  $300^\circ\text{C}$  under 200 mbar of hydrogen, followed by cool-down at which evacuation started at around  $227^\circ\text{C}$ . Both mixed supports ( $MO_x/Al_2O_3$  and  $M^I O_x/M^{II} O_x/Al_2O_3$ ) and the supported gold-based catalysts were pretreated in this way. An IR spectrum was recorded at  $40^\circ\text{C}$  and  $1 \cdot 10^{-5}$  mbar after this treatment and was used as the reference to later-recorded spectra of the same sample.

Thereafter, 20 mbar of NH<sub>3</sub> was introduced, held for 20 min, and evacuated at 40<sup>0</sup>C. A stepwise temperature-programmed desorption (sTPD) was performed sequentially at 40, 55, 70, 90, 120, 150, 200, 250, and 300<sup>0</sup>C under vacuum, where an IR spectrum was taken at every temperature. Afterwards the sample was cooled down to 40<sup>0</sup>C, exposed to NH<sub>3</sub> and a stepwise temperature-programmed oxidation (sTPO) experiment was carried out, which was essentially an sTPD in the presence of ca. 20 mbar of oxygen. No useful information could be extracted within the region of the N-H stretching modes, because most spectra were very noisy in that region. Figure 3.3 shows a schematic representation of the infrared set-up used.

### 3.5 References

- [1] R. J. H. Grisel, *Supported gold catalysts for environmental applications*, PhD thesis, Leiden University (2002).
- [2] R. J. H. Grisel, P. J. Kooyman, B. E. Nieuwenhuys, *J. Catal.* 191 (2000) 430.
- [3] H. H. Kung, *Transition metal oxides: Surface chemistry and catalysis*, in *Stud. Surf. Sci. Catal.*, Elsevier, Amsterdam, 45 (1989) 86.
- [4] S. Ivanova, C. Petit, V. Pitchon, *Appl. Catal. A* 267 (2004) 191.
- [5] M. Haruta, N. Yamada, T. Kobayashi, S. Iijima, *J. Catal.* 115 (1989) 301.
- [6] D. Andreeva, V. Idakiev, T. Tabakova, L. Ilieva, P. Falaras, A. Bourlinos, A. Travlos, *Catal. Today* 72 (2002) 51.
- [7] A. Knell, P. Barnickel, A. Baiker, A. Wokaun, *J. Catal.* 137 (1992) 306.
- [8] P. Buffat, J.-P. Borel, *Phys. Rev. A* 13 (1976) 2287.
- [9] S. J. Gregg, K. S. W. Sing, *Adsorption, Surface Area and Porosity*, Academic Press Inc., London, New York 1967, p. 67.
- [10] P. Scherrer, *Nachr. K. Ges. Wiss., Gottingen* 98 (1918).
- [11] Q. Xu, K. C. C. Kharas, A. K. Datye, *Stud. Surf. Sci. Catal.* 139 (2001) 157.
- [12] Q. Xu, K. C. C. Kharas, A. K. Datye, *Catal. Lett.* 85 (2003) 229.
- [13] P. Claus, A. Bruckner, C. Mohr, H. Hofmeister, *J. Am. Chem. Soc.* 122 (2000) 11430 and refs. therein.
- [14] A. C. Gluhoi, M. A. P. Dekkers, B. E. Nieuwenhuys, *J. Catal.* 219 (2003) 197.



# Chapter 4

## Alumina-supported gold based catalysts.

### Characterization results

*The as-prepared Au/Al<sub>2</sub>O<sub>3</sub>, Au/MO<sub>x</sub>/Al<sub>2</sub>O<sub>3</sub> and Au/M<sup>I</sup>O<sub>x</sub>/M<sup>II</sup>O<sub>x</sub>/Al<sub>2</sub>O<sub>3</sub> (M, M<sup>I</sup> and M<sup>II</sup>: Li, Rb, Ba, Mg, Cr, Mn, Fe, Co, Ni, Cu, Zn, Zr, Ti, Ce, La, V and Y) catalysts have been characterized by means of various characterization techniques: AAS, BET, XRD, HRTEM, SEM, DR/UV-Vis, XPS and TPR. The variation in gold loading of these catalysts is relatively small. All the additives: MO<sub>x</sub>, M<sup>I</sup>O<sub>x</sub> and M<sup>II</sup>O<sub>x</sub> act as a structural promoter, in the sense that the small gold crystallites are preserved during the preparation and subsequent heat treatments. Sintering of the gold particles during a reaction cycle eventually proceeds above 500<sup>o</sup>C. DR/UV-Vis and XPS techniques did not indicate the presence of ionic gold (Au<sup>3+</sup> or Au<sup>+</sup>); only Au<sup>0</sup> was detected. However, the TPR studies carried out over some selected Au-catalysts showed the presence of ionic gold (Au<sup>3+</sup>) in the dried samples, but the reduction to Au<sup>0</sup> already proceeded at 150<sup>o</sup>C. It is concluded that a catalyst in working state contains mainly Au<sup>0</sup>.*

## 4.1 Outline

This chapter presents a comprehensive study of the physico-chemical properties of various gold-based catalysts. Section 4.2 presents results concerning the gold loading (AAS technique), BET surface area, average size of the gold particles (XRD and HRTEM) and macroscopic changes of the support after the addition of Au (SEM). Section 4.3 deals with DR/UV-Vis results, and section 4.4 is devoted to temperature-programmed reduction studies (TPR) of some of the gold-based catalysts. Section 4.5 presents some XPS results and a general discussion of all the results is found in Section 4.6. Section 4.7 summarizes the most important conclusions.

## 4.2 Gold loading (AAS), BET surface area, XRD, HRTEM and SEM results

### 4.2.1 Unpromoted Au/Al<sub>2</sub>O<sub>3</sub> catalysts

Gold has a much lower melting point (1063<sup>0</sup>C) than the Pt group metals (Pd: 1550<sup>0</sup>C, Pt: 1769<sup>0</sup>C). Moreover, the melting point of gold in a highly dispersed state may be as low as 327<sup>0</sup>C due to the quantum size effect [1]. It is, therefore, difficult to synthesize highly dispersed gold catalysts. It was found that the deposition of gold during the preparation step is rather high, especially if it is considered that the gold precursor is not used in excess, as is the case when the coprecipitation method is employed. In addition, the HDP method has more advantages for the preparation of gold catalysts: the gold deposition onto the support is high, none of the gold is buried within the support, and a narrow particle size distribution is obtained [2]. The gold loading, as determined by AAS for unpromoted Au/Al<sub>2</sub>O<sub>3</sub> is 4.1 wt-% Au (see Table 4.1).

In general, the carrier, although it does not possess catalytic properties, plays an important role in the final catalytic properties of the active component. For example, it ensures a high dispersion of the active phase (gold in this case). Therefore the support should display a high thermal and mechanical strength, high surface area and no reactivity. The  $\gamma$ -Al<sub>2</sub>O<sub>3</sub> used as a carrier has a BET surface area of 275 m<sup>2</sup>g<sup>-1</sup>. After gold deposition, the BET surface area of Au/Al<sub>2</sub>O<sub>3</sub> was not significantly decreased and is around 260 m<sup>2</sup>g<sup>-1</sup> (Table 4.1).

A comparison of the XRD results obtained for Au/Al<sub>2</sub>O<sub>3</sub> catalysts in two different states (calcined at 300<sup>0</sup>C in an oxygen flow or dried at 80<sup>0</sup>C), support-only (Al<sub>2</sub>O<sub>3</sub>) and Au-sponge are depicted in Figure 4.1. The XRD pattern of Au sponge shows the typical diffraction pattern of metallic Au, i.e. the presence of two diffraction lines at  $2\theta = 38.2^{\circ}$  ( $d = 2.35 \text{ \AA}$ ) and  $2\theta = 43.4^{\circ}$  ( $d = 2.03 \text{ \AA}$ ). As expected, dried-Au/Al<sub>2</sub>O<sub>3</sub> does not show any diffraction pattern characteristic of metallic gold, it only resembles the structure of  $\gamma$ -Al<sub>2</sub>O<sub>3</sub>. On the other hand, calcined-Au/Al<sub>2</sub>O<sub>3</sub> shows mainly the diffraction lines of  $2\theta = 38.2^{\circ}$  which is, however, relatively broad, typical for relatively small crystallites. The average size of the gold particles as calculated by using the main diffraction line of  $2\theta = 38.2^{\circ}$  and according to the formula (3.4), is around 4.3 nm. A much smaller diffraction line is visible at  $2\theta = 43.4^{\circ}$ .

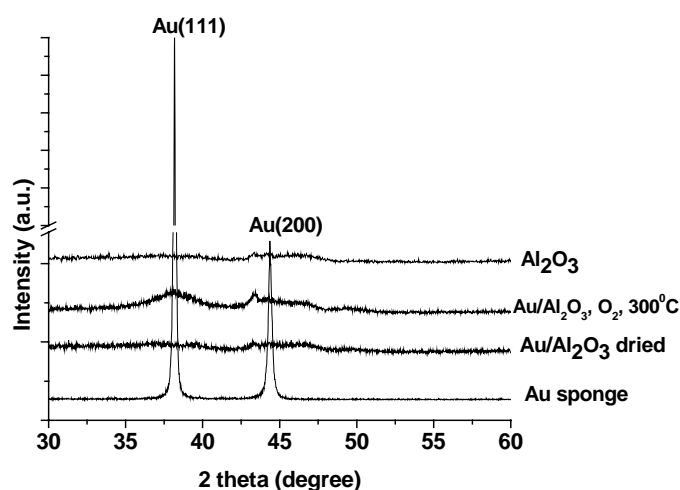


**Figure 4.1:** Comparison of XRD patterns of calcined-Au/Al<sub>2</sub>O<sub>3</sub> (300<sup>o</sup>C, O<sub>2</sub>), dried-Au/Al<sub>2</sub>O<sub>3</sub>, Au sponge and Al<sub>2</sub>O<sub>3</sub> support.

More recently, attention has also been paid to the effect of the calcination temperature. It was reported that for Au/TiO<sub>2</sub> [3, 4], Au/Fe<sub>2</sub>O<sub>3</sub> [4-6], and Au/MnO<sub>x</sub> [7] catalysts, calcination at mild temperature (100-200<sup>o</sup>C) results in more active catalysts than calcined at higher temperatures. There are also reports that uncalcined Au/Al<sub>2</sub>O<sub>3</sub> [8] or Au/Y [9] can be very active. In addition, a higher calcination temperature may cause a severe sintering of the gold crystallites [10, 11]. On the other hand, it has been reported that a higher calcination temperature may positively influence the catalytic activity of Au/TiO<sub>2</sub> in the sense that a stronger interaction between Au and support is created and this phenomenon leads to a higher catalytic efficiency, even though gold particles grow to larger ones [10]. Therefore, the influence of the pretreatment temperature and the nature of the gas on the structure of Au/Al<sub>2</sub>O<sub>3</sub> were studied by means of XRD. These catalysts have been tested, in particular, for CO oxidation (*Chapter 9*). Figure 4.2 shows the influence of the pretreatment (H<sub>2</sub> or O<sub>2</sub>) and various temperatures (150, 300 and 500<sup>o</sup>C) on the structure of Au/Al<sub>2</sub>O<sub>3</sub> as determined by XRD technique.

Interestingly, a pretreatment in either O<sub>2</sub> or H<sub>2</sub> at 150<sup>o</sup>C is able to generate metallic gold (diffraction line at  $2\theta = 38.2^{\circ}$ ). The Au crystallite size is around 3 nm. In addition, no significant difference was found in the size of the gold particles for pretreatment in H<sub>2</sub> and O<sub>2</sub>. By increasing the calcination temperature, the average size of Au particles increases slightly (treatment at 300<sup>o</sup> in O<sub>2</sub> forms gold particles of 4.3 nm). In an atmosphere of hydrogen a further increase in treatment temperature (500<sup>o</sup>C) causes a minor increase in the particle size from 4.3 nm to 4.8 nm, whereas no change was observed for heating in O<sub>2</sub> (4.3 nm). However, the difference caused by using H<sub>2</sub> or O<sub>2</sub> is not large, even at 500<sup>o</sup>C large agglomeration of the gold crystallites was not found.



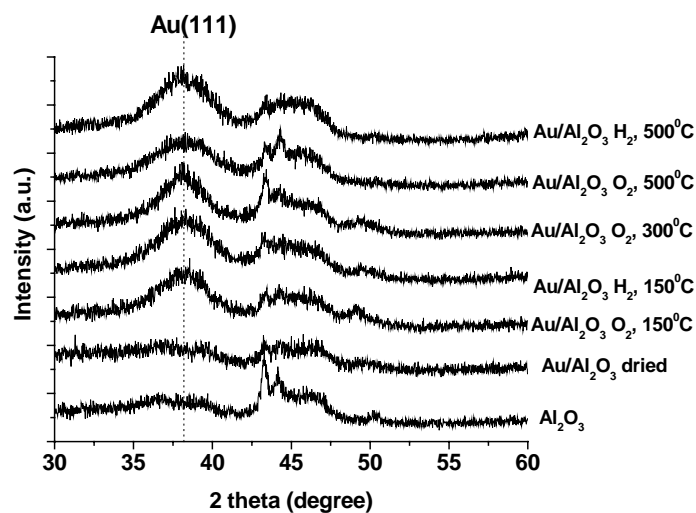


**Figure 4.2:** The influence of the pretreatment (gas and temperature) on the structure of Au/Al<sub>2</sub>O<sub>3</sub> catalysts (XRD measurements).

A typical HRTEM image of the gold particles of Au/Al<sub>2</sub>O<sub>3</sub> catalyst is shown in Figure 4.3. The gold particles (black dots in Fig. 4.3) are fairly homogeneously distributed over the alumina support (grey regions). In agreement with the XRD data, the gold particles were, on average, rather large (5.2 nm). In addition, it is also visible in Figure 4.3 that some of the gold particles do not exhibit a round shape, but rather a truncated one.

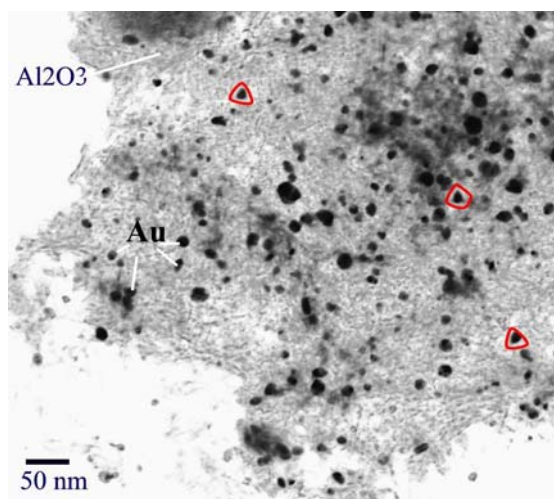


**Figure 4.3:** HRTEM image of Au/Al<sub>2</sub>O<sub>3</sub>. Gold particles are visible as black dots distributed over the support (grey patches).

Possible macroscopic changes in the structure of alumina after gold deposition have been followed by SEM. It was found that, in line with the results obtained by BET, the support

structure is preserved after Au deposition. Two SEM pictures of alumina and Au/Al<sub>2</sub>O<sub>3</sub> are shown in Figures 4.4A-B.

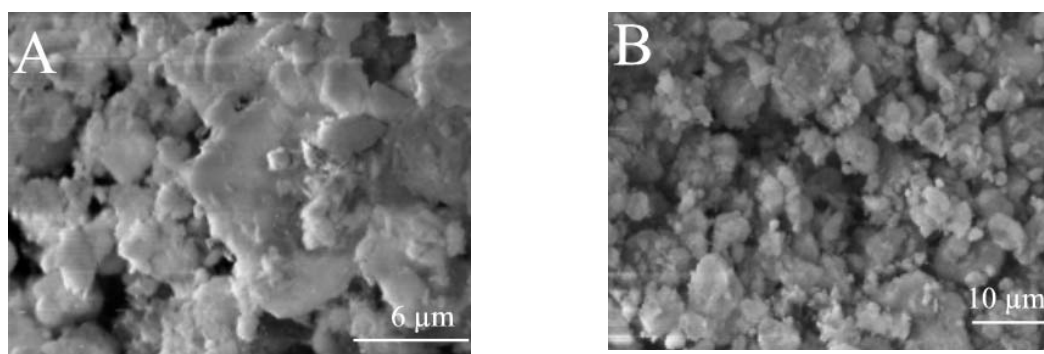


**Figure 4.4:** SEM pictures of  $\gamma$ -Al<sub>2</sub>O<sub>3</sub> (A) and Au/Al<sub>2</sub>O<sub>3</sub> (B).

#### 4.2.2 Promoted Au/Al<sub>2</sub>O<sub>3</sub> catalysts

Often, gold-based catalysts are used in combination with additives, and one of their roles is to stabilize the small gold particles against sintering. For example, Grisel stated that MgO has a beneficial effect on the particle size of Au for alumina-supported gold catalysts [11, 12]. This thesis presents a more detailed study of the effect of various additives on the structure and catalytic performance of gold-based catalysts. The additives added to Au/Al<sub>2</sub>O<sub>3</sub> may be classified as follows:

- i) alkali (earth) metal oxides, for example: Li<sub>2</sub>O, Rb<sub>2</sub>O, MgO and BaO;
- ii) transition metal oxides, TMO (MnO<sub>x</sub>, CoO<sub>x</sub>, FeO<sub>x</sub>, TiO<sub>2</sub>, NiO, CrO<sub>x</sub>, ZrO<sub>x</sub>, V<sub>2</sub>O<sub>5</sub>, Y<sub>2</sub>O<sub>3</sub>), ZnO, ceria (CeO<sub>x</sub>) and copper oxide (CuO);
- iii) two different metal oxides, for example alkali(earth) metal oxide + ceria or TMO + ceria.

Unless otherwise specified, the intended Au loading was 5 wt-%. Concerning the loading of various MO<sub>x</sub> used as additives, the atomic ratios used were M:Al = 1:15 and M<sup>I</sup>:M<sup>II</sup>:Al = 1:1:15 (see also *Chapter 3*). The characterization results will be discussed according to the type of additives or their combination.

##### *Alkali (earth) metal oxides as additives*

Following the addition of the alkali (earth) metal oxides to  $\gamma$ -Al<sub>2</sub>O<sub>3</sub>, and then gold deposition, the gold loading varies between 3.5 wt-% (Au/Rb<sub>2</sub>O/Al<sub>2</sub>O<sub>3</sub>) and 4.2 wt-% (Au/MgO/Al<sub>2</sub>O<sub>3</sub>). A summary of the obtained results for the promoted Au/MO<sub>x</sub>/Al<sub>2</sub>O<sub>3</sub> (M: Li, Rb, Mg and Ba) is presented in Table 4.1.

Regarding the BET surface area, the measurements show a rather broad variation in between the limits of 224 m<sup>2</sup>g<sup>-1</sup> (Au/MgO/Al<sub>2</sub>O<sub>3</sub>) and 294 m<sup>2</sup>g<sup>-1</sup> (Au/Rb<sub>2</sub>O/Al<sub>2</sub>O<sub>3</sub>). It is possible that during the vacuum impregnation step, the promoter has blocked some of the Al<sub>2</sub>O<sub>3</sub> pores resulting in a slight decrease in S<sub>BET</sub>, compared with the support. Interestingly, the addition of Rb<sub>2</sub>O resulted in an increase of the BET surface area of the bare support. Possibly, the rubidium nitrate has changed (i.e. expanded) the structure of alumina during the

impregnation. The summary of all the results concerning the BET surface area is presented in Table 4.1.

A comparison of the XRD patterns of Au/Al<sub>2</sub>O<sub>3</sub>, Au/Li<sub>2</sub>O/Al<sub>2</sub>O<sub>3</sub> and Au/MgO/Al<sub>2</sub>O<sub>3</sub> is presented in Fig. 4.5. The shape of the line at  $2\theta = 38.2^\circ$  differs significantly between the samples. This sharpest line found for Au/Al<sub>2</sub>O<sub>3</sub> (large gold particles) becomes broader (smaller gold particles) in the presence of MgO or Li<sub>2</sub>O.

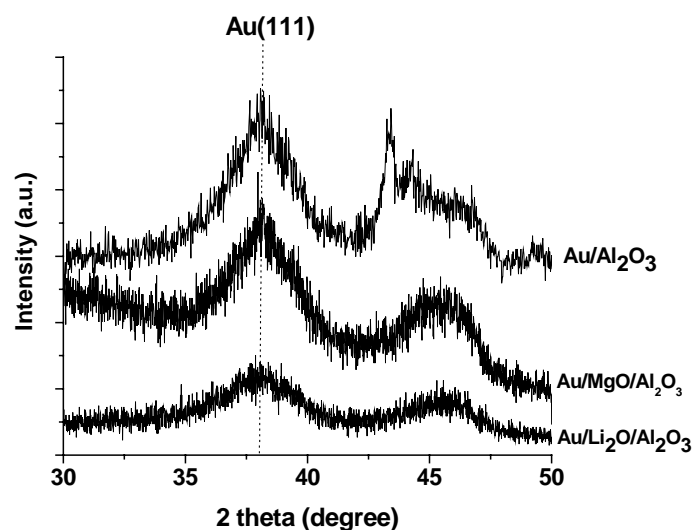


**Figure 4.5:** The influence of Li<sub>2</sub>O and MgO on the gold particle size of Au/Al<sub>2</sub>O<sub>3</sub>.

The results concerning the average gold particle size of the gold-based catalysts with alkali (earth) metal oxides as additives are summarized in Table 4.1. In addition, where possible, the metallic surface area of gold was estimated based on the equations described in Chapter 3.

**Table 4.1:** Catalysts characterization by means of AAS, BET, XRD and HRTEM

Catalyst	Au, (wt-%)	S <sub>BET</sub> (m <sup>2</sup> g <sup>-1</sup> )	d <sub>Au</sub> <sup>a</sup> (nm)	S <sub>Au</sub> <sup>a</sup> (m <sup>2</sup> g <sup>-1</sup> )	d <sub>Au</sub> <sup>b</sup> (nm)	S <sub>Au</sub> <sup>b</sup> (m <sup>2</sup> g <sup>-1</sup> )	D <sub>Au</sub> (%)
Al <sub>2</sub> O <sub>3</sub>	–	275±5	–	–	–	–	–
Au/Al <sub>2</sub> O <sub>3</sub>	4.1±0.1	260±5	4.3±0.1	2.4±0.2	5.2±0.3	1.5±0.3	11.5±1.1
Au/Li <sub>2</sub> O/Al <sub>2</sub> O <sub>3</sub>	4.0±0.3	278±7	3.2±0.1	3.0±0.4	3.0±0.1	2.5±0.1	19±1.0
Au/Rb <sub>2</sub> O/Al <sub>2</sub> O <sub>3</sub>	3.5±0.1	294±3	<3.0	–	2.6±0.3	3.6±0.3	33±1.1
Au/MgO/Al <sub>2</sub> O <sub>3</sub>	4.2±0.1	224±10	4.0±0.1	2.6±0.3	n.m.	–	–
Au/BaO/Al <sub>2</sub> O <sub>3</sub>	3.6±0.2	240±8	<3.0	–	1.5±0.2	6.2±0.02	55±1.2

d<sub>Au</sub><sup>a</sup>: mean diameter of gold particles, XRD, fresh catalysts (nm); d<sub>Au</sub><sup>b</sup>: mean diameter of gold particles, HRTEM, fresh catalysts (nm); S<sub>Au</sub><sup>a</sup>: gold surface area, XRD (m<sup>2</sup>g<sup>-1</sup>); S<sub>Au</sub><sup>b</sup>: gold surface area, HRTEM (m<sup>2</sup>g<sup>-1</sup>); D<sub>Au</sub>: gold dispersion, HRTEM; n.m.: not measured.

XRD was not always able to detect the gold signal, i.e. when very small gold crystallites or amorphous phases are present (Au/BaO/Al<sub>2</sub>O<sub>3</sub> and Au/Rb<sub>2</sub>O/Al<sub>2</sub>O<sub>3</sub>). Comparing the values

of  $d_{Au}^a$  (Table 4.1) it is clear that the presence of the alkali (earth) metal oxides has a beneficial effect on the stabilization of the small Au crystallites. However, it appears that this beneficial effect is connected with the oxide identity, since the effect of MgO for example, was modest, compared with the effect of BaO or Rb<sub>2</sub>O.

The loading of the oxidic additives was probably rather low to obtain large crystallites and for this reason XRD did not identify their presence.

The corresponding gold surface area, calculated according to (3.5), changes as a function of the additive, from 2.6 m<sup>2</sup>g<sup>-1</sup> (Au/MgO/Al<sub>2</sub>O<sub>3</sub>) to 3.3 m<sup>2</sup>g<sup>-1</sup> (Au/Li<sub>2</sub>O/Al<sub>2</sub>O<sub>3</sub>). The metallic surface area of Au/Al<sub>2</sub>O<sub>3</sub> is slightly smaller, 2.4 m<sup>2</sup>g<sup>-1</sup>.

HRTEM detected for Au/Rb<sub>2</sub>O/Al<sub>2</sub>O<sub>3</sub> and Au/BaO/Al<sub>2</sub>O<sub>3</sub> very small Au particles (below 3.0 nm) - Table 4.1. The Au particle size distribution of Au/Al<sub>2</sub>O<sub>3</sub>, Au/Rb<sub>2</sub>O/Al<sub>2</sub>O<sub>3</sub> and Au/BaO/Al<sub>2</sub>O<sub>3</sub> is presented in Figure 4.6.

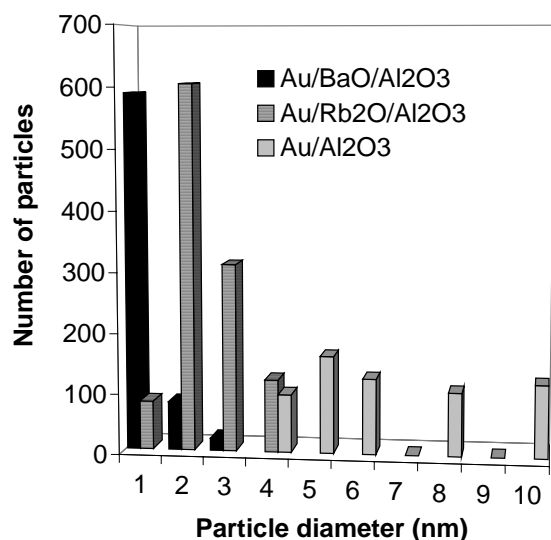


**Figure 4.6:** Particle size distribution as determined by HRTEM for Au/Al<sub>2</sub>O<sub>3</sub>, Au/Rb<sub>2</sub>O/Al<sub>2</sub>O<sub>3</sub> and Au/BaO/Al<sub>2</sub>O<sub>3</sub>.

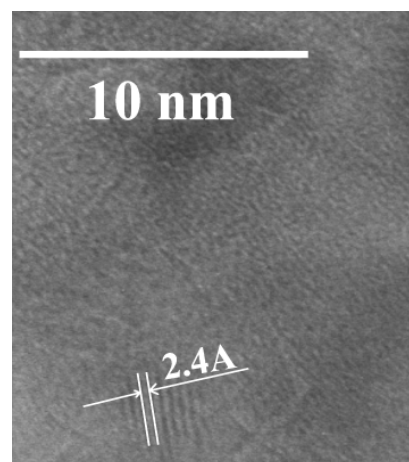


**Figure 4.7:** HRTEM micrograph of Au/Rb<sub>2</sub>O/Al<sub>2</sub>O<sub>3</sub>.

At least 500 particles were counted to estimate the distribution of the gold particles. There is a significant difference concerning the particle size distribution of the samples with or without additive. The growth of the large gold particles at the expense of the smaller Au crystallites found for Au/Al<sub>2</sub>O<sub>3</sub> is prevented in the presence of alkali (earth) metal oxides.

A sufficiently high resolution was achieved by HRTEM such that the lattice spacing of Au for Au/Rb<sub>2</sub>O/Al<sub>2</sub>O<sub>3</sub> could be measured. The corresponding HRTEM micrograph is shown in Figure 4.7 and the lattice spacing measured is 2.4 Å. This is, within experimental error, the (111) reflection of metallic gold (JCPDS powder diffraction data base reports 2.36 Å [13]).

The metallic surface area (HRTEM) varies between 1.5 m<sup>2</sup>g<sup>-1</sup> (Au/Al<sub>2</sub>O<sub>3</sub>) and 6.2 m<sup>2</sup>g<sup>-1</sup> (Au/BaO/Al<sub>2</sub>O<sub>3</sub>). The differences between the values of the gold surface area determined by HRTEM and XRD may be related to the experimental limitations of each technique.

However, it should be emphasized that both techniques are not really suitable for this type of determinations and that the results may be considered only as a relative measure of the metallic surface area of the catalysts. A dispersion of 55% was calculated for Au/BaO/Al<sub>2</sub>O<sub>3</sub>, which considerably exceeds the estimated dispersion of Au/Al<sub>2</sub>O<sub>3</sub> (11.5%).

### **Transition metal oxides (TMO), Ceria, ZnO and CuO as additives**

Table 4.2 summarizes the gold loading, the average size of gold particles as determined by XRD and HRTEM measurements, as well as the total and metallic surface area of the catalysts that contain various transition metal oxides, ceria and copper oxide as additives. The gold dispersion is also shown in Table 4.2.

The gold loading, as summarized in Table 4.2, is higher than 4%-wt for all the catalysts, with one exception: Au/ZrO<sub>2</sub>/Al<sub>2</sub>O<sub>3</sub> (3.2 wt-% Au). The CuO-containing gold-based catalysts were prepared using different Au and CuO concentrations: 4 wt-% Au and 6 wt-% CuO (Au/CuO/Al<sub>2</sub>O<sub>3</sub>-A) and 7.4 wt-% Au and 12 wt-% CuO (Au/CuO/Al<sub>2</sub>O<sub>3</sub>-B).

In all cases, the BET surface area is above 200 m<sup>2</sup>g<sup>-1</sup> for all samples. However, a decrease of the total surface area to 207 m<sup>2</sup>g<sup>-1</sup> (Au/CoO<sub>x</sub>/Al<sub>2</sub>O<sub>3</sub>) or 212 m<sup>2</sup>g<sup>-1</sup> (Au/CuO/Al<sub>2</sub>O<sub>3</sub>-B) was also found. Similarly to the previous results, it is possible that the additives block some of the Al<sub>2</sub>O<sub>3</sub> pores during the vacuum impregnation step, resulting in a decrease of S<sub>BET</sub>.

**Table 4.2:** Catalysts characterization by means of AAS, BET, XRD and HRTEM

Catalyst	Au (wt-%)	S <sub>BET</sub> (m <sup>2</sup> g <sup>-1</sup> )	d <sub>Au</sub> <sup>a</sup> (nm)	S <sub>Au</sub> <sup>a</sup> (m <sup>2</sup> g <sup>-1</sup> )	d <sub>Au</sub> <sup>b</sup> (nm)	S <sub>Au</sub> <sup>b</sup> (m <sup>2</sup> g <sup>-1</sup> )	D <sub>Au</sub> (%)
Au/Al <sub>2</sub> O <sub>3</sub>	4.1±0.1	260±5	4.3±0.1	2.4±0.2	5.2±0.3	1.5±0.3	11.5±1.1
Au/CeO <sub>x</sub> /Al <sub>2</sub> O <sub>3</sub>	4.5±0.1	218±11	<3.0	—	1.7±0.2	7.1±0.2	52±1.3
Au/CoO <sub>x</sub> /Al <sub>2</sub> O <sub>3</sub>	4.3±0.2	207±8	5.0±0.1	2.2±0.1	8.0±0.1	2.2±0.1	8±0.7
Au/MnO <sub>x</sub> /Al <sub>2</sub> O <sub>3</sub>	4.3±0.4	222±12	8.0±0.1	1.4±0.1	4.9±0.3	1.4±0.3	20±1
Au/FeO <sub>x</sub> /Al <sub>2</sub> O <sub>3</sub>	4.4±0.1	234±7	<3.0	—	n.m.	—	—
Au/TiO <sub>2</sub> /Al <sub>2</sub> O <sub>3</sub>	4.7±0.3	243±9	<3.0	—	n.m.	—	—
Au/ZrO <sub>2</sub> /Al <sub>2</sub> O <sub>3</sub>	3.2±0.1	270±13	3.1±0.3	2.7±0.3	n.m.	—	—
Au/CuO/Al <sub>2</sub> O <sub>3</sub> -A	4.0±0.3	253±15	3.0±0.1	2.7±0.1	2.3±0.2	3.6±0.2	30±1.2
Au/CuO/Al <sub>2</sub> O <sub>3</sub> -B	7.4±0.3	212±7	6.8±0.2	2.7±0.2	n.m.	—	—

d<sub>Au</sub><sup>a</sup>: mean diameter of gold particles, XRD, fresh catalysts (nm); d<sub>Au</sub><sup>b</sup>: mean diameter of gold particles, HRTEM, fresh catalysts (nm); S<sub>Au</sub><sup>a</sup>: gold surface area, XRD (m<sup>2</sup>g<sup>-1</sup>); S<sub>Au</sub><sup>b</sup>: gold surface area, HRTEM (m<sup>2</sup>g<sup>-1</sup>); D<sub>Au</sub>: gold dispersion, HRTEM; n.m.: not measured.

The XRD results for the as-prepared supported gold catalysts (Table 4.2) show a relatively large variation in the size of the gold particles. As in the case of alkali (earth) metal oxides as additives, the various MO<sub>x</sub> affect the growth of the gold particles during the heat treatment in a different way. Some of the catalysts (Au/CeO<sub>x</sub>/Al<sub>2</sub>O<sub>3</sub>, Au/FeO<sub>x</sub>/Al<sub>2</sub>O<sub>3</sub> and Au/TiO<sub>2</sub>/Al<sub>2</sub>O<sub>3</sub>) displayed very small gold particles, below the detection limit of the technique. On the other hand, relatively large gold particles have been measured for Au/MnO<sub>x</sub>/Al<sub>2</sub>O<sub>3</sub>, Au/CuO/Al<sub>2</sub>O<sub>3</sub>-B and Au/CoO<sub>x</sub>/Al<sub>2</sub>O<sub>3</sub>. It is possible, however, that these catalysts also contain very small gold crystallites, below the XRD detection limit (~3 nm). Supplementary HRTEM measurements should clarify this point. In addition, no diffraction

lines of  $\text{Au}_2\text{O}_3$  or  $\text{Au}_2\text{O}$  were found for all these gold-based catalysts. As mentioned before, the loading of the additives is relatively low and their state is rather amorphous, but some of them were identified by XRD ( $\text{CeO}_2$ ,  $\text{CuO}$ ,  $\text{MnO}_2$ ).

The XRD of  $\text{Au}/\text{CuO}/\text{Al}_2\text{O}_3\text{-A}$ ,  $\text{Au}/\text{CuO}/\text{Al}_2\text{O}_3\text{-B}$  and the corresponding supports are shown in Fig. 4.8. For comparison, the diffraction pattern of  $\text{CuO}$  is also presented. The main diffraction lines of bulk  $\text{CuO}$  appear at  $2\theta = 35.2^\circ$  ( $d = 2.52 \text{ \AA}$ ) and  $38.1^\circ$  ( $d = 2.32 \text{ \AA}$ ). The formation of the crystalline  $\text{CuO}$  phase is detected by XRD for  $\text{CuO}/\text{Al}_2\text{O}_3\text{-B}$  and  $\text{Au}/\text{CuO}/\text{Al}_2\text{O}_3\text{-B}$ .

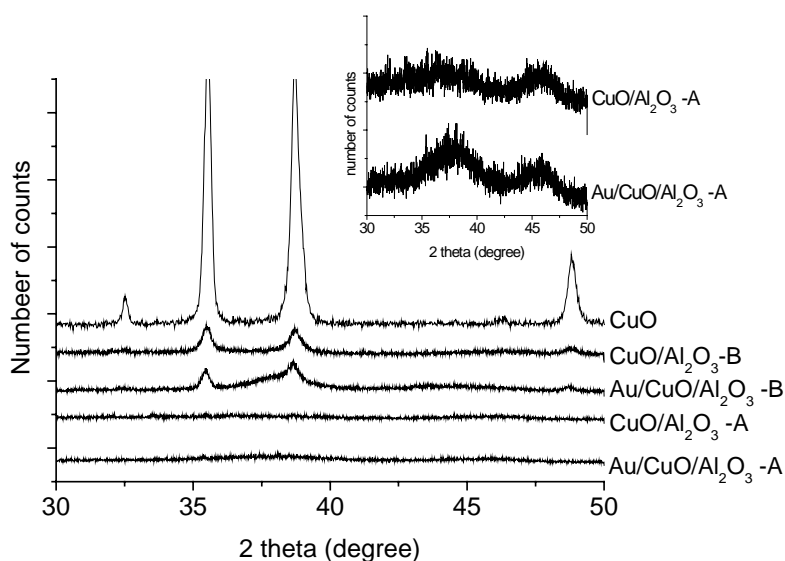


**Figure 4.8:** XRD patterns of  $\text{CuO}$ ,  $\text{Au}/\text{CuO}/\text{Al}_2\text{O}_3\text{-A}$ ,  $\text{Au}/\text{CuO}/\text{Al}_2\text{O}_3\text{-B}$  and the corresponding supports.

The XRD patterns of  $\text{Au}/\text{CuO}/\text{Al}_2\text{O}_3\text{-A}$  and  $\text{CuO}/\text{Al}_2\text{O}_3\text{-A}$  are shown in detail in the inset of the Fig. 4.8. The pattern of crystalline  $\text{CuO}$  is hardly visible for  $\text{CuO}/\text{Al}_2\text{O}_3\text{-A}$  and the peak intensity of  $2\theta = 38.2^\circ$  increases after gold deposition ( $\text{Au}/\text{CuO}/\text{Al}_2\text{O}_3\text{-A}$ ).

The average gold particle size of  $\text{Au}/\text{CuO}/\text{Al}_2\text{O}_3\text{-B}$  as determined by XRD is around 6.8 nm. Possibly, the mean diameter of Au particles is overestimated due to the overlap of  $\text{CuO}$  and Au signals at  $2\theta = 38.2^\circ$ , and, hence, the real size of Au particles in  $\text{Au}/\text{CuO}/\text{Al}_2\text{O}_3\text{-B}$  may be smaller than 6.8 nm. However, it is expected that at high Au loading, larger Au particles are formed. It should be mentioned that  $\text{Cu}^0$  and  $\text{Cu}^+$  have not been detected by any technique employed (i.e. XRD, DR/UV-Vis, XPS), neither in  $\text{Au}/\text{CuO}/\text{Al}_2\text{O}_3$ , nor in  $\text{CuO}/\text{Al}_2\text{O}_3$ .

The Au surface area (XRD) varies between  $1.4 \text{ m}^2\text{g}^{-1}$  ( $\text{Au}/\text{MnO}_x/\text{Al}_2\text{O}_3$ ) and  $2.7 \text{ m}^2\text{g}^{-1}$  ( $\text{Au}/\text{ZrO}_2/\text{Al}_2\text{O}_3$  and  $\text{CuO}$ -containing gold-based catalysts).

Very small gold particles have been detected for  $\text{Au}/\text{CeO}_x/\text{Al}_2\text{O}_3$  and  $\text{Au}/\text{CuO}/\text{Al}_2\text{O}_3\text{-A}$  by means of HRTEM (Table 4.2), whilst larger particles were found for  $\text{Au}/\text{MnO}_x/\text{Al}_2\text{O}_3$  (5 nm). Occasionally, the lattice parameter of the  $\text{MO}_x$  could be detected. For example, for  $\text{Au}/\text{CeO}_x/\text{Al}_2\text{O}_3$  catalyst, it was possible to measure the lattice parameter of the oxidic phase

present and to identify the  $\text{CeO}_2$  present. A HRTEM micrograph is displayed in Figure 4.9A. As visible in Figs. 4.9A-B, the gold nanoparticles are mainly located on the crystalline ceria (visible as dark grey patches in the Figs. 4.9A-B) and to a lesser extent on alumina. The second HRTEM micrograph of  $\text{Au/CeO}_x/\text{Al}_2\text{O}_3$  presented in Figure 4.9B shows a measured lattice spacing of Au of 2.76 Å that corresponds to the (111) reflection.

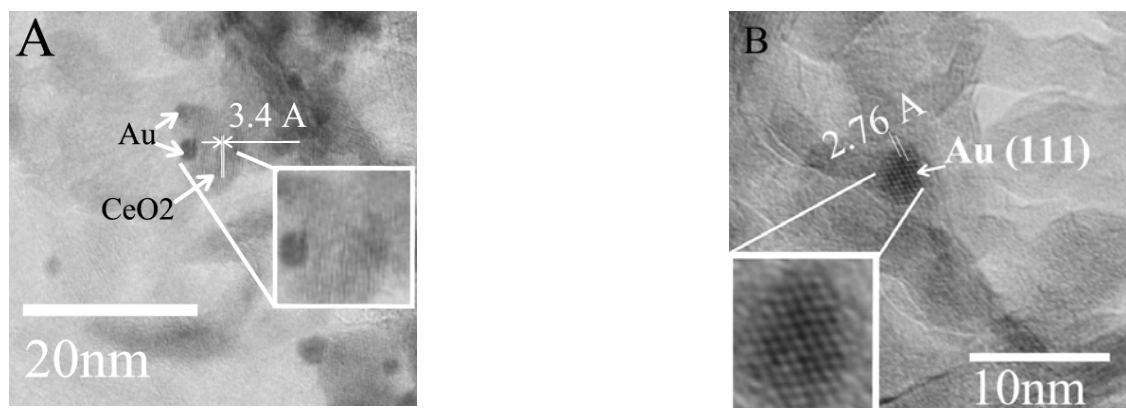


**Figure 4.9:** HRTEM micrographs of  $\text{Au/CeO}_x/\text{Al}_2\text{O}_3$ : (A) illustrates the lattice parameter of  $\text{CeO}_2$  and the arrangement of Au particles, (B) shows the lattice parameter of Au (black dots represent Au particles, dark grey patches:  $\text{CeO}_2$  and light grey regions: alumina).

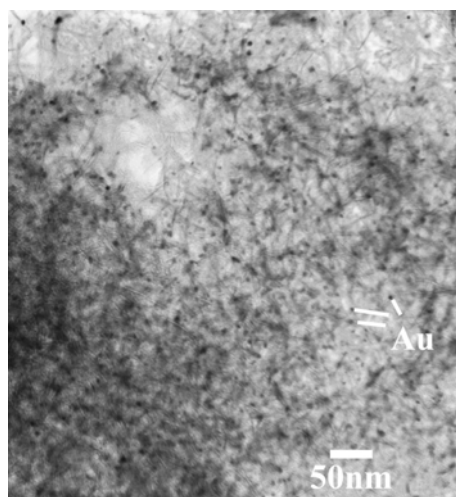


**Figure 4.10:** HRTEM micrograph of  $\text{Au/MnO}_x/\text{Al}_2\text{O}_3$ .

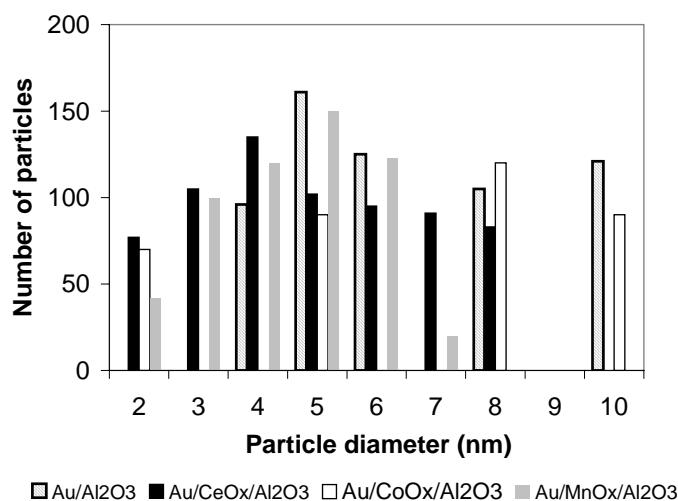


**Figure 4.11:** Au particle size distribution for various gold-based catalysts (HRTEM).

The HRTEM micrograph of  $\text{Au/MnO}_x/\text{Al}_2\text{O}_3$  is presented in Figure 4.10. A lot of small gold particles are visible (black dots), homogeneously distributed over the support. However, the Au particles are larger than what was visualized for  $\text{Au/CeO}_x/\text{Al}_2\text{O}_3$ . Figure 4.11

illustrates the Au particle size distribution of several supported gold catalysts, based on HRTEM. Whereas the gold particles on Au/CeO<sub>x</sub>/Al<sub>2</sub>O<sub>3</sub> are mainly below 5nm, the other gold-based catalysts display a much broader particle size distribution. It appears that ceria influences both the size of the gold nano-crystallites and their distribution.

The largest metallic gold surface area calculated from the HRTEM measurements was found for Au/CeO<sub>x</sub>/Al<sub>2</sub>O<sub>3</sub>: 7.1 m<sup>2</sup>g<sup>-1</sup>. For the other samples, the metallic surface area is much smaller. As expected, the highest dispersion corresponds to Au/CeO<sub>x</sub>/Al<sub>2</sub>O<sub>3</sub>, 52%.

The macroscopic structure of this class of catalysts as followed by SEM is not significantly changed by the presence of additives. A SEM picture of Au/CeO<sub>x</sub>/Al<sub>2</sub>O<sub>3</sub> is presented in Figure 4.12.

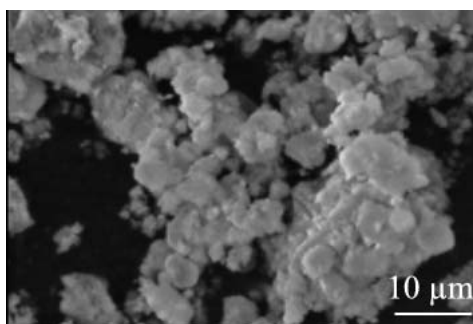


**Figure 4.12:** SEM picture of Au/CeO<sub>x</sub>/Al<sub>2</sub>O<sub>3</sub>.

#### ***Multicomponent gold-based catalysts Au/M<sup>I</sup>O<sub>x</sub>/M<sup>II</sup>O<sub>x</sub>/Al<sub>2</sub>O<sub>3</sub>***

As previously discussed, the addition of alkali (earth) metal oxides produced very small gold particles, with a relatively narrow distribution of the gold nanocrystallites. On the other hand, the role of TMO, ceria or CuO is believed to be more than that of a structural promoter due to their intrinsic catalytic activities for various reactions, including hydrocarbon oxidation. The effect of the presence of two different oxides as additives on the catalytic performance of gold-based catalysts has not been studied in detail and only a few combinations have been investigated [11, 14]. Accordingly, previously described results present the synergy obtained after combining MgO with MnO or FeO<sub>x</sub>. First, the support was modified by MgO, since this oxide was found efficient in stabilization of small gold particles. Subsequently, gold was deposited on MgO/Al<sub>2</sub>O<sub>3</sub> via HDP with urea. Finally, iron nitrate or manganese nitrate were added via impregnation, such that the final composition of the catalysts was either FeO<sub>x</sub>/Au/MnO<sub>x</sub>/Al<sub>2</sub>O<sub>3</sub>, or MnO<sub>x</sub>/Au/MgO/Al<sub>2</sub>O<sub>3</sub> [11, 14]. The catalysts have been successfully tested in preferential oxidation of CO in the presence of hydrogen [11, 14].

Based on the results presented above, other combinations of metal oxides were studied as mixed supports for gold catalysts. In general, one of the additives was ceria. This choice is based on its properties, such as its high oxygen storage capacity, which makes this oxide valuable in total oxidation reactions, and also its stabilization effect on carriers such as alumina [15-17]. The second additive used was either an alkali (earth) metal oxide (Li<sub>2</sub>O, Rb<sub>2</sub>O, MgO or BaO) or a TMO (ZrO<sub>2</sub> or Y<sub>2</sub>O<sub>3</sub>). In addition, two other catalysts have been



prepared: one contains  $\text{CoO}_x$  and  $\text{Li}_2\text{O}$ , whilst the other consists of  $\text{MnO}_x$  and  $\text{MgO}$  (for the purpose of comparison with the previously reported work [11, 14]). The aim was to examine whether the presence of two different oxides (one – presumably acting as a structural promoter and the other one – as a structural and chemical promoter) is able to produce a synergistic effect and to enhance the catalytic performance of gold.

Table 4.3 summarizes the physical characteristics of the multicomponent gold-based catalysts. The information correlates the gold loading, the average gold particle size (XRD and HRTEM) and the metallic surface area (XRD and HRTEM).

**Table 4.3:** Physico-chemical characterization of  $\text{Au}/\text{M}^{\text{I}}\text{O}_x/\text{M}^{\text{II}}\text{O}_x/\text{Al}_2\text{O}_3$ .

Catalyst	Au, (wt-%)	$S_{\text{BET}}$ ( $\text{m}^2\text{g}^{-1}$ )	$d_{\text{Au}}^{\text{a}}$ (nm)	$S_{\text{Au}}^{\text{a}}$ ( $\text{m}^2\text{g}^{-1}$ )	$d_{\text{Au}}^{\text{b}}$ (nm)	$S_{\text{Au}}^{\text{b}}$ ( $\text{m}^2\text{g}^{-1}$ )	$D_{\text{Au}}$ (%)
$\text{Au}/\text{Li}_2\text{O}/\text{CeO}_x/\text{Al}_2\text{O}_3$	$4.6\pm 0.2$	$262\pm 10$	$<3.0$	–	$2.9\pm 0.1$	$3.8\pm 0.1$	$27\pm 5$
$\text{Au}/\text{Rb}_2\text{O}/\text{CeO}_x/\text{Al}_2\text{O}_3$	$4.5\pm 0.3$	$275\pm 7$	$<3.0$	–	$2.8\pm 0.2$	$2.6\pm 0.2$	$20\pm 4$
$\text{Au}/\text{CoO}_x/\text{Li}_2\text{O}/\text{Al}_2\text{O}_3$	$4.6\pm 0.1$	$247\pm 11$	$<3.0$	–	n.m.	–	–
$\text{Au}/\text{MnO}_x/\text{MgO}/\text{Al}_2\text{O}_3$	$4.5\pm 0.2$	$265\pm 15$	$<3.0$	–	$3.9\pm 0.3$	$2.1\pm 0.3$	$15\pm 4$
$\text{Au}/\text{ZrO}_2/\text{CeO}_x/\text{Al}_2\text{O}_3$	$3.2\pm 0.1$	$251\pm 9$	$<3.0$	–	$6.6\pm 0.1$	$1.2\pm 0.1$	$12\pm 5$
$\text{Au}/\text{Y}_2\text{O}_3/\text{CeO}_x/\text{Al}_2\text{O}_3$	$4.3\pm 0.4$	$249\pm 11$	$<3.0$	–	$1.6\pm 0.2$	$5.6\pm 0.2$	$40\pm 7$
$\text{Au}/\text{BaO}/\text{CeO}_x/\text{Al}_2\text{O}_3$	$4.4\pm 0.2$	$259\pm 7$	$<3.0$	–	$3.3\pm 0.1$	$3\pm 0.1$	$23\pm 5$

$d_{\text{Au}}^{\text{a}}$ : mean diameter of gold particles, XRD, fresh catalysts (nm);  $d_{\text{Au}}^{\text{b}}$ : mean diameter of gold particles, HRTEM, fresh catalysts (nm);  $S_{\text{Au}}^{\text{a}}$ : gold surface area, XRD ( $\text{m}^2\text{g}^{-1}$ );  $S_{\text{Au}}^{\text{b}}$ : gold surface area, HRTEM ( $\text{m}^2\text{g}^{-1}$ );  $D_{\text{Au}}$ : gold dispersion, HRTEM; n.m.: not measured.

The degree of gold deposition onto the mixed support  $\text{M}^{\text{I}}\text{O}_x/\text{M}^{\text{II}}\text{O}_x/\text{Al}_2\text{O}_3$  is rather high. In general, a much higher  $S_{\text{BET}}$  was found for all these multicomponent catalysts.

Interestingly, XRD was not able to detect any gold signal for all the catalysts. The very small size of the gold particles leads to a very broad signal at  $2\theta = 38.2^\circ$  and an estimate of the metallic surface area based on XRD measurements was not possible. A comparison of the XRD patterns of various gold-based catalysts is presented in Figure 4.13.

After the addition of ceria, the average gold particle decreases, as compared with the reference ( $\text{Au}/\text{Al}_2\text{O}_3$ ). A similar situation is found when  $\text{Li}_2\text{O}$  is added. However, for the multicomponent catalyst  $\text{Au}/\text{Li}_2\text{O}/\text{CeO}_x/\text{Al}_2\text{O}_3$ , the region where the gold signal can be found becomes even broader.

The XRD patterns of the other oxides were not identified, except for  $\text{CeO}_x$  and  $\text{MnO}_x$  ( $x = 2$ ). However, the presence of cerium oxide and manganese oxide with  $x < 2$  cannot be excluded. For the rest of the samples, the  $\text{MO}_x$  crystallites are either too small for detection, or  $\text{MO}_x$  is in an amorphous state.

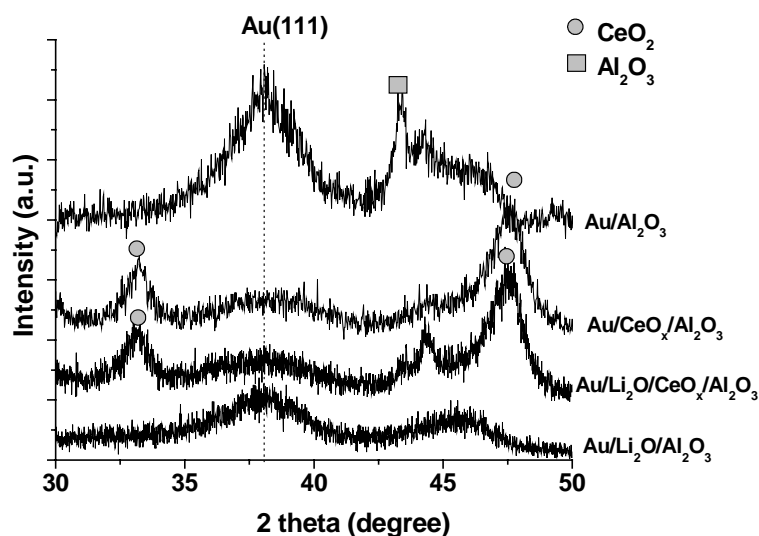


**Figure 4.13:** XRD patterns of Au/Al<sub>2</sub>O<sub>3</sub>, Au/Li<sub>2</sub>O/Al<sub>2</sub>O<sub>3</sub>, Au/CeO<sub>x</sub>/Al<sub>2</sub>O<sub>3</sub> and Au/Li<sub>2</sub>O/CeO<sub>x</sub>/Al<sub>2</sub>O<sub>3</sub>. In addition to the diffraction peak of gold, the diffraction patterns of ceria (circle) and alumina (square) are shown.

According to the HRTEM results, the average size of the gold particles was around 3.8 nm for Au/MnO<sub>x</sub>/MgO/Al<sub>2</sub>O<sub>3</sub>, and 3.3 nm for Au/BaO/CeO<sub>x</sub>/Al<sub>2</sub>O<sub>3</sub>. It was interesting to observe that for Au/BaO/CeO<sub>x</sub>/Al<sub>2</sub>O<sub>3</sub> many gold particles are not spherical but rather truncated. An illustration of different shapes of gold particles in Au/BaO/CeO<sub>x</sub>/Al<sub>2</sub>O<sub>3</sub> is shown in Figs. 4.14A-B. Figure 4.14B shows a HRTEM picture of the same catalyst where the lattice spacing of gold for two different particles could be measured.

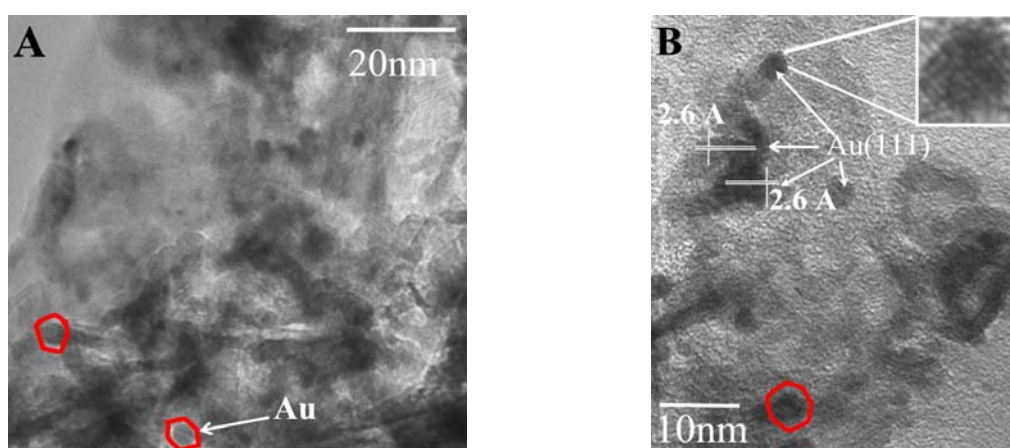


**Figure 4.14:** HRTEM photographs of Au/BaO/CeO<sub>x</sub>/Al<sub>2</sub>O<sub>3</sub>: (A) different shapes of gold particles and (B) lattice spacing of two gold particles, determined as 2.6Å.

Very small gold particles, uniformly distributed over the support have also been found for Au/Y<sub>2</sub>O<sub>3</sub>/CeO<sub>x</sub>/Al<sub>2</sub>O<sub>3</sub>. Figure 4.15 shows one of the HRTEM micrographs of Au/Y<sub>2</sub>O<sub>3</sub>/CeO<sub>x</sub>/Al<sub>2</sub>O<sub>3</sub> and the measured lattice spacing is 2.3 Å.

A summary of the particle size distribution of different gold-based catalysts is presented in Figure 4.16. The beneficial effects of different oxides on both the size and the distribution of the gold particles are clearly represented in the figure.

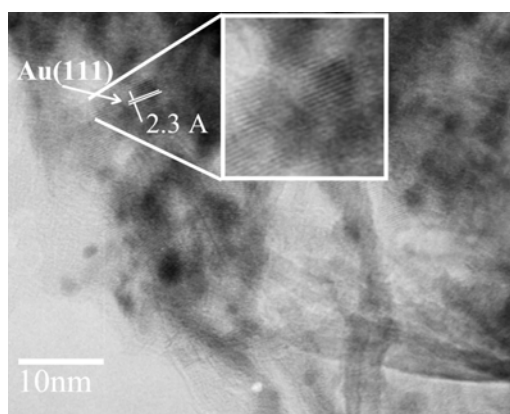


**Figure 4.15:** HRTEM micrograph of Au/Y<sub>2</sub>O<sub>3</sub>/CeO<sub>x</sub>/Al<sub>2</sub>O<sub>3</sub>.

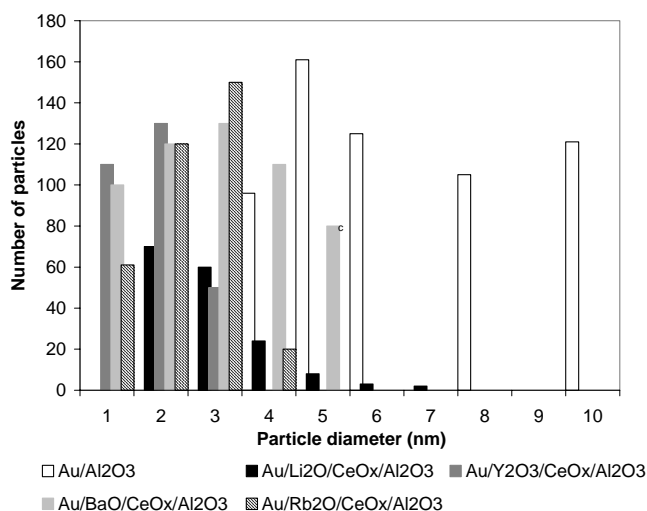


**Figure 4.16:** Particle size distribution (HRTEM).

The metallic surface area (Table 4.3) varies between 1.2 m<sup>2</sup>g<sup>-1</sup> (Au/CeO<sub>x</sub>/ZrO<sub>2</sub>/Al<sub>2</sub>O<sub>3</sub>) and 5.6 m<sup>2</sup>g<sup>-1</sup> (Au/Y<sub>2</sub>O<sub>3</sub>/CeO<sub>x</sub>/Al<sub>2</sub>O<sub>3</sub>). Accordingly, the dispersion lies between 12% (Au/CeO<sub>x</sub>/ZrO<sub>2</sub>/Al<sub>2</sub>O<sub>3</sub>) and 40% (Au/Y<sub>2</sub>O<sub>3</sub>/CeO<sub>x</sub>/Al<sub>2</sub>O<sub>3</sub>). Hence, a combination that includes ceria and an alkali earth metal oxide (i.e. BaO) is the most efficient to manufacture nano-sized gold, highly dispersed on the support. In fact, it is possible that the effect of ceria predominates over that of the alkali (earth) metal oxides. This is also reflected on the variation of S<sub>Au</sub> (7.1 m<sup>2</sup>g<sup>-1</sup>) and D<sub>Au</sub> (52%) for Au/CeO<sub>x</sub>/Al<sub>2</sub>O<sub>3</sub>. Also other combinations that contain ceria are rather efficient (Table 4.3), but if ceria is replaced by MnO<sub>x</sub> or CoO<sub>x</sub>, the overall effect is less pronounced.

An illustration of the structure of Au/Rb<sub>2</sub>O/CeO<sub>x</sub>/Al<sub>2</sub>O<sub>3</sub> as determined by SEM, is presented in Figure 4.17. The structure of the multicomponent catalyst resembles the structure of γ-Al<sub>2</sub>O<sub>3</sub>.

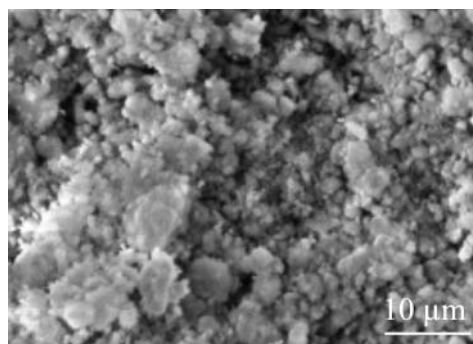


**Figure 4.17:** SEM picture of Au/Rb<sub>2</sub>O/CeO<sub>x</sub>/Al<sub>2</sub>O<sub>3</sub>.

### 4.3 Diffuse-reflectance ultra-violet measurements, DR/UV-Vis

Metal nanoparticles have optical properties that are absent in the bulk material as well as for the individual atoms. These optical properties are determined by both their size and shape [18]. Their origin is attributed to the collective oscillation of the free conduction electrons induced by an interacting electromagnetic field. These resonances are also denoted as surface plasmons and are observed when the wavelength of the incident light far exceeds the particle diameter.

Because the surface plasmon resonance is distinct for each (noble) metal, optical absorption spectroscopy is well suited for a complete in-depth structural characterization of gold-based catalysts. Fine gold particles, in the nanometer range, exhibit a surface plasmon peak centered between 500 and 600 nm. The relation between the mean particle diameter, the shape of the particles and the peak position is also influenced by the dielectric function of the supporting or surrounding medium, as well as by possible particle interactions deviating from the single-particle assumption of Mie's theory [19].

Although the peak position of Au in the metallic state is generally accepted (between 500-600 nm), the peak positions of the ionic gold species are still under discussion. However, it was reported that Au<sup>+</sup> cations display an absorption band around 240 nm, whereas small clusters such as (Au)<sub>n</sub><sup>δ+</sup> exhibit a band around 390 nm [20].

Figure 4.18 presents the optical spectra of Au/Al<sub>2</sub>O<sub>3</sub> calcined at 300<sup>o</sup>C in O<sub>2</sub>, dry-Au/Al<sub>2</sub>O<sub>3</sub>, Au-sponge and Al<sub>2</sub>O<sub>3</sub>. It should be mentioned that dry-Au/Al<sub>2</sub>O<sub>3</sub>, i.e. the as-prepared catalyst, corresponds to Au<sub>2</sub>O<sub>3</sub>/Al<sub>2</sub>O<sub>3</sub>. As expected, dry-Au/Al<sub>2</sub>O<sub>3</sub> does not exhibit the plasmonic oscillation mode of nanosized gold particles, since no metallic gold is present in the sample. However, the optical spectra of dry-Au/Al<sub>2</sub>O<sub>3</sub> showed a small shoulder around 260 nm. This peak corresponds to the same wavelength as the one reported in literature for Au<sup>+</sup> [20]. On the other hand, if the optical spectrum of Au-sponge is analyzed, a similar shoulder exists too, although a little shifted to lower wavelength (240 nm) and less intense than in the case of dry-Au/Al<sub>2</sub>O<sub>3</sub>. Thus, the assignment of the peak at 260 nm to Au<sup>+</sup> appears unlikely, since Au-sponge contains only Au<sup>0</sup>. More investigations are needed to clarify the origin of this peak. For the calcined-Au/Al<sub>2</sub>O<sub>3</sub>, the typical plasmon band of small Au particles at 540 nm appears very clearly in Figure 4.18.

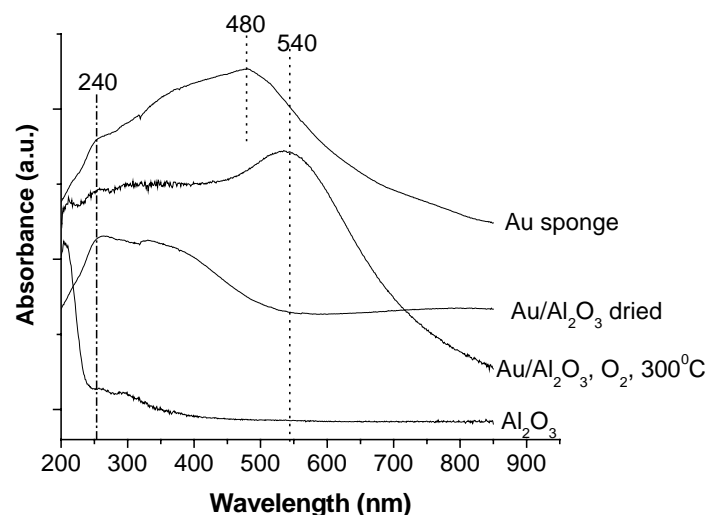


**Figure 4.18:** DR/UV-Vis spectra of calcined-Au/Al<sub>2</sub>O<sub>3</sub>, dried-Au/Al<sub>2</sub>O<sub>3</sub>, Au-sponge and Al<sub>2</sub>O<sub>3</sub> support.

The same peak but with different shape and also shifted to lower wavelength (480 nm) is visible for sponge-Au. As was mentioned before, the shape of the peak, interpreted as the full-width-at-half-maximum (FWHM) of the peak, strongly depends on the shape and the size of the gold particles. Thus, the relatively large shift, from 540 nm to 480 nm, accompanied by the variation of FWHM may be explained in terms of the huge difference in the size of gold particles of the two samples. XRD points to an average size of sponge-Au of 74 nm, while the mean diameter of Au particles for calcined-Au/Al<sub>2</sub>O<sub>3</sub> is 4.3 nm. Usually, smaller gold particles cause a red shift in the absorption peak, accompanied by a larger FWHM in the “intrinsic size region” (mean diameter smaller than 25 nm) [18]. On the other hand, it was reported that very large particles induce the opposite effect; the FWHM increases with increasing size, in the “extrinsic size region” (mean diameter larger than 25 nm). Thus, the apparent differences in optical spectra of calcined-Au/Al<sub>2</sub>O<sub>3</sub> and Au-sponge can be explained on the basis of the size effect. It is also possible that the shape of the gold particles differs significantly for the two samples, resulting in an additional optical difference.

The evolution of the optical behaviour was also used to follow the appearance of the plasmon peak for the Au/Al<sub>2</sub>O<sub>3</sub> catalyst subjected to various thermal treatments, under oxygen or hydrogen flow. Figure 4.19A presents the evolution of the plasmon peak of Au/Al<sub>2</sub>O<sub>3</sub> catalyst under the influence of O<sub>2</sub> and temperature (150<sup>0</sup>C, 200<sup>0</sup>C, 300<sup>0</sup>C and 500<sup>0</sup>C). Figure 4.19B summarizes the DR/UV-Vis spectra of Au/Al<sub>2</sub>O<sub>3</sub> treated in hydrogen at 150<sup>0</sup>C, 200<sup>0</sup>C and 300<sup>0</sup>C.

As was already discussed, dry-Au/Al<sub>2</sub>O<sub>3</sub> does not exhibit any plasmon peak in the interval 500-600 nm. Interestingly, the typical plasmon band of Au nanocrystallites appears already after a heat-treatment at 150<sup>0</sup>. Moreover, there is no particular influence of the nature of the gas on the formation of the Au<sup>0</sup>. Thus, it can be concluded that the formation of Au<sup>0</sup> proceeds already at 150<sup>0</sup>C. Of course, the extent of reduction cannot be quantified by these measurements. The results obtained by using temperature programmed reduction (TPR)

technique are presented in the next section. The small peak at 260 nm (dry-Au/Al<sub>2</sub>O<sub>3</sub>) decreases upon heating and, eventually, is weaker if H<sub>2</sub> is used. Although the evolution of this peak changes with the temperature, we still cannot conclude that this peak belongs to Au<sup>+</sup>, since Au-sponge reveals a similar feature in that region of the spectra.

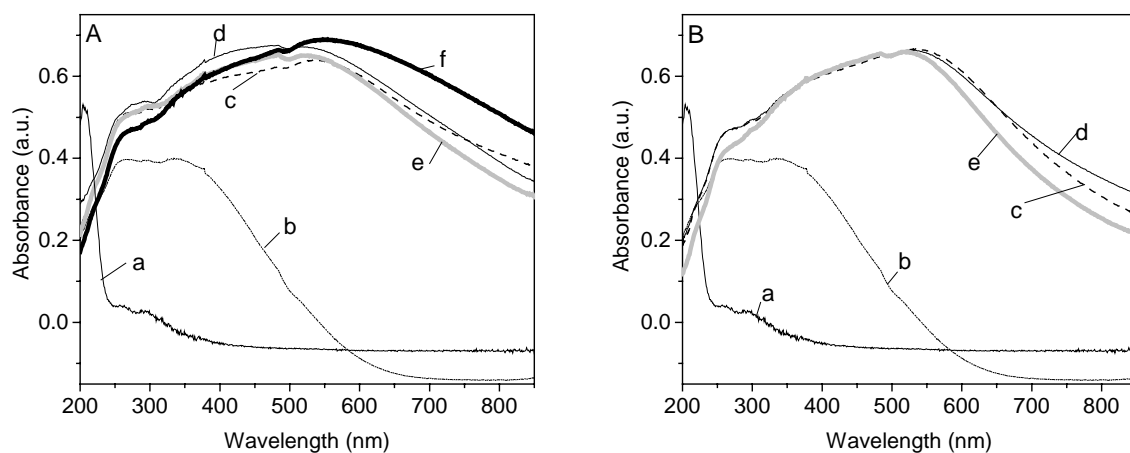


**Figure 4.19:** DR/UV-Vis spectra of samples pretreated in O<sub>2</sub> (A) and H<sub>2</sub> (B). Al<sub>2</sub>O<sub>3</sub> (a), dried-Au/Al<sub>2</sub>O<sub>3</sub> (b), Au/Al<sub>2</sub>O<sub>3</sub> 150<sup>0</sup>C (c), Au/Al<sub>2</sub>O<sub>3</sub> 200<sup>0</sup>C (d), Au/Al<sub>2</sub>O<sub>3</sub> 300<sup>0</sup>C (e), Au/Al<sub>2</sub>O<sub>3</sub> 500<sup>0</sup>C (f).

The variation of the FWHM of the above-discussed catalysts with the temperature and the gas used (H<sub>2</sub> or O<sub>2</sub>) is shown in Figure 4.20.

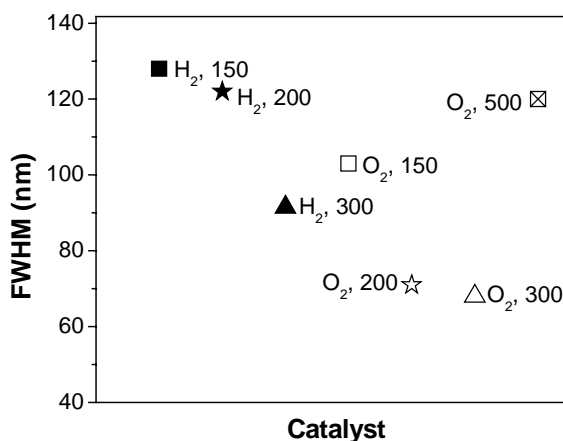


**Figure 4.20:** The variation in FWHM for various Au/Al<sub>2</sub>O<sub>3</sub> catalysts as a result of heat-treatment and the nature of the gas. Filled symbols: H<sub>2</sub> treatment, open symbols: O<sub>2</sub> treatment.

The FWHM data for H<sub>2</sub> pretreatment are marked by filled symbols, while the FWHM data characteristic for the oxygen pretreatment are marked by open symbols. In general, the plasmon bandwidth is found to follow the predicted behaviour as it increases with decreasing

size. However, a relatively large bandwidth was found for Au/Al<sub>2</sub>O<sub>3</sub> treated in O<sub>2</sub> at 500<sup>0</sup>C. This unexpected behaviour may be attributed to either a change in the gold distribution over the surface due to the temperature effect, and/or modification of the shape of the gold particles as a result of the heat-treatment. This conclusion is supported by the following proofs. First, the optical spectrum of Au/Al<sub>2</sub>O<sub>3</sub>/O<sub>2</sub>/500<sup>0</sup>C (Fig. 4.19A, curve f) looks quite different, compared with the other spectra, especially the intensity and the shape of the peak at 550 nm. The average Au particle size does not vary significantly, compared with the other samples (*Section 4.2.1* and *Chapter 9*). Therefore, a redistribution of the Au nanoparticles as a result of thermal treatment seems a reasonable explanation.

In addition, several used samples (i.e. used in N<sub>2</sub>O reduction, *Chapter 8*) have been studied by means of DR/UV-Vis and the results are presented in Figs. 4.21A-B.

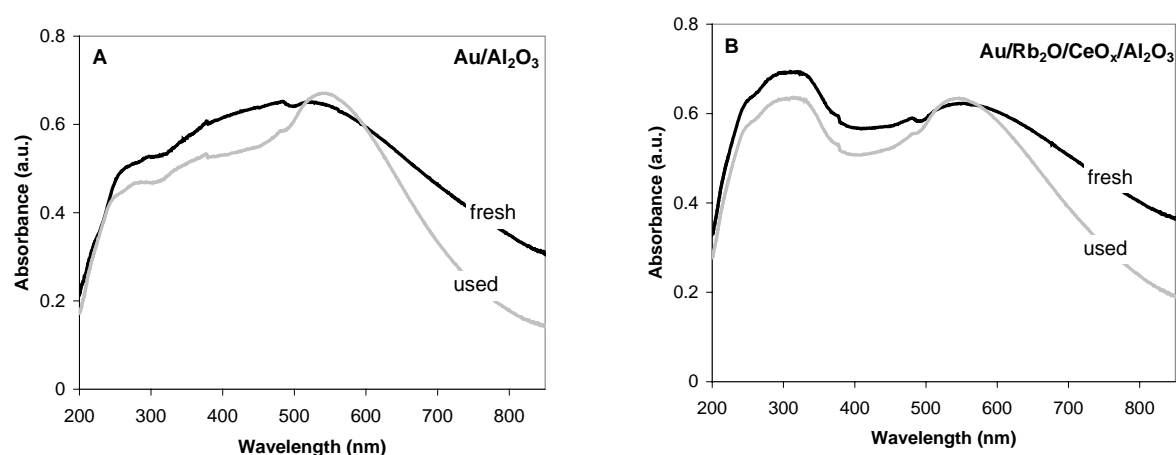


**Figure 4.21:** DR/UV-Vis spectra of fresh and used (N<sub>2</sub>O+H<sub>2</sub>) Au/Al<sub>2</sub>O<sub>3</sub> (A) and Au/Rb<sub>2</sub>O/CeO<sub>x</sub>/Al<sub>2</sub>O<sub>3</sub> (B).

The DR/UV-Vis spectra of the used catalysts show a different shape, compared with the fresh samples, especially the peak at ~ 550 nm. The XRD data do not indicate a severe sintering of the Au particles during the catalytic test (*Chapter 8*), thus other factors are responsible for the change in the DR/UV-Vis spectra (e.g. redispersion, shape of the Au crystallites). However, information concerning the dispersion and the shape of the Au particles for the used catalysts does not exist. Similar findings have been reported for Au/ZrO<sub>2</sub> after being used in CO oxidation [21].

The variation of the plasmon band of small gold particles for the bicomponent gold-based catalysts with alkali (earth) metal oxides as additives is presented in Figure 4.22. For comparison, the DR/UV-Vis spectra of the supports are also included. The support signal was not subtracted, in order to avoid the appearance of false peaks. The plasmon band of Au<sup>0</sup> is visible for all the samples. In addition, the variation of the FWHM with the size of the gold particles obeys the general rule, viz. increases if the gold particle size decreases. Notice the very broad bands for Au/Rb<sub>2</sub>O/Al<sub>2</sub>O<sub>3</sub> and Au/BaO/Al<sub>2</sub>O<sub>3</sub> and a slight shift of the peak maximum due to the size effect.

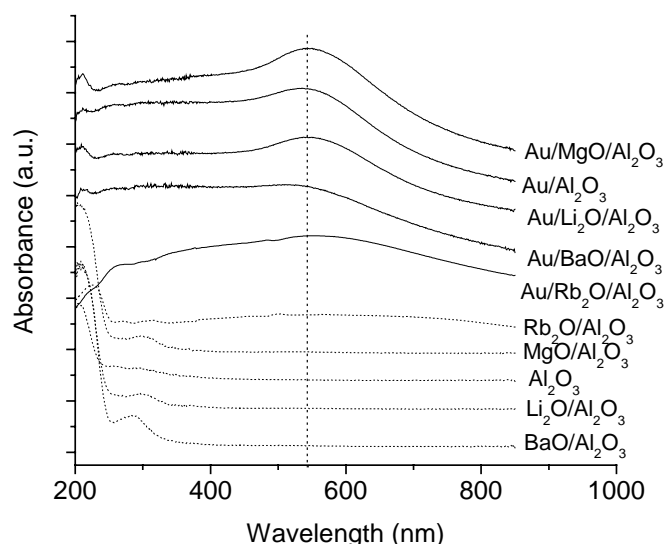


**Figure 4.22:** DR/UV-Vis optical spectra of different gold-based catalysts and the corresponding supports.

The effect of the TMO and ceria on the optical spectra of gold-based catalysts and  $\text{MO}_x/\text{Al}_2\text{O}_3$  is shown in Figure 4.23A. Figure 4.23B shows the optical spectra of the CuO-containing gold-based catalysts and the corresponding supports.

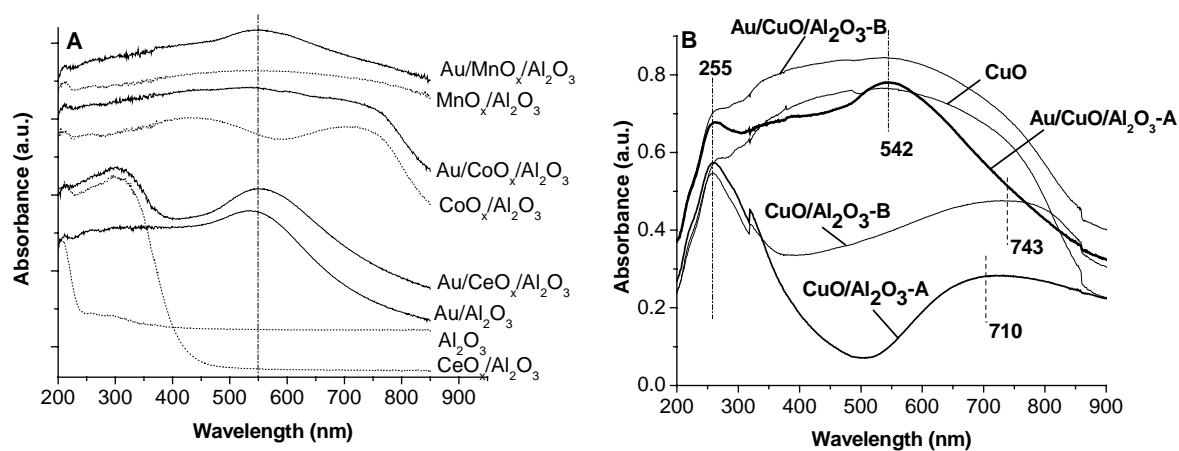


**Figure 4.23:** DR/UV-Vis spectra of promoted gold-based catalysts: (A) with TMO and ceria as promoters and (B) with CuO. In addition, for comparison, spectrum (B) also contains the optical signal of pure CuO.

As expected, in Figure 4.23A the typical plasmon resonance peak of metallic gold ( $\sim 540$  nm) clearly appears. Other additional absorption bands (due to ionic gold or partly charged Au nanoclusters) are not detected. Moreover, the shoulder at the lower wavelength previously found for  $\text{Au}/\text{Al}_2\text{O}_3$ , is not detected anymore. It appears that this absorption band disappears if additives such as TMO or ceria are present. In addition, a small shift of the plasmon band towards higher wavelength takes place in the presence of ceria (smaller gold particles).

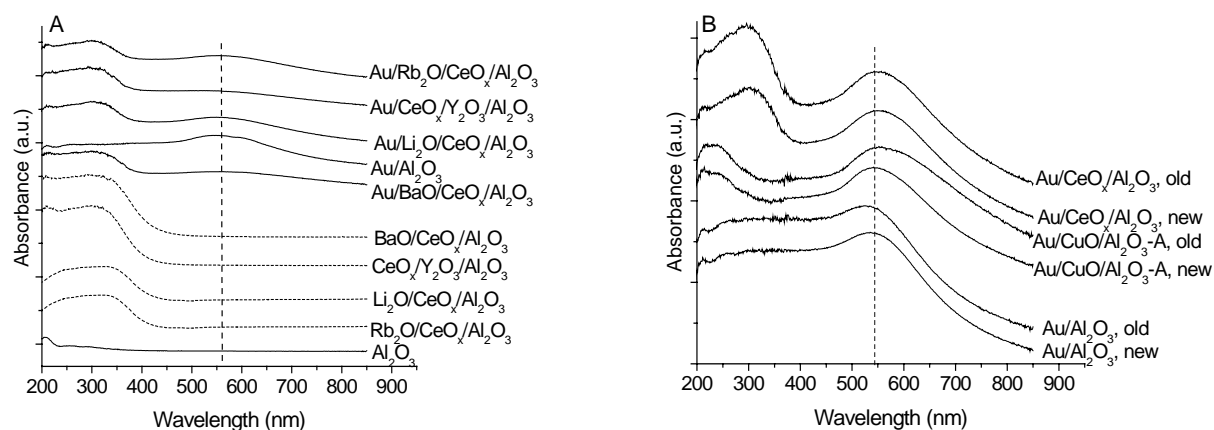


Figure 4.23B presents a more complex situation because of the presence of CuO, by itself optically active in the visible region. The main optical feature of Au/CuO/Al<sub>2</sub>O<sub>3</sub>-A is the plasmon peak at 542 nm, as the fingerprint of metallic Au. A similar absorption peak does not appear very clearly in the optical spectra of Au/CuO/Al<sub>2</sub>O<sub>3</sub>-B. In fact, the spectrum looks similar to that of bulk CuO. The higher CuO loading of Au/CuO/Al<sub>2</sub>O<sub>3</sub>-B catalyst compared with Au loading makes the detection of Au nanoparticles difficult. Moreover, the colour of Au/CuO/Al<sub>2</sub>O<sub>3</sub>-B catalyst is almost black, that indicates the presence of CuO, but is also a strong impediment in DR/UV-Vis data acquisition. The absorption band around 255 nm is assigned to the charge transfer band in CuO [22]. The main absorption band for CuO/Al<sub>2</sub>O<sub>3</sub>-B is around 734 nm, whereas for CuO/Al<sub>2</sub>O<sub>3</sub>-A it is at 710 nm. This band is assigned to Cu<sup>2+</sup> in octahedral symmetry [22-24] but slightly tetragonally distorted. In addition, the shape of this peak is different for CuO/Al<sub>2</sub>O<sub>3</sub>-A and CuO/Al<sub>2</sub>O<sub>3</sub>-B (Figure 4.23B): for CuO/Al<sub>2</sub>O<sub>3</sub>-B it is asymmetric to shorter wavelength, whereas CuO/Al<sub>2</sub>O<sub>3</sub>-A showed an asymmetry at higher wavelength. This asymmetry may be explained on the basis of structural differences of the two samples: an asymmetry towards shorter wavelength is an indication of the presence of bulk CuO with semiconducting properties (CuO/Al<sub>2</sub>O<sub>3</sub>-B) [23], whereas the asymmetry at longer wavelength is characteristic of more isolated Cu<sup>2+</sup> ions (CuO/Al<sub>2</sub>O<sub>3</sub>-A). The absorption band of Cu<sup>+</sup> has not been found (peak around 400nm). Also, there is no indication of the presence of CuAl<sub>2</sub>O<sub>4</sub> (~1600 nm). In conclusion, DR/UV-Vis spectroscopy confirms the previous experimental data: metallic Au is detected as the only Au-containing species, and depending on CuO loading, a very well dispersed (Au/CuO/Al<sub>2</sub>O<sub>3</sub>-A), or more crystalline CuO phase (Au/CuO/Al<sub>2</sub>O<sub>3</sub>-B) may be formed. The CuO dispersion will influence both the reduction temperature as well as the chemical interaction with Au.

The DR/UV-Vis results of the multicomponent gold-based catalysts are shown in Figure 4.24A. No additional aspects appear for this situation, as compared with the singly promoted gold-based catalysts. However, the plasmon band of Au<sup>0</sup> is the most pronounced for Au/Al<sub>2</sub>O<sub>3</sub> (4.3 nm) and least pronounced for Au/BaO/CeO<sub>x</sub>/Al<sub>2</sub>O<sub>3</sub> and Au/Y<sub>2</sub>O<sub>3</sub>/CeO<sub>2</sub>/Al<sub>2</sub>O<sub>3</sub>, in line with the HRTEM findings (Table 4.3).

The optical response of gold-based catalysts under UV-Vis light was also used to follow the changes of the plasmon peak with time, accompanied by eventual appearance of new peaks. For this purpose, a second set of optical measurements has been carried out for some selected gold-based catalysts at an interval of one year. The results are presented in Figure 4.24B. The optical response of the support was not subtracted from that of gold-containing samples.

After one year there is no noticeable change in the structure of gold-based catalysts. The results indicate that the nanosized gold particles are rather stable in time and no clear agglomeration of gold particles is noticed, nor the appearance of other species such as ionic gold. However, it should be mentioned that the catalysts have been stored at low temperature (4°C), in order to avoid the growth of Au particles.



**Figure 4.24:** DR/UV-Vis spectra of multicomponent gold-based catalysts and their corresponding supports (A). The stability in time of gold-based catalysts as studied by DR/UV-Vis (B).

#### 4.4 Temperature-programmed reduction, TPR

TPR spectroscopy was used to study in more detail the reduction of a few selected gold-based catalysts in the presence of hydrogen. This technique has not been used often in relation with gold-based catalysts. Therefore, just a few reports are found in the literature. In addition, a rather broad range of the reduction temperature of alumina-supported gold catalysts is reported. For example, for Au/Al<sub>2</sub>O<sub>3</sub> it was reported that reduction of Au proceeds in three steps: first at  $-93^{\circ}\text{C}$  Au<sup>s</sup>O<sub>x</sub><sup>1</sup> is being reduced, then at  $27^{\circ}\text{C}$  the reduction of Au<sup>s</sup>Cl<sub>y</sub> takes place, while upon further increasing the temperature, at  $727^{\circ}\text{C}$  the reduction occurs of gold ions (Au<sup>1</sup>) incorporated into the subsurface of alumina support [25]. Another paper reported that the reduction of Au in Au/MgO takes place during a single process with a maximum at  $142^{\circ}\text{C}$ , whilst if Fe or Mn are added to Au/MgO, the reduction temperature of Au increases slightly to  $156^{\circ}\text{C}$  and  $170^{\circ}\text{C}$  respectively [26]. No information was provided about the reduction process of the Fe and Mn oxides additives. If gold was present as Au(CH<sub>3</sub>)<sub>2</sub>(acac)<sub>2</sub><sup>2</sup>, the reduction of Au particles was found at around  $148^{\circ}\text{C}$ , while if gold was present as supported mononuclear Au, the temperature increased to  $208^{\circ}\text{C}$  [27]. All these papers, although very different temperatures were reported for gold reduction, agree that gold was present initially as Au<sup>3+</sup>. On the other hand, other papers report only the influence of gold addition on the reducibility of CeO<sub>2</sub>, FeO<sub>x</sub> or Co<sub>3</sub>O<sub>4</sub>, without any evidence for gold reduction [28, 29]. However, different results may be partly caused by experimental differences, such as in heating ramp, flow rate or the concentration of the reducing gas.

<sup>1</sup> “s” corresponds to the atoms exposed to the surface of gold particles and “x” denotes the reduction stoichiometry

<sup>2</sup> acac corresponds to acetylacetonate

The first TPR results presented here concern the reduction of  $\text{Au}_2\text{O}_3$  (Aldrich), as reference. The reduction profile is depicted in Figure 4.25A, while Figure 4.25B shows a comparison between the TPR spectra of  $\text{Au}_2\text{O}_3/\text{Al}_2\text{O}_3$  and  $\text{Au}/\text{Al}_2\text{O}_3$ .

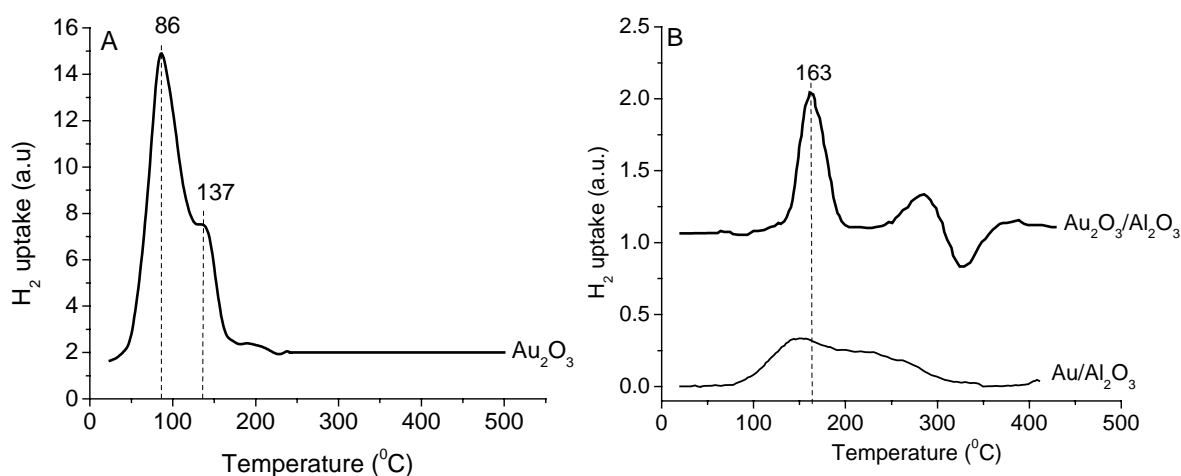


**Figure 4.25:** TPR reduction profile of  $\text{Au}_2\text{O}_3$  (A) and  $\text{Au}_2\text{O}_3/\text{Al}_2\text{O}_3$  and  $\text{Au}/\text{Al}_2\text{O}_3$  (B). The reducing gas consisted of 5.5 %  $\text{H}_2$  in Ar, at a total flow of  $25 \text{ ml min}^{-1}$ .

The reduction of  $\text{Au}_2\text{O}_3$ , proceeds at  $86^\circ\text{C}$  and corresponds to the reduction of  $\text{Au}^{3+}$  to  $\text{Au}^0$ . The small shoulder at  $137^\circ\text{C}$  is due to the reduction of  $\text{Au}^+$  to  $\text{Au}^0$ , which is, however, much smaller than the main peak at  $86^\circ\text{C}$ . When gold is deposited on alumina, viz.  $\text{Au}_2\text{O}_3/\text{Al}_2\text{O}_3$ , the reduction profile looks quite different (Figure 4.25B). The reduction of  $\text{Au}^{3+}$  to  $\text{Au}^0$  proceeds in one single step and is shifted to higher temperature ( $163^\circ\text{C}$ ). The calculated amount of  $\text{Au}^{3+}$  which is reduced to  $\text{Au}^0$  corresponds to 3.65 wt-% Au, in line with the AAS results. This reduction temperature is in agreement with previous results reported in [26]. The difference in the reduction profiles of  $\text{Au}_2\text{O}_3$  and  $\text{Au}_2\text{O}_3/\text{Al}_2\text{O}_3$  may be explained upon considering that in the former case the size of the gold oxide particles is much larger than in the latter case. For this reason, during the first reduction step of  $\text{Au}_2\text{O}_3$ , partly reduced Au grains are formed, which probably encapsulate small ionic gold grains. These will be further reduced to metallic gold in the next reduction step. When gold is deposited on alumina, the gold concentration is much lower than in the case of  $\text{Au}_2\text{O}_3$  and, consequently, the gold particles are more accessible to hydrogen from the gas phase. In addition, the interaction formed during the preparation step between Au and the support shifts the reduction temperature of the gold species to higher temperature, compared to unsupported  $\text{Au}_2\text{O}_3$ . In addition, a large difference in the hydrogen consumption is observed upon comparison of the intensity peaks of  $\text{Au}_2\text{O}_3$  and  $\text{Au}_2\text{O}_3/\text{Al}_2\text{O}_3$ . The negative peak observed at higher temperature for  $\text{Au}_2\text{O}_3/\text{Al}_2\text{O}_3$  might be due to some desorption process, since this sample was not subjected to precalcination. The “hydrogen consumption” of  $\text{Au}/\text{Al}_2\text{O}_3$  is much less, compared with that of  $\text{Au}_2\text{O}_3/\text{Al}_2\text{O}_3$  and based on the TPR profile of  $\text{Au}_2\text{O}_3/\text{Al}_2\text{O}_3$ , all the gold is in its reduced state at  $300^\circ\text{C}$ .

Figure 4.26 shows the reduction profiles of  $\text{Au}_2\text{O}_3/\text{Li}_2\text{O}/\text{CeO}_x/\text{Al}_2\text{O}_3$ ,  $\text{Li}_2\text{O}/\text{CeO}_x/\text{Al}_2\text{O}_3$  and  $\text{CeO}_x/\text{Al}_2\text{O}_3$ . The reduction of ionic gold takes place at  $146^\circ\text{C}$ , which is shifted by  $17^\circ\text{C}$

towards lower temperature, compared with  $\text{Au}_2\text{O}_3/\text{Al}_2\text{O}_3$ . In addition, the peak shape differs for  $\text{Au}_2\text{O}_3/\text{Li}_2\text{O}/\text{CeO}_x/\text{Al}_2\text{O}_3$  and  $\text{Au}_2\text{O}_3/\text{Al}_2\text{O}_3$ . The former catalyst shows a rather sharp peak, whereas the latter one shows a slightly broader peak. The reason may be due to the influence of the additives in the former case, but also to the difference in the gold-support interaction.

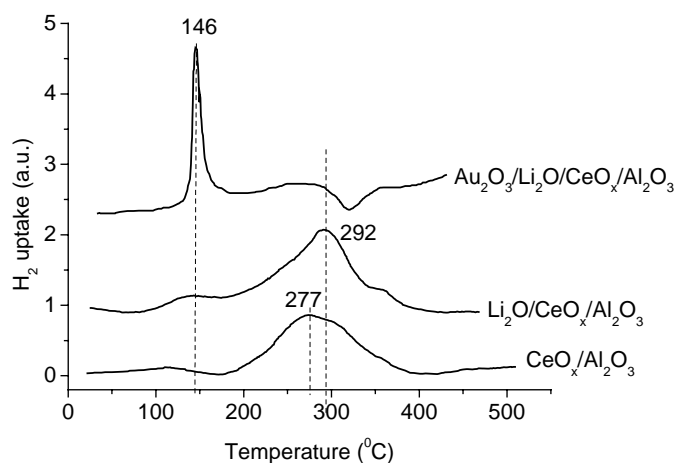


**Figure 4.26:** TPR reduction profile of  $\text{Au}_2\text{O}_3/\text{Li}_2\text{O}/\text{CeO}_x/\text{Al}_2\text{O}_3$ ,  $\text{Li}_2\text{O}/\text{CeO}_x/\text{Al}_2\text{O}_3$  and  $\text{CeO}_x/\text{Al}_2\text{O}_3$ . Experimental conditions are similar as in Figure 4.25.

Moreover, the presence of the additives seems to increase the amount of hydrogen consumed for  $\text{Au}^{3+}$  reduction, but this may be partly due to partial reduction of  $\text{Ce}^{4+}$  in the same temperature range. The amount of  $\text{Au}^{3+}$  reduced to  $\text{Au}^0$  calculated on the basis of the CuO reference corresponds to approximately 4.5 wt-% Au, which is in line with AAS results.

The main conclusion is that all the gold-based catalysts under working conditions (after calcination in  $\text{O}_2$  flow at  $300^\circ\text{C}$  and in-situ hydrogen pretreatment) consist of only  $\text{Au}^0$ .

In the examined temperature range, the cerium oxide sample shows one reduction peak with a maximum at  $292^\circ\text{C}$  for  $\text{Li}_2\text{O}/\text{CeO}_x/\text{Al}_2\text{O}_3$ , and at  $277^\circ\text{C}$  for  $\text{CeO}_x/\text{Al}_2\text{O}_3$ . This is attributed to the reduction of the surface oxygen of ceria, known also as capping oxygen [29]. The reduction of bulk oxygen of cerium oxide has been reported to occur at temperatures above  $700^\circ\text{C}$  [29].

The TPR reduction profile of  $\text{Au}/\text{CuO}/\text{Al}_2\text{O}_3\text{-A}$  and the corresponding support are presented in Figure 4.27. In this case, the catalyst and the support were already subjected to calcination at  $300^\circ\text{C}$  for 2 hours. The TPR profile of  $\text{CuO}/\text{Al}_2\text{O}_3\text{-A}$  shows a single reduction peak at  $194^\circ\text{C}$ . According to literature data, it is established that the reduction of pure CuO occurs around  $257^\circ\text{C}$  [30], whereas for  $\text{CuO}/\text{Al}_2\text{O}_3$ , a reduction temperature between  $204^\circ\text{C}$  [30] and  $272^\circ\text{C}$  [23] was reported, depending on the experimental conditions used. The hydrogen consumption measured, calculated from the area under the peak corresponds to a CuO content of 6.4 wt-% (by AAS this sample contains 6 wt-% CuO). This result implies that CuO was reduced in one step to  $\text{Cu}^0$ .

For Au/CuO/Al<sub>2</sub>O<sub>3</sub>-A the main reduction peak is slightly shifted towards lower temperatures, viz. 183<sup>o</sup>C. This indicates that the presence of Au has some positive effect on the reduction of CuO and the maximum reduction temperature is shifted with approximately 11<sup>o</sup> towards lower temperatures. In addition, a small shoulder appears around 236<sup>o</sup>C. The amount of CuO which was reduced, calculated on the basis of hydrogen consumption from the main peak, is 5.8 wt-%, and indicates nearly full reduction of Cu<sup>2+</sup> to Cu<sup>0</sup>.

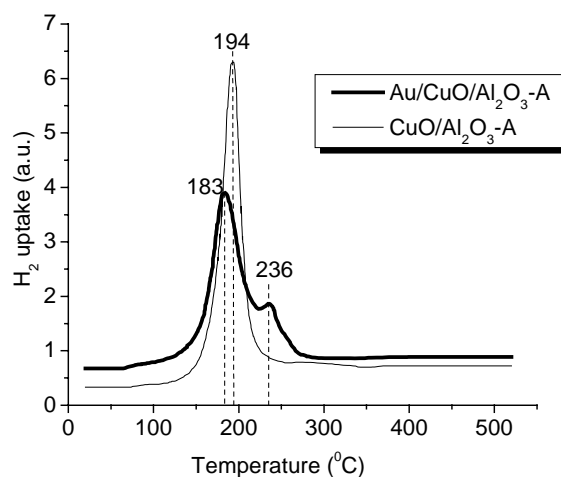


**Figure 4.27:** TPR profile of Au/CuO/Al<sub>2</sub>O<sub>3</sub>-A and CuO/Al<sub>2</sub>O<sub>3</sub>-A.

The small shoulder at 236<sup>o</sup>C may have two origins: either it is due to a very small reduction of Au<sup>3+</sup> to Au<sup>0</sup>, or to a supplementary CuO reduction. The first possibility appears unlikely (see above). Thus, it is suggested that this peak corresponds to the reduction of a small amount of crystalline CuO. The calculated amount of the reduced CuO would be around 0.3 wt-%. There is no direct evidence for CuAl<sub>2</sub>O<sub>4</sub> formation that could eventually cause this reduction shoulder.

#### 4.5 X-ray photoelectron spectroscopy, XPS

Some of the gold-based catalysts have been characterized by XPS. The results are presented in the Fig. 4.28 and correspond to the core level signal of Au. Unfortunately, a very noisy spectrum was recorded for the reference Au/Al<sub>2</sub>O<sub>3</sub> catalyst, and no useful information could be obtained. It is possible that the Au surface concentration of this catalyst was too low, in spite of a bulk concentration of 4.1 wt-%, as determined by AAS (Table 4.1). The XPS data were recorded without any additional thermal or gas pretreatment.

The reported XPS signals of bulk gold are at 84.0 eV (4f<sub>7/2</sub>) and 87.7 eV (4f<sub>5/2</sub>) [13]. The binding energy (BE) of Au 4f<sub>7/2</sub> for these catalysts varies between 84.2 eV and 84.5 eV. The reported 4f<sub>7/2</sub> signal of Au<sub>2</sub>O<sub>3</sub> is around 85.5 eV, whereas Au<sub>2</sub>O should present a peak centered at 86.5 eV [13].

The results presented below point to the existence of metallic gold as the only species and are in a good agreement with other results obtained by DR/UV-Vis and TPR. A summary of the BEs of the gold-based catalysts is presented in Table 4.6.

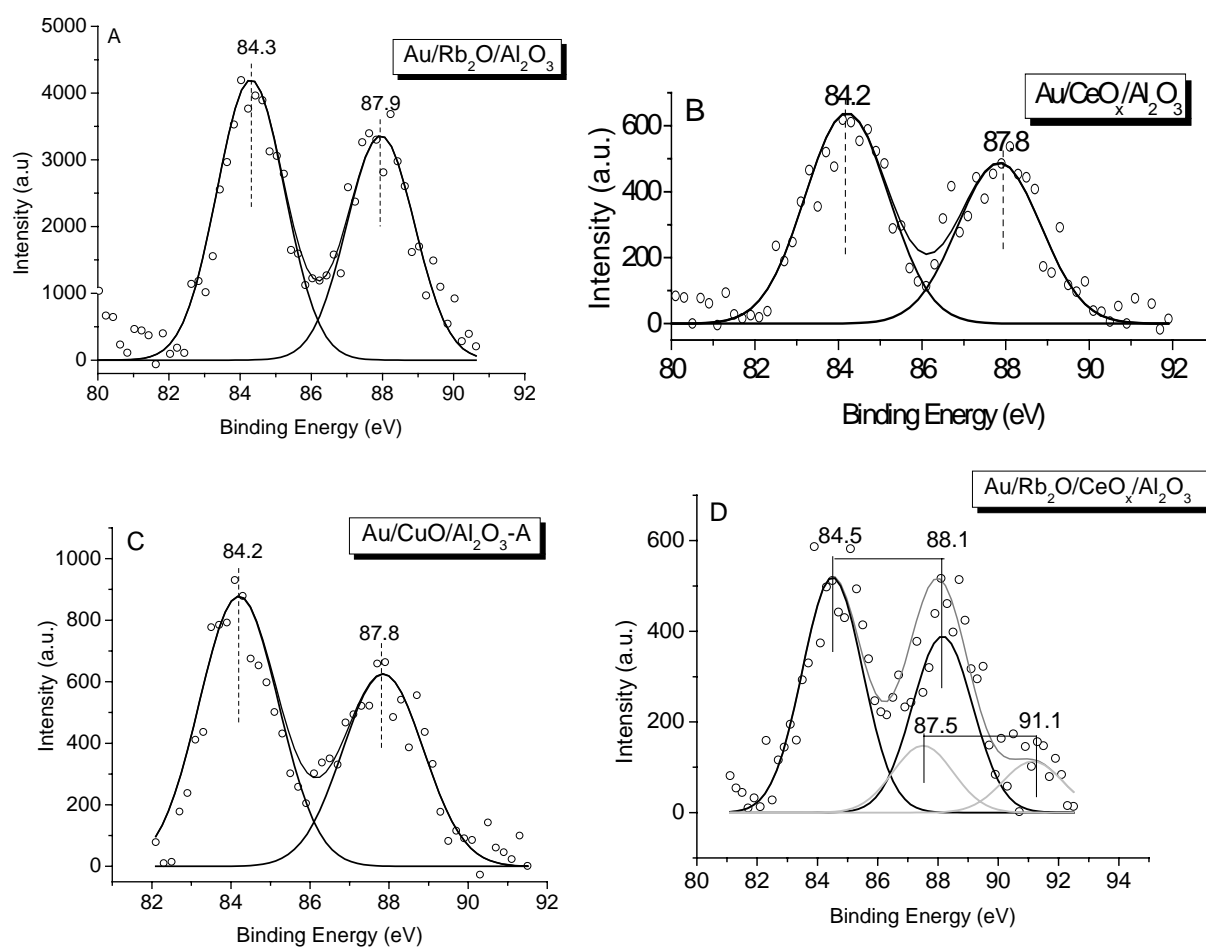


**Figure 4.28:** Au 4f spectra of: Au/Rb<sub>2</sub>O/Al<sub>2</sub>O<sub>3</sub> (A), Au/CeO<sub>x</sub>/Al<sub>2</sub>O<sub>3</sub> (B), Au/CuO/Al<sub>2</sub>O<sub>3</sub>-A (C), Au/Rb<sub>2</sub>O/CeO<sub>x</sub>/Al<sub>2</sub>O<sub>3</sub> (D).

**Table 4.6:** XPS study of alumina-supported gold catalysts

Catalyst	XPS binding energy (eV)	
	$4f_{7/2}$	$4f_{5/2}$
Au/Rb <sub>2</sub> O/Al <sub>2</sub> O <sub>3</sub>	84.3	87.9
Au/CeO <sub>x</sub> /Al <sub>2</sub> O <sub>3</sub>	84.2	87.8
Au/CuO/Al <sub>2</sub> O <sub>3</sub> -A	84.2	87.8
Au/Rb <sub>2</sub> O/CeO <sub>x</sub> /Al <sub>2</sub> O <sub>3</sub>	84.5	88.1
	87.5	91.1

The positive shift of no more than 0.5 eV in the BE of Au 4f<sub>7/2</sub> has been attributed to various phenomena, including “chemical shift” due to chemical binding or electron transfer, or “matrix effects” associated with differences in crystal potential, work function and relaxation energy [7]. Matrix effects become important for very small particles, where Au loses its metallic character (particle size less than 2 nm). The average gold particle size as determined by various techniques (see above) is in general larger than 2 nm, thus “matrix

effects” are not expected to be important. On the other hand, the “chemical shift” can be due to metal-support interaction or a change of the Au oxidation state. The latter is unlikely, since oxidic Au would create a much larger BE shift (at least 1.5 eV) than the one observed [7, 31]. In addition, negatively charged Au particles are also unlikely to be present, since a negative shift of the BE would be observed in that case [31]. Thus, it is possible that the observed shift in the BE observed for these catalysts may be due to some kind of metal-support interaction.

An interesting XPS signal was obtained for Au/Rb<sub>2</sub>O/CeO<sub>x</sub>/Al<sub>2</sub>O<sub>3</sub> (sample (D) in Figure 4.28). The experimental data could be fitted with two different pairs of peaks. One pair is the couple Au 4f<sub>7/2</sub> = 84.5 eV and 4f<sub>5/2</sub> = 88.1 eV, and the other pair consists of Au 4f<sub>7/2</sub> = 87.5 eV and 4f<sub>5/2</sub> = 91.1 eV. More interestingly is that both pairs appear as the signal of Au<sup>0</sup>, in the sense that the ratio between the areas of the peaks is 0.75, in line with [13], and the width of the peaks is ~ 2 eV, also in line with the theory. The 4f<sub>5/2</sub> signal of “basic” Au<sup>0</sup> is positively shifted by 0.5 eV. There is no correlation with the already reported data. It is possible that the presence of small amounts of positively charged Au particles may cause the shift in the BE along with the other two small peaks. However, Au/Rb<sub>2</sub>O/CeO<sub>x</sub>/Al<sub>2</sub>O<sub>3</sub> did not show any indication of the presence of Au<sup>δ+</sup>, as revealed by DR/UV-Vis investigations. An alternative explanation may take into account a different distribution of the gold particles. That means that the Au particles with an average size around 3 nm give rise to a “normal” XPS spectrum, whereas other Au particles, very different in shape and, presumably, very small, may generate the red shift in the binding energy of about 3 eV.

## 4.6 General discussion

### *Unpromoted Au/Al<sub>2</sub>O<sub>3</sub> catalyst*

Deposition-precipitation with urea proved to be an efficient method to prepare unpromoted Au/Al<sub>2</sub>O<sub>3</sub> catalyst. The gold loading was relatively close to the target (5 wt-%) and the dispersion was rather high. However, these characteristics can be further improved by using different classes of additives. Moreover, it was found that the preparation method did not produce a significant change in BET surface area and the structure of the alumina. After a thermal treatment in H<sub>2</sub> or O<sub>2</sub> at 150<sup>0</sup>C, gold is already present in metal form and the degree of reduction increases by increasing the temperature (XRD data). These findings are further supported by DR/UV-Vis and TPR measurements. However, it should be emphasized that by varying the treatment (H<sub>2</sub> or O<sub>2</sub>), and heating up to 500<sup>0</sup>C, no significant effect related to the growth of the Au particles was found. These results are in contradiction with literature data, where it was reported that a heat treatment at a temperature above 400<sup>0</sup>C causes gold to agglomerate [11]. XRD and HRTEM pointed to the formation of relatively small gold particles (≤ 5 nm) distributed over the alumina support. Other shapes than spherical could be visualized by HRTEM (i.e. truncated, see Figs. 4.3, 4.14A-B). A treatment at 200<sup>0</sup>C or above causes total reduction of ionic gold to Au<sup>0</sup>. However, agglomeration of Au particles was found in the present investigations when the samples were used in methane oxidation (*Chapter 6*) at a maximum temperature of 740<sup>0</sup>C.

### *Promoted Au/Al<sub>2</sub>O<sub>3</sub> catalysts*

The different classes of additives used for Au/Al<sub>2</sub>O<sub>3</sub> catalyst influence the characteristics of the final catalyst. The preparation method used was HDP with urea and was based on work previously reported in [11]. The route to prepare Au/MO<sub>x</sub>/Al<sub>2</sub>O<sub>3</sub> or Au/M<sup>I</sup>O<sub>x</sub>/M<sup>II</sup>O<sub>x</sub>/Al<sub>2</sub>O<sub>3</sub> consisted of first modifying the support (alumina) and then depositing gold. This method proved to be rather reproducible and efficient in obtaining highly dispersed gold.

The identity of the additive is important. Thus, by considering various alkali (earth) metal oxides as additives, the best result obtained was with BaO. This catalyst was superior to the one previously reported, Au/MgO [11, 32]. The final dispersion of Au when BaO was present reached 55%. However, the exact role of these additives is not yet fully understood. It was speculated that in the presence of MO<sub>x</sub>, part of the defect sites of the support, directly responsible for Au nucleation, are covered by a layer of M(OH)<sub>x</sub>, which, during subsequent thermal treatments, leads to the formation of a surface spinel which will influence the final gold particle size distribution [11]. None of the samples studied in this thesis displayed a spinel-like structure formed by alumina and MO<sub>x</sub>. However, it is possible that this structure is not stable or detectable. On the other hand, by adding different kinds of additives, especially of the type of alkali (earth) metal oxides, the surface acidity/basicity of alumina is modified and it changes from acidic to basic. As a consequence, the starting pH of the carrier is not 2.5, but higher, and gold deposition is facilitated; the nucleation and growth processes are shortened in this way, compared with alumina-only. Finally, gold-based catalysts with smaller particles are obtained. In fact, the importance of the “point of zero charge” is well known for this type of synthesis. This might explain why better results are obtained when BaO is used, compared with MgO or Li<sub>2</sub>O. On the other hand, the distinct role of these additives as structural promoters might also be related to the interaction between these additives and gold and is most probably stronger than between Au and alumina. This type of additives acts as structural promoters by stabilizing Au nanoparticles against sintering. Efficient stabilization concerning the gold nanoparticles was found with ceria as well, where the final gold dispersion reached 52%.

HRTEM identified very small gold particles for the multicomponent catalysts and it was also possible to visualize different shapes of gold nanoparticles. The identification of metallic gold and the absence of ionic species were further confirmed by DR/UV-Vis, TPR and XPS techniques. In addition, very small gold particles contain an increased number of low coordinated gold atoms with, possibly, a much stronger interaction between Au and support. This strong gold-support interaction is probably responsible for the modification of the electronic structure of gold nanoparticles at the interface with the support and, in turn, for their superior catalytic activity. Further support for the existence of a strong metal support interaction between gold and support was evidenced by means of XPS.

## **4.7 Conclusions**

Various unpromoted and promoted Au/Al<sub>2</sub>O<sub>3</sub> were successfully prepared by HDP with urea. This method proved to be rather reproducible concerning the gold loading and gold particle size. Various additives improved the final characteristics of the catalysts.



Very small Au particles, homogeneously distributed over the support were obtained when different types of additives were added to the alumina carrier. As a consequence of the very small gold particles, the dispersion and the metallic surface area are significantly increased. The variety of characterization techniques employed (DR/UV-Vis, TPR and XPS) did not identify the existence of ionic gold. The existence of a strong Au-support interaction was evidenced by TPR and XPS. However, the existence of a small amount of partly charged gold particles cannot be completely ruled out (Au/Rb<sub>2</sub>O/CeO<sub>x</sub>/Al<sub>2</sub>O<sub>3</sub>).

#### 4.8 References

- [1] P. Buffat, J.-P. Borel, *Phys. Rev. A* 13 (1976) 2287.
- [2] G. C. Bond, D. T. Thompson, *Catal. Rev. Sci. Eng.* 41 (1999) 319.
- [3] F. Boccuzzi, A. Chiorino, M. Manzoli, P. Lu, T. Akita, S. Ichikawa, M. Haruta, *J. Catal.* 202 (2001) 256.
- [4] E. D. Park, J. S. Lee, *J. Catal.* 186 (1999) 1.
- [5] N. A. Hodge, C. J. Kiely, R. Whyman, M. R. H. Siddiqui, G. J. Hutchings, Q. A. Pankhurst, F. E. Wagner, R. R. Rajaram, S. E. Golunski, *Catal. Today* 72 (2002) 133.
- [6] S. Minico, S. Scire, C. Crisafulli, S. Galvagno, *Appl. Catal. B* 34 (2001) 277.
- [7] S.-J. Lee, A. Gavrilidis, Q. A. Pankhurst, A. Kyek, F. E. Wagner, P. C. L. Wong, K. L. Yeung, *J. Catal.* 200 (2001) 298.
- [8] A. Wolf, F. Schuth, *Appl. Catal. A* 226 (2002) 1.
- [9] J.-N. Lin, J.-H. Chen, C.-Y. Hsiao, Y.-M. Kang, B.-Z. Wan, *Appl. Catal. B* 36 (2002) 19.
- [10] S. Tsubota, T. Nakamura, K. Tanaka, M. Haruta, *Catal. Lett.* 56 (1998) 131.
- [11] R. J. H. Grisel, *Supported gold catalysts for environmental applications*, PhD thesis, Leiden University (2002).
- [12] R. J. H. Grisel, B. E. Nieuwenhuys, *Catal. Today* 64 (2001) 69.
- [13] JCPDS Powder Diffraction File, International Centre for Diffraction Data.
- [14] R. J. H. Grisel, C. J. Weststrate, A. C. Gluhoi, B. E. Nieuwenhuys, *Gold Bull.* 35 (2002) 39.
- [15] M. A. Centeno, M. Paulis, M. Montes, J. A. Odriozola, *Appl. Catal. A* 234 (2002) 65.
- [16] M. A. Centeno, P. Malet, I. Carrizosa, J. A. Odriozola, *J. Phys. Chem. B* 104 (2000) 3310.
- [17] A. Martinez-Arias, M. Fernandez-Garcia, L. N. Salamanca, R. X. Valenzuela, J. C. Conesa, J. Soria, *J. Phys. Chem. B* 104 (2000) 4038.
- [18] S. Link, M. A. El-Sayed, *J. Phys. Chem. B* 103 (1999) 4212 and refs. therein.
- [19] P. Claus, A. Bruckner, C. Mohr, H. Hofmeister, *J. Am. Chem. Soc.* 122 (2000) 11430 and refs. therein.
- [20] J. L. Margitfalvi, A. Fasi, M. Hegedus, F. Lonyi, S. Gobolos, N. Bogdanchikova, *Catal. Today* 72 (2002) 157 and ref. therein.
- [21] F. Boccuzzi, G. Cerrato, F. Pinna, G. Strukul, *J. Phys. Chem. B* 102 (1998) 5733.
- [22] M. C. Marion, E. Garbowski, M. Primet, *J. Chem. Soc.-Farad. Trans.* 86 (1990) 3027.
- [23] M. C. Marion, E. Garbowski, M. Primet, *J. Chem. Soc.-Farad. Trans* 87 (1991) 1795.
- [24] Z. H. Zhu, H. Y. Zhu, S. B. Wang, G. Q. Lu, *Catal. Lett.* 91 (2003) 73.
- [25] C.-K. Chang, Y.-J. Chen, C.-T. Yeh, *Appl. Catal. A* 174 (1998) 13.
- [26] J. L. Margitfalvi, M. Hegedus, A. Szegedi, I. Sajo, *Appl. Catal. A* 272 (2004) 87.
- [27] J. Guzman, B. C. Gates, *J. Phys. Chem. B* 107 (2003) 2242 and refs. therein.
- [28] D. Andreeva, *Gold Bull.* 35 (2002) 82.
- [29] S. Scire, S. Minico, C. Crisafulli, C. Satriano, A. Pistone, *Appl. Catal. B* 40 (2003) 43.
- [30] L. Dong, Y. Hu, M. Shen, T. Jin, J. Wang, W. Ding, Y. Chen, *Chem. Matter.* 13 (2001) 4227.
- [31] J. Radnik, C. Mohr, P. Claus, *Phys. Chem. Chem. Phys.* 5 (2003) 172.
- [32] G. K. Bethke, H.H. Kung, *Appl. Catal. A* 194 (2000) 43.

# Chapter 5

## Oxidation of unsaturated hydrocarbons: total oxidation of propene

*Total oxidation of  $C_3H_6$  at low temperatures over unpromoted- and promoted-  $Au/Al_2O_3$  catalysts has been investigated.  $Au/Al_2O_3$  is active in low temperature  $C_3H_6$  oxidation and all the additives used enhance the catalytic performance of Au. The main role of alkali (earth) metal oxide additives is to decrease the size of the gold particles through the preparation step and to stabilize them against sintering during the reaction. In turn, a direct dependence of the catalytic performance on the size of the gold particles is found. The role of this kind of additives is that of a structural promoter and not of a chemical promoter. If the additives are of the TMO/Ceria type, their role is mainly related to that of an active participant throughout the reaction process, as cocatalyst. It is experimentally shown that these oxides are able to supply active oxygen via a Mars and van Krevelen mechanism. The composition of the oxide is then restored by oxygen from the gas phase. Propene is activated on gold or at the gold-support interface. A large enhancement of the catalytic activity in propene oxidation is found if two different  $MO_x$  are added, i.e. an alkali (earth) metal oxide and ceria.*

## 5.1 Outline

This chapter describes a detailed study concerning the total oxidation of propene over unpromoted- and promoted- Au/Al<sub>2</sub>O<sub>3</sub> catalysts. The additives are either alkali (earth) metal oxides, TMO/Ceria/CuO, or a combination of these oxides. Additional information concerning the experimental procedure is described in Section 5.2. Section 5.3 is devoted to the catalytic activity results, which are further discussed in Section 5.4. The most important conclusions are summarized in Section 5.5.

## 5.2 Experimental

The unpromoted- and promoted- gold-based catalysts (5 wt-% Au) have been prepared using the preparation method previously described (i.e. homogeneous deposition precipitation with urea, *Chapter 3* and thereafter). MO<sub>x</sub>/Al<sub>2</sub>O<sub>3</sub> and M<sup>I</sup>O<sub>x</sub>/M<sup>II</sup>O<sub>x</sub>/Al<sub>2</sub>O<sub>3</sub> (M: Rb, Li, Ba, Mg, Mn, Fe, Cr, Ni, Co, Ti, Zn, Zr, Cu, Ce, V, Pr, Y) catalysts were prepared by pore volume impregnation. The characterization results are discussed in detail in *Chapter 4*.

The experimental set-up used for catalytic activity measurements is described in *Chapter 3*. The samples were reactivated *in-situ* under hydrogen flow, at 300<sup>o</sup>C, unless otherwise stated. The oxidation of propene was carried out under a high excess of oxygen, C<sub>3</sub>H<sub>6</sub>:O<sub>2</sub> = 1:9 and using a total flow of 30 ml min<sup>-1</sup> (GHSV ~ 1800 h<sup>-1</sup>). All the gases were 4 vol % /He. The outlet gas stream was analysed either by means of a GC, or MS. The reaction cycle consisted of at least two consecutive heating-cooling cycles until the maximum reaction temperature of 400 (Au-containing samples), or 450<sup>o</sup>C (supports only). Because the total flow and the catalyst weight were always constant (30 ml min<sup>-1</sup> and 0.2 g), the conversion plot of the second heating cycle is considered for comparison. However, the specific reaction rate, *r*, was also estimated and considered as a measure of the catalytic performance, especially because the theoretical gold loading was set to 5 wt-%, but AAS results showed lower values. The morphological changes of the catalyst structure after the reaction test were followed by XRD.

## 5.3 Catalytic performance in C<sub>3</sub>H<sub>6</sub> oxidation

### *Alkali (earth) metal oxides as additives*

Figure 5.1A shows the catalytic performance of Au/Al<sub>2</sub>O<sub>3</sub> during two consecutive heating-cooling cycles. One can see that deactivation is relatively small because the first heating-cooling cycle is almost equal to the second one. The stability of any catalyst is important for long-term operation, but is crucial for Au, due to its very low melting point temperature, compared with Pt or Pd. Figure 5.1B compares the catalytic performance of unpromoted- and alkali (earth) promoted- Au/Al<sub>2</sub>O<sub>3</sub> (second heating stage). The additives include Rb<sub>2</sub>O, Li<sub>2</sub>O, MgO and BaO. For comparison, the catalytic activity of alumina is also included. The mixed supports MO<sub>x</sub>/Al<sub>2</sub>O<sub>3</sub> (M=Li, Rb, Mg and Ba) have also been tested in propene oxidation and were found to be negligibly active under the reaction conditions used here.

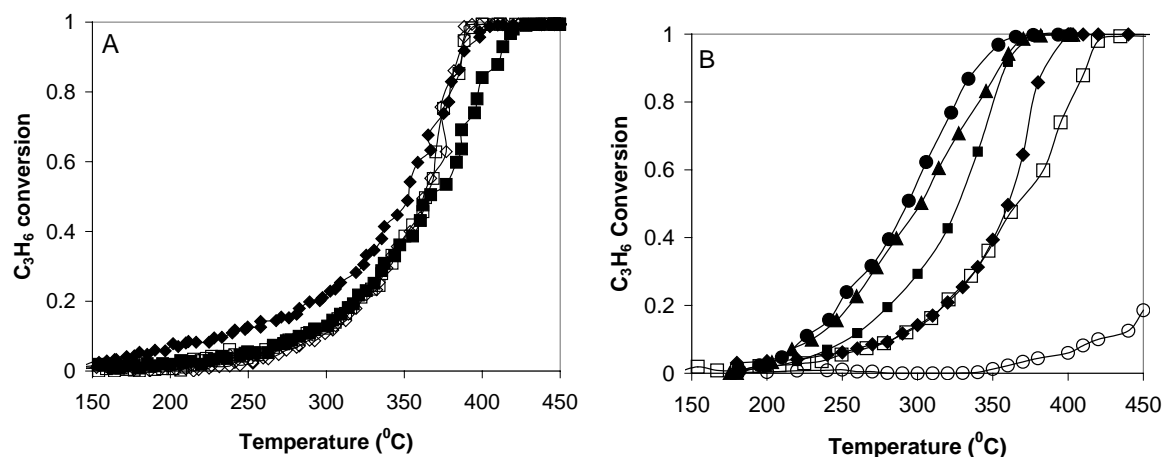


**Figure 5.1:** The catalytic conversion of propene vs. temperature over  $Au/Al_2O_3$ , heating #1 ( $\blacklozenge$ ), cooling #1 ( $\diamond$ ), heating #2 ( $\blacksquare$ ), cooling #2 ( $\square$ ) (A);  $Au/Al_2O_3$  ( $\square$ ),  $Au/MgO/Al_2O_3$  ( $\blacklozenge$ ),  $Au/Li_2O/Al_2O_3$  ( $\blacksquare$ ),  $Au/Rb_2O/Al_2O_3$  ( $\blacktriangle$ )  $Au/BaO/Al_2O_3$  ( $\bullet$ ),  $Al_2O_3$  ( $\circ$ ) (B).

The only C-containing molecule obtained as product is  $CO_2$ . The introduction of alkali (earth) metal oxides improves the catalytic performance of  $Au/Al_2O_3$  over the whole temperature range. Thus, the  $T_{50\%}$  (the temperature of 50% propene conversion, Table 5.1) decreases from  $365^\circ C$  ( $Au/Al_2O_3$ ) to  $290^\circ C$  ( $Au/BaO/Al_2O_3$ ). Contrary to reactions where alkali metal oxides act as poison, i.e. the selective reduction of NO with  $NH_3$  over  $TiO_2$ -supported  $V_2O_5$  [1], or the H-D isotopic exchange reaction between OH groups of H-ZSM-5 and  $D_2$  in the gas phase [2], their presence is beneficial for gold-based catalysts in propene oxidation.

The change of the gold particle size during the catalytic cycle was followed by XRD and the results are summarized in Table 5.1 as  $d_{Au}^b$  and compared with  $d_{Au}^a$  (fresh Au-based catalysts). In general the gold particles do not sinter significantly during the catalytic reaction. However, the gold crystallites of the catalysts that contain an additive are more stable against sintering. In addition, new crystalline planes, corresponding to new solid phases, have not been detected.

DR/UV-Vis was used to follow the plasmon peak of nano Au particles situated at  $\sim 550$  nm. All the optical spectra are presented in Chapter 4, Fig. 4.21. Table 5.1 summarizes the values of the full-width-at-half-maximum (FWHM), as estimated from the peak shape of the optical spectra. The FWHM value decreases from 189.4 nm ( $Au/BaO/Al_2O_3$ -very small particles) to 71.1 nm ( $Au/Al_2O_3$ -large gold particles), in line with the variation of the size of gold particles. However, the relation between the mean particle diameter, the peak position and the FWHM is also influenced by the interaction between the gold particles and the support [3, 4].

The specific reaction rate,  $r$ , calculated at  $260^\circ C$ , and defined as the moles of  $C_3H_6$  transformed over the moles gold per second, is presented in Table 5.1. The specific reaction rate varies between  $1.38 \times 10^{-4}$  (moles  $C_3H_6 \times \text{moles}^{-1} Au \times \text{s}^{-1}$ ) -  $Au/Al_2O_3$ , and  $8.1 \times 10^{-4}$  (moles  $C_3H_6 \times \text{moles}^{-1} Au \times \text{s}^{-1}$ ) -  $Au/BaO/Al_2O_3$ . BaO addition to  $Au/Al_2O_3$  produces a six-

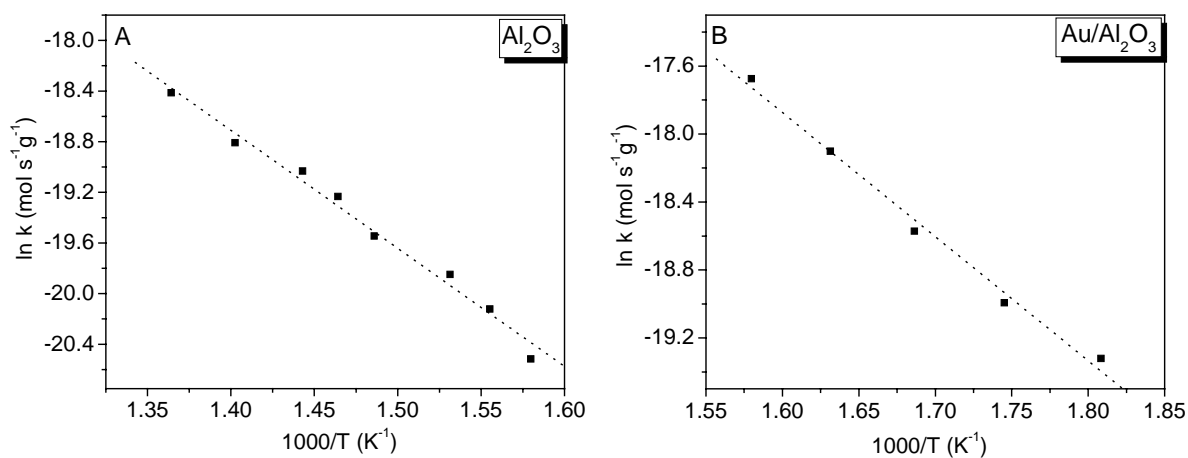
fold increase in the reaction rate. The values for the other gold-containing catalysts are in between these limits. The ranking of the catalysts based on  $r$  values is: Au/Al<sub>2</sub>O<sub>3</sub> < Au/Li<sub>2</sub>O/Al<sub>2</sub>O<sub>3</sub> < Au/Rb<sub>2</sub>O/Al<sub>2</sub>O<sub>3</sub> < Au/BaO/Al<sub>2</sub>O<sub>3</sub> and is in line with the trend observed in Fig. 5.1B. The variation in the specific reaction rate is clearly affected by the change in the size of the Au particles. As a direct consequence of the smaller gold particle size in the presence of an alkali (earth) metal oxide, the metallic surface area as estimated from HRTEM strongly increases by the addition of the oxides (Table 5.1 and Chapter 4). A larger metallic surface area/smaller average Au particle size is beneficial for the catalytic performance, if the noble metal is the active component of the catalyst.

**Table 5.1:** The temperature of 50% propene conversion, the specific reaction rate,  $r$ , the metallic surface area (HRTEM results), the average size of the gold particles for the fresh  $d_{\text{Au}}^{\text{a}}$  and used (after reaction)  $d_{\text{Au}}^{\text{b}}$  gold-based catalysts and the full-width-at-half-maximum (FWHM) as estimated from DR/UV-Vis measurements.

Catalyst	$d_{\text{Au}}^{\text{a}}$ (nm)	$d_{\text{Au}}^{\text{b}}$ (nm)	$S_{\text{Au}}^{\text{a}}$ (m <sup>2</sup> g <sup>-1</sup> )	$T_{50\%}$ (°C)	$r \times 10^4$ (moles C <sub>3</sub> H <sub>6</sub> moles <sup>-1</sup> Au s <sup>-1</sup> )	$E_{\text{a}}$ (kJ mol <sup>-1</sup> )	FWHM (nm)
Au/Al <sub>2</sub> O <sub>3</sub>	4.3±0.1	4.5±0.2	1.5	365	1.4±0.1	67±3	71.1±1.2
Au/BaO/Al <sub>2</sub> O <sub>3</sub>	n.d.	n.d.	6.2	290	8. ±0.1	66±2	189.4±1.2
Au/MgO/Al <sub>2</sub> O <sub>3</sub>	4.0±0.1	4.0±0.2	n.m.	359	1.9±0.1	61±4	100.7±3.4
Au/Li <sub>2</sub> O/Al <sub>2</sub> O <sub>3</sub>	3.2±0.1	3.4±0.1	2.5	327	3.2±0.2	65±3	86.4±8.3
Au/Rb <sub>2</sub> O/Al <sub>2</sub> O <sub>3</sub>	n.d.	3.3±0.1	3.6	307	6.9±0.2	65±2	164.5±15
Al <sub>2</sub> O <sub>3</sub>	–	–	–	>450	0	90±2	–

n.m.: not measured; n.d.: not detected.

The Arrhenius plots for propene oxidation over support-only, unpromoted- and alkali (earth) promoted- Au/Al<sub>2</sub>O<sub>3</sub> catalysts are presented in Figs. 5.2A-D. The apparent activation energy ( $E_{\text{a}}$ ) was calculated at conversions ranging from 0.05 to 0.2 (Table 5.1).



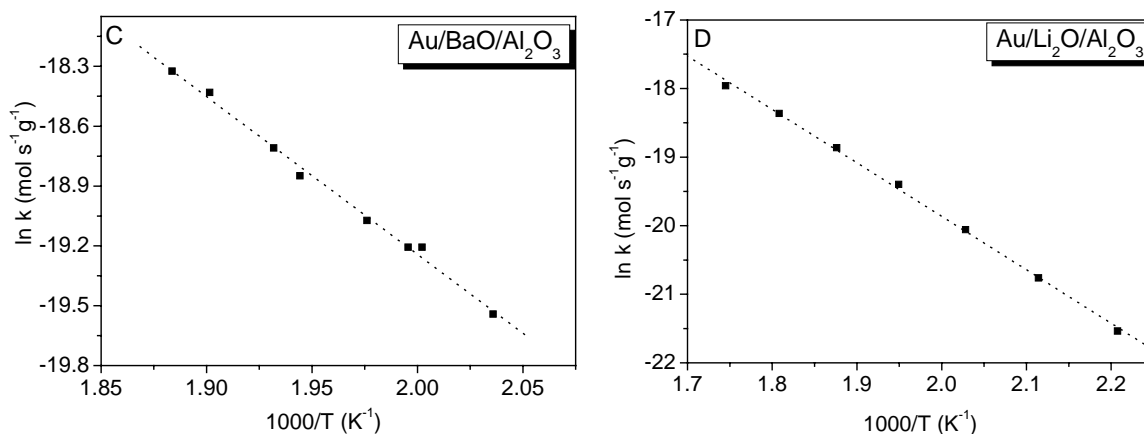


**Figure 5.2:** Arrhenius plots for propene oxidation over  $\text{Al}_2\text{O}_3$  (A),  $\text{Au}/\text{Al}_2\text{O}_3$  (B),  $\text{Au}/\text{BaO}/\text{Al}_2\text{O}_3$  (C),  $\text{Au}/\text{Li}_2\text{O}/\text{Al}_2\text{O}_3$  (D).

First, it is found that  $E_a$  decreases after gold addition to  $\text{Al}_2\text{O}_3$ , from *ca*  $90 \text{ kJ mol}^{-1}$  ( $\text{Al}_2\text{O}_3$ ) to  $67 \text{ kJ mol}^{-1}$  ( $\text{Au}/\text{Al}_2\text{O}_3$ ), indicating that gold is the active species in  $\text{C}_3\text{H}_6$  oxidation. Secondly, it is found that the presence/nature of the alkali (earth) metal oxide does not significantly change the apparent activation energy. The negligible effect of  $\text{MO}_x$  addition ( $\text{M}=\text{Li}, \text{Rb}, \text{Mg}, \text{Ba}$ ) on  $E_a$  suggests that the presence of  $\text{MO}_x$  does not create new reaction paths for  $\text{C}_3\text{H}_6$  oxidation. Presumably, their role is mostly related to the stabilization of the small gold particles.

### ***TMO, rare earth metal oxides and copper oxide as additives***

This section deals with the effect of various TMOs, rare earth metal oxides ( $\text{CeO}_x, \text{PrO}_x$ ) - Fig. 5.3A, and different loadings of copper oxide - Fig. 5.3B, on the catalytic performance of  $\text{Au}/\text{Al}_2\text{O}_3$ . In general the catalysts performed slightly better during the first heating-cooling cycle, but the difference between the cycles did not exceed  $40^\circ\text{C}$ . Results obtained during the third or fourth heating cycle were similar to those obtained during the second run. The results presented below correspond to the second heating cycle.

All the additives positively influence the catalytic activity of unpromoted  $\text{Au}/\text{Al}_2\text{O}_3$ . From the Fig. 5.3A, it is concluded that the most active catalyst is  $\text{Au}/\text{CeO}_x/\text{Al}_2\text{O}_3$ , with a temperature of 50% propene conversion of  $192^\circ\text{C}$ . This catalyst also displays the largest Au dispersion, based on HRTEM results, i.e. 52% (*Chapter 4*). Important synergistic effects were observed for all the catalysts. It should be noted that none of the supports except the CuO-containing supports are significantly active under the reaction conditions used here. A comprehensive summary for all the catalysts in terms of  $T_{50\%}$  and the specific reaction rate at  $260^\circ\text{C}$ ,  $r$ , is presented in Table 5.2. It should be mentioned that for CuO-containing Au-based catalysts the specific reaction rate was also estimated by taking into account the loading of CuO, either separately, or in combination with Au. The same table also contains the data regarding the variation of the gold particle size after the catalytic run,  $d_{\text{Au}}^b$ . It was noticed that all the catalysts showed good stability during the catalytic runs.

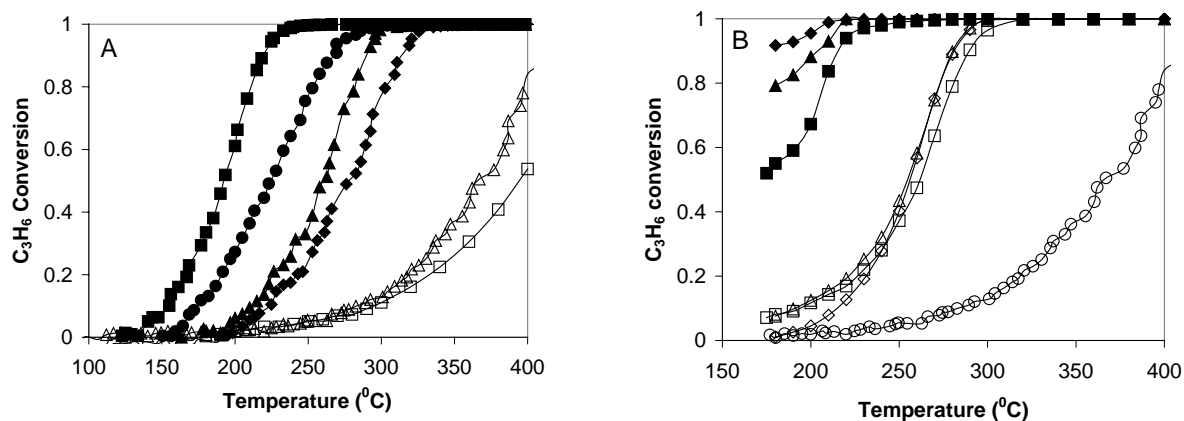


**Figure 5.3:** Propene oxidation vs. temperature over: Au/CeO<sub>x</sub>/Al<sub>2</sub>O<sub>3</sub> (■), Au/CoO<sub>x</sub>/Al<sub>2</sub>O<sub>3</sub> (◆), Au/MnO<sub>x</sub>/Al<sub>2</sub>O<sub>3</sub> (▲), Au/FeO<sub>x</sub>/Al<sub>2</sub>O<sub>3</sub> (●), Au/Al<sub>2</sub>O<sub>3</sub> (Δ), CeO<sub>x</sub>/Al<sub>2</sub>O<sub>3</sub> (□) (A). Au/CuO/Al<sub>2</sub>O<sub>3</sub>-A (■), Au/CuO/Al<sub>2</sub>O<sub>3</sub>-B (◆), Au/CuO/Al<sub>2</sub>O<sub>3</sub>-C (▲), CuO/Al<sub>2</sub>O<sub>3</sub>-A (□), CuO/Al<sub>2</sub>O<sub>3</sub>-B (◇), CuO/Al<sub>2</sub>O<sub>3</sub>-C (Δ), Au/Al<sub>2</sub>O<sub>3</sub> (○) (B).

**Table 5.2:** The temperature of 50% propene conversion, the specific reaction rate,  $r$  and the average size of the gold particles for the fresh  $d_{Au}^a$  and used (after reaction)  $d_{Au}^b$  gold-based catalysts.

Catalyst	$d_{Au}^a$ (nm)	$d_{Au}^b$ (nm)	$T_{50\%}$ (°C)	$r \times 10^4$ (moles C <sub>3</sub> H <sub>6</sub> moles <sup>-1</sup> M s <sup>-1</sup> )
Au/Al <sub>2</sub> O <sub>3</sub>	4.3±0.1	4.5±0.2	365	1.4±0.1
Au/CoO <sub>x</sub> /Al <sub>2</sub> O <sub>3</sub>	5.0±0.1	5.9±0.1	280	8.3±0.2
Au/MnO <sub>x</sub> /Al <sub>2</sub> O <sub>3</sub>	8.0±0.1	11.0±0.1	262	12±0.1
Au/FeO <sub>x</sub> /Al <sub>2</sub> O <sub>3</sub>	<3.0	3.1±0.2	224	21±0.2
Au/CeO <sub>x</sub> /Al <sub>2</sub> O <sub>3</sub>	<3.0	<3.0	192	26±0.2
Au/ZrO <sub>x</sub> /Al <sub>2</sub> O <sub>3</sub>	3.1±0.3	3.1±0.3	342	1.5±0.1
Au/ZnO/Al <sub>2</sub> O <sub>3</sub>	<3.0	3.2±0.1	358	1.6±0.1
Au/NiO/Al <sub>2</sub> O <sub>3</sub>	<3.0	<3.0	317	4.5±0.1
Au/VO <sub>x</sub> /Al <sub>2</sub> O <sub>3</sub>	<3.0	3.2±0.1	260	9.1±0.2
Au/PrO <sub>x</sub> /Al <sub>2</sub> O <sub>3</sub>	3.0±0.3	3.5±0.1	290	6.4±0.1
Au/YO <sub>x</sub> /Al <sub>2</sub> O <sub>3</sub>	<3.0	<3.0	256	13.0±0.1
Au/CrO <sub>x</sub> /Al <sub>2</sub> O <sub>3</sub>	4.8±0.1	4.8±0.3	302	3.4±0.1
Au/CuO/Al <sub>2</sub> O <sub>3</sub> -A	3.0±0.1	3.1±0.1	<180	$(26.5±0.2)^1/(5.7±0.1)^2/(7.3±0.2)^3$
Au/CuO/Al <sub>2</sub> O <sub>3</sub> -B	6.8±0.2	7.1±0.3	<180	$(14.4±0.2)^1/(2.9±0.2)^2/(3.6±0.1)^3$
Au/CuO/Al <sub>2</sub> O <sub>3</sub> -C	<3.0	<3.0	<180	$(22.2±0.2)^1/(4.3±0.1)^2/(5.4±0.2)^3$
CuO/Al <sub>2</sub> O <sub>3</sub> -A	—	—	262	3.5±0.2
CuO/Al <sub>2</sub> O <sub>3</sub> -B	—	—	256	2.0±0.1
CuO/Al <sub>2</sub> O <sub>3</sub> -C	—	—	254	3.1±0.1
CeO <sub>x</sub> /Al <sub>2</sub> O <sub>3</sub>	—	—	397	~0
MnO <sub>x</sub> /Al <sub>2</sub> O <sub>3</sub>	—	—	335	~0
FeO <sub>x</sub> /Al <sub>2</sub> O <sub>3</sub>	—	—	342	~0
Al <sub>2</sub> O <sub>3</sub>	—	—	>400	0

<sup>1</sup> $r$  was estimated based on the Au loading; <sup>2</sup> $r$  was estimated based on the (Au+CuO) loading; <sup>3</sup> $r$  was estimated based on the CuO loading. M: Au, Cu.

The variation of the specific reaction rate,  $r$ , is related to the identity of the additives. The least promoting effect is observed if  $ZrO_x$  or  $ZnO$  are added. On the other hand, an increase of more than 19 times is obtained in the presence of ceria. Iron oxide produces a 15-fold increase of  $r$ . Also  $VO_x$  and  $YO_x$  are considered as significant enhancers. It is interesting to note that  $Au/MnO_x/Al_2O_3$  with relatively big Au particles (8 nm) is very active and converts  $C_3H_6$  at a temperature lower than, for instance,  $Au/CoO_x/Al_2O_3$ . However, we cannot rule out that  $Au/MnO_x/Al_2O_3$  also contains very small gold crystallites, below the XRD detection limit ( $\sim 3$  nm).

Thus, from these results it may be concluded that for catalysts containing a transition metal oxide, or more generally an easily reducible metal oxide as additive, the mean diameter of the gold particles is not that crucial to obtain an active catalyst. The reason may reside in the intrinsic properties of the additives that may act not only as a structural promoter (by stabilizing gold particles against sintering - a phenomenon which starts early in the preparation step), but also as chemical promoter, or as cocatalyst.

Regarding the catalytic activity of the CuO-containing gold-based catalysts, if only the results presented in Fig. 5.3B are considered, the best performance is obtained when the highest content in both Au and CuO is used. Thus,  $Au/CuO/Al_2O_3$ -B (7.4 wt-% Au, 12 wt-% CuO) is the most active; this catalyst is followed by  $Au/CuO/Al_2O_3$ -C (4.8 wt-% Au, 8 wt-% CuO) and  $Au/CuO/Al_2O_3$ -A (4 wt-% Au, 6 wt-% CuO). However, the catalytic performance per gram of catalyst of  $CuO/Al_2O_3$  is almost similar for the three catalysts with different CuO loadings and  $r$  decreases when the loading of CuO is increased (Table 5.2). The same trend is found for  $Au/CuO/Al_2O_3$  catalysts with various Au and CuO concentrations. As a final remark, for  $Au/CuO/Al_2O_3$ -B the average size of the gold particles is relatively large, but the influence of this factor on the overall activity appears to be not very important.

### ***Two different metal oxides as additives***

The catalytic performance of various multicomponent gold-based catalysts is presented in Figs. 5.4A-B in terms of propene conversion versus temperature. The results for all the gold-based catalysts consisting of two different metal oxides are summarized in Table 5.3 in terms of  $T_{50\%}$ , the specific reaction rate,  $r$ , estimated at  $260^\circ C$ ,  $d_{Au}^a$  (fresh catalysts) and  $d_{Au}^b$  (used catalysts). It should be mentioned that for  $Au/CuO/CeO_x/Al_2O_3$  catalyst the specific reaction rate was also estimated by taking into account the loading of CuO, either separately, or in combination with Au.

As illustrated in Fig. 5.4A, the difference in the catalytic performance is not large for combinations of  $Li_2O-CeO_x$ ,  $Rb_2O-CeO_x$  and  $BaO-CeO_x$ . Concerning the results presented in Fig. 5.4B,  $YO_x-CeO_x$  and  $MnO_x-MgO$  are less efficient promoters than  $CeO_x-ZrO_x$ . An interesting situation is observed for  $Au/CeO_x/Al_2O_3$ .



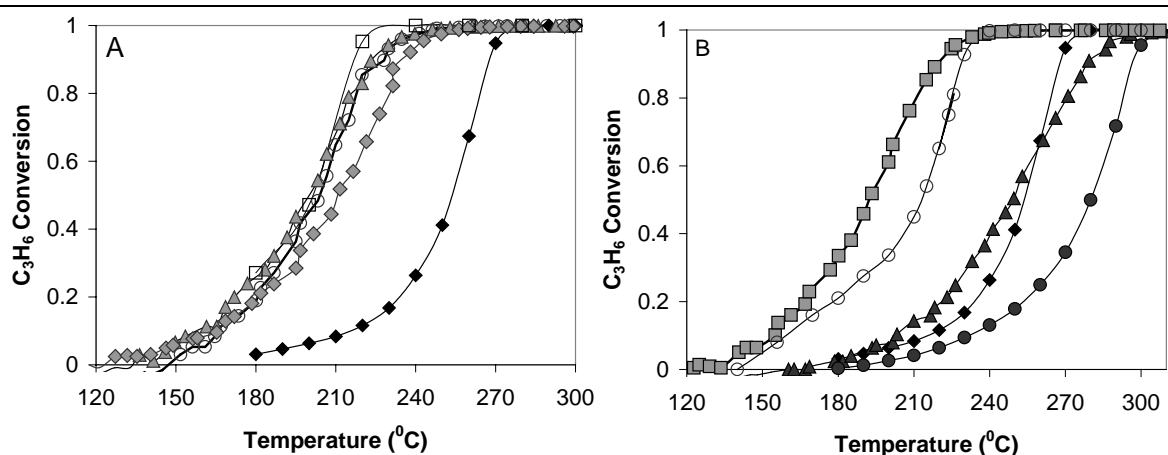


**Figure 5.4:** The propene conversion vs. temperature over Au/Rb<sub>2</sub>O/CeO<sub>x</sub>/Al<sub>2</sub>O<sub>3</sub> (□), Au/BaO/CeO<sub>x</sub>/Al<sub>2</sub>O<sub>3</sub> (○), Au/Li<sub>2</sub>O/CeO<sub>x</sub>/Al<sub>2</sub>O<sub>3</sub> (▲), Au/MgO/CeO<sub>x</sub>/Al<sub>2</sub>O<sub>3</sub> (◆), Au/CeO<sub>x</sub>/Al<sub>2</sub>O<sub>3</sub> (♦) (A); Au/ZrO<sub>x</sub>/CeO<sub>x</sub>/Al<sub>2</sub>O<sub>3</sub> (○), Au/YO<sub>x</sub>/CeO<sub>x</sub>/Al<sub>2</sub>O<sub>3</sub> (▲), Au/MnO<sub>x</sub>/MgO/Al<sub>2</sub>O<sub>3</sub> (●), Au/CeO<sub>x</sub>/Al<sub>2</sub>O<sub>3</sub> (♦), Au/CeO<sub>x</sub>/Al<sub>2</sub>O<sub>3</sub>\* (■) (B).

Fig. 5.4B shows the catalytic performance of two batches of ceria-containing gold-based catalysts. Their catalytic performance differs quite a lot even though their preparation procedure was the same. Thus, if the catalytic behaviour of the multicomponent catalysts is compared with Au/CeO<sub>x</sub>/Al<sub>2</sub>O<sub>3</sub> marked by (♦), the synergistic effects found are rather significant. However, the other Au/CeO<sub>x</sub>/Al<sub>2</sub>O<sub>3</sub>\* (■) is more active than any of the multicomponent catalysts. The large difference in the catalytic behaviour of these two batches with ceria as additive may have different origins. First, the average size of the gold particles plays an important role. The most active sample, i.e. Au/CeO<sub>x</sub>/Al<sub>2</sub>O<sub>3</sub> (■), displays an average gold particle size around 1.7 nm, with the corresponding metallic surface area of 7.25 m<sup>2</sup> g<sup>-1</sup> and a 52% Au dispersion (*Chapter 4*). The gold particles of the other catalyst have an average size of around 4.8 nm, and much smaller values for the metallic surface area (2.13 m<sup>2</sup> g<sup>-1</sup>) and dispersion (15%). This large difference regarding the active phase can induce a large difference in the catalytic behaviour. The second reason is related to the ceria crystallites. Cerium ions influence the anchoring of Au particles on the support. In addition, as was suggested earlier [5], ceria stabilizes the small size of the gold particles. The gold-ceria interface may also play an important role in the catalytic performance. It was reported that the crystallite size of CeO<sub>2</sub> is also important for high activity [6]. The mean particle size of CeO<sub>2</sub>, estimated by XRD measurements, is around 7.5 nm for the most active catalyst and around 9 nm for the least active catalyst. These results indicate that besides the size of the gold particles, also the mean particle diameter of the metal oxide additive is important. This can be easily understood if it is considered that ceria, due to its redox properties, may improve the catalytic behaviour of the catalyst by increasing the supply of active oxygen and thus the size of the ceria particles becomes important [7].

**Table 5.3:** The temperature of 50% propene conversion, the specific reaction rate,  $r$  and the average size of the gold particles for the fresh  $d_{Au}^a$  and used (after reaction)  $d_{Au}^b$  multicomponent gold-based catalysts.

Catalyst	$d_{Au}^a$ (nm)	$d_{Au}^b$ (nm)	$T_{50\%}$ ( $^{\circ}C$ )	$r \times 10^4$ (moles $C_3H_6$ moles $^{-1}M$ s $^{-1}$ )
Au/Al <sub>2</sub> O <sub>3</sub>	4.3±0.1	4.5±0.2	365	1.4±0.1
Au/CeO <sub>x</sub> /ZrO <sub>x</sub> /Al <sub>2</sub> O <sub>3</sub>	<3.0	<3.0	212	33.3±0.2
Au/MnO <sub>x</sub> /MgO/Al <sub>2</sub> O <sub>3</sub>	<3.0	5.3±0.4	282	5.9±0.1
Au/Li <sub>2</sub> O/CeO <sub>x</sub> /Al <sub>2</sub> O <sub>3</sub>	<3.0	<3.0	199	23.1±0.2
Au/Rb <sub>2</sub> O/CeO <sub>x</sub> /Al <sub>2</sub> O <sub>3</sub>	<3.0	<3.0	200	23.7±0.1
Au/Rb <sub>2</sub> O/MnO <sub>x</sub> /Al <sub>2</sub> O <sub>3</sub>	5.0±0.3	5.8±0.1	260	12.9±0.2
Au/BaO/CeO <sub>x</sub> /Al <sub>2</sub> O <sub>3</sub>	<3.0	<3.0	205	24.2±0.1
Au/MgO/CeO <sub>x</sub> /Al <sub>2</sub> O <sub>3</sub>	<3.0	<3.0	210	25.8±0.1
Rb <sub>2</sub> O/Au/CeO <sub>x</sub> /Al <sub>2</sub> O <sub>3</sub>	3.3±0.3	3.7±0.1	205	25.8±0.2
Au/YO <sub>x</sub> /CeO <sub>x</sub> /Al <sub>2</sub> O <sub>3</sub>	<3.0	3.5±0.1	250	16.8±0.1
Au/CuO/CeO <sub>x</sub> /Al <sub>2</sub> O <sub>3</sub>	16.8±0.1	17.0±0.3	200	(13.4±0.1) <sup>1</sup> /(2.5±0.1) <sup>2</sup> /(3.1±0.1) <sup>3</sup>
Au/CeO <sub>x</sub> /Al <sub>2</sub> O <sub>3</sub> <sup>*</sup>	4.8±0.1	4.9±0.3	253	17.5±0.2
MnO <sub>x</sub> /MgO/Al <sub>2</sub> O <sub>3</sub>	–	–	295	0
CeO <sub>x</sub> /ZrO <sub>x</sub> /Al <sub>2</sub> O <sub>3</sub>	–	–	385	0

<sup>\*</sup> $d_{Ce} = 9.0$  nm; <sup>1</sup> $r$  was estimated based on the Au loading; <sup>2</sup> $r$  was estimated based on the (Au+CuO) loading; <sup>3</sup> $r$  was estimated based on the CuO loading. M: Au, Cu.

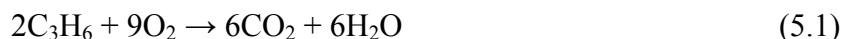
If the catalysts are discussed in terms of  $r$  variation, the combination ceria-zirconia is the most active, with a 24-fold increase, compared with unpromoted Au/Al<sub>2</sub>O<sub>3</sub>, and 1.3 times if only ceria is present. It was reported that Au/MnO<sub>x</sub>/MgO/Al<sub>2</sub>O<sub>3</sub> is an efficient catalyst for CO oxidation [8, 9]. However, this behaviour is not found for propene oxidation. The efficiency of Au-based catalysts increases upon combining alkali (earth) metal oxides with ceria, with BaO and MgO being the most efficient. The best results are found in the presence of ZrO<sub>2</sub>+CeO<sub>x</sub>. Finally, these results emphasize the role of ceria on the catalytic performance of Au containing catalysts.

The gold particles are preserved during the catalytic test and no significant sintering was observed by XRD (Table 5.3).

## 5.4 Discussion

### The influence of MO<sub>x</sub> addition. Active sites

The oxidation of propene proceeds via the following reaction:



The experiments have been carried out under large excess of oxygen ( $C_3H_6:O_2 = 1:9$ ), and no by-products were formed.

The addition of various MO<sub>x</sub> to Au/Al<sub>2</sub>O<sub>3</sub> influences both the sintering behaviour of Au nano-particles and the catalytic performance. Due to the additives, small gold particles were preserved during the preparation. These small Au particles are more active than larger gold

particles. Figure 5.5 illustrates the possible relation between the size of the gold particles and the  $T_{50\%}$ .

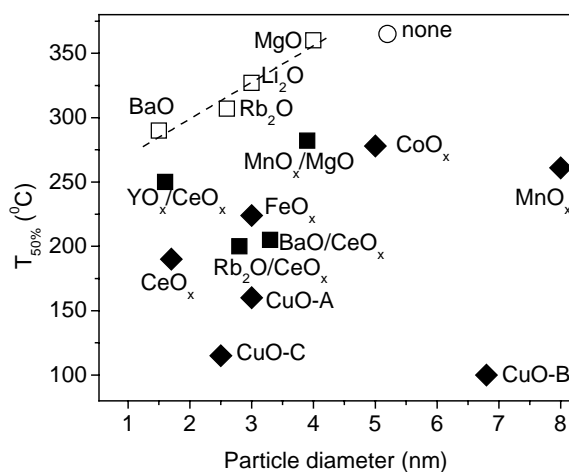


**Figure 5.5:**  $T_{50\%}$  vs. the average gold particle size for the unpromoted (○), alkali (earth) (□), TM/ceria/CuO (◆) and two different metal oxides (■) promoted gold catalysts.

It is observed that the variation of  $T_{50\%}$  is directly related to the size of the Au particles for the Au/Al<sub>2</sub>O<sub>3</sub> catalysts with alkali (earth) metal oxides added. Because the mixed supports are hardly active towards propene oxidation, most probably  $T_{50\%}$  is directly correlated with  $d_{Au}$ . For the Au-based catalysts with TMO, CuO, or rare earth metal oxides as additives, the situation is not clear. Catalysts with small gold particles are highly active (ceria), and  $T_{50\%}$  shifts to higher temperatures (FeO<sub>x</sub> and CoO<sub>x</sub>) with increasing Au particle size. However, Au/MnO<sub>x</sub>/Al<sub>2</sub>O<sub>3</sub>, with an average Au particle size of 8 nm is also very active. Thus, not only the size of the Au particles is important. It is therefore concluded that the catalytic performance in propene oxidation is directly correlated with both the particle size of gold and the identity of the additive.

Two different parameters have been considered in order to evaluate the active sites, i.e. surface versus perimeter sites. Thus, if the catalyst activity would reside exclusively on surface sites, a linear variation of the activity with  $1/D_s$  would be expected, with  $D_s$  the surface average diameter. Alternatively, if the catalyst activity were located exclusively at the perimeter, the activity should scale as  $1/D_p^2$ , with  $D_p$  the perimeter average diameter [10, 11]. The calculations of these two parameters have been done according to the following equations and as described in Chapter 3:

$$D_p = \frac{D_n^2 + D_s^2}{D_n + D_s} \quad (5.2)$$

$$D_s = \frac{\sum n_i \cdot d_i^3}{\sum n_i \cdot d_i^2} \quad (5.3)$$

$$D_n = \frac{\sum n_i \cdot d_i}{\sum n_i} \quad (5.4)$$

where:

- $n_i$ : number of gold particles (HRTEM) with the diameter  $d_i$ ;
- $D_p$ : the perimeter average;
- $D_s$ : the surface average diameter;
- $D_n$ : the average diameter.

It should be mentioned that these formulas do not distinguish between the perimeter or surface average  $\text{Au-M}^{\text{I}}\text{O}_x$  and  $\text{Au-M}^{\text{II}}\text{O}_x$  for the multicomponent catalysts and the results are a contribution of both.

Figure 5.6A shows the variation of  $r$  with the number of the active sites situated at the perimeter gold-support ( $1/D_p^2$ ) or at the surface,  $1/D_s$  for alkali (earth) metal oxides added to  $\text{Au}/\text{Al}_2\text{O}_3$ . The same parameters are plotted in Fig. 5.6B for the TMO/ceria as additives, and the variation of  $1/D_p^2$  and  $1/D_s$  for the multicomponent catalysts is shown in Fig. 5.6C.

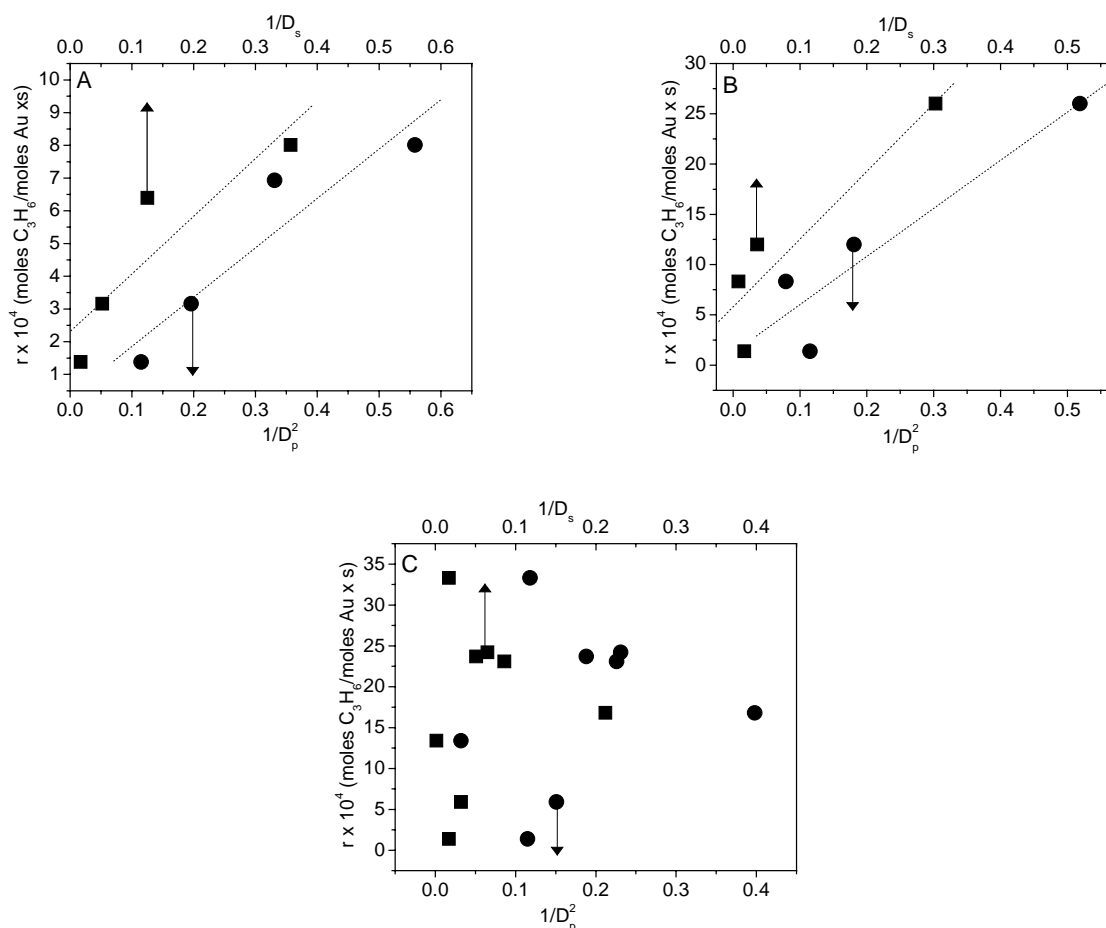


**Figure 5.6:** The variation of  $r$  with the active sites situated at the perimeter  $1/D_p^2$  ( $\bullet$ ), or at the surface  $1/D_s$  ( $\blacksquare$ ) of the catalyst. Alkali (earth) metal oxides (A), TMO/ceria (B), multicomponent catalysts (C). The arrows indicate the corresponding axis.

The fit is reasonable for both models in Fig. 5.6A. Therefore, these two competing models for the reactivity of Au catalysts cannot be discriminated. The situation is more complex in Fig. 5.6B, but there is still a reasonable fit for both models. The most complex situation is found for the multicomponent Au catalysts (Fig. 5.6C), where none of the models correlate with the variation of the specific reaction rate,  $r$ . It is clear that the reaction mechanism is more complex and no clear correlation exists between  $r$  and the fraction of sites on the surface or on the perimeter. Finally, these results emphasize that not only gold particles are important for the activity, the support/additives also play an important role.

Alkali (earth) metal oxides do not have any ability to supply active oxygen. Therefore, the promoter effect of alkali (earth) metal oxides cannot be explained in terms of a redox mechanism. The variation of the  $E_a$  after Au addition to  $\text{Al}_2\text{O}_3$  indicates that gold is the active species in this reaction (bare alumina is hardly active under these reaction conditions). On the other hand, the absence of a significant effect of the addition of the alkali (earth) metal oxides on the apparent activation energy of Au/ $\text{Al}_2\text{O}_3$  suggests that the presence/nature of these additives do not create new reaction paths for  $\text{C}_3\text{H}_6$  oxidation. The activation of propene proceeds on gold, or, possibly, at the gold-support interface. This situation is completely different from what is known for ammonia synthesis, where the role of alkali metal oxides ( $\text{K}_2\text{O}$ ,  $\text{Cs}_2\text{O}$ ) on Fe- and Ru-based catalysts is that of a chemical promoter by lowering the  $\text{N}_2$  dissociation barrier [12-15]. In propene oxidation, the experimental data prove that the role of  $\text{MO}_x$  is mostly that of a stabilizer for small gold particles (XRD and HRTEM data), and no direct effect on the chemical process could be detected by means of  $E_a$ . Thus, the role of alkali (earth) metal oxides is rather to increase the concentration of the Au active sites, without creating new reaction pathways. These additives appear to act only as structural promoters.

Cobalt oxide, chromium oxide and copper oxide are reported to belong to the most active oxides for catalytic combustion [16-18]. Also, spinel-like materials, such as  $\text{CoCr}_2\text{O}_4$ ,  $\text{CuCr}_2\text{O}_4$ ,  $\text{ZnCr}_2\text{O}_4$  [19, 20], and perovskite-like compounds,  $\text{LaMO}_3$  (with M: Sr, Ba, K, Cs, Ni, Zn, Cu, Mn) [21, 22] are reported to be promising due to their high activity and stability at high temperatures. If these types of oxides are combined with gold, a more complex situation is obtained compared with the alkali (earth) metal oxide promoted systems. The identity of these oxides is very important to obtain an active catalyst and the catalytic activity does not correlate anymore with the gold particle size. This is because these oxides are intrinsically active (i.e. copper oxide), or they have the ability to provide active oxygen during the reaction cycle ( $\text{CeO}_x$ ,  $\text{MnO}_x$ ,  $\text{FeO}_x$ ). It has been reported, for example, that for the total oxidation of some volatile organic compounds, VOCs (2-propanol, methanol and toluene), the catalytic activity of Au/ $\text{Al}_2\text{O}_3$  and Au/ $\text{CeO}_2$  is directly related to the capacity of gold to increase the mobility of the metal oxide lattice oxygen which is involved in the oxidation of VOCs through a Mars and van Krevelen mechanism [23, 24].

As already shown, the best promoting effect observed for the various TMO and rare earth metal oxides examined was found for ceria. This oxide is very well known for its oxygen storage capacity (OSC) defined as the capacity to release/accept oxygen under fuel-rich/lean

conditions in the gas stream. Centeno and co-workers [5] have studied the catalytic combustion of VOCs on Au/CeO<sub>x</sub>/Al<sub>2</sub>O<sub>3</sub> and they concluded that the presence of cerium ions exerts a positive influence on the fixation and the final dispersion of gold on alumina support. In addition, ceria stabilizes the gold particles with low crystallite size. Besides these beneficial features, ceria, due to its redox properties, may improve the catalytic behaviour of the catalyst by increasing the supply of active oxygen. A similar model has been proposed by Scire *et al.* [24] based on their study of VOCs oxidation over Au/CeO<sub>2</sub>.

The mechanism of hydrocarbon oxidation over ceria and other reducible metal oxides is usually considered to be of the redox or Mars and van Krevelen type [5, 24-26]. The key steps of this mechanism are believed to be the supply of the active oxygen by the readily reducible oxide and its reoxidation by oxygen. As previously described, the size of the ceria crystallites also plays an important role, since the active oxygen is supplied by CeO<sub>2</sub>. The interfacial effect created by metal-support interaction appears at least as important as the mean diameter of the gold particles. Under these reaction conditions, XRD revealed no significant change of the diameter of ceria particles for the used catalyst. This finding implies a high stability of ceria during the catalytic test.

The oxygen availability of CeO<sub>x</sub> and, in turn, the presence of a Mars and van Krevelen mechanism in propene oxidation, has been discussed for pre-reduced (H<sub>2</sub>, 300°C, 30minutes) CeO<sub>x</sub>/Al<sub>2</sub>O<sub>3</sub> [7]. During the catalytic run, oxygen was replaced by argon. Hence, the feed passing through the catalyst bed consisted of 4 vol% C<sub>3</sub>H<sub>6</sub> in He co-fed with Ar. Interestingly, besides propene consumption and water formation, a relatively large amount of CO<sub>2</sub> was detected. This is a direct indication that, although CeO<sub>x</sub>/Al<sub>2</sub>O<sub>3</sub> was subjected to mild hydrogen pretreatment at 300°C during 30 minutes prior the reaction, there is still lattice oxygen available for reaction with C<sub>3</sub>H<sub>6</sub> to form CO<sub>2</sub> and H<sub>2</sub>O. The conversion of propene versus temperature for Au/CeO<sub>x</sub>/Al<sub>2</sub>O<sub>3</sub> and CeO<sub>x</sub>/Al<sub>2</sub>O<sub>3</sub> is shown in Fig. 5.7A.

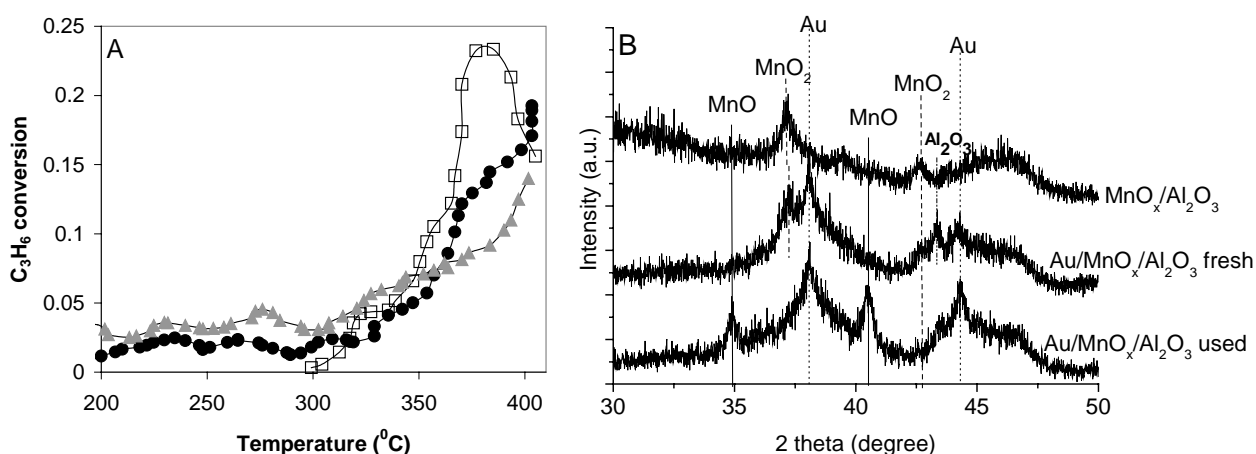


**Figure 5.7:** Propene conversion vs. temperature over Au/CeO<sub>x</sub>/Al<sub>2</sub>O<sub>3</sub> (●), CeO<sub>x</sub>/Al<sub>2</sub>O<sub>3</sub> (□) and Au/MnO<sub>x</sub>/Al<sub>2</sub>O<sub>3</sub> (▲) (A); XRD patterns of MnO<sub>x</sub>/Al<sub>2</sub>O<sub>3</sub>, fresh-Au/MnO<sub>x</sub>/Al<sub>2</sub>O<sub>3</sub> and used-Au/MnO<sub>x</sub>/Al<sub>2</sub>O<sub>3</sub> (B).

Clearly, the consumption of  $C_3H_6$  starts around  $300^{\circ}C$ , the same temperature range at which  $C_3H_6$  is oxidized in the presence of  $O_2$  (see Fig. 5.3A). At the end of the experiment, some coke deposition was visible on the topmost part of the catalyst bed. Apparently, the rate of C formation and deposition was higher than its transformation into  $CO_2$ . Hence, in the case of  $CeO_x/Al_2O_3$ , a Mars and van Krevelen type of mechanism is operative, and the lattice oxygen of  $CeO_x$  is accessible for the reaction with  $C_3H_6$ .

A similar experiment has been performed over a mildly pre-reduced  $Au/CeO_x/Al_2O_3$  catalyst. As should be expected,  $CO_2$  and  $H_2O$  are formed and propene is consumed in the same temperature range ( $\sim 300^{\circ}C$ ) as found for  $CeO_x/Al_2O_3$ . The  $C_3H_6$  conversion was slightly lower than was found for  $CeO_x/Al_2O_3$ . Nevertheless, a 20% conversion of  $C_3H_6$  could be achieved over  $Au/CeO_x/Al_2O_3$  in this temperature range without  $O_2$  in the feed (see Fig. 5.7A). This experiment proves that the oxygen of ceria is highly mobile and plays an active role in  $C_3H_6$  oxidation into  $CO_2$ . X-ray diffraction experiments performed on the used  $Au/CeO_x/Al_2O_3$  did not reveal any change, neither in the structure of  $CeO_2$ , nor in that of Au. Probably only the near surface oxygen, known as highly mobile species, plays an active role in the oxidation and the reaction temperature was not sufficiently high to convert the  $CeO_2$  to  $Ce_2O_3$ . In addition, no change of the structure of Au was detected using XRD and the average size of the gold particles as estimated by the FWHM of  $2\theta = 38.2^{\circ}$  ( $d = 2.35 \text{ \AA}$ ) was not affected by this experiment. Coke deposition has not been observed for  $Au/CeO_x/Al_2O_3$ . Possibly, the presence of gold prevents coke formation during  $C_3H_6$  oxidation.

Another base oxide that can easily change the valence of the metal ion is  $MnO_x$ . In order to prove any direct involvement of this oxide in propene oxidation, a similar experiment as the one described for  $Au/CeO_x/Al_2O_3$ , has been done using mildly pre-reduced  $Au/MnO_x/Al_2O_3$ . In the absence of  $O_2$ , a maximum  $C_3H_6$  conversion of 14% was found in the first heating run (Fig. 5.7A).

In addition, XRD measurements performed on the used  $Au/MnO_x/Al_2O_3$  revealed a dramatic change of the structure of the catalyst. Fig. 5.7B shows the XRD patterns for  $MnO_x/Al_2O_3$ , fresh- $Au/MnO_x/Al_2O_3$  and used- $Au/MnO_x/Al_2O_3$ . One can see that the XRD pattern of fresh- $Au/MnO_x/Al_2O_3$  consists of several lines that belong either to the  $MnO_x/Al_2O_3$  ( $2\theta = 37.2^{\circ}$ ,  $d = 2.41 \text{ \AA}$ ,  $2\theta = 43.3^{\circ}$ ,  $d = 2.08 \text{ \AA}$ ,  $x = 2$  [27]), metallic gold ( $2\theta = 38.2^{\circ}$ ,  $d = 2.35 \text{ \AA}$ ,  $2\theta = 44.3^{\circ}$ ,  $d = 2.04 \text{ \AA}$ ), and  $Al_2O_3$  ( $2\theta = 43.3^{\circ}$ ,  $d = 2.08 \text{ \AA}$ ). For the used- $Au/MnO_x/Al_2O_3$  (Fig. 5.7B) the XRD pattern of  $MnO_2$  had disappeared and new lines at  $2\theta = 34.8^{\circ}$  ( $d = 2.57 \text{ \AA}$ ) and  $2\theta = 40.5^{\circ}$  ( $d = 2.22 \text{ \AA}$ ) -  $MnO$  [27] - have appeared. In addition, the line intensity of metallic gold increases, especially the one from  $2\theta = 44.3^{\circ}$  ( $d = 2.04 \text{ \AA}$ ). Thus,  $Au/MnO_x/Al_2O_3$  suffers drastic changes upon reaction with propene in the absence of  $O_2$ , whereas with  $Au/CeO_x/Al_2O_3$  the whole structure of ceria is preserved in the form of  $CeO_2$  and only a minor reduction takes place. Thermodynamic data suggest that the reduction of  $MnO_2$  to  $MnO$  requires  $135 \text{ kJ mol}^{-1}$ . On the other hand, for formation of  $Ce_2O_3$  from  $CeO_2$  the much higher energy of  $378 \text{ kJ mol}^{-1}$  is needed. These data confirm the experimental results, i.e. that the reduction of  $MnO_2$  to  $MnO$  proceeds more easily than the reduction of  $CeO_2$  to  $Ce_2O_3$ . As a consequence,  $MnO$  is obtained with only  $C_3H_6$  in the gas stream, while  $CeO_2$  is only little affected by the reducing gas.

On the basis of these results it is concluded that, indeed, the Mars and van Krevelen mechanism plays a significant role in propene oxidation over Au/CeO<sub>x</sub>/Al<sub>2</sub>O<sub>3</sub> and Au/TMO/Al<sub>2</sub>O<sub>3</sub> catalysts. Hence, the readily reducible oxide can provide the active oxygen required for the reaction, and, probably, there is a direct relationship between oxygen availability (based on our calculations mainly the near surface oxygen of ceria is involved in the reaction) and the catalytic performance. This oxidation mechanism may also explain the gold particle size effect, i.e. why Au/MnO<sub>x</sub>/Al<sub>2</sub>O<sub>3</sub> ( $d^{\text{XRD}}_{\text{Au}} = 8 \text{ nm}$ ) is still a very effective catalyst in C<sub>3</sub>H<sub>6</sub> oxidation in spite of its large gold particles: the active oxygen is provided by MnO<sub>x</sub> and propene may be activated on Au or at the gold/support interface. Additionally, other factors may also play a role in the observed catalytic performance of Au/MO<sub>x</sub>/Al<sub>2</sub>O<sub>3</sub>. Density-functional calculations on Au clusters show that O<sub>2</sub> and CO can adsorb on Au atoms if the coordination number (CN) is less than 8 [28]. In turn, the concentration of low coordinated Au atom depends both on the size and the shape of the particle [29]. In this case the direct relationship between the size of gold particles and the catalytic activity in C<sub>3</sub>H<sub>6</sub> oxidation does not always apply (see above). For some of the catalysts other shapes than spherical were visualized by HRTEM (*Chapter 4*). On the other hand, the interaction of Au with the support is stronger on a surface with oxygen defects, increased number of steps or adatoms. As was already discussed, ceria, for example, may have a relatively high concentration of oxygen vacancies due to its very facile redox cycle Ce<sup>4+</sup>/Ce<sup>3+</sup>. As a result, the characteristics of the support may influence both the Au anchoring process and the overall catalytic activity.

It is concluded that over gold-based catalysts that contain TMO, rare earth metal oxides or copper oxide, the oxidation of propene is facilitated by the available oxygen coming from the additives via the Mars and van Krevelen mechanism. This mechanism implies that propene is most likely activated on gold or at the gold-support interface and will react with oxygen from the lattice of the oxide. In the next step the oxygen from the gas phase will refill the O-vacancy. These additives simultaneously act as structural promoters, stabilizing the small gold particles against sintering. Recently, direct evidence for activation of propene on gold was obtained by XPS [30].

It is expected that a similar chemistry takes place over the gold-based catalysts that contain a TMO/ceria/copper oxide and an alkali (earth) metal oxide. However, it is clear that ceria is the most important additive in order to obtain a highly active oxidation catalyst and the identity of the other additive is (slightly) less important. It is also possible that the crystalline structure of ceria is stabilized by the other additive (i.e. ZrO<sub>x</sub>, MgO, BaO, Li<sub>2</sub>O, Rb<sub>2</sub>O), because the latter do not have real abilities to change metal ion valency during the catalytic reaction.

## 5.5 Conclusions

The variation of the T<sub>50%</sub> and the specific reaction rate,  $r$ , clearly indicate a particle size effect of gold on the activity for Au/Al<sub>2</sub>O<sub>3</sub> catalysts containing additives such as alkali (earth) metal oxides. Moreover, the values of the apparent activation energy,  $E_a$ , for Au/Al<sub>2</sub>O<sub>3</sub> and Au/MO<sub>x</sub>/Al<sub>2</sub>O<sub>3</sub> (M: alkali (earth) metals) reveal that the additives (Li<sub>2</sub>O, Rb<sub>2</sub>O, MgO and



BaO) are not directly responsible for the higher catalytic activity. The deactivation process can be prevented by the presence of these additives. Based on the experimental results it is concluded that the role of this kind of additives is to increase the concentration of the Au active sites, by acting as structural promoters. The best promoting effect is obtained when BaO is used.

The variation of the  $T_{50\%}$  and  $r$  does not directly correlate with the average size of the Au particles if the additives are TM/rare earth metal oxides. These additives are directly involved in the stabilization of the gold particles against sintering. However, besides this function of a structural promoter, these additives act as cocatalysts as well. It is experimentally proven that for these gold-based catalysts a Mars and van Krevelen mechanism is valid. This mechanism implies that the reactant (propene) is activated on gold or the gold-support interface and that the active oxygen comes from the lattice of the metal oxide. Recently, direct evidence for activation of propene on gold was obtained by XPS [30]. In addition, the structure of the metal oxide is important because it can affect the anchoring process of gold particles, but it is also directly involved in supplying the active oxygen, and the average particle size of  $MO_x$  is important as well. The most active catalysts comprise Au and  $CeO_x$ , both in the nanometer range.

Active multicomponent Au-based catalysts contain either two readily reducible metal oxides, or TMO/ceria in combination with alkali (earth) metal oxides. The most active catalysts are obtained by combining ceria with zirconia or with alkali (earth) metal oxides. The same mechanism (Mars and van Krevelen) is expected to proceed over these catalysts.

## 5.6 References

- [1] J. P. Chen, R. T. Yang, *Appl. Catal. A* 80 (1992) 135.
- [2] T. Baba, Y. Inoue, Y. Ono, *J. Catal.* 159 (1996) 230.
- [3] K.-J. Berg, A. Berger, H. Hofmeister, *Z. Phys. D* 20 (1991) 309.
- [4] P. Claus, A. Bruckner, C. Mohr, H. Hofmeister, *J. Am. Chem. Soc.* 122 (2000) 11430 and refs. therein.
- [5] M. A. Centeno, M. Paulis, M. Montes, J. A. Odriozola, *Appl. Catal. A* 234 (2002) 65.
- [6] S. Carrettin, P. Concepcion, A. Corma, J. M. Lopez Nieto, V. F. Puentes, *Angew. Chem. Int. Ed.* (2004) 2538.
- [7] A. C. Gluhoi, N. Bogdanchikova, B. E. Nieuwenhuys, *J. Catal.* 229 (2005) 154.
- [8] R. J. H. Grisel, C. J. Weststrate, A. C. Gluhoi, B. E. Nieuwenhuys, *Gold Bull.* 35 (2002) 39.
- [9] R. J. H. Grisel, *Supported gold catalysts for environmental applications*, PhD thesis, Leiden University (2002).
- [10] Q. Xu, K. C. C. Kharas, A. K. Datye, *Stud. Surf. Sci. Catal.* 139 (2001) 157.
- [11] Q. Xu, K. C. C. Kharas, A. K. Datye, *Catal. Lett.* 85 (2003) 229.
- [12] Z. Kowalczyk, J. Sentek, S. Jodzis, M. Muhler, O. Hinrichsen, *J. Catal.* 169 (1997) 407.
- [13] Z. Kowalczyk, M. Krukowski, W. Rarog-Pilecka, D. Szmigiel, J. Zielinski, *Appl. Catal. A* 248 (2003) 67.
- [14] D. Szmigiel, H. Bielawa, M. Kurtz, O. Hinrichsen, M. Muhler, W. Rarog, S. Jodzis, Z. Kowalczyk, L. Znak, J. Zielinski, *J. Catal.* 205 (2002) 205.
- [15] R. A. van Santen, J. W. Niemantsverdriet, *Chemical Kinetics and Catalysis*, Plenum Press, New York 1995.
- [16] J. E. Germain, *Catalytic Conversion of Hydrocarbons*, Academic Press 1967.
- [17] G. K. Boreskov, *Catalysis Science and Technology*, Vol. 3, Springer-Verlag, Berlin 1985.
- [18] E. Garbowski, M. Guenin, M. C. Marion, M. Primet, *Appl. Catal.* 64 (1990) 209.
- [19] L. Y. Margolis, *Adv. Catal.* 14 (1963) 429.
- [20] A. Terleckibaricevic, B. Grbic, D. Jovanovic, S. Angelov, D. Mehandziev, C. Marinova, P. Kirilovstefanov, *Appl. Catal.* 47 (1989) 145.

- [21] F. C. Buciuman, F. Patcas, J. C. Menezo, J. Barbier, T. Hahn, H. G. Lintz, *Appl. Catal. B* 35 (2002) 175.
- [22] V. Blain-Aube, J. Belkouch, L. Monceaux, *Appl. Catal. B* 43 (2003) 175.
- [23] S. Minico, S. Scire, C. Crisafulli, R. Maggiore, S. Galvagno, *Appl. Catal. B* 28 (2000) 245.
- [24] S. Scire, S. Minico, C. Crisafulli, C. Satriano, A. Pistone, *Appl. Catal. B* 40 (2003) 43.
- [25] E. Finocchio, G. Busca, V. Lerezelli, V. S. Escribano, *J. Chem. Soc.-Farad. Trans.* 92 (1996) 1587.
- [26] E. Finocchio, R. J. Willey, G. Busca, V. Lorenzelli, *J. Chem. Soc.-Farad. Trans.* 93 (1997) 175.
- [27] JCPDS Powder Diffraction File, International Centre for Diffraction Data.
- [28] N. Lopez, J. K. Norskov, *J. Am. Chem. Soc.* 124 (2002) 11262.
- [29] N. Lopez, J. K. Norskov, T. V. W. Janssens, A. Carlsson, A. Puig-Molina, B. S. Clausen, J. D. Grunwaldt, *J. Catal.* 225 (2004) 86.
- [30] C. P. Vinod, J. W. Niemantsverdriet, B. E. Nieuwenhuys, to be published.



# Chapter 6

## Oxidation of saturated hydrocarbons: total oxidation of methane and propane

*Unpromoted- and promoted- Au/Al<sub>2</sub>O<sub>3</sub> have been used as catalysts for combustion of the saturated hydrocarbons methane and propane. As expected, higher temperatures are required to oxidize CH<sub>4</sub> compared with C<sub>3</sub>H<sub>8</sub>. A direct relationship is found between the catalytic performance and the average size of the gold particles in the presence of additives such as alkali (earth) metal oxides. The effect of the gold particle size becomes less important for additives of the type of transition metal oxides, ceria or CuO. Particularly good results have been obtained for MnO<sub>x</sub> and CoO<sub>x</sub> as additives. The results suggest that the role of the alkali (earth) metal oxides is more related to the stabilization of the gold nano- particles, whereas additives such as TMO, CuO and ceria may be involved in oxygen activation.*

## 6.1 Outline

This chapter describes the catalytic performance of unpromoted- and promoted- ( $\text{MO}_x$  or  $\text{M}^{\text{I}}\text{O}_x/\text{M}^{\text{II}}\text{O}_x$ )  $\text{Au}/\text{Al}_2\text{O}_3$  ( $\text{M} = \text{Li}, \text{Rb}, \text{Ba}, \text{Cu}, \text{Cr}, \text{Fe}, \text{Mn}, \text{Co}, \text{Cu}, \text{Ti}, \text{V}, \text{Ce}, \text{Zr}, \text{Zn}, \text{Y}, \text{Pr}$ ) in the total oxidation of methane and propane. Section 6.2 presents a short summary of the experimental details, and Section 6.3 is devoted to the results of the catalytic activity concerning both oxidation reactions. Section 6.4 presents a discussion of the results and Section 6.5 summarizes the most important findings regarding the oxidation reactions of methane and propane over gold-based catalysts.

## 6.2 Experimental

The unpromoted- and promoted- ( $\text{MO}_x$  or  $\text{M}^{\text{I}}\text{O}_x/\text{M}^{\text{II}}\text{O}_x$ ) gold-based catalysts (5 wt-% Au) were prepared by HDP with urea (*Chapter 3*). The mixed supports in the form of either  $\text{MO}_x/\text{Al}_2\text{O}_3$ , or  $\text{M}^{\text{I}}\text{O}_x/\text{M}^{\text{II}}\text{O}_x/\text{Al}_2\text{O}_3$  ( $\text{M}: \text{Rb}, \text{Li}, \text{Ba}, \text{Mg}, \text{Mn}, \text{Fe}, \text{Cr}, \text{Co}, \text{Ti}, \text{Zn}, \text{Zr}, \text{Cu}, \text{Ce}, \text{V}, \text{Pr}, \text{Y}$ ) were obtained by pore volume impregnation of alumina with the corresponding nitrates (solution). *Chapter 4* presents a comprehensive description of the results concerning the physico-chemical characteristics of these catalysts.

$\text{Pt}/\text{Al}_2\text{O}_3$  (5 wt-% Pt) was prepared by vacuum impregnation of  $\gamma\text{-Al}_2\text{O}_3$  with the corresponding amount of  $\text{H}_2\text{PtCl}_6$  (Aldrich). After impregnation, the precursor was dried in static air at  $80^\circ\text{C}$  for 16 h and then calcined in oxygen flow at  $350^\circ\text{C}$ .

A description of the lab-scale flow system used for the catalytic activity measurements can be found in *Chapter 3*. The samples were reactivated in-situ under hydrogen flow at  $300^\circ\text{C}$ , unless otherwise stated. The oxidation of methane was carried out in excess of oxygen,  $\text{CH}_4:\text{O}_2 = 1:4$ , and the total oxidation of propane was carried out using a reactant ratio  $\text{C}_3\text{H}_8:\text{O}_2 = 1:16$ . For the latter reaction a second reactant ratio of  $\text{C}_3\text{H}_8:\text{O}_2 = 1:7.5$  was also employed for  $\text{Au}/\text{Al}_2\text{O}_3$ . The total flow was set to  $30 \text{ ml min}^{-1}$  (GHSV  $\sim 1800 \text{ h}^{-1}$ ). All the gases were 4 vol % /He. The outlet gas stream was analysed by means of GC or MS. The reaction cycle consisted of at least two consecutive heating-cooling cycles to a maximum reaction temperature of  $750^\circ\text{C}$  (methane) or  $450^\circ\text{C}$  (propane). Because the total flow and the catalyst weight were always constant ( $30 \text{ ml min}^{-1}$  and 0.2 g), the catalytic performance is compared in terms of the conversion versus temperature (second heating cycle) plots. However, the specific reaction rate,  $r$  (the amount of methane and propane (moles) converted per total amount of Au (moles) and second) was considered as a more precise measure of the catalytic performance, especially because the gold loading is less than 5 wt-% and it varies among the samples. It should be mentioned that for the CuO-containing  $\text{Au}/\text{Al}_2\text{O}_3$  catalysts, the specific reaction rate was calculated by taking into account the loading of CuO, either separately, or in combination with Au.

After performing the test reactions, the catalysts were again analysed by XRD. This analysis is expected to be informative especially for methane oxidation, since the maximum temperature used exceeded  $700^\circ\text{C}$  and sintering of the gold nanoparticles is expected at these high temperatures.

## 6.3 Catalytic activity measurements

### 6.3.1 Methane oxidation

Figure 6.1A shows the catalytic performance of the unpromoted Au/Al<sub>2</sub>O<sub>3</sub> catalyst during two consecutive heating-cooling cycles. In addition, the corresponding plot of Al<sub>2</sub>O<sub>3</sub> (second heating cycle) is also depicted. The addition of gold to alumina produces an important shift of the methane conversion to lower temperatures.

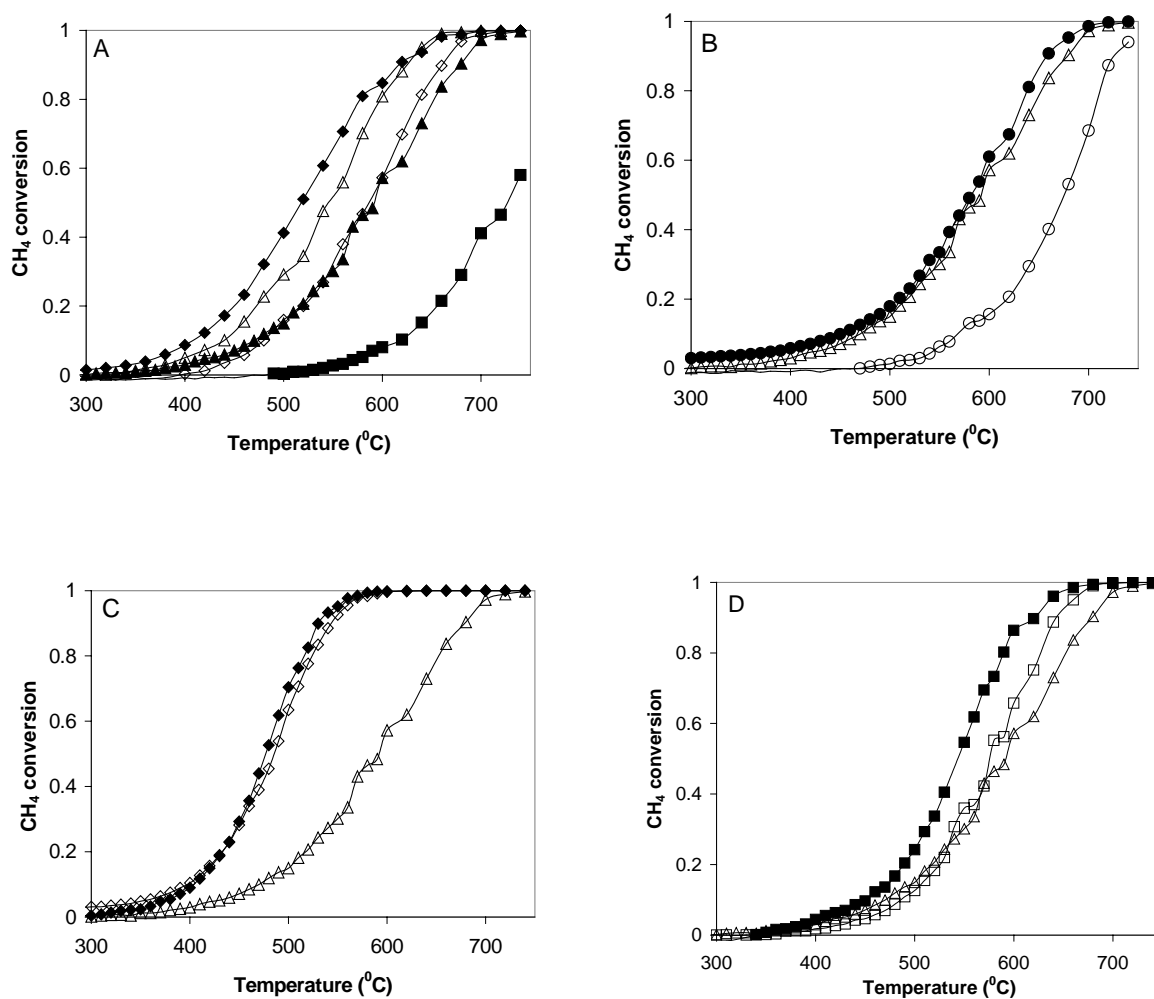


**Figure 6.1:** Methane conversion vs. temperature over heating #1 (◆), cooling #1 (◇), heating #2 (▲), cooling #2 (△) of Au/Al<sub>2</sub>O<sub>3</sub> and Al<sub>2</sub>O<sub>3</sub> (■) (A); Au/CoO<sub>x</sub>/Al<sub>2</sub>O<sub>3</sub> (●), CoO<sub>x</sub>/Al<sub>2</sub>O<sub>3</sub> (○), Au/Al<sub>2</sub>O<sub>3</sub> (△) (B); Au/CuO/Al<sub>2</sub>O<sub>3</sub>-A (◆), CuO/Al<sub>2</sub>O<sub>3</sub>-A (◇), Au/Al<sub>2</sub>O<sub>3</sub> (△) (C); Au/FeO<sub>x</sub>/Al<sub>2</sub>O<sub>3</sub> (■), FeO<sub>x</sub>/Al<sub>2</sub>O<sub>3</sub> (□), Au/Al<sub>2</sub>O<sub>3</sub> (△) (D). Reactant ratio: CH<sub>4</sub>:O<sub>2</sub> = 1:4.

The difference between the first (#h1) and subsequent heating-cooling cycles is relatively large and the best performance is achieved during the first heating cycle. This is most probably due to some sintering of the Au particles because of the high operating temperature and the exothermic character of the reaction. The least active branch corresponds to the second heating branch, and both cooling branches exhibit a slightly higher conversion than

the second heating branch. Subsequent heating-cooling cycles did not show any additional deactivation. The slightly higher conversion observed during the cooling branches compared to the heating branch may have different origins. The difference observed between heating and cooling branches may be due to a deviation in temperature measurement by the thermocouple, which is close to the catalyst bed, but not in intimate contact with it. However, it also might be a kind of “activation” process of the catalyst during the cooling branches such that the catalytic conversion is slightly shifted to lower temperatures.

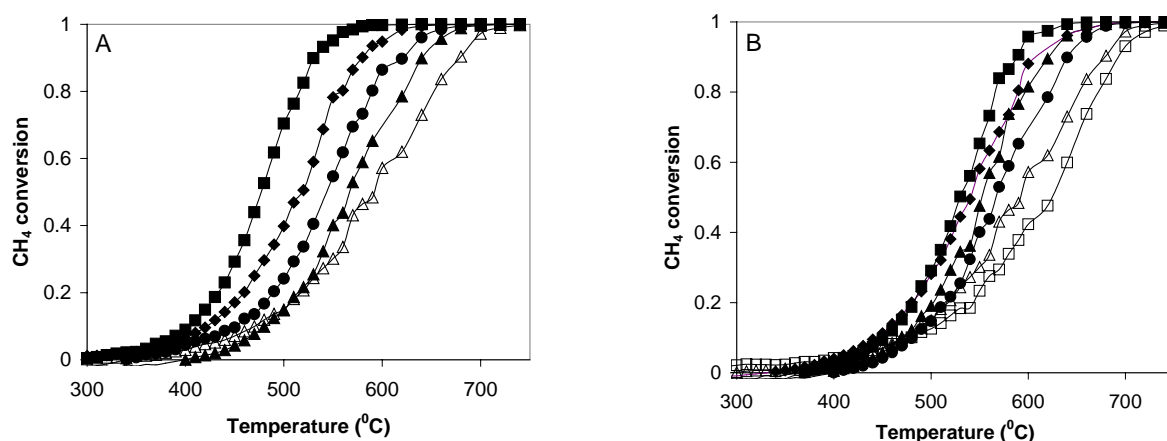
Fig. 6.1B shows that after Au addition to the  $\text{CoO}_x/\text{Al}_2\text{O}_3$  support, the catalytic activity is greatly improved, but compared with the unpromoted  $\text{Au}/\text{Al}_2\text{O}_3$ , no further improvement of the catalytic performance is obtained.  $\text{Au}/\text{Al}_2\text{O}_3$  performs better than  $\text{CoO}_x/\text{Al}_2\text{O}_3$ , in spite of the well-known activity of the transition metal oxides for this kind of reaction [1], but no synergy is created if the two active materials (Au and  $\text{CoO}_x$ ) are combined, with respect to the reference  $\text{Au}/\text{Al}_2\text{O}_3$ .

Fig. 6.1C compares the catalytic performance of CuO-containing  $\text{Au}/\text{Al}_2\text{O}_3$  catalyst, the corresponding  $\text{CuO}/\text{Al}_2\text{O}_3$  catalyst and the unpromoted-  $\text{Au}/\text{Al}_2\text{O}_3$  catalyst. The catalytic activity of the multicomponent  $\text{Au}/\text{CuO}/\text{Al}_2\text{O}_3\text{-A}$  is superior to that of  $\text{Au}/\text{Al}_2\text{O}_3$  and a significant shift towards lower temperatures is visible. However, the gold-free  $\text{CuO}/\text{Al}_2\text{O}_3$  exhibits approximately the same performance as the multicomponent  $\text{Au}/\text{CuO}/\text{Al}_2\text{O}_3\text{-A}$ . Hence, the synergy created for these samples is not significant, at least with respect to the performance of  $\text{CuO}/\text{Al}_2\text{O}_3$ . Clearly,  $\text{CuO}/\text{Al}_2\text{O}_3$  is the most active component of the  $\text{Au}/\text{CuO}/\text{Al}_2\text{O}_3$ .

Figure 6.1D compares the catalytic performance of  $\text{Au}/\text{FeO}_x/\text{Al}_2\text{O}_3$  with that of  $\text{FeO}_x/\text{Al}_2\text{O}_3$  and  $\text{Au}/\text{Al}_2\text{O}_3$ . The synergy between Au and iron oxide makes the multicomponent  $\text{Au}/\text{FeO}_x/\text{Al}_2\text{O}_3$  more active than the mixed support  $\text{FeO}_x/\text{Al}_2\text{O}_3$  or the unpromoted  $\text{Au}/\text{Al}_2\text{O}_3$  catalyst.

Figures 6.2A-B depict the conversion of methane versus temperature over various gold-based catalysts, either with one  $\text{MO}_x$  (Fig. 6.2A), or two  $\text{MO}_x$ s (Fig. 6.2B). The data presented in Fig. 6.2A point to the conclusion that the catalytic performance of  $\text{MO}_x$  promoted  $\text{Au}/\text{Al}_2\text{O}_3$  is directly related to the nature of the  $\text{MO}_x$  and its intrinsic activity.

The same holds for the results presented in Fig. 6.2B. The most active catalyst is  $\text{Au}/\text{FeO}_x/\text{CrO}_x/\text{Al}_2\text{O}_3$ , but in this case the mixed support displays some catalytic activity as well (Table 6.1). The next active catalyst is  $\text{MnO}_x/\text{Au}/\text{MgO}/\text{Al}_2\text{O}_3$ , followed by  $\text{Au}/\text{MnO}_x/\text{MgO}/\text{Al}_2\text{O}_3$  and  $\text{Au}/\text{MnO}_x/\text{Al}_2\text{O}_3$ . The addition of  $\text{MnO}_x$  to  $\text{Au}/\text{MgO}/\text{Al}_2\text{O}_3$  produces a catalyst slightly more active than  $\text{Au}/\text{MnO}_x/\text{MgO}/\text{Al}_2\text{O}_3$ . On the other hand, the addition of MgO to  $\text{Au}/\text{Al}_2\text{O}_3$  negatively influences the overall catalytic performance. The average gold particle size of  $\text{MnO}_x/\text{Au}/\text{MgO}/\text{Al}_2\text{O}_3$  catalyst is around 4.4 nm, and for  $\text{MgO}/\text{Au}/\text{Al}_2\text{O}_3$  it is 6.3 nm. This variation of the gold particle size as a function of the additives' order indicates the important role played by the oxides such as alkali (earth) metal oxides in stabilization of small gold particles if they are added *prior* to Au deposition. On the other hand, the identity of the top additive, potentially (in)active in the activation of the reactants may play a role as well.



**Figure 6.2:** Methane conversion vs. temperature over Au/CuO/Al<sub>2</sub>O<sub>3</sub>-A (■), Au/CrO<sub>x</sub>/Al<sub>2</sub>O<sub>3</sub> (◆), Au/FeO<sub>x</sub>/Al<sub>2</sub>O<sub>3</sub> (●), Au/MnO<sub>x</sub>/Al<sub>2</sub>O<sub>3</sub> (▲), Au/Al<sub>2</sub>O<sub>3</sub> (Δ) (A); Au/FeO<sub>x</sub>/CrO<sub>x</sub>/Al<sub>2</sub>O<sub>3</sub> (■), MnO<sub>x</sub>/Au/MgO/Al<sub>2</sub>O<sub>3</sub> (◆), Au/MnO<sub>x</sub>/MgO/Al<sub>2</sub>O<sub>3</sub> (▲), Au/MnO<sub>x</sub>/Al<sub>2</sub>O<sub>3</sub> (●), MgO/Au/Al<sub>2</sub>O<sub>3</sub> (□), Au/Al<sub>2</sub>O<sub>3</sub> (Δ) (B). Reaction conditions: CH<sub>4</sub>:O<sub>2</sub> = 1:4.

Table 6.1 summarizes the T<sub>50%</sub> (temperature of 50% methane conversion), the specific reaction rate, *r* (550<sup>o</sup>C), the apparent activation energy, *E<sub>a</sub>*, calculated for the conversion ranging between 0.05 and 0.2 and the variation of the Au particle size before (*d<sub>Au</sub><sup>a</sup>*) and after (*d<sub>Au</sub><sup>b</sup>*) catalytic reaction.

**Table 6.1:** T<sub>50%</sub>, the specific reaction rate, *r*, the apparent activation energy, *E<sub>a</sub>*, the average size of the gold particles for fresh *d<sub>Au</sub><sup>a</sup>* and used (after reaction) *d<sub>Au</sub><sup>b</sup>* gold-based catalysts (XRD).

Catalyst	<i>d<sub>Au</sub><sup>a</sup></i> (nm)	<i>d<sub>Au</sub><sup>b</sup></i> (nm)	T <sub>50%</sub> ( <sup>o</sup> C)	<i>r</i> x 10 <sup>3</sup> (moles CH <sub>4</sub> moles <sup>-1</sup> Au s <sup>-1</sup> )	<i>E<sub>a</sub></i> (kJ mol <sup>-1</sup> )
Au/Al <sub>2</sub> O <sub>3</sub>	4.3±0.1	6.0±0.3	592	1.7±0.1	74±2
Au/MgO/Al <sub>2</sub> O <sub>3</sub>	4.0±0.1	5.0±0.5	598	1.4±0.1	83±2
Au/CeO <sub>x</sub> /Al <sub>2</sub> O <sub>3</sub>	<3.0	5.8±0.3	590	1.4±0.2	68±2
Au/CoO <sub>x</sub> /Al <sub>2</sub> O <sub>3</sub>	5.0±0.1	6.0±0.4	580	1.8±0.1	71±3
Au/CrO <sub>x</sub> /Al <sub>2</sub> O <sub>3</sub>	4.8±0.1	10.5±0.2	520	5.0±0.1	74±2
Au/CuO/Al <sub>2</sub> O <sub>3</sub> -A	3.0±0.1	8.7±0.3	476	(5.8±0.2) <sup>1</sup> /(1.3±0.1) <sup>2</sup> /(1.6±0.1) <sup>3</sup>	91±1
Au/FeO <sub>x</sub> /Al <sub>2</sub> O <sub>3</sub>	<3.0	10.2±0.5	543	3.0±0.1	70±2
Au/MnO <sub>x</sub> /Al <sub>2</sub> O <sub>3</sub>	8.0±0.1	14.1±0.6	565	2.4±0.2	66±3
Au/ZnO/Al <sub>2</sub> O <sub>3</sub>	<3.0	3.9±0.5	604	1.4±0.1	79±2
Au/ZrO <sub>x</sub> /Al <sub>2</sub> O <sub>3</sub>	3.1±0.3	5.5±0.4	620	1.5±0.1	82±2
MgO/Au/Al <sub>2</sub> O <sub>3</sub>	6.3±0.1	8.1±0.1	624	1.3±0.1	80±2
Au/MnO <sub>x</sub> /MgO/Al <sub>2</sub> O <sub>3</sub>	<3.0	6.2±0.3	552	2.4±0.2	79±2
MnO <sub>x</sub> /Au/MgO/Al <sub>2</sub> O <sub>3</sub>	4.4±0.2	7.3±0.3	541	3.5±0.2	80±3
Au/FeO <sub>x</sub> /CrO <sub>x</sub> /Al <sub>2</sub> O <sub>3</sub>	<3.0	3.5±0.4	530	4±0.2	96±4
Al <sub>2</sub> O <sub>3</sub>	—	—	725	0	120±3
CoO <sub>x</sub> /Al <sub>2</sub> O <sub>3</sub>	—	—	674	~0	130±2
CrO <sub>x</sub> /Al <sub>2</sub> O <sub>3</sub>	—	—	495	0.8±0.1	114±3
CuO/Al <sub>2</sub> O <sub>3</sub> -A	—	—	486	1.4±0.1	70±2
FeO <sub>x</sub> /Al <sub>2</sub> O <sub>3</sub>	—	—	577	0.4±0.1	111±3
MnO <sub>x</sub> /Al <sub>2</sub> O <sub>3</sub>	—	—	600	0.3±0.1	101±3
FeO <sub>x</sub> /CrO <sub>x</sub> /Al <sub>2</sub> O <sub>3</sub>	—	—	507	~0	128±4



<sup>1</sup>r was estimated based on the Au loading; <sup>2</sup>r was estimated based on the (Au+CuO) loading; <sup>3</sup>r was estimated based on the CuO loading.

According to the variation of  $T_{50\%}$ , the effect of Au on the catalytic activity of  $MO_x/Al_2O_3$  varies from insignificant (Au/CuO/ $Al_2O_3$ ), to positive (Au/ $CoO_x/Al_2O_3$ , Au/ $FeO_x/Al_2O_3$ , Au/ $MnO_x/Al_2O_3$ ) or negative (Au/ $CrO_x/Al_2O_3$ , Au/ $FeO_x/CrO_x/Al_2O_3$ ). A comparison of the catalytic performance on the basis of the specific reaction rate, reveal that among various  $MO_x/Al_2O_3$ , only CuO/ $Al_2O_3$ -A shows a significant  $r$ , compared with Au/ $Al_2O_3$ . However, it has to be emphasised that according to the variation of  $r$ , CuO/ $Al_2O_3$ -A is less active than Au/ $Al_2O_3$ , although the results concerning the conversion presented in Fig. 6.1C suggest that the former is more active. This is an important result, since CuO is well known as an active oxidation catalyst. In addition, the most significant enhancers of the catalytic activity of Au/ $Al_2O_3$  are  $CrO_x$  and  $FeO_x$ . The small discrepancy between these data and previously reported results [2] might be due to a misinterpretation of the loading for both Au and CuO for the latter.

The apparent activation energy,  $E_a$  strongly decreased after Au addition to  $Al_2O_3$ , from  $120 \text{ kJ mol}^{-1}$  to  $74 \text{ kJ mol}^{-1}$ . The Arrhenius plots of methane oxidation over Au/ $Al_2O_3$  and Au/ $CeO_x/Al_2O_3$  are shown in Fig. 6.3A-B.

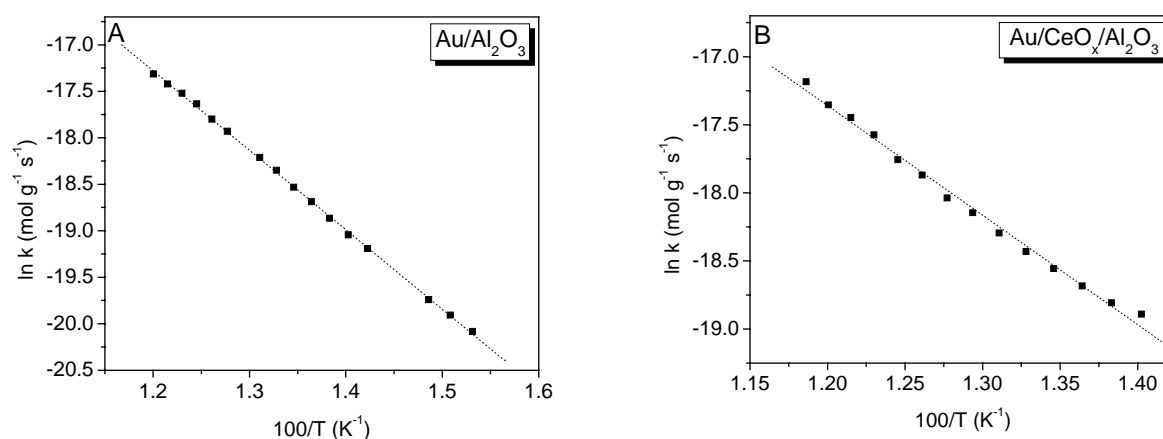


**Figure 6.3:** Arrhenius plots of methane oxidation over Au/ $Al_2O_3$  (A) and Au/ $CeO_x/Al_2O_3$  (B).

A large number of promoted- Au/ $Al_2O_3$  catalysts have a similar  $E_a$  as the unpromoted- Au/ $Al_2O_3$  (i.e. ranging from  $71 \text{ kJ mol}^{-1}$  to  $83 \text{ kJ mol}^{-1}$ ). There are a few samples that exhibit higher  $E_a$  ( $90\text{-}100 \text{ kJ mol}^{-1}$ ), whereas the  $E_a$  found for Au/ $MnO_x/Al_2O_3$  is slightly lower, as compared with Au/ $Al_2O_3$  ( $66 \text{ kJ mol}^{-1}$ ). On the other hand, the  $E_a$  of  $MO_x$  is, with one exception (CuO/ $Al_2O_3$ -A), above  $100 \text{ kJ mol}^{-1}$ .

Regarding the stability of the gold particles during the reaction test, it was found by XRD that sintering is rather significant. This is expected, since the temperature used is quite high and exceeds by far the Tamman temperature of Au. However, some of the catalysts appear less affected by the temperature, probably because for those catalysts the additives worked more efficiently as structural promoters.

### 6.3.2 Propane oxidation

The catalytic conversion of propane over unpromoted Au/Al<sub>2</sub>O<sub>3</sub> is shown in Fig. 6.4A for two consecutive heating-cooling cycles, reactant ratio C<sub>3</sub>H<sub>8</sub>:O<sub>2</sub> = 1:16. For comparison, also the catalytic conversion of propane over alumina is included (second heating cycle). The deactivation of the unpromoted Au/Al<sub>2</sub>O<sub>3</sub> eventually proceeds during the first heating cycle, since all the other cycles are slightly shifted to lower temperatures, compared with the first one. In fact no noticeable difference exists between cooling 1 and 2 and very little between heating 1 and 2. The maximum propane conversion over Au/Al<sub>2</sub>O<sub>3</sub> during heating #2 is around 53%, and it increases to 60% during the second cooling cycle. The oxidation of propane proceeds at much lower temperatures than that of methane. A maximum propane conversion of about 15% was found over alumina-only. The only C-containing product molecule was CO<sub>2</sub>.

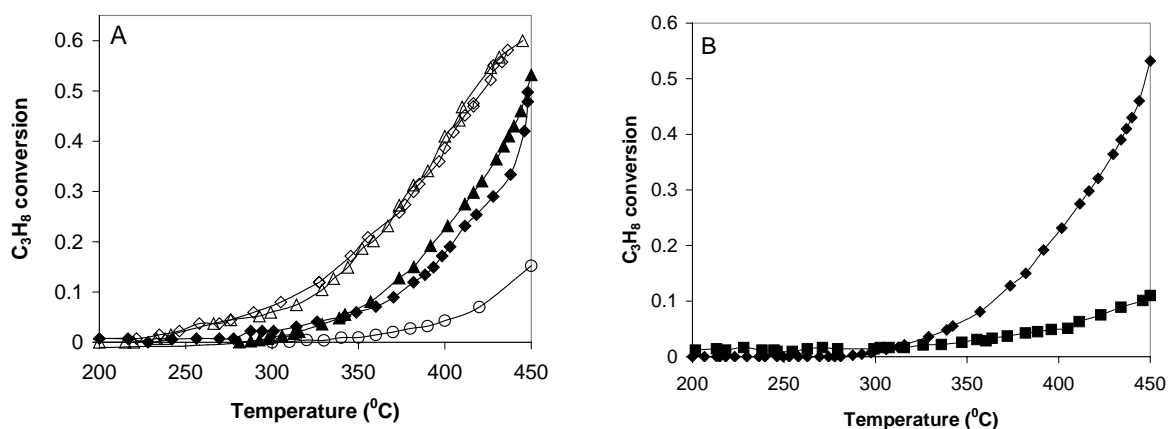


**Figure 6.4:** Propane conversion vs. temperature during heating #1 (◆), cooling #1 (◇), heating #2 (▲), cooling #2 (△) of Au/Al<sub>2</sub>O<sub>3</sub> and Al<sub>2</sub>O<sub>3</sub> (○), C<sub>3</sub>H<sub>8</sub>:O<sub>2</sub> = 1:16 (A); Au/Al<sub>2</sub>O<sub>3</sub> C<sub>3</sub>H<sub>8</sub>:O<sub>2</sub> = 1:16 (◆), C<sub>3</sub>H<sub>8</sub>:O<sub>2</sub> = 1:7.5 (■) (B).

Fig. 6.4B compares the catalytic performance of Au/Al<sub>2</sub>O<sub>3</sub> using two different reactant ratios. Both reactant ratios correspond to excess of oxygen (total oxidation). One experiment has been performed with 1.5 times more O<sub>2</sub> (C<sub>3</sub>H<sub>8</sub>:O<sub>2</sub> = 1:7.5) than the stoichiometric value, and the second experiment was carried out with 3.2 times more O<sub>2</sub> (C<sub>3</sub>H<sub>8</sub>:O<sub>2</sub> = 1:16). The difference in propane conversion is significant: 53% for C<sub>3</sub>H<sub>8</sub>:O<sub>2</sub> = 1:16 and only 11% for C<sub>3</sub>H<sub>8</sub>:O<sub>2</sub> = 1:7.5 at the maximum temperature used, viz. 450°C.

Fig. 6.5 illustrates the influence of the nature of the support on propane conversion, by comparing the catalytic activity of Au/Al<sub>2</sub>O<sub>3</sub> (d<sub>Au</sub> = 4.3 nm) with that of Au/SiO<sub>2</sub>-Al<sub>2</sub>O<sub>3</sub> (d<sub>Au</sub> = 10 nm). The catalytic performance of Pt/Al<sub>2</sub>O<sub>3</sub> is also depicted.

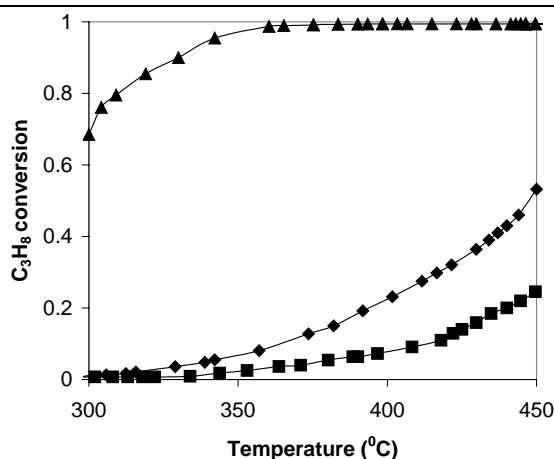


**Figure 6.5:** Propane conversion vs. temperature over Au/Al<sub>2</sub>O<sub>3</sub> (◆), Au/SiO<sub>2</sub>-Al<sub>2</sub>O<sub>3</sub> (■) and Pt/Al<sub>2</sub>O<sub>3</sub> (▲). Reactant ratio C<sub>3</sub>H<sub>8</sub>:O<sub>2</sub> = 1:16.

### Alkali (earth) metal oxides as additives

The effect of alkali (earth) metal oxides on the catalytic performance of Au/Al<sub>2</sub>O<sub>3</sub> is shown in Fig. 6.6A. The beneficial effect of these additives is not that significant as for other reactions (*Chapters 5 and 8*). However, the best results are obtained if Au is combined with Rb<sub>2</sub>O ( $T_{50\%} = 430^{\circ}\text{C}$ ), or BaO ( $T_{50\%} = 423^{\circ}\text{C}$ ). According to the data presented in Fig. 6.6A and Table 6.2, Li<sub>2</sub>O does not promote the catalytic performance of Au/Al<sub>2</sub>O<sub>3</sub> ( $T_{50\%} = 450^{\circ}\text{C}$ ). All catalysts are superior to alumina ( $T_{50\%} > 450^{\circ}\text{C}$ ). MO<sub>x</sub>/Al<sub>2</sub>O<sub>3</sub> did not show relevant conversion in the reaction temperature used.

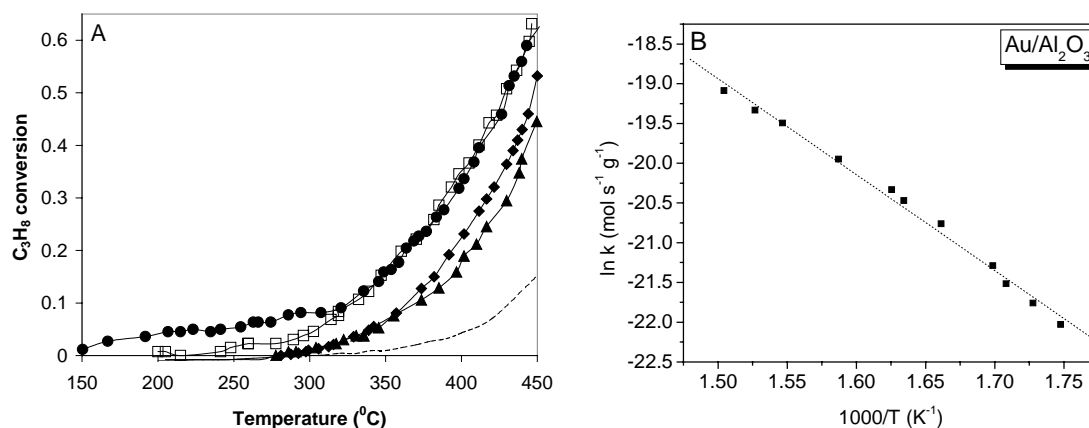


**Figure 6.6:** Propane oxidation over Au/Rb<sub>2</sub>O/Al<sub>2</sub>O<sub>3</sub> (●), Au/BaO/Al<sub>2</sub>O<sub>3</sub> (□), Au/Al<sub>2</sub>O<sub>3</sub> (◆), Au/Li<sub>2</sub>O/Al<sub>2</sub>O<sub>3</sub> (▲), Al<sub>2</sub>O<sub>3</sub> (--) (A). Arrhenius plot for Au/Al<sub>2</sub>O<sub>3</sub> (B).

Table 6.2 summarizes the  $T_{50\%}$ , the specific reaction rate,  $r$ , at  $370^{\circ}\text{C}$ , the apparent activation energy,  $E_a$ , and the average size of the gold particles for fresh ( $d_{\text{Au}}^a$ ) and used ( $d_{\text{Au}}^b$ ) catalysts. The addition of Rb<sub>2</sub>O to Au/Al<sub>2</sub>O<sub>3</sub> causes a two-fold increase of the specific reaction rate  $r$ . The Arrhenius plot of propane oxidation over Au/Al<sub>2</sub>O<sub>3</sub> is shown in Fig. 6.6B. The addition of Au to Al<sub>2</sub>O<sub>3</sub> decreases the apparent activation energy. The  $E_a$  is in the same

range as found for CH<sub>4</sub>. After the catalytic reaction slight sintering of the gold particles was observed (XRD).

**Table 6.2:** T<sub>50%</sub>, the specific reaction rate, *r*, the apparent activation energy, *E<sub>a</sub>*, the average size of the gold particles for fresh d<sub>Au</sub><sup>a</sup> and used (after reaction) d<sub>Au</sub><sup>b</sup> gold-based catalysts (XRD).

Catalyst	d <sub>Au</sub> <sup>a</sup> (nm)	d <sub>Au</sub> <sup>b</sup> (nm)	T <sub>50%</sub> (°C)	<i>r</i> x 10 <sup>4</sup> (moles C <sub>3</sub> H <sub>8</sub> moles <sup>-1</sup> Au s <sup>-1</sup> )	<i>E<sub>a</sub></i> (kJ mol <sup>-1</sup> )
Au/Al <sub>2</sub> O <sub>3</sub>	4.3±0.1	5.1±0.4	447	1.7±0.1	81±1
Au/SiO <sub>2</sub> -Al <sub>2</sub> O <sub>3</sub>	10.0±0.3	15.1±0.5	>450	0.7±0.1	86±2
Au/Li <sub>2</sub> O/Al <sub>2</sub> O <sub>3</sub>	3.2±0.1	4.3±0.4	450	1.3±0.1	80±2
Au/Rb <sub>2</sub> O/Al <sub>2</sub> O <sub>3</sub>	<3.0.	3.8±0.2	430	3.5±0.1	75±2
Au/BaO/Al <sub>2</sub> O <sub>3</sub>	<3.0.	4.1±0.1	423	3.3±0.2	74±3
Al <sub>2</sub> O <sub>3</sub>	–	–	>450	–	112±2

### TMO, rare earth metal oxides and copper oxide as additives

Fig. 6.7A illustrates the changes in the catalytic activity of Au/Al<sub>2</sub>O<sub>3</sub> after addition of some TMOs, CuO and ceria. In addition, the same figure depicts the catalytic performance of Pt/Al<sub>2</sub>O<sub>3</sub> (5 wt-% Pt).

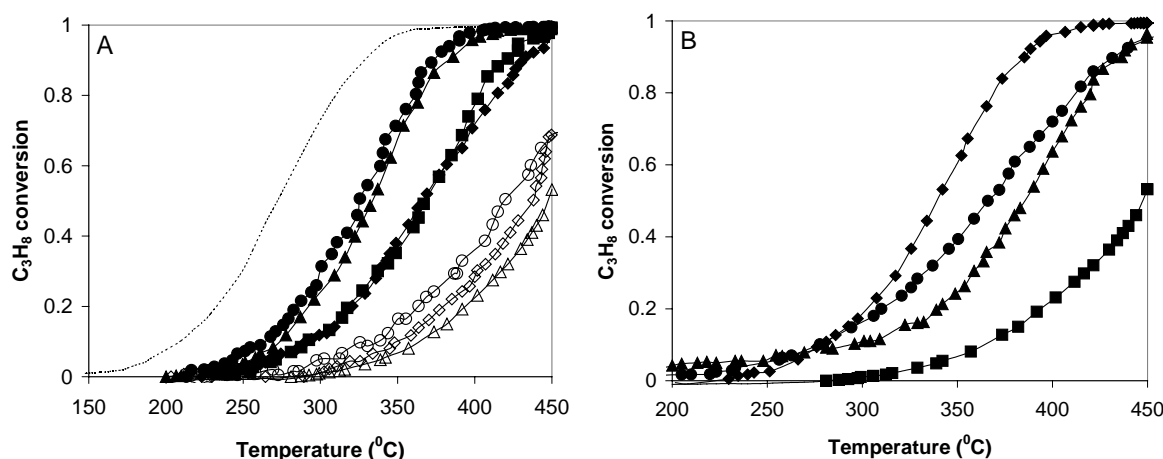


**Figure 6.7:** Propane oxidation vs. temperature over Pt/Al<sub>2</sub>O<sub>3</sub> (–), Au/MnO<sub>x</sub>/Al<sub>2</sub>O<sub>3</sub> (●), Au/CoO<sub>x</sub>/Al<sub>2</sub>O<sub>3</sub> (▲), Au/FeO<sub>x</sub>/Al<sub>2</sub>O<sub>3</sub> (■), Au/CeO<sub>x</sub>/Al<sub>2</sub>O<sub>3</sub> (◆), Au/TiO<sub>x</sub>/Al<sub>2</sub>O<sub>3</sub> (○), Au/VO<sub>x</sub>/Al<sub>2</sub>O<sub>3</sub> (◇), Au/Al<sub>2</sub>O<sub>3</sub> (Δ) (A); Au/CuO/Al<sub>2</sub>O<sub>3</sub>-A (◆), Au/CuO/Al<sub>2</sub>O<sub>3</sub>-B (●), CuO/Al<sub>2</sub>O<sub>3</sub>-A (▲), Au/Al<sub>2</sub>O<sub>3</sub> (■) (B).

Among the gold-containing catalysts, the most efficient one contains MnO<sub>x</sub> as additive. Obviously, this high catalytic activity is not critically related to the average size of the gold particles, around 8 nm (Table 6.3). Almost the same degree of C<sub>3</sub>H<sub>8</sub> conversion is obtained over Au/CoO<sub>x</sub>/Al<sub>2</sub>O<sub>3</sub>. FeO<sub>x</sub>- and CeO<sub>x</sub>- containing Au/Al<sub>2</sub>O<sub>3</sub> are slightly less active, but still superior to samples with TiO<sub>x</sub>- or VO<sub>x</sub> as additives. It should be mentioned that the catalysts comprising TiO<sub>x</sub> or VO<sub>x</sub> contain very small Au particles. Small Au particles are not sufficient to obtain high activity. Interestingly, a different ranking of the catalysts is observed, as

compared with that found for propene oxidation (*Chapter 5*). Thus, based on the results presented in Fig. 6.7A, the most active catalyst does not contain ceria, as in the case of propene total oxidation, nor  $\text{CoO}_x$ , as reported by Haruta [3], but  $\text{MnO}_x$ . However, the difference in performance between the catalysts with  $\text{MnO}_x$  and  $\text{CoO}_x$  is small and the most active Au-based catalyst is still inferior to  $\text{Pt}/\text{Al}_2\text{O}_3$ . This comparison was made because earlier reports claimed  $\text{Au}/\text{Co}_3\text{O}_4$  (10 wt-% Au) as a very efficient catalyst for total oxidation of saturated hydrocarbons ( $\text{CH}_4$  and  $\text{C}_3\text{H}_8$ ) [3], even exceeding the performance of 1 wt-%  $\text{Pt}/\text{Al}_2\text{O}_3$  or 1 wt-%  $\text{Pd}/\text{Al}_2\text{O}_3$ .

The catalytic performance of CuO-containing  $\text{Au}/\text{Al}_2\text{O}_3$  with two different compositions, namely  $\text{Au}/\text{CuO}/\text{Al}_2\text{O}_3$ -A (4 wt-% Au, 6 wt-% CuO) and  $\text{Au}/\text{CuO}/\text{Al}_2\text{O}_3$ -B (7.4 wt-% Au, 12 wt-% CuO) is depicted in Fig. 6.7B. The catalytic performance of  $\text{CuO}/\text{Al}_2\text{O}_3$ -A is also depicted. The best performance is achieved if both Au and CuO are used in small amounts.

All the relevant data ( $T_{50\%}$ ,  $r$ ,  $E_a$  and the variation of the size of the gold particles after the catalytic reaction) are summarized in Table 6.3.

**Table 6.3:**  $T_{50\%}$ , the specific reaction rate,  $r$ , the apparent activation energy,  $E_a$ , the average size of the gold particles for fresh  $d_{\text{Au}}^a$  and used (after reaction)  $d_{\text{Au}}^b$  gold-based catalysts (XRD).

Catalyst	$d_{\text{Au}}^a$ (nm)	$d_{\text{Au}}^b$ (nm)	$T_{50\%}$ ( $^{\circ}\text{C}$ )	$r \times 10^4$ (moles $\text{C}_3\text{H}_8$ moles $^{-1}\text{M s}^{-1}$ )	$E_a$ (kJ mol $^{-1}$ )
$\text{Au}/\text{MnO}_x/\text{Al}_2\text{O}_3$	8.0±0.1	9.2±0.1	325	11.3±0.2	81 ±1
$\text{Au}/\text{CoO}_x/\text{Al}_2\text{O}_3$	5.0±0.1	5.5±0.2	333	10.3±0.1	83±2
$\text{Au}/\text{CeO}_x/\text{Al}_2\text{O}_3$	<3.0	3.4±0.3	372	7.2±0.1	75±1
$\text{Au}/\text{FeO}_x/\text{Al}_2\text{O}_3$	<3.0	3.6±0.5	368	6.4±0.1	80±2
$\text{Au}/\text{PrO}_x/\text{Al}_2\text{O}_3$	3.0±0.3	3.2±0.3	401	3.6±0.1	78±2
$\text{Au}/\text{TiO}_x/\text{Al}_2\text{O}_3$	<3.0	3.7±0.4	419	2.7±0.1	78±1
$\text{Au}/\text{VO}_x/\text{Al}_2\text{O}_3$	<3.0	3.3±0.2	419	1.5±0.1	83±1
$\text{Au}/\text{ZrO}_x/\text{Al}_2\text{O}_3$	3.1±0.3	3.9±0.1	450	2.1±0.1	85±2
$\text{Au}/\text{YO}_x/\text{Al}_2\text{O}_3$	<3.0	3.8±0.6	384	5.3±0.2	82±2
$\text{Au}/\text{CuO}/\text{Al}_2\text{O}_3$ -A	3.0±0.1	4.0±0.6	339	$(11.1±0.2)^1/(\mathbf{2.3±0.1})^2/(3±0.1)^3$	74±1
$\text{Au}/\text{CuO}/\text{Al}_2\text{O}_3$ -B	6.8±0.2	7.5±0.2	365	$(3.7±0.1)^1/(\mathbf{0.8±0.1})^2/(1±0.1)^3$	79±1
$\text{MnO}_x/\text{Al}_2\text{O}_3$	—	—	359	0.7±0.1	120±2
$\text{CoO}_x/\text{Al}_2\text{O}_3$	—	—	365	2.4±0.2	101±3
$\text{CuO}/\text{Al}_2\text{O}_3$ -A	—	—	386	1.4±0.1	40±1
$\text{Pt}/\text{Al}_2\text{O}_3$	—	—	274	10.7±0.2	68±1

<sup>1</sup> $r$  was estimated based on the Au loading; <sup>2</sup> $r$  was estimated based on the (Au+CuO) loading; <sup>3</sup> $r$  was estimated based on the CuO loading. M: Au, Cu, Pt.

More than a six-fold increase of the specific reaction rate,  $r$ , calculated at 370 $^{\circ}\text{C}$ , is found after  $\text{MnO}_x$  addition to  $\text{Au}/\text{Al}_2\text{O}_3$ . For most of the samples, the apparent activation energies,  $E_a$  for the  $\text{MO}_x$ -promoted  $\text{Au}/\text{Al}_2\text{O}_3$  resemble the value found for  $\text{Au}/\text{Al}_2\text{O}_3$ . The apparent activation energies of the  $\text{MO}_x/\text{Al}_2\text{O}_3$  are larger than  $E_a$  of  $\text{Au}/\text{MO}_x/\text{Al}_2\text{O}_3$ . There is, however, one exception,  $\text{CuO}/\text{Al}_2\text{O}_3$ -A, with a much lower  $E_a$  than what was found for the other samples. Possibly, the reaction was here in the diffusion regime where the apparent  $E_a$  is half of the real  $E_a$ . This supposition is supported by the calculated value for the specific reaction

rate,  $r$ , which is relatively low (Table 6.3). The apparent activation energy of Pt/Al<sub>2</sub>O<sub>3</sub> is much lower than for the gold-based catalysts, around 68 kJ mol<sup>-1</sup>, and in line with previously reported results [4].

Sintering of the gold nano-particles does not proceed significantly under the experimental conditions used.

### Two different metal oxides as additives

The catalytic performance of various multicomponent gold-based catalysts is presented in Fig. 6.8 in terms of propane conversion versus temperature (second heating stage). Table 6.4 summarizes the  $T_{50\%}$ ,  $r$  (370°C) and the apparent activation energy,  $E_a$ .

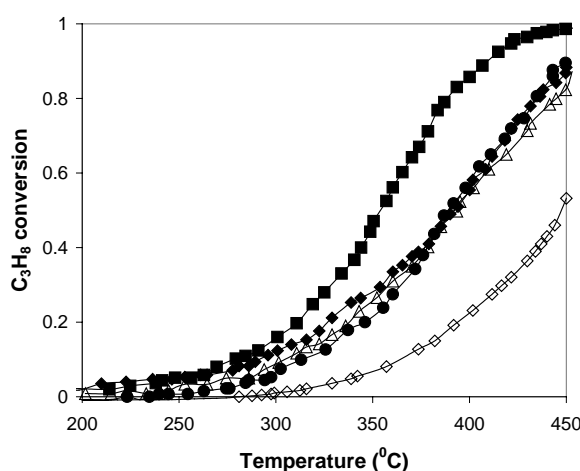


**Figure 6.8:** Propane oxidation vs. temperature over Au/CuO/CeO<sub>x</sub>/Al<sub>2</sub>O<sub>3</sub> (■), Au/CeO<sub>x</sub>/ZrO<sub>x</sub>/Al<sub>2</sub>O<sub>3</sub> (◆), Au/BaO/CeO<sub>x</sub>/Al<sub>2</sub>O<sub>3</sub> (Δ), Au/Li<sub>2</sub>O/CeO<sub>x</sub>/Al<sub>2</sub>O<sub>3</sub> (●) and Au/Al<sub>2</sub>O<sub>3</sub> (◇).

From Fig. 6.8, Au/CuO/CeO<sub>x</sub>/Al<sub>2</sub>O<sub>3</sub> appears to be the most active catalyst. A rather similar catalytic performance was observed for Au/CeO<sub>x</sub>/ZrO<sub>x</sub>/Al<sub>2</sub>O<sub>3</sub>, Au/BaO/CeO<sub>x</sub>/Al<sub>2</sub>O<sub>3</sub> and Au/Li<sub>2</sub>O/CeO<sub>x</sub>/Al<sub>2</sub>O<sub>3</sub>, especially at temperatures above 350°C.

However, according to the variation of  $r$ , Au/CuO/CeO<sub>x</sub>/Al<sub>2</sub>O<sub>3</sub> is not the most active catalyst, but its performance is still significantly high, considering the average size of the Au particles. Among the catalysts with an alkali (earth) metal oxide + CeO<sub>x</sub>, the best performance in terms of  $r$  is shown by Au/BaO/CeO<sub>x</sub>/Al<sub>2</sub>O<sub>3</sub>. A close similarity exists between these results and what was found in *Chapter 5*. The most active catalyst in C<sub>3</sub>H<sub>6</sub> oxidation also performs the best in C<sub>3</sub>H<sub>8</sub> oxidation. It was reported that zirconia modifies the structure of ceria and also that zirconia has a positive effect in stabilization of the ceria defects [5]. Besides, ceria is well known for its oxygen storage capacity. The XRD data did not indicate any alteration of the ceria structure in the presence of ZrO<sub>2</sub>.

Sintering of the small gold particles was not detected by XRD.

**Table 6.4:**  $T_{50\%}$ , the specific reaction rate,  $r$ , the apparent activation energy,  $E_a$ , the average size of the gold particles for fresh  $d_{Au}^a$  and used (after reaction)  $d_{Au}^b$  gold-based catalysts (XRD).

Catalyst	$d_{Au}^a$ (nm)	$d_{Au}^b$ (nm)	$T_{50\%}$ ( $^{\circ}C$ )	$r \times 10^4$ (moles $C_3H_8$ moles $^{-1}M$ s $^{-1}$ )	$E_a$ (kJ mol $^{-1}$ )
Au/CuO/CeO $_x$ /Al $_2$ O $_3$	16.8 $\pm$ 0.1	17.2 $\pm$ 0.6	354	(5.8 $\pm$ 0.1) $^1$ /(1.1 $\pm$ 0.1) $^2$ /(1.4 $\pm$ 0.1) $^3$	73 $\pm$ 2
Au/BaO/CeO $_x$ /Al $_2$ O $_3$	<3.0	3.4 $\pm$ 0.2	394	4.5 $\pm$ 0.2	76 $\pm$ 1
Au/Li $_2$ O/CeO $_x$ /Al $_2$ O $_3$	<3.0	3.3 $\pm$ 0.3	382	4 $\pm$ 0.1	81 $\pm$ 3
Au/Rb $_2$ O/CeO $_x$ /Al $_2$ O $_3$	<3.0	3.5 $\pm$ 0.2	392	4.3 $\pm$ 0.1	72 $\pm$ 2
Au/CeO $_x$ /ZrO $_x$ /Al $_2$ O $_3$	<3.0	3.0 $\pm$ 0.5	392	6.4 $\pm$ 0.2	74 $\pm$ 3
Au/YO $_x$ /CeO $_x$ /Al $_2$ O $_3$	<3.0	3.1 $\pm$ 0.1	416	2.9 $\pm$ 0.1	81 $\pm$ 2
Au/CoO $_x$ /Li $_2$ O/Al $_2$ O $_3$	<3.0	3.5 $\pm$ 0.3	444	1.3 $\pm$ 0.1	89 $\pm$ 3

$^1r$  was estimated based on the Au loading;  $^2r$  was estimated based on the (Au+CuO) loading;  $^3r$  was estimated based on the CuO loading. M: Au, Cu.

## 6.4 Discussion

### The influence of the reactant ratio and nature of the support in $C_3H_8$ oxidation

As shown in Fig. 6.4B, there is a strong dependence of the reaction rate on the oxygen concentration. This dependence may be explained in terms of site competition. More oxygen in the gas stream implies less propane (total flow = constant) in these experiments. If both reactants compete for the same adsorption sites and the fraction of adsorbed propane on the surface is larger compared with  $O_2$ , the surface will be covered by carbonaceous species that may act as poison. This direct dependence of propane conversion on the  $O_2$  concentration may also indicate that the reaction order of oxygen is positive. However, a more detailed study would be necessary before kinetic conclusions are drawn.

It was shown earlier that, for propane oxidation, Pt deposited on a strong acidic support is more efficient than if it is deposited on a basic support such as  $ZrO_2$  [6]. The results depicted in Fig. 6.5 shows that Pt-based catalysts are more active than the Au-based catalysts and that for the Au-based catalysts, a more acidic support produces a less active catalyst. Au deposited on  $SiO_2$ - $Al_2O_3$  (strongly acidic) displayed very large Au particles. The reason is the PZC of  $SiO_2$ - $Al_2O_3$ , which is around 2 and HDP is not suitable for this kind of supports. The significantly larger Au particles formed on  $SiO_2$ - $Al_2O_3$  are probably the main reason for the low catalytic activity. Besides, the reaction mechanism on Pt-based catalysts may differ from that on Au. However, more experiments are necessary in order to formulate a valid model.

### The effect of $MO_x$ addition on the hydrocarbon oxidation activity

C-H bond activation in saturated hydrocarbons is a crucial step in the combustion of these compounds [7-10]. Once the first bond is broken, sequential reactions to  $CO_2$  and  $H_2O$  are more facile. Methane is the most difficult compound to activate, whereas propane activation is of intermediate difficulty [11]. This activation is partly related to the ease of adsorption of these hydrocarbons. An important factor is the “stickiness” of the molecules to a metallic or oxidized surface. Since the C-H bond in methane is only very weakly acidic ( $pK_a = 46$ ), it follows that surface sites capable of deprotonation of methane must be very basic. However,

such sites would be expected to adsorb  $\text{CO}_2$  rather strongly, and so they might be expected to be rapidly self-poisoned [7]. Besides the basic sites, also the acidic sites were proposed as important for saturated hydrocarbon oxidation [12]. All these models are, however, based on metal oxide-like catalysts. If the catalyst is a metal-based catalyst, the rate of activation of the C-H bond depends on the nature of the hydrocarbon, the nature of the metal, and the reaction conditions. In general the surface composition of a metal catalyst depends on the reaction conditions and varies from more oxidized surface (oxygen-rich conditions) to more reduced surface (fuel-rich conditions). For methane oxidation, it is well established that Pd is the most active catalyst, but that Pt is a better catalyst for the oxidation of higher hydrocarbons [13, 14]. On the other hand, Haruta reported that Au deposited on  $\text{Co}_3\text{O}_4$  is more efficient in total oxidation of the saturated hydrocarbons than Pt or Pd deposited on alumina [3]. However, their results were obtained using a huge difference in the loading of the active metal, from 10 wt-% (Au/ $\text{Co}_3\text{O}_4$ ) to 1 wt-% (Pt and Pd).

Hardly any results regarding the oxidation of either methane or propane over gold-based catalysts have been reported [2]. This is partly due to the high inertness of methane, as was already discussed, and partly to the fact that sintering of the gold particles becomes very important at reaction temperatures above  $500^\circ\text{C}$ . The current results indicate that the presence of  $\text{MO}_x$  has a larger influence on the catalytic performance of the gold-based catalysts in propane oxidation, than for methane oxidation. However, TMOs appear to be the most suited for both oxidation reactions, exceeding the effect of alkali (earth) metal oxides. This is most likely because TMOs are intrinsically active (i.e.  $\text{MnO}_x$ ,  $\text{CoO}_x$ ), whereas the alkali (earth) metal oxides are only structural promoters. In the case of CuO-containing catalysts most of the catalytic action can be attributed to the CuO sites.

Regarding the particle size effect, the oxidation of methane over gold-based catalysts is related to the size of the gold particles, but this is not the only effect that controls the catalytic activity. An illustration of the dependence of the  $T_{50\%}$  with the average gold particle size is presented in Figs. 6.9A-B for methane and propane oxidation. As previously found for propene oxidation (*Chapter 5*), the size of the gold particles is important. Methane conversion is strongly related to the size of the gold particles, but also to the identity of the  $\text{MO}_x$ . According to  $T_{50\%}$ , most of the catalysts are active between 500 and  $600^\circ\text{C}$ . However, some of these Au-based catalysts do not perform better than the  $\text{MO}_x/\text{Al}_2\text{O}_3$  counterpart (i.e. the samples marked by italics in Fig. 6.9A), whereas some of them are considerably more active than  $\text{MO}_x/\text{Al}_2\text{O}_3$  (the samples underlined in Fig. 6.9A). Among them, Au/ $\text{MnO}_x/\text{Al}_2\text{O}_3$  and Au/ $\text{CoO}_x/\text{Al}_2\text{O}_3$  should be in particular considered, because these catalysts have relatively large gold particles. The anomalous effects observed for both methane and propane oxidation and the absence of correlation between activity and particle size could be attributed to the metal-support interaction. A stronger metal-support interaction affects the geometry/structure of the Au nanoparticles. Thus, the Au nanoparticles may change their shape from spherical to flat. Flat Au particles are reported to be more active [15]. Moreover, TMO and ceria contain an increased number of defects, useful as anchoring sites for Au.



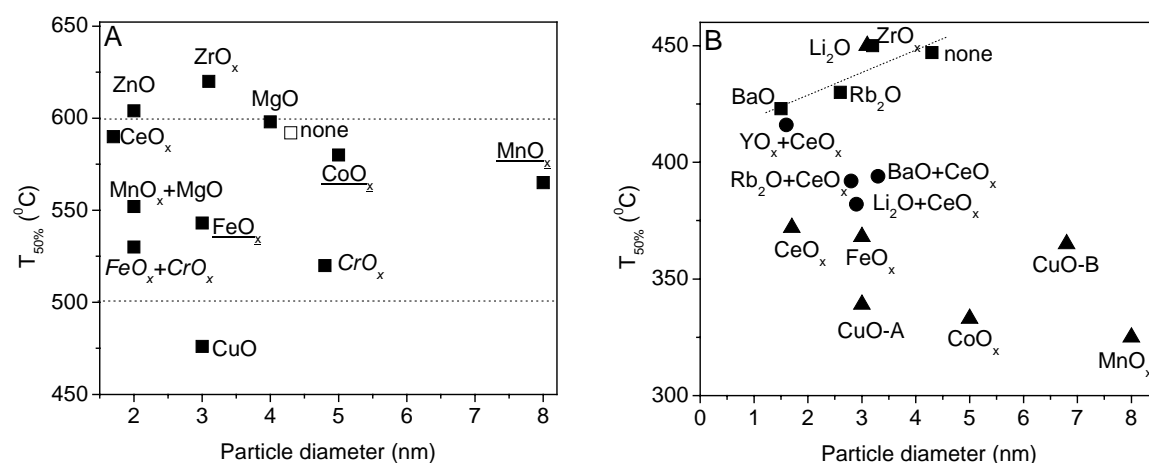


**Figure 6.9:**  $T_{50\%}$  vs. particle diameter for methane (A) and propane (B) oxidation.

Similar conclusions can be drawn concerning the results presented in Fig. 6.9B. However, a more pronounced effect of the additives on the catalytic performance of Au/Al<sub>2</sub>O<sub>3</sub> is observed for propane oxidation. Only the alkali (earth) metal oxides exhibit a direct dependence of the catalytic performance with the size of Au particles. For the rest of the samples, a size of  $\sim 3$  nm is particularly important for a high catalytic activity, next to the identity of the additive.

### Active sites

As was already mentioned, oxidation of hydrocarbons involves C-H bond activation as a crucial step. For both methane and propane oxidation, after Au addition to Al<sub>2</sub>O<sub>3</sub> the apparent activation energy decreases drastically. This decrease implies that Au plays an active role in the activation of these hydrocarbons. Grisel reported similar results for methane oxidation over Au-based catalysts [2]. A similar model as the one already published for methane oxidation over Pd/Al<sub>2</sub>O<sub>3</sub> [14] was used to explain his results obtained for Au/Al<sub>2</sub>O<sub>3</sub> [2]: the  $E_a$  was seen as an “average value” on the basis of different Au particles, with variable size. This is a reasonable suggestion, since it is known that smaller Au particles have an increased number of kinks and steps where the activation of various molecules is more likely to proceed. Larger Au particles, on the other hand, resemble the characteristics of inactive bulk-Au.

Next to the particle size effect the identity of the additives is very important, especially in propane oxidation. These additives are directly responsible for the existence of a certain metal/support interaction and may also contribute to the availability of surface oxygen and its overall mobility. The presence of MO<sub>x</sub> (MO<sub>x</sub>: TMO, ceria, CuO) seems essential for the fast and complete oxidation. Although at sufficiently high temperatures the catalytic oxidation takes place even on catalysts with non-redox couple oxides, for example Au/MgO/Al<sub>2</sub>O<sub>3</sub>, the presence of M<sup>n+</sup> with strong redox capacity is more beneficial. The overall reaction rate may be controlled either by the activation of the C-H bond, or by the reoxidation of M<sup>n-1</sup>O<sub>x</sub> to M<sup>n+</sup>O<sub>x</sub>. The activation of the C-H bond appears to be directly related to the presence of Au, whereas the availability of appropriate oxygen species is connected to the identity of M<sup>n+</sup>O<sub>x</sub>.

This may explain the differences found in the catalytic performance between methane and propane oxidation. The two different processes (C-H bond activation and oxygen activation) may also explain the difference found in  $E_a$  for both oxidation reactions. However, the reason of different ranking orders for the oxidation of saturated and unsaturated hydrocarbons is not clear and a more detailed study of each individual reaction step may give more insights into these differences.

In addition, some relationship between the catalytic activity and the acid/base character of the additives may exist. Thus, if the additive has a relatively strong acidic character, such as  $\text{VO}_x$  or  $\text{SiO}_2\text{-Al}_2\text{O}_3$ , the catalytic performance in  $\text{C}_3\text{H}_8$  oxidation is very low. However, most of the oxides used as additives have a basic character (Lewis acid) which varies from weak ( $\text{Al}_2\text{O}_3$ ) to strong or very strong ( $\text{MgO}$ ,  $\text{BaO}$ ,  $\text{NiO}$ ,  $\text{CuO}$ ,  $\text{ZnO}$ ). Moreover, the basic strength of the  $\text{MO}_x$  does not reflect the variation in the catalytic performance. Thus, an oxide with a medium-weak basic character such as  $\text{FeO}_x$  appears to have a more pronounced effect on the activity of  $\text{Au/Al}_2\text{O}_3$  than a medium-strong ( $\text{ZrO}_x$ ) or very strong ( $\text{BaO}$ ) oxide. The conclusion is that oxides with a basic character are beneficial compared with those with an acidic character. This model would be important, however, if these additives are directly involved in the activation of the reactants. If their role is, as already discussed, rather to supply active oxygen, then their acid/base character is less important. More likely, the hydrocarbons are activated on gold or at the Au-support interface, whereas oxygen is activated/supplied by the mixed support.

## 6.5 Conclusions

The significant decrease of  $T_{50\%}$  and  $E_a$ , accompanied by an increase in  $r$  by addition of Au to  $\text{MO}_x/\text{Al}_2\text{O}_3$  clearly indicates that Au is active in the oxidation of saturated hydrocarbons such as methane and propane. The results clearly show that a direct relationship exists between the catalytic performance and the average size of the Au particles, especially in the presence of alkali (earth) metal oxide additives. Their role is probably that of a structural promoter. On the other hand, if the additives are of the type of transition metal oxides and ceria, the size of Au particles does not seem to be that crucial anymore. These additives may function as a cocatalyst, i.e. as supplier of oxygen. Promising catalysts are those with  $\text{BaO}$  or  $\text{Rb}_2\text{O}$  as promoters. However, the efficiency of the Au-based catalysts can be even further improved if oxides such as  $\text{MnO}_x$ ,  $\text{FeO}_x$ ,  $\text{CoO}_x$  or  $\text{CeO}_x$  are added. Although the catalytic performance of  $\text{CuO}$  cannot be neglected and has to be considered for any further discussions,  $\text{Au/Al}_2\text{O}_3$  is slightly more active than  $\text{CuO/Al}_2\text{O}_3$ .

Regarding the stability of the gold nano-particles in propane oxidation, the presence of the additives prevents their sintering even during an extended period in the reactor. However, the temperatures needed to activate  $\text{CH}_4$  are rather high and (very) small Au particles grow.

## 6.6 References

- [1] J. E. Germain, *Catalytic Conversion of Hydrocarbons*, Academic Press 1967.
- [2] R. J. H. Grisel, *Supported gold catalysts for environmental applications*, PhD thesis, Leiden University (2002).

- [3] M. Haruta, *Catal. Today* 36 (1997) 153.
- [4] T. F. Garetto, E. Rincon, C. R. Apesteguia, *Appl. Catal. B* 48 (2004) 167.
- [5] J. A. Rodriguez, *Catal. Today* 85 (2003) 177.
- [6] H. C. Wu, L. C. Liu, S. M. Yang, *Appl. Catal. A* 211 (2001) 159.
- [7] R. Burch, D. J. Crittle, M. J. Hayes, *Catal. Today* 47 (1999) 229.
- [8] G. Busca, M. Daturi, E. Finocchio, V. Lorenzelli, G. Ramis, R. J. Wiley, *Catal. Today* 33 (1997) 239.
- [9] G. Busca, E. Finocchio, G. Ramis, G. Ricchiardi, *Catal. Today* 32 (1996) 133.
- [10] M. Alifanti, J. Kirchnerova, B. Delmon, D. Klvana, *Appl. Catal. A* 262 (2004) 167.
- [11] T. V. Choudhary, S. Banerjee, V. R. Choudhary, *Appl. Catal. A* 234 (2002) 1.
- [12] V. R. Choudhary, V. H. Rane, *J. Catal.* 130 (1991) 411.
- [13] F. H. Ribeiro, M. Chow, R. A. Dalla Betta, *J. Catal.* 146 (1994) 537.
- [14] R. F. Hicks, H. H. Qi, M. L. Young, R. G. Lee, *J. Catal.* 122 (1990) 280.
- [15] N. Lopez, J. K. Norskov, T. V. W. Janssens, A. Carlsson, A. Puig-Molina, B. S. Clausen, J. D. Grunwaldt, *J. Catal.* 225 (2004) 86.

# Chapter 7

## Ammonia oxidation over mono- and multi-component gold-based catalysts

*Various gold-based catalysts were prepared via HDP with urea and tested for the selective catalytic oxidation of ammonia (SCO). The effect of different oxidic additives,  $MO_x$  ( $M = Li, Rb, Mg, Cu, Fe, Ce, Mn, Cr, Zr$  and  $Ti$ ) on the catalytic performance of  $Au/Al_2O_3$  was examined. It was found that the presence of  $Au$  enhances the SCO activity. The selectivity can be steered into the desired direction by a proper choice of the additives. The most active catalyst ( $Au/CuO/Al_2O_3$ ) shows high selectivity to  $N_2$  (more than 90%), whereas  $Au/Li_2O/CeO_x/Al_2O_3$  exhibits high selectivity to  $N_2O$ . In addition, the catalytic performance of supported gold catalysts was compared with  $Ag$  and  $Ag-CuO$  deposited on alumina. FT-IR spectroscopy shows bands following  $NH_3$  adsorption that can be attributed to imide-like ( $-NH$ ) adspecies, in addition to  $NH_4^+$  (on Brønsted acid sites) and coordinated  $NH_3$  (on Lewis acid sites). The presence of  $Au$  enhances the band intensity of imide-like adspecies, which may be responsible for the improved SCO activity in the presence of  $Au$ .*

## 7.1 Outline

This chapter describes the catalytic performance of Au/Al<sub>2</sub>O<sub>3</sub>, Au/MO<sub>x</sub>/Al<sub>2</sub>O<sub>3</sub> and Au/M<sup>I</sup>O<sub>x</sub>/M<sup>II</sup>O<sub>x</sub>/Al<sub>2</sub>O<sub>3</sub> (M, M<sup>I</sup> and M<sup>II</sup>: Li, Rb, Mg, Mn, Fe, Cu, Zr, Ce and Ti) in NH<sub>3</sub> oxidation. In addition, a comparison of the catalytic performance of supported gold catalysts with Ag and Ag-CuO combinations is described. Section 7.2 presents some experimental details concerning the preparation of the samples and the experimental set-up. Section 7.3 illustrates the catalytic performance (activity and selectivity) of the as-prepared supported gold catalysts in NH<sub>3</sub> oxidation, reactant ratio NH<sub>3</sub>/O<sub>2</sub> = 1. Section 7.4 illustrates the changes in the catalytic performance and product distribution under a large excess of oxygen. Section 7.5 presents FTIR spectroscopy results. Section 7.6 presents a general discussion. The most important conclusions are summarized in section 7.7.

## 7.2 Experimental

The mono- and multi- component gold based catalysts have been prepared by HDP with urea, as described in *Chapter 3*. Au/Fe<sub>2</sub>O<sub>3</sub> and Au/TiO<sub>2</sub> were prepared in a similar way using commercial TiO<sub>2</sub> (Eurotitania 1) and Fe<sub>2</sub>O<sub>3</sub> prepared by the precipitation from Fe(NO<sub>3</sub>)<sub>3</sub>·6 H<sub>2</sub>O (Aldrich). Unless mentioned, the atomic ratio used to prepare the catalysts was Au:M:Al = 1:5:15, which corresponds to approximately 5 wt-% Au. Three Au-based catalysts deposited on CuO/Al<sub>2</sub>O<sub>3</sub> have been prepared: Au/CuO/Al<sub>2</sub>O<sub>3</sub>-A (4 wt-% Au, 6 wt-% CuO), Au/CuO/Al<sub>2</sub>O<sub>3</sub>-B (7.4 wt-% Au, 12 wt-% CuO) and Au/CuO/Al<sub>2</sub>O<sub>3</sub>-C (4.8 wt-% Au, 8 wt-% CuO).

Ag/Al<sub>2</sub>O<sub>3</sub> was prepared by vacuum impregnation of  $\gamma$ -Al<sub>2</sub>O<sub>3</sub> with the necessary amount of silver nitrate (Aldrich), such that the atomic ratio Ag:Al = 1:10 (17 wt-% Ag). After impregnation, the cake was dried in static air at 80<sup>o</sup>C for 16h and then calcined in oxygen flow at 350<sup>o</sup>C. Ag/CuO/Al<sub>2</sub>O<sub>3</sub> was prepared similar to the mixed support M<sup>I</sup>O<sub>x</sub>/M<sup>II</sup>O<sub>x</sub>/Al<sub>2</sub>O<sub>3</sub>, such that the atomic ratio employed was Ag:Cu:Al=1:1:10. XRD analysis showed that Ag is present mainly as Ag<sup>0</sup> on all Ag-containing samples.

The experiments were performed in a total flow of NH<sub>3</sub>+O<sub>2</sub> of 30 ml min<sup>-1</sup>. The gases (4 vol % in He) were mixed using the ratio NH<sub>3</sub>:O<sub>2</sub> = 1:1. However, some selected gold-based catalysts were also tested in ammonia oxidation under excess of oxygen. In this case the reactant ratio used was NH<sub>3</sub>:O<sub>2</sub> = 1:10. The catalysts were pretreated in-situ with hydrogen up to 300<sup>o</sup>C, followed by a cool-down under He to RT. The test procedures started with feeding 4 vol % O<sub>2</sub> until the gas composition was stabilized, subsequently adding an equal flow rate of 4 vol % NH<sub>3</sub> until stabilized. At least two heating-cooling cycles were applied up to 400<sup>o</sup>C using a heating/cooling rate of 5<sup>o</sup>C min<sup>-1</sup>. The effluent composition was analyzed by mass spectrometry. The monitored mass signals included 2, 14, 16, 17, 18, 28, 30, 32, 44, and 46. After correction of the signal intensities for the fragmentation signals of the different compounds, the effluent mass balance in the heating sequences was correct within  $\pm 10\%$  of the feed, but not in the cooling sequences. The erroneous mass balance in the cooling sequences was attributed to the slow pumping/slow desorption of H<sub>2</sub>O and NH<sub>3</sub>. Therefore, only the data in the heating sequences is used for activity analysis. After performing the test reaction, the used catalysts were again analysed by XRD.

FTIR analysis was carried out using a commercial instrument (*Mattson, Galaxy 2020*) equipped with a controlled-atmosphere chamber [1]. The experimental details concerning the complete procedure are described in *Chapter 3, Section 3.4.6*.

### 7.3 Ammonia oxidation, reactant ratio $\text{NH}_3:\text{O}_2 = 1:1$

#### Catalytic activity

The results presented in Figs. 7.1A-B correspond to the first heating stage, but subsequent heating-cooling cycles eventually caused a maximum shift in conversion of 30 – 40°C towards higher temperature. A comparison of the temperatures needed to achieve 50% conversion during subsequent heating cycles is provided in Table 7.1.

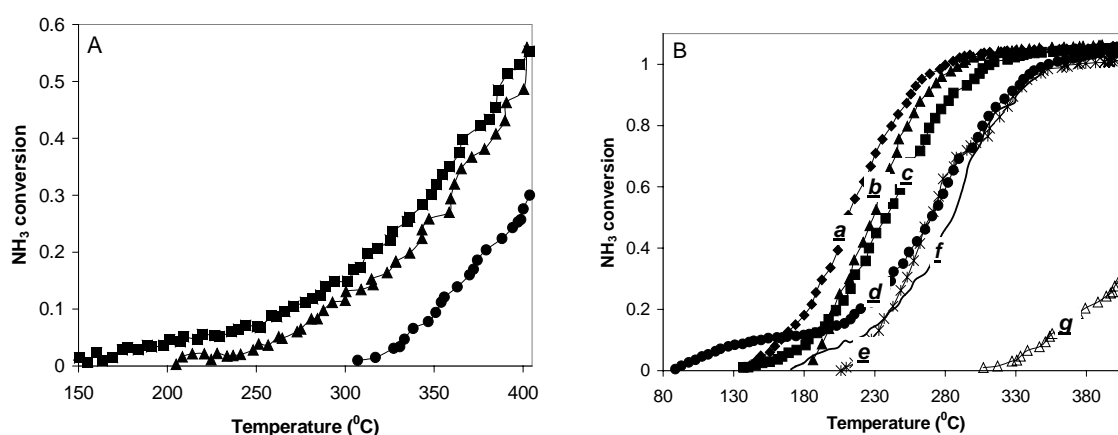


**Figure 7.1:**  $\text{NH}_3$  conversion vs. temperature over  $\text{Au}/\text{Al}_2\text{O}_3$  (●),  $\text{Au}/\text{Li}_2\text{O}/\text{Al}_2\text{O}_3$  (▲) and  $\text{Au}/\text{Rb}_2\text{O}/\text{Al}_2\text{O}_3$  (■) (A);  $\text{Au}/\text{CuO}/\text{Al}_2\text{O}_3$ -C (a),  $\text{Au}/\text{CuO}/\text{Al}_2\text{O}_3$ -B (b),  $\text{Au}/\text{CuO}/\text{Al}_2\text{O}_3$ -A (c),  $\text{CuO}/\text{Al}_2\text{O}_3$ -A (d),  $\text{CuO}/\text{Al}_2\text{O}_3$ -C (e),  $\text{CuO}/\text{Al}_2\text{O}_3$ -B (f) and  $\text{Au}/\text{Al}_2\text{O}_3$  (g) (B).

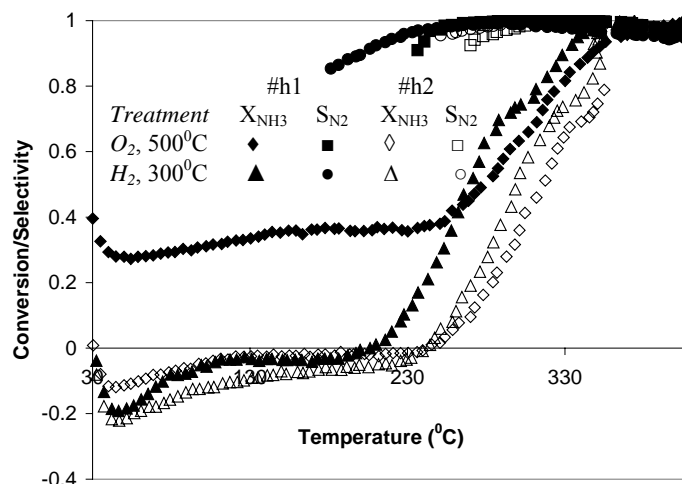
Fig. 7.1A compares the catalytic performance of  $\text{Au}/\text{Al}_2\text{O}_3$  and  $\text{Li}_2\text{O}$ - and  $\text{Rb}_2\text{O}$ -promoted gold catalysts. Oxidation of ammonia starts on  $\text{Au}/\text{Al}_2\text{O}_3$  above 300°C [1, 2]. Addition of additives such as alkali metal oxides produces a significant shift of  $\text{NH}_3$  conversion to lower temperatures. However, the influence of these additives on the catalytic performance of  $\text{Au}/\text{Al}_2\text{O}_3$  in  $\text{NH}_3$  oxidation is less pronounced than that found for other reactions (i.e. propene oxidation and nitrous oxide reduction) [3, 4]. In addition, the catalytic performance of both alkali-promoted  $\text{Au}/\text{Al}_2\text{O}_3$  catalysts is quite similar. It should be mentioned that  $\text{Al}_2\text{O}_3$  and  $\text{MO}_x/\text{Al}_2\text{O}_3$  (M: Li, Rb) were also tested and found negligibly active under the reaction conditions employed here.

Fig. 7.1B shows the variation of the  $\text{NH}_3$  conversion with increasing temperature over  $\text{Au}/\text{CuO}/\text{Al}_2\text{O}_3$  and  $\text{CuO}/\text{Al}_2\text{O}_3$  catalysts with different CuO loadings. The samples  $\text{Au}/\text{CuO}/\text{Al}_2\text{O}_3$ -A,  $\text{Au}/\text{CuO}/\text{Al}_2\text{O}_3$ -B,  $\text{CuO}/\text{Al}_2\text{O}_3$ -A and  $\text{CuO}/\text{Al}_2\text{O}_3$ -B have been already discussed in detail in *Chapter 4*. The samples  $\text{Au}/\text{CuO}/\text{Al}_2\text{O}_3$ -C and  $\text{CuO}/\text{Al}_2\text{O}_3$ -C contain 8 wt-% CuO and 4.8 wt-% Au. The peculiar line shape of the data at lower temperatures (below 150°C) is due to initial  $\text{NH}_3$  adsorption at room temperature and subsequent  $\text{NH}_3$  desorption

from 40 to 150°C. Adsorption results in higher apparent conversions in the beginning of the heating sequence, while NH<sub>3</sub> desorption results in negative conversions. Oxygen consumption was not observed in this temperature range. CuO/Al<sub>2</sub>O<sub>3</sub> catalysts show a conversion light off at 250°C. The variation in the CuO content (6, 8 or 12 wt-% CuO) in CuO/Al<sub>2</sub>O<sub>3</sub> did not result in a significantly different behaviour (Fig. 7.1B, curves d, e and f).

The onset temperature is defined as the temperature corresponding to  $\geq 10\%$  NH<sub>3</sub> conversion. Fig. 7.1B shows that the onset temperatures over Au/CuO/Al<sub>2</sub>O<sub>3</sub> catalysts are 30 - 50°C lower than over CuO/Al<sub>2</sub>O<sub>3</sub>. Hence, it can be concluded that the Au/CuO/Al<sub>2</sub>O<sub>3</sub> catalysts are clearly more active than CuO/Al<sub>2</sub>O<sub>3</sub>. This indicates that the presence of Au enhances the activity. Among the three different CuO loadings, CuO/Al<sub>2</sub>O<sub>3</sub>-C seems to give the best activity for Au/CuO/Al<sub>2</sub>O<sub>3</sub>. However, the activity recorded in the second heating sequence indicates that the catalytic activity of CuO/Al<sub>2</sub>O<sub>3</sub>-B and CuO/Al<sub>2</sub>O<sub>3</sub>-C showed similar activities though they are both still more active than Au/CuO/Al<sub>2</sub>O<sub>3</sub>-A. This is because all catalysts except Au/CuO/Al<sub>2</sub>O<sub>3</sub>-C showed a ca. 5-10% activity decrease in the second heating sequence compared to the first heating cycle. The XRD data shown in Fig. 4.8 (Chapter 4) indicate the presence of CuO-aggregates in the CuO/Al<sub>2</sub>O<sub>3</sub>-B and the corresponding Au/CuO/Al<sub>2</sub>O<sub>3</sub>-B catalysts. 12 wt-% CuO (CuO/Al<sub>2</sub>O<sub>3</sub>-B) is higher than needed for one theoretical monolayer coverage, whereas 8% CuO (CuO/Al<sub>2</sub>O<sub>3</sub>-C) is close to a monolayer. The absence of CuO-aggregates in the CuO/Al<sub>2</sub>O<sub>3</sub>-C suggests that CuO tends to spread over the Al<sub>2</sub>O<sub>3</sub> surface to form well-dispersed CuO. At the highest CuO loading XRD detects CuO aggregates. That the Au/CuO/Al<sub>2</sub>O<sub>3</sub>-A catalyst showed a lower activity than the other two Au/CuO/Al<sub>2</sub>O<sub>3</sub> catalysts with higher CuO loadings may be due to an incomplete coverage of CuO on Al<sub>2</sub>O<sub>3</sub>. This suggests that a well-dispersed CuO surface works as a better substrate for Au than bare Al<sub>2</sub>O<sub>3</sub>. The presence of a CuO-aggregate in Au/CuO/Al<sub>2</sub>O<sub>3</sub>-B seems to result in a larger Au particle size than those with lower CuO loading, as indicated by the Au XRD signals shown in Fig. 4.8 and Table 4.2. This may be a reason for the somewhat lower activity of CuO/Al<sub>2</sub>O<sub>3</sub>-B as compared with CuO/Al<sub>2</sub>O<sub>3</sub>-C.

Gang *et al.* [5] reported that CuO/Al<sub>2</sub>O<sub>3</sub> and Cu-Ag/Al<sub>2</sub>O<sub>3</sub> after calcination at 500°C exhibit an excellent activity and N<sub>2</sub> selectivity for the SCO reaction to N<sub>2</sub>. For comparison, the CuO/Al<sub>2</sub>O<sub>3</sub>-C catalyst was also tested following calcination at 500°C. Fig. 7.2 compares its activity and selectivity to that after pretreatment with H<sub>2</sub> at 300°C. It is interesting to note that calcination of this catalyst indeed resulted in an improved activity. It is expected that an O<sub>2</sub> treatment at 500°C will result in oxidized Cu, which readily catalyzes NH<sub>3</sub> oxidation even at room temperature. However, the improved activity was found only at the beginning of the first heating sequence. This is illustrated in Fig. 7.2, which shows the NH<sub>3</sub> conversion and the selectivity during the first and second heating cycle for calcined and reduced CuO/Al<sub>2</sub>O<sub>3</sub>-C. The oxidized Cu became partly reduced under the reaction conditions used in this study and the N<sub>2</sub> selectivity is more than 90%. The effect of the pretreatment on the selectivity is very small.



**Figure 7.2:** Effect of pretreatment of CuO/Al<sub>2</sub>O<sub>3</sub>-C on the NH<sub>3</sub> oxidation during two heating sequences.

Fig. 7.3A compares the ammonia oxidation over other singly-promoted Au/Al<sub>2</sub>O<sub>3</sub> catalysts during the first heating cycles, whereas Fig. 7.3B presents the conversion of ammonia versus temperature over some multicomponent gold-based catalysts. Au/FeO<sub>x</sub>/Al<sub>2</sub>O<sub>3</sub> (Fig. 7.3A) showed a high initial activity.

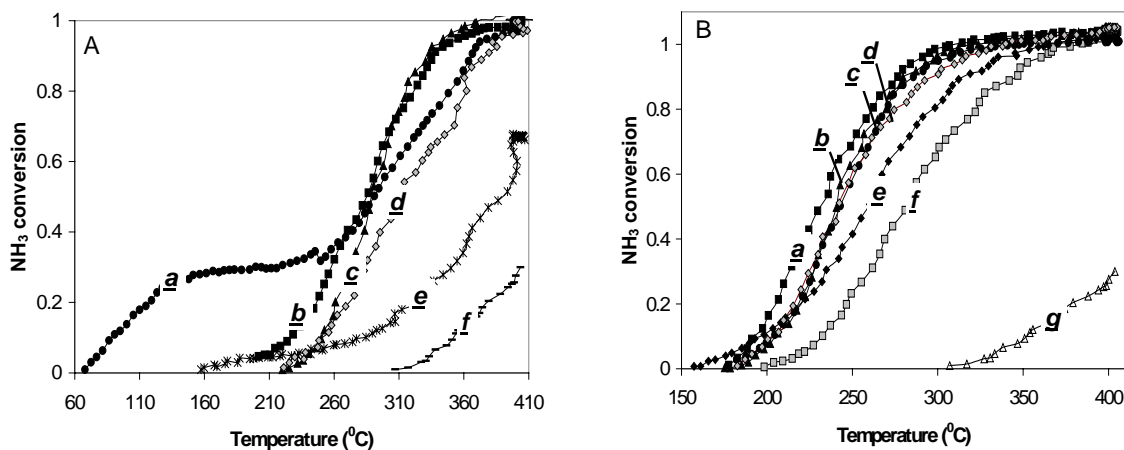


**Figure 7.3:** NH<sub>3</sub> conversion vs. temperature over Au/FeO<sub>x</sub>/Al<sub>2</sub>O<sub>3</sub> (a), Au/CeO<sub>x</sub>/Al<sub>2</sub>O<sub>3</sub> (b), Au/CrO<sub>x</sub>/Al<sub>2</sub>O<sub>3</sub> (c), Au/Fe<sub>2</sub>O<sub>3</sub> (d), Au/ZrO<sub>x</sub>/Al<sub>2</sub>O<sub>3</sub> (e), Au/Al<sub>2</sub>O<sub>3</sub> (f) (A); Au/FeO<sub>x</sub>/CuO/Al<sub>2</sub>O<sub>3</sub> (a), Au/CuO/CeO<sub>x</sub>/Al<sub>2</sub>O<sub>3</sub> (b), Au/Li<sub>2</sub>O/CeO<sub>x</sub>/Al<sub>2</sub>O<sub>3</sub> (c), Au/CeO<sub>x</sub>/ZrO<sub>x</sub>/Al<sub>2</sub>O<sub>3</sub> (d), Au/MnO<sub>x</sub>/MgO/Al<sub>2</sub>O<sub>3</sub> (e), FeO<sub>x</sub>/CuO/Al<sub>2</sub>O<sub>3</sub> (f), Au/Al<sub>2</sub>O<sub>3</sub> (g) (B).

However, the observed activity of Au/FeO<sub>x</sub>/Al<sub>2</sub>O<sub>3</sub> in the second heating sequence is almost the same as that shown for Au/Fe<sub>2</sub>O<sub>3</sub>. Subsequent heating cycles did not affect the performance of Au/Fe<sub>2</sub>O<sub>3</sub>. Au/FeO<sub>x</sub>/Al<sub>2</sub>O<sub>3</sub>, similar to CuO/Al<sub>2</sub>O<sub>3</sub> catalyst, displays a slightly higher initial activity in the first heating cycle than in the second and further cycles. The



lowest catalytic performance of the singly-promoted gold-based catalysts was displayed by Au/ZrO<sub>x</sub>/Al<sub>2</sub>O<sub>3</sub>.

A strong effect on the catalytic activity of Au/Al<sub>2</sub>O<sub>3</sub> was obtained in the presence of two different additives. Among them, Au/FeO<sub>x</sub>/CuO/Al<sub>2</sub>O<sub>3</sub> (curve a in Fig. 7.3B) showed the best performance, whereas the least active catalyst was Au/MnO<sub>x</sub>/MgO/Al<sub>2</sub>O<sub>3</sub> (curve e in Fig. 7.3B). As already observed, among the mixed supports, only CuO/Al<sub>2</sub>O<sub>3</sub> and FeO<sub>x</sub>/Al<sub>2</sub>O<sub>3</sub> show catalytic activity. The other oxides used as additives were found negligibly active in NH<sub>3</sub> oxidation. For comparison, the catalytic activity of FeO<sub>x</sub>/CuO/Al<sub>2</sub>O<sub>3</sub> is also shown in Fig. 7.3B (curve f). This indicates that, except for the samples with CuO and/or FeO<sub>x</sub> as additives, the catalytic activity shown in Fig. 7.3B is mainly from the presence of Au. XRD analyses (Table 7.1) of these fresh Au catalysts indicate that the Au particle size sequence did not match to the activity sequence, since catalysts with very small gold particles, i.e. Au/Li<sub>2</sub>O/Al<sub>2</sub>O<sub>3</sub> (3.2 nm) or Au/Rb<sub>2</sub>O/Al<sub>2</sub>O<sub>3</sub> (< 3 nm) were less active catalysts than Au/CuO/Al<sub>2</sub>O<sub>3</sub>-B (~ 7 nm). Hence, the nature of the support plays a decisive role in the differences in SCO activity of the catalysts tested. The identity of the additives greatly influences the product selectivity as well, and will be discussed in the next section. Additives such as ceria or zirconia are not truly beneficial for selective ammonia oxidation to N<sub>2</sub>. This can be due to the well known “oxygen storage capacity”, more pronounced for ceria than zirconia, which may not be required for this reaction.

Table 7.1 also summarizes the temperature of 50% conversion (for the first heating stage, #h1, and the second and further heating stages, #h2) and the corresponding selectivity to N<sub>2</sub> during #h1. In the same table are also mentioned the corresponding values of the specific reaction rate, *r*, expressed as the moles of NH<sub>3</sub> transformed over the moles of Au per second (300°C). For the Au-containing catalysts with active supports, viz. CuO-, and FeO<sub>x</sub>-containing catalysts, the specific reaction rate, *r*, was also calculated by taking into account both the loading of Au and MO<sub>x</sub>.

In general, the difference between the first and second (and further) heating cycles does not exceed 40°C. Moreover, the average gold particle size is preserved during the reaction cycle and more than 10 hours in the gas stream did not cause severe sintering.

If the catalysts are discussed in terms of the specific reaction rate, *r*, some changes in the ranking order of the catalysts are noticed. First, addition of Li<sub>2</sub>O causes an increase of more than a factor of 10 in *r*, as compared with unpromoted Au/Al<sub>2</sub>O<sub>3</sub>. The maximum increase is found for Au/CeO<sub>x</sub>/ZrO<sub>x</sub>/Al<sub>2</sub>O<sub>3</sub>, more than 120 times. This is an interesting result, since if only ceria or zirconia was added to Au/Al<sub>2</sub>O<sub>3</sub>, the result was a catalyst with intermediate activity. The reason why such huge synergy results upon combining ceria and zirconia is not very clear. A possible explanation may be related to the well-known effect of zirconia on the stability of ceria, with the former acting more like a structural promoter and the latter as a chemical one [6].

**Table 7.1:**  $T_{50\%}$  during first heating (#h1) and second heating cycle (#h2), the corresponding selectivity to  $N_2$  during (#h1), the specific reaction rate,  $r$ , the average gold particle size for fresh ( $d_{Au}^a$ ) and used ( $d_{Au}^b$ ) catalysts (XRD).  $NH_3:O_2=1$ .

Catalyst	$d_{Au}^a$ (nm)	$d_{Au}^b$ (nm)	$T_{50\%}$ , #h1, ( $^{\circ}C$ )	$T_{50\%}$ , #h2, ( $^{\circ}C$ )	$S_{N_2}$ , (%)	$r \times 10^3$ (moles $NH_3$ moles $M^{-1} s^{-1}$ )
Au/ $Al_2O_3$	4.3±0.1	5.0±0.1	>400	>400	-	~0
Au/ $Li_2O/Al_2O_3$	3.2±0.1	3.5±0.2	396	350	77	1.5±0.1
Au/ $Rb_2O/Al_2O_3$	<3.0	3.0±0.2	390	>400	82	2.0±0.1
Au/ $CuO/Al_2O_3$ -A	3.0±0.1	3.2±0.3	245	255	96	$(11.2±0.2)^1/(2.3±0.1)^2/(3.0±0.1)^3$
Au/ $CuO/Al_2O_3$ -B	6.8±0.2	7.5±0.3	286	298	96	$(6.5±0.1)^1/(2.5±0.2)^2/(4.0±0.1)^3$
Au/ $CuO/Al_2O_3$ -C	<3.0	3.5±0.2	211	230	94	$(10.1±0.2)^1/(2.0±0.1)^2/(2.4±0.1)^3$
Au/ $FeO_x/Al_2O_3$	<3.0	3.4±0.4	291	337	77	$(8.2±0.2)^1/(2.4±0.1)^2/(3.4±0.2)^3$
Au/ $Fe_2O_3$	3.6±0.1	4.5±0.2	312	330	94	$(2.9±0.2)^1/(0.5±0.1)^2/(0.5±0.1)^3$
Au/ $CrO_x/Al_2O_3$	3.4±0.2	4.5±0.1	290	288	94	7.6±0.2
Au/ $CeO_x/Al_2O_3$	<3.0	3.3±0.3	280	295	45	7.1±0.1
Au/ $ZrO_x/Al_2O_3$	3.1±0.3	4.0±0.2	393	>400	66	2.1±0.1
Au/ $TiO_2/Al_2O_3$	<3.0	3.1±0.4	>400	>400	-	~0
Au/ $CeO_x/ZrO_x/Al_2O_3$	<3.0	3.5±0.1	242	244	72	13.3±0.2
Au/ $FeO_x/CuO/Al_2O_3$	<3.0	4.0±0.2	232	247	97	$(11.3±0.2)^1/(1.6±0.1)^2/(1.9±0.1)^3$
Au/ $CuO/CeO_x/Al_2O_3$	16.8±0.1	17.3±0.3	240	230	90	$(9.0±0.2)^1/(0.5±0.1)^2/(0.6±0.1)^3$
Au/ $MnO_x/MgO/Al_2O_3$	<3.0	4.2±0.1	260	273	80	2.5±0.1
Au/ $Li_2O/CeO_x/Al_2O_3$	<3.0	3.1±0.1	243	258	58	9.7±0.2
$CuO/Al_2O_3$ -A	-	-	276	316	95	2.3±0.1
$CuO/Al_2O_3$ -B	-	-	286	320	96	1.6±0.1
$CuO/Al_2O_3$ -C	-	-	263	295	99	1.7±0.1
$FeO_x/CuO/Al_2O_3$	-	-	282	300	97	1.1±0.1
$CeO_x/ZrO_x/Al_2O_3$	-	-	>400	>400	-	0
$CuO/CeO_x/Al_2O_3$	-	-	270	290	95	1.4±0.1

<sup>1</sup>r was estimated based on the Au loading; <sup>2</sup>r was estimated based on the (Au+ $MO_x$ ) loading; <sup>3</sup>r was estimated based on the  $MO_x$  loading. M: Au, Cu, Fe.

Among the multicomponent catalysts, if the  $NH_3$  conversion is normalized to the real loading of various active components, Au/ $FeO_x/CuO/Al_2O_3$  and Au/ $CuO/CeO_x/Al_2O_3$  are less active than, for example, Au/ $CeO_x/ZrO_x/Al_2O_3$ . Nevertheless, these catalysts remain very attractive due to their  $T_{50\%}$  and  $S_{N_2}$ . However, as mentioned before, the identity of the additives is crucial and influences both the  $NH_3$  conversion and selectivity to various products.

Previously reported results [5, 7, 8] showed that Ag- and Cu-based catalysts are very efficient for ammonia oxidation and with high selectivity to  $N_2$ . Therefore, some catalysts have been prepared and tested, based on either Ag, or on a combination of Ag with CuO and Au. The aim was to compare the performance of Au in  $NH_3$  oxidation with those of the other elements of the Group IB, Cu and Ag and also to examine the effect of combining these metals on the conversion and the selectivity. The results of the catalytic activity tests are depicted in Fig. 7.4.

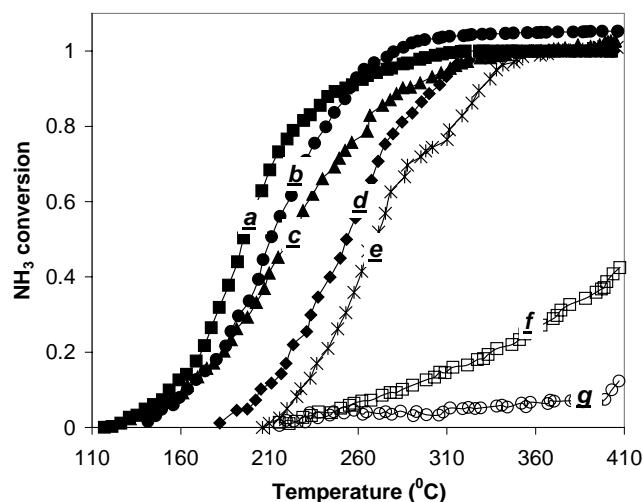


**Figure 7.4:**  $\text{NH}_3$  conversion vs. temperature over:  $\text{Ag}/\text{Al}_2\text{O}_3$  (a),  $\text{Au}/\text{CuO}/\text{Al}_2\text{O}_3\text{-C}$  (b),  $\text{Ag}/\text{CuO}/\text{Al}_2\text{O}_3$  (c),  $\text{Au}/\text{Ag}/\text{CuO}/\text{Al}_2\text{O}_3$  (d),  $\text{CuO}/\text{Al}_2\text{O}_3\text{-C}$  (e),  $\text{Au}/\text{Al}_2\text{O}_3$  (f),  $\text{Au}/\text{Ag}/\text{Al}_2\text{O}_3$  (g).

Apparently,  $\text{Ag}/\text{Al}_2\text{O}_3$  (curve a) is the most active catalyst, followed by  $\text{Au}/\text{CuO}/\text{Al}_2\text{O}_3\text{-C}$  (curve b). The least active catalyst is  $\text{Au}/\text{Ag}/\text{Al}_2\text{O}_3$ . However, due to the fact that the catalysts contain different metal loadings, a comparison based on  $r$  is requested. The results concerning the temperature of 50%  $\text{NH}_3$  conversion during #h1 and #h2, the corresponding selectivity to  $\text{N}_2$ , as well as the variation of the specific reaction rate  $r$  at  $300^\circ\text{C}$  are summarized in Table 7.2. XRD detected only the diffraction pattern of  $\text{Ag}^0$ .

**Table 7.2:**  $T_{50\%}$  for #h1 and #h2, the corresponding  $S_{\text{N}_2}$  (#h1) and the specific reaction rate,  $r$  ( $300^\circ\text{C}$ ) for Ag-, CuO- and Au- containing catalysts.  $\text{NH}_3:\text{O}_2 = 1$ .

Catalyst	$T_{50\%}$ (#h1, $^\circ\text{C}$ )	$T_{50\%}$ (#h2, $^\circ\text{C}$ )	$S_{\text{N}_2}$ (%)	$r \times 10^3$ (moles $\text{NH}_3$ moles $\text{M}^{-1} \text{s}^{-1}$ )
$\text{Ag}/\text{Al}_2\text{O}_3$	195	220	90	$1.5 \pm 0.1$
$\text{Au}/\text{Al}_2\text{O}_3$	>400	>400	-	$\sim 0$
$\text{CuO}/\text{Al}_2\text{O}_3\text{-C}$	263	295	99	$1.7 \pm 0.1$
$\text{Au}/\text{Ag}/\text{Al}_2\text{O}_3$	>400	>400	-	$\sim 0$
$\text{Au}/\text{CuO}/\text{Al}_2\text{O}_3\text{-C}$	211	230	94	$(10.1 \pm 0.2)^1 / (2.0 \pm 0.1)^2 / (2.4 \pm 0.1)^3$
$\text{Ag}/\text{CuO}/\text{Al}_2\text{O}_3$	222	260	100	$1.6 \pm 0.1$
$\text{Au}/\text{Ag}/\text{CuO}/\text{Al}_2\text{O}_3$	254	282	99.5	$(8.1 \pm 0.2)^1 / (2.5 \pm 0.1)^2 / (0.8 \pm 0.1)^3$

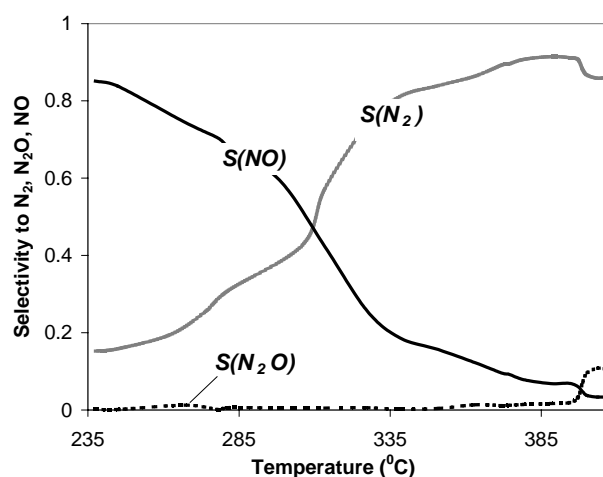
<sup>1</sup> $r$  was estimated based on the Au loading; <sup>2</sup> $r$  was estimated based on the  $(\text{Au} + \text{MO}_x)$  loading; <sup>3</sup> $r$  was estimated based on the  $\text{MO}_x$  loading. M: Au, Ag, Cu.

High selectivity to  $\text{N}_2$  was found for all the catalysts, except  $\text{Au}/\text{Al}_2\text{O}_3$ . The ranking of the catalysts is different on the basis of the specific reaction rate. A minor improvement of the catalytic performance is obtained after combining Ag with CuO.  $\text{Au}/\text{Ag}/\text{Al}_2\text{O}_3$  is completely inactive. This might be due to the very large Au particles formed during the preparation (25.2 nm-XRD). The addition of Au to  $\text{Ag}/\text{CuO}/\text{Al}_2\text{O}_3$  does not significantly influence the selectivity to  $\text{N}_2$  (see below).

**Product distribution,  $NH_3:O_2 = 1$** 

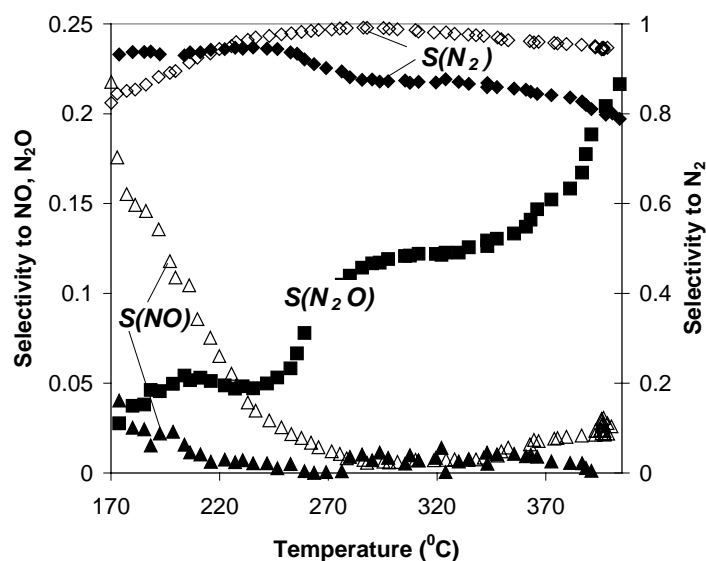
During oxidation of ammonia over gold-based catalysts, four N-containing products may be obtained, viz.  $N_2O$ ,  $NO$ ,  $N_2$  or  $NO_2$ . The production of the above-mentioned molecules was found to depend strongly on the nature of the additives as well as on the temperature.

Fig. 7.5 shows the product distribution for the unpromoted  $Au/Al_2O_3$  catalyst. The main product in the low temperature range is  $NO$ , but by increasing the temperature,  $N_2$  starts to be formed and at the highest reaction temperature used, the selectivity to  $N_2$  is about 80%.  $N_2O$  and  $NO_2$  were not formed. However, the unpromoted  $Au/Al_2O_3$  catalyst is not a real choice for SCO of  $NH_3$  to  $N_2$ , since this catalyst shows a maximum  $NH_3$  conversion of 30% at  $400^\circ C$  and a high selectivity to  $NO$  in the low-temperature range. This high selectivity to  $NO$  may be interesting for the low-temperature production of  $NO$ , if  $NH_3$  conversion would be slightly improved.



**Figure 7.5:** Product distribution vs. temperature during  $NH_3$  oxidation over  $Au/Al_2O_3$ ;  $S_{NO}$ : black line,  $S_{N_2}$ : grey line,  $S_{N_2O}$ : dotted line.

A comparison between the product distribution of  $Au/CuO/Al_2O_3-C$  and  $CuO/Al_2O_3-C$  is shown in Fig. 7.6. Both  $CuO/Al_2O_3-C$  and  $Au/CuO/Al_2O_3-C$  show a high selectivity to  $N_2$  in the whole temperature range studied. However, a slight drop in the  $S_{N_2}$  was observed at temperatures exceeding  $300^\circ C$ . In addition to  $N_2$ , some  $N_2O$  was also formed over  $Au/CuO/Al_2O_3-C$ . However, the maximum selectivity to  $N_2O$  did not exceed 20% at  $400^\circ C$ . On the other hand,  $NO$  was not formed after  $Au$  addition to  $CuO/Al_2O_3-C$ .



**Figure 7.6:** Product distribution vs. temperature during NH<sub>3</sub> oxidation over Au/CuO/Al<sub>2</sub>O<sub>3</sub>-C (full symbols) and CuO/Al<sub>2</sub>O<sub>3</sub>-C (open symbols): S<sub>N<sub>2</sub></sub> (◆), S<sub>NO</sub> (▲), S<sub>N<sub>2</sub>O</sub> (■).

The product distribution of Au/CeO<sub>2</sub>/Al<sub>2</sub>O<sub>3</sub> (full symbols) and Au/Li<sub>2</sub>O/CeO<sub>2</sub>/Al<sub>2</sub>O<sub>3</sub> (open symbols) is shown in Fig. 7.7.

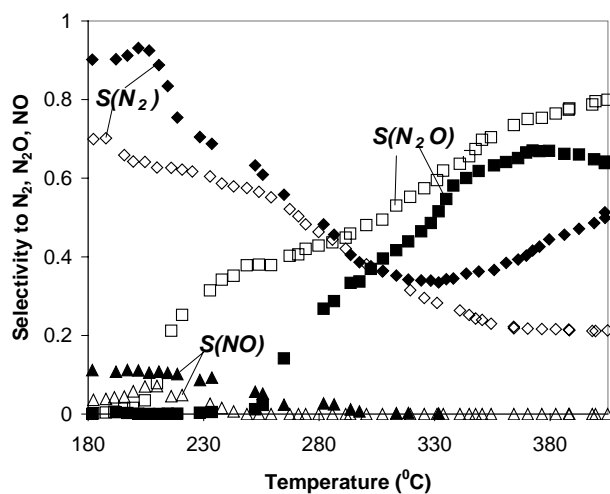


**Figure 7.7:** Product distribution vs. temperature during NH<sub>3</sub> oxidation over Au/CeO<sub>x</sub>/Al<sub>2</sub>O<sub>3</sub> (full symbols) and Au/Li<sub>2</sub>O/CeO<sub>x</sub>/Al<sub>2</sub>O<sub>3</sub> (open symbols): S<sub>N<sub>2</sub></sub> (◆), S<sub>NO</sub> (▲), S<sub>N<sub>2</sub>O</sub> (■).

It should be noted that the support did not show significant activity under these reaction conditions. The distribution profile for the different products over the CeO<sub>x</sub>-containing catalysts is totally different than for the catalysts previously presented (Fig. 7.5, 7.6). In the low temperature range both gold-based catalysts produce mainly N<sub>2</sub>. However, Au/CeO<sub>x</sub>/Al<sub>2</sub>O<sub>3</sub> produces somewhat larger amounts of N<sub>2</sub>. When the reaction temperature exceeds 250<sup>0</sup>C, the selectivity to N<sub>2</sub> decreases significantly. However, whereas for Au/Li<sub>2</sub>O/CeO<sub>x</sub>/Al<sub>2</sub>O<sub>3</sub> the fall is continuous, Au/CeO<sub>x</sub>/Al<sub>2</sub>O<sub>3</sub> shows a second maximum in N<sub>2</sub>

production at 400<sup>0</sup>C. More interesting is the formation of N<sub>2</sub>O with increasing temperature. Thus, for Au/CeO<sub>x</sub>/Al<sub>2</sub>O<sub>3</sub> the production of N<sub>2</sub>O reached a plateau around 350<sup>0</sup>C, and Au/Li<sub>2</sub>O/CeO<sub>x</sub>/Al<sub>2</sub>O<sub>3</sub> shows a continuous increase in N<sub>2</sub>O production. It is expected that if the temperature would exceed 400<sup>0</sup>C (the maximum temperature used here), the production of N<sub>2</sub>O would increase further. This finding may have a practical applicability, since N<sub>2</sub>O may be used for SCO of hydrocarbons [9, 10]. Therefore, it would be interesting to develop a catalyst with a high selectivity to N<sub>2</sub>O. Other by-products were very small concentrations of NO in the low temperature range (below 230<sup>0</sup>C).

Fig. 7.8 shows the product distribution for Ag/Al<sub>2</sub>O<sub>3</sub> (full symbols) and Au/Ag/CuO/Al<sub>2</sub>O<sub>3</sub> (empty symbols) during ammonia oxidation.

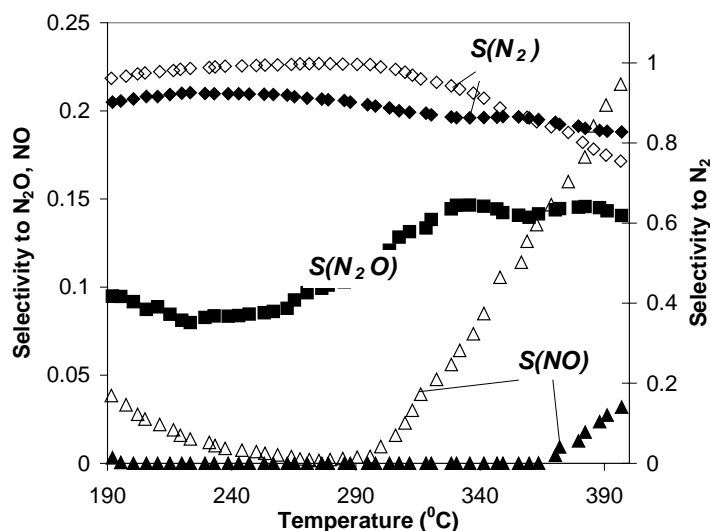


**Figure 7.8:** Product distribution vs. temperature during NH<sub>3</sub> oxidation over for Ag/Al<sub>2</sub>O<sub>3</sub> (full symbols) and Au/Ag/CuO/Al<sub>2</sub>O<sub>3</sub> (open symbols). S<sub>N<sub>2</sub></sub> (◆), S<sub>N<sub>2</sub>O</sub> (▲), S<sub>NO</sub> (■).

N<sub>2</sub> is the main reaction product for both catalysts. However, a very small amount of N<sub>2</sub>O is formed over Ag/Al<sub>2</sub>O<sub>3</sub>, whereas Au/Ag/CuO/Al<sub>2</sub>O<sub>3</sub> produces NO at high temperature (maximum 20% at 400<sup>0</sup>C).

Clearly, by using different additives the product distribution is drastically influenced.

#### 7.4 Ammonia oxidation, reactant ratio NH<sub>3</sub>:O<sub>2</sub> = 1:10

##### Catalytic activity

The effect of excess oxygen on the catalytic performance in ammonia oxidation of various catalytic materials such as Pt/CuO/Al<sub>2</sub>O<sub>3</sub> or CuO/Al<sub>2</sub>O<sub>3</sub> was reported to be negative for both NH<sub>3</sub> conversion and N<sub>2</sub> selectivity [11]. Several supported gold-based catalysts have been selected and their performance in ammonia oxidation was followed under O<sub>2</sub>-rich conditions. It was found that both the ammonia conversion and the selectivity are greatly affected by the oxygen concentration in the gas stream.

A comparison between ammonia conversion in a high excess of oxygen (open symbols) and  $\text{NH}_3:\text{O}_2 = 1:1$  (filled symbols) is shown for  $\text{Au}/\text{Al}_2\text{O}_3$  in Fig. 7.9A and for  $\text{Au}/\text{CuO}/\text{Al}_2\text{O}_3\text{-C}$  in Fig. 7.9B.

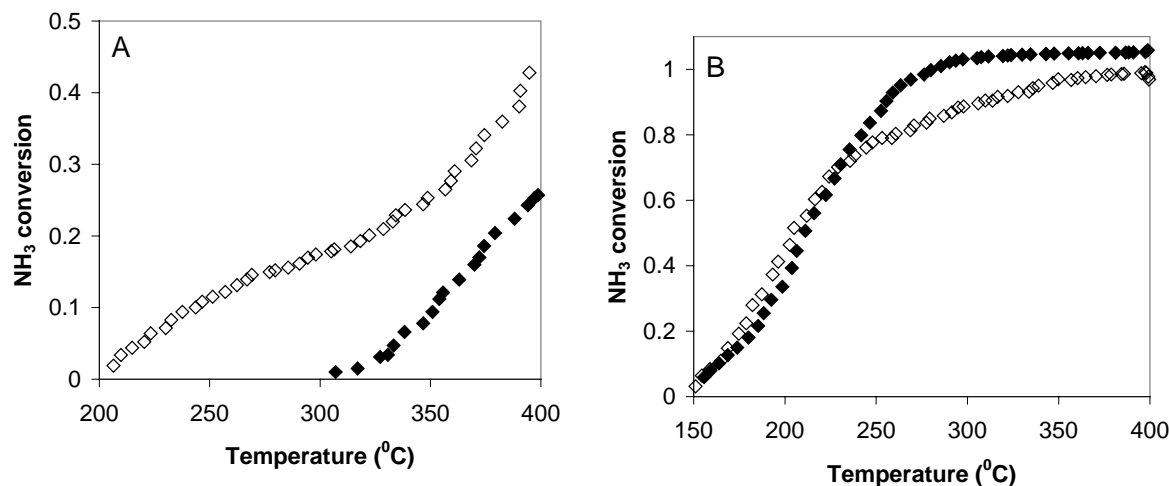


**Figure 7.9:**  $\text{NH}_3$  conversion vs. temperature over  $\text{Au}/\text{Al}_2\text{O}_3$  (A) and  $\text{Au}/\text{CuO}/\text{Al}_2\text{O}_3\text{-C}$  (B).  $\text{NH}_3:\text{O}_2 = 1:1$  ( $\blacklozenge$ ),  $\text{NH}_3:\text{O}_2 = 1:10$  ( $\diamond$ ).

For  $\text{Au}/\text{Al}_2\text{O}_3$  the ammonia conversion is drastically improved when a high excess of oxygen is used (Fig. 7.9A). However, a much smaller effect of the oxygen concentration on the  $\text{NH}_3$  conversion was found for the more active  $\text{Au}/\text{CuO}/\text{Al}_2\text{O}_3\text{-C}$  (Fig. 7.9B). In fact, in the higher temperature range an excess of oxygen appears to slightly inhibit  $\text{NH}_3$  conversion over  $\text{Au}/\text{CuO}/\text{Al}_2\text{O}_3\text{-C}$ .

A comparison of the ammonia conversion ( $X_{\text{NH}_3}$ ) for the  $\text{NH}_3:\text{O}_2$  ratios 1:10 and 1:1 is provided in Table 7.3 for three different temperatures.

**Table 7.3:**  $X_{\text{NH}_3}$  over various gold-based catalysts and different reactant ratios  $\text{NH}_3:\text{O}_2$ .

Catalyst	$X_{\text{NH}_3}$ ( $\text{NH}_3:\text{O}_2=1:1$ ), %			$X_{\text{NH}_3}$ ( $\text{NH}_3:\text{O}_2=1:10$ ), %		
	180 <sup>o</sup> C	240 <sup>o</sup> C	300 <sup>o</sup> C	180 <sup>o</sup> C	240 <sup>o</sup> C	300 <sup>o</sup> C
$\text{Au}/\text{Al}_2\text{O}_3$	0	0	0	0	9	17
$\text{Ag}/\text{Al}_2\text{O}_3$	31	85	99	66	76	93
$\text{Au}/\text{CuO}/\text{Al}_2\text{O}_3\text{-C}$	18	80	100	28	75	89
$\text{CuO}/\text{Al}_2\text{O}_3\text{-C}$	4	26	80	24	62	92
$\text{Au}/\text{CeO}_x/\text{Al}_2\text{O}_3$	0	21	72	0	33	78
$\text{Au}/\text{CuO}/\text{CeO}_x/\text{Al}_2\text{O}_3$	0	50	98	0	32	76

The results summarized in Table 7.3 divide the catalysts into three classes. The first class corresponds to a situation where an excess of oxygen has a beneficial effect in the whole temperature range. It is the case for  $\text{Au}/\text{Al}_2\text{O}_3$ ,  $\text{CuO}/\text{Al}_2\text{O}_3\text{-C}$  and  $\text{Au}/\text{CeO}_x/\text{Al}_2\text{O}_3$ . For the second class a beneficial effect of excess of  $\text{O}_2$  is observed in the low temperature range, but

at higher temperature the effect is either slightly positive or even negative. This is the case for Ag/Al<sub>2</sub>O<sub>3</sub> and Au/CuO/Al<sub>2</sub>O<sub>3</sub>-C. The last class is where the excess of oxygen is detrimental in the whole temperature range, i.e. Au/CuO/CeO<sub>x</sub>/Al<sub>2</sub>O<sub>3</sub>. Different behaviour is observed, depending on the identity of the catalyst. If an excess of oxygen does decrease the catalytic performance, possibly NH<sub>3</sub> and O<sub>2</sub> compete for the same adsorption sites. This could be the situation for those catalysts where an excess of oxygen inhibits the ammonia conversion in the whole temperature range. On the other hand, during the reaction at least two different sources of oxygen exist: oxygen adsorbed on the metal, and promoter lattice oxygen. The activation of oxygen on gold is a very difficult step and it is, most probably, a temperature activated process [12]. On the other hand, the mobility of the lattice oxygen is a function of the nature of the oxide and increases with temperature as well. Thus, the reaction mechanism might be different from one sample to another.

Of course, the role of Au is highly important, most probably for the activation of ammonia. Some evidence for this will be presented in the section devoted to FTIR measurements.

#### Product distribution, NH<sub>3</sub>:O<sub>2</sub> = 1:10

The influence of the excess oxygen (open symbols) on the product distribution during ammonia oxidation is illustrated for two samples: Au/CuO/Al<sub>2</sub>O<sub>3</sub>-C (Fig. 7.10A) and Au/CeO<sub>x</sub>/Al<sub>2</sub>O<sub>3</sub> (Fig. 7.10B). Surprisingly, in a large excess of oxygen, the selectivity to N<sub>2</sub> is increased for Au/CuO/Al<sub>2</sub>O<sub>3</sub>-C and no other by-products are formed, i.e. the NO production is completely suppressed. Thus, this catalyst may find practical applications because it performs as an active and highly selective catalyst even in a large excess of oxygen.

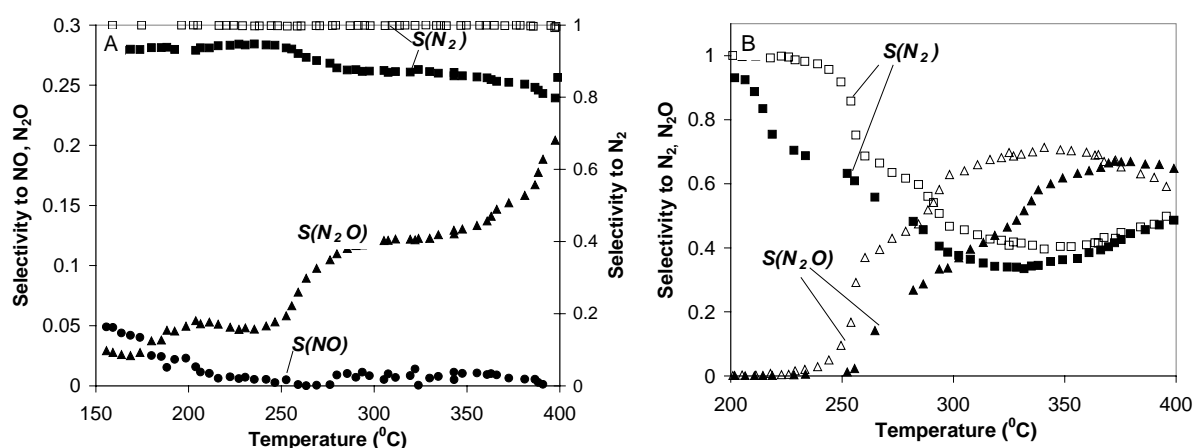


**Figure 7.10:** Product distribution vs. temperature over Au/CuO/Al<sub>2</sub>O<sub>3</sub>-C (A) and Au/CeO<sub>x</sub>/Al<sub>2</sub>O<sub>3</sub> (B) for two different reactant ratios. Full symbols: NH<sub>3</sub>:O<sub>2</sub> = 1:1, open symbols: NH<sub>3</sub>:O<sub>2</sub> = 1:10.



For Au/CeO<sub>x</sub>/Al<sub>2</sub>O<sub>3</sub>, an excess of oxygen affects both the conversion (see above) and the product distribution. The selectivity towards N<sub>2</sub> is positively affected in the lower temperature range up to about 260<sup>0</sup>C. However, in the high temperature range, it equals S<sub>N<sub>2</sub></sub> corresponding to NH<sub>3</sub>:O<sub>2</sub> = 1:1.

The selectivity to N<sub>2</sub>O is also greatly affected by excess oxygen. The production of N<sub>2</sub>O starts at lower temperature with a maximum around 70%, whereas it is about 60% for NH<sub>3</sub>:O<sub>2</sub> = 1:1. This result is not unexpected, since more oxygen in the gas stream would promote the formation of oxygenated compounds such as N<sub>2</sub>O. No other N-containing products were formed.

## 7.5 FTIR spectroscopy measurements

### *FTIR of NH<sub>3</sub> adsorbed over MO<sub>x</sub>/Al<sub>2</sub>O<sub>3</sub> catalysts*

On oxide surfaces ammonia can adsorb on both Brønsted and Lewis acid sites. Infrared absorption of NH<sub>4</sub><sup>+</sup> adspecies (on Brønsted acid sites) is found at 1450-1480 and 1660-1690 cm<sup>-1</sup> for the asymmetric and symmetric deformation modes, respectively. The bands reported for coordinated NH<sub>3</sub> adspecies (on Lewis acid sites) are at 1250-1300 and 1600-1630 cm<sup>-1</sup>, respectively [13]. Fig. 7.11 shows the FTIR spectra of NH<sub>3</sub> adsorption on several MO<sub>x</sub>/Al<sub>2</sub>O<sub>3</sub> at 40<sup>0</sup>C. It is clear that most of the NH<sub>3</sub> absorption bands can be attributed to these adsorption modes. This indicates that NH<sub>3</sub> adsorbs mainly on Brønsted and Lewis sites. However, these bands have different intensity ratios on the various MO<sub>x</sub>/Al<sub>2</sub>O<sub>3</sub> catalysts. By qualitatively comparing the intensity ratios of δ<sub>sym,NH<sub>3</sub></sub> (ca. 1620 cm<sup>-1</sup>) to δ<sub>sym,NH<sub>4</sub><sup>+</sup></sub> (ca. 1690 cm<sup>-1</sup>), it can be concluded that the fraction of Lewis acid sites increases according to: Li<sub>2</sub>O/Al<sub>2</sub>O<sub>3</sub> < CeO<sub>x</sub>/Al<sub>2</sub>O<sub>3</sub> < TiO<sub>x</sub>/Al<sub>2</sub>O<sub>3</sub> < FeO<sub>x</sub>/Al<sub>2</sub>O<sub>3</sub> < Al<sub>2</sub>O<sub>3</sub> < CuO/Al<sub>2</sub>O<sub>3</sub>.

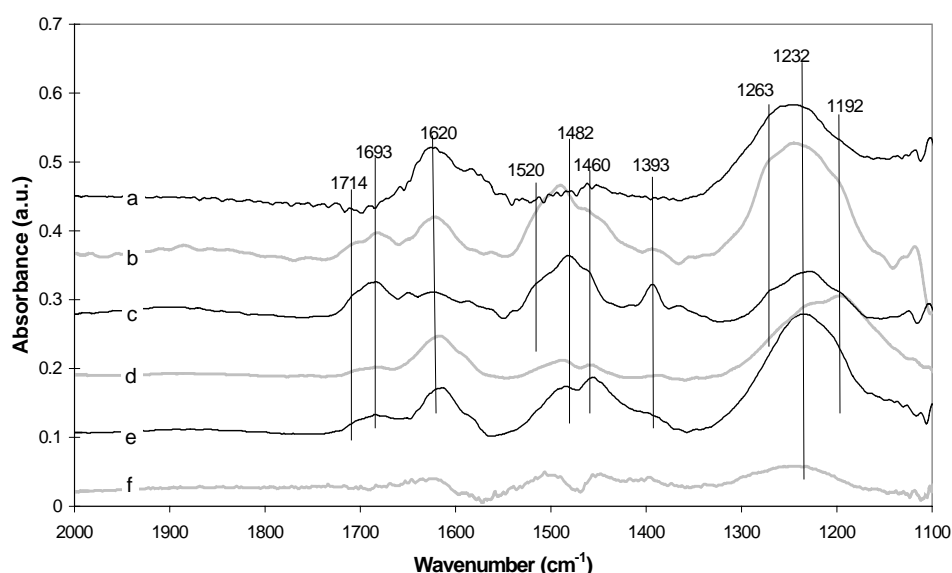


**Fig. 7.11:** FTIR spectra of NH<sub>3</sub> adsorption (40<sup>0</sup>C) on: CuO/Al<sub>2</sub>O<sub>3</sub> (a), CeO<sub>x</sub>/Al<sub>2</sub>O<sub>3</sub> (b), Li<sub>2</sub>O/Al<sub>2</sub>O<sub>3</sub> (c), FeO<sub>x</sub>/Al<sub>2</sub>O<sub>3</sub> (d), TiO<sub>x</sub>/Al<sub>2</sub>O<sub>3</sub> (e) and Al<sub>2</sub>O<sub>3</sub> (f).

The observation that CuO/Al<sub>2</sub>O<sub>3</sub> (curve a) shows no Brønsted acid sites is consistent with earlier reports [14-16]. Clearly, the order in concentration of the Lewis-acid sites and Brønsted acid sites do not match the trend of increasing ammonia oxidation activity shown in Figs. 7.1A-B and 7.3. This suggests that the Lewis acid site density on oxide surfaces cannot account for all the differences in the catalytic activities.

A closer examination of the spectra shown in Fig. 7.11 indicates that the spectra are more complicated and, hence, that an explanation in terms of just NH<sub>4</sub><sup>+</sup> and coordinated NH<sub>3</sub> adspecies is too simple. Both the broad bands at 1150-1300 and 1450-1550 cm<sup>-1</sup> seem to contain more than one absorption band. For example, Li<sub>2</sub>O/Al<sub>2</sub>O<sub>3</sub> exhibits a broad band at 1150-1300 cm<sup>-1</sup> that can be identified as a more intense peak at 1232 cm<sup>-1</sup> with two shoulders at 1192 and 1263 cm<sup>-1</sup>. The same band on FeO<sub>x</sub>/Al<sub>2</sub>O<sub>3</sub> appears to be a combination of the 1192 and 1232 cm<sup>-1</sup> bands where the 1192 cm<sup>-1</sup> peak is more intense. By considering that all the MO<sub>x</sub>/Al<sub>2</sub>O<sub>3</sub> were subjected to an H<sub>2</sub> treatment at 300<sup>o</sup>C before IR analysis, the observed 1232 and 1192 cm<sup>-1</sup> bands are consistent with coordinated NH<sub>3</sub> on oxidized and reduced Fe<sub>2</sub>O<sub>3</sub> at 1220 and 1190 cm<sup>-1</sup>, respectively, as reported in [13]. This indicates that FeO<sub>x</sub>/Al<sub>2</sub>O<sub>3</sub> may be partially reduced following the pretreatment used in this study. The presence of oxidic Fe in Au/FeO<sub>x</sub>/Al<sub>2</sub>O<sub>3</sub> was considered to be responsible for the initial activity enhancement as mentioned earlier. However, in case of Li<sub>2</sub>O/Al<sub>2</sub>O<sub>3</sub> it is clear that the broad band at around 1230 cm<sup>-1</sup> cannot be attributed to a partially reduced surface. Alternatively, the multiple-band absorption in this range can be assigned to the presence of different kinds of Lewis acid sites [13, 15-21].

### FTIR of NH<sub>3</sub> adsorbed over Au/MO<sub>x</sub>/Al<sub>2</sub>O<sub>3</sub> catalysts

Fig. 7.12 shows the FTIR spectra of adsorbed NH<sub>3</sub> at 40<sup>o</sup>C on various supported Au catalysts.

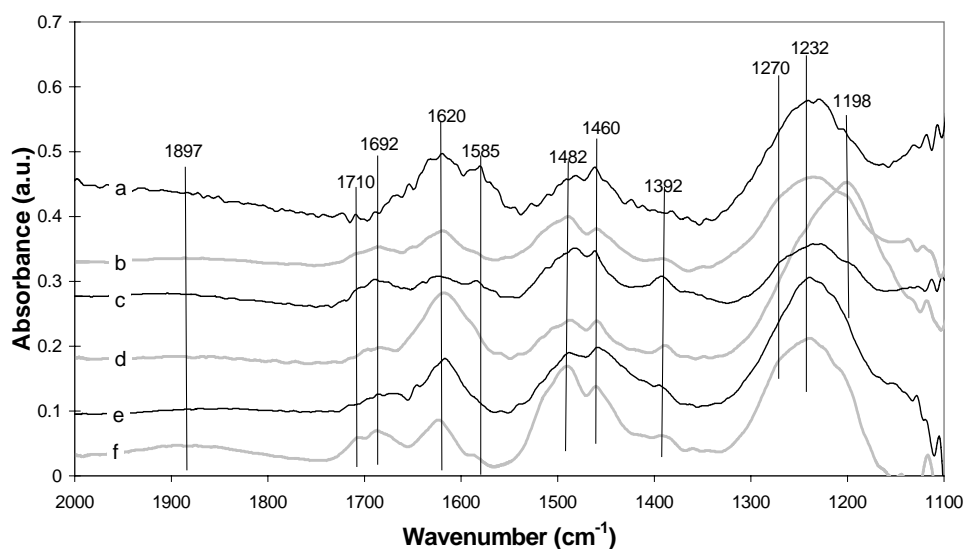


**Fig. 7.12:** FTIR spectra of NH<sub>3</sub> adsorption (40<sup>o</sup>C) on: Au/CuO/Al<sub>2</sub>O<sub>3</sub> (a), Au/CeO<sub>x</sub>/Al<sub>2</sub>O<sub>3</sub> (b), Au/Li<sub>2</sub>O/Al<sub>2</sub>O<sub>3</sub> (c), Au/FeO<sub>x</sub>/Al<sub>2</sub>O<sub>3</sub> (d), Au/TiO<sub>x</sub>/Al<sub>2</sub>O<sub>3</sub> (e) and Au/Al<sub>2</sub>O<sub>3</sub> (f).

Gold-based catalysts exhibit absorption bands at 1232, 1392, 1460, 1482, 1585, 1620, 1692 and 1897  $\text{cm}^{-1}$ . The bands at 1393, 1482 and 1692  $\text{cm}^{-1}$  are close to the bands attributed to the deformation modes of  $\text{NH}_4^+$  on  $\gamma\text{-Al}_2\text{O}_3$  at 1393, 1478, and 1686  $\text{cm}^{-1}$  [21] and are consistent with earlier reports [13, 22]. The bands at 1232 and 1620  $\text{cm}^{-1}$  in Fig. 7.12 could be assigned to  $\text{NH}_3$  adspecies on  $\gamma\text{-Al}_2\text{O}_3$  [13, 21, 22]. On the other hand, the 1232  $\text{cm}^{-1}$  band and its shoulders could have another origin. It was reported that amide-like ( $-\text{NH}_2$ ) adspecies (or hydrazine) might be present following  $\text{NH}_3$  adsorption on different (mixed) oxides [13-20, 22-24].

Peri [22] assigned a 1510  $\text{cm}^{-1}$  band to the  $-\text{NH}_2$  bending mode on  $\text{Al}_2\text{O}_3$ . Bands at 1187, 1210, 1560 and 1610  $\text{cm}^{-1}$  were assigned to the  $\text{NH}_2$  rocking,  $\nu_{\text{N-N}}$ ,  $\delta_{\text{asy,NH}_2}$  and  $\delta_{\text{sym,NH}_2}$  modes of hydrazine on  $\text{Cu/TiO}_2$  [18]. The presence of hydrazine may explain the 1192, 1232, and 1585  $\text{cm}^{-1}$  bands in Fig. 7.12. The presumed 1610  $\text{cm}^{-1}$  peak of surface hydrazine may overlap with the symmetric deformation mode of coordinated- $\text{NH}_3$  at around 1620  $\text{cm}^{-1}$ .

Following the band assignments of  $\text{NH}_4^+$ , coordinated- $\text{NH}_3$ , and amide (or hydrazine) adspecies on  $\text{Au/MO}_x/\text{Al}_2\text{O}_3$ , this still leaves the 1460 and the broad 1897  $\text{cm}^{-1}$  bands in Figure 7.12 unassigned. Kagami *et al.* attributed a 1410  $\text{cm}^{-1}$  band to the imido ( $-\text{NH}$ ) species following  $\text{NH}_3$  adsorption on  $\text{MgO}$  [23]. Bi-dentate  $\text{NH}$  surface species at 1480  $\text{cm}^{-1}$  were reported on  $\text{CuO/TiO}_2$  [20] and at 1440-1450  $\text{cm}^{-1}$  on  $\text{MO}_x/\text{TiO}_2$  [19]. This is close to the 1460  $\text{cm}^{-1}$  band in Fig. 7.12 and, therefore, this band is tentatively assigned to an imide-like adspecies. By comparing Fig. 7.11 and 7.12, it is noteworthy that the presence of Au increases the relative intensity of the 1460 and 1585  $\text{cm}^{-1}$  bands, (with respect to, e.g., the 1620  $\text{cm}^{-1}$  band intensity) on some  $\text{Au/MO}_x/\text{Al}_2\text{O}_3$ . The presence of Au enhances the relative intensity of these two bands on  $\text{CuO/Al}_2\text{O}_3$ ,  $\text{CeO}_x/\text{Al}_2\text{O}_3$  and  $\text{Li}_2\text{O/Al}_2\text{O}_3$ . On the other hand, those bands on  $\text{FeO}_x/\text{Al}_2\text{O}_3$  were only slightly promoted by Au and for  $\text{TiO}_x/\text{Al}_2\text{O}_3$  no enhancement was found. Since Au significantly promotes the activity of  $\text{MO}_x/\text{Al}_2\text{O}_3$ , it is suggested that Au enhances the SCO activity via increasing the surface concentration of the amide- and imide-like intermediates. The  $\text{Au/TiO}_x/\text{Al}_2\text{O}_3$  showed almost no increase in this band intensity compared to  $\text{TiO}_x/\text{Al}_2\text{O}_3$ . This seems to be consistent with its low activity found in this study. On the other hand,  $\text{CuO/Al}_2\text{O}_3$  is the only  $\text{MO}_x/\text{Al}_2\text{O}_3$  catalyst that showed significant SCO activity in this study, but imide-like adspecies are not present on this catalyst, as indicated by Fig. 7.11. The SCO over  $\text{CuO/Al}_2\text{O}_3$  may occur via a different mechanism. The higher SCO activity of  $\text{Au/CuO/Al}_2\text{O}_3$  compared to  $\text{CuO/Al}_2\text{O}_3$  may indicate a synergistic effect of a gold-promoted  $\text{NH}_x$  intermediate and the reactivity of the  $\text{CuO}$ -phase.

The FTIR spectra of a stepwise TPD (sTPD) experiment of  $\text{NH}_3$  adsorbed on  $\text{Au/Li}_2\text{O/Al}_2\text{O}_3$  are shown in Fig. 7.13. Similar experiments have been done for the other catalysts. However, only the results obtained for  $\text{Au/Li}_2\text{O/Al}_2\text{O}_3$  are shown because these spectra contain almost all the absorption features observed in the study described in this chapter.

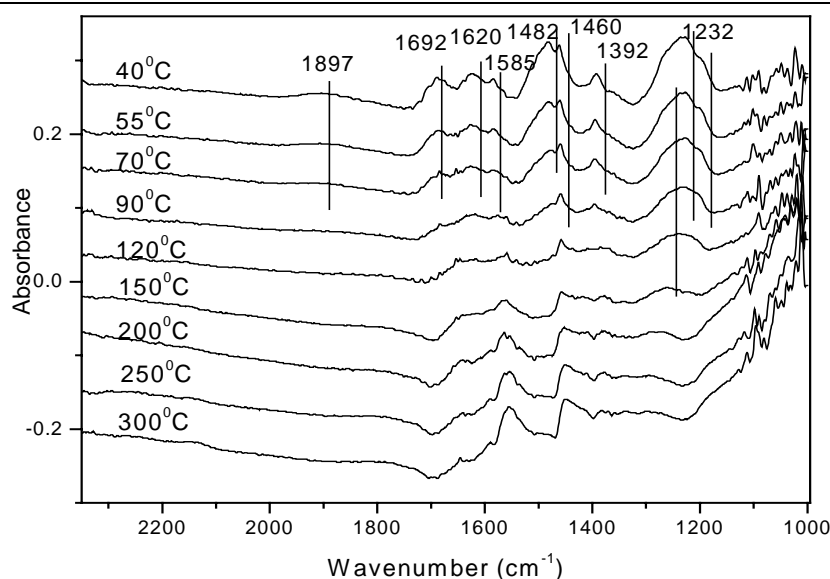


**Figure 7.13:** FTIR spectra during a stepwise TPD of  $\text{NH}_3$  on  $\text{Au}/\text{Li}_2\text{O}/\text{Al}_2\text{O}_3$ .

Upon heating first the  $\text{NH}_4^+$  adspecies disappear, then, subsequently, the bands ascribed to surface  $-\text{NH}_2$ , the coordinated  $\text{NH}_3$  on Lewis acid sites, and, finally, the  $1460\text{ cm}^{-1}$  (imido) band. This desorption sequence seems to coincide with the expected adsorption strength of these adspecies. It is also interesting to note that the band at  $1460\text{ cm}^{-1}$  and a new band at around  $1560\text{ cm}^{-1}$  constitute the main IR absorption features above  $200^\circ\text{C}$ . The peak around  $1560\text{ cm}^{-1}$  is near the reported NO stretching band of nitroxyl species [16, 17, 19-21]. This implies that  $-\text{NH}$  adspecies may be converted to nitroxyl species at higher temperature. This suggests that an in-situ SCR mechanism proposed earlier by Amblard *et al.* [25] may be involved for the gold-based catalysts. According to this mechanism, surface  $\text{NO}_x$  may be formed and react with surface  $\text{NH}_x$ . Readsorption of  $\text{NH}_3$  at  $40^\circ\text{C}$  after this sTPD results in the same absorption bands as shown in Fig. 7.13, although the band intensities are a little bit smaller. This suggests that a sTPD experiment does not significantly alter the catalyst. A subsequent sTPO (sTPD under  $2 \cdot 10^3\text{ Pa O}_2$ , Fig. 7.14) does not generate any new absorption bands on  $\text{Au}/\text{Li}_2\text{O}/\text{Al}_2\text{O}_3$  up to  $150^\circ\text{C}$ .

However, the  $\text{NH}_3$  adspecies seem to be more stable in the presence of  $2 \cdot 10^3\text{ Pa O}_2$ , as indicated by the prevalence of absorption bands to higher temperatures compared to the sTPD in Fig. 7.13. In addition, the  $1460\text{ cm}^{-1}$  band in sTPO became more intense than that in sTPD. It should be mentioned that bands at  $2192$  and  $2232\text{ cm}^{-1}$  were observed in the sTPO of  $\text{CuO}/\text{Al}_2\text{O}_3$ ,  $\text{Au}/\text{Al}_2\text{O}_3$ ,  $\text{Au}/\text{TiO}_x/\text{Al}_2\text{O}_3$ ,  $\text{Au}/\text{FeO}_x/\text{Al}_2\text{O}_3$ , and  $\text{Au}/\text{CuO}/\text{Al}_2\text{O}_3$  starting from  $120^\circ\text{C}$  or  $150^\circ\text{C}$  in sTPO experiments. These two bands have been attributed to the N-N stretching mode of  $\text{N}_2^-$  adspecies [15-20]. However, the presence of this band did not warrant either a high SCO activity or a high selectivity to  $\text{N}_2$  when compared to the reaction results presented here.

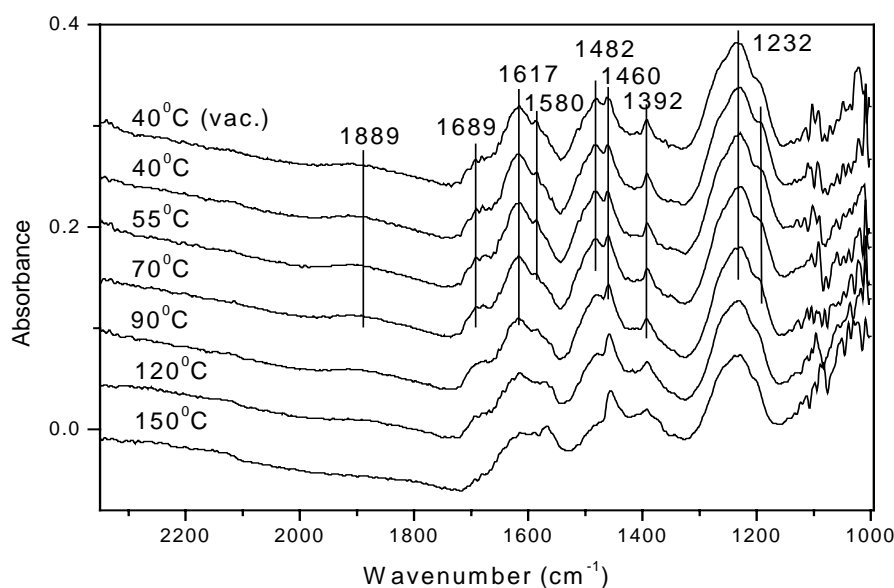


**Figure 7.14:** FTIR spectra during a stepwise TPO on Au/Li<sub>2</sub>O/Al<sub>2</sub>O<sub>3</sub>.

## 7.6 Discussion

The oxidation of ammonia can proceed via 3 overall reactions:



Reaction (7a) is the so-called Ostwald process used to produce nitric acid. Reaction (7b) is potentially an ideal technology to remove ammonia from waste gases. Reaction (7c) may find applications for the production of N<sub>2</sub>O, as an oxidizing agent for, for example, selective oxidation of hydrocarbons [9, 10].

Unsupported [26] and supported oxide catalysts [8, 27-30] were found to give quite a good N<sub>2</sub> selectivity but their activities are not sufficient at temperatures below 300°C. Noble metal catalysts were reported to be more active in this temperature range, but less selective to N<sub>2</sub> than oxide catalysts [31, 32]. Amblard *et al.* reported that Ni/Al<sub>2</sub>O<sub>3</sub> could be a good SCO catalyst [25, 33]. Long and Yang recently reported a better SCO performance for Fe-ZSM5 compared to other metal-exchanged ZSM-5 catalysts [34]. Cu-Y was reported to act as more active catalyst compared to other metal-exchanged NaY or Al<sub>2</sub>O<sub>3</sub>-supported metal oxides [29].

Gold-based catalysts are known for their unusually high oxidation activity at low temperatures, especially toward CO [12, 35]. However, ammonia oxidation over gold-based catalysts has not been reported in the literature, although the catalytic performance of the rest of the Group IB metals has been extensively studied.

The results reported in the literature regarding the variation of NH<sub>3</sub> conversion with increasing NH<sub>3</sub> concentration [1] indicate that the NH<sub>3</sub> partial pressure may only have a slight

effect on the conversion. This suggests a low, maybe close to zero reaction order of  $\text{NH}_3$  for this reaction. The presence of  $\text{O}_2$  does not affect the IR absorption bands of  $\text{NH}_3$ , also pointing to a low  $\text{NH}_3$  dependency. This implies that  $\text{NH}_3$  is more abundant than oxygen on the surface. As a consequence, it is very likely that the reaction rate will be more dependent on the oxygen concentration. This is supported by the results obtained under a large excess of oxygen (section 7.4).

Fig. 7.2 indicates a strong effect of the pretreatment on the performance of  $\text{CuO}/\text{Al}_2\text{O}_3$ . It implies that oxidic Cu is more active for SCO than reduced Cu. It was reported that on  $\text{Cu}(110)$  the surface oxygen favours abstraction of hydrogen from  $\text{NH}_3$  [36]. This kind of mechanism has been discussed earlier: surface oxygen abstracts hydrogen from  $\text{NH}_3$  to form surface hydroxyl and amide. Imide and adsorbed N are formed in subsequent abstraction steps. However, the reaction mechanism may be quite different for a reduced metallic surface than for an oxidic surface [7, 36, 37]. Based on the results presented in Fig. 7.2, it appears that the reaction conditions used here keep the surface more reduced, because the activity in the second heating cycle of the calcined  $\text{CuO}/\text{Al}_2\text{O}_3$  was almost the same as that of the reduced one.

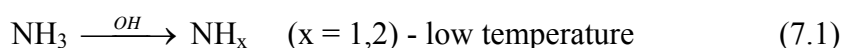
Another factor that may affect the SCO activity is the surface acidity. It is expected that an acidic surface should enhance  $\text{NH}_3$  adsorption. However, such an enhanced adsorption could have a negative effect on SCO because surface  $\text{NH}_3$  may be the more abundant species as discussed earlier. This is supported by the observation that a post treatment with  $\text{NaOH}$  increases the SCO activity of several catalysts [29, 38]. On the other hand, Long and Yang attributed the observed performance for SCO of  $\text{Fe-TiO}_2$  prepared from sulphate precursor to the effect of surface sulphate [30]. However, this sulphate-containing  $\text{Fe-TiO}_2$  actually showed a lower  $\text{NH}_3$  conversion but a somewhat higher  $\text{N}_2$  selectivity, similar to the effect of the inclusion of  $\text{SO}_2$  in the feed [8, 32]. Therefore, a less acidic surface may favour a high activity in SCO.

From the trend of concurrent band disappearance during sTPD and sTPO, the shoulder around  $1190\text{ cm}^{-1}$  can be attributed to the rocking mode of  $-\text{NH}_2$  associated with surface amide or hydrazine. Adsorbed amide and hydrazine species can only be distinguished by the  $\nu_{\text{N-N}}$  mode of hydrazine. However, on  $\text{TiO}_2$  and  $\text{TiO}_2$ -supported  $\text{CrO}_x$ ,  $\text{CoO}_x$ ,  $\text{Fe}_2\text{O}_3$ , and  $\text{CuO}$  [15, 16, 19, 20], this mode was assigned to a band at  $1210\text{-}1225\text{ cm}^{-1}$ , which is close to the region of the symmetric deformation mode of  $\text{NH}_3$  coordinated on Lewis acid sites. Amblard *et al.* [25] also questioned the possibility of surface hydrazine based on the tendency of hydrazine decomposition into  $\text{NH}_3$ . Actually, it has been reported that both  $\text{NH}_3$  and  $\text{N}_2\text{H}_4$  adsorption result in very similar IR spectra on calcined  $\text{Ni}/\text{Al}_2\text{O}_3$  [25] and  $\text{TiO}_2$ -supported oxides [15, 16, 19]. This makes a definite assignment of surface hydrazine almost impossible. Nevertheless, IR studies can clearly identify the presence of  $-\text{NH}_2$  surface species by its less controversial rocking and asymmetric deformation modes around  $1160\text{-}1190$  and  $1550\text{-}1580\text{ cm}^{-1}$ , respectively.

The presence of surface  $-\text{NH}_2$  indicates the dissociative adsorption of  $\text{NH}_3$  and/or the presence of H-abstraction on the surface. Its subsequent dissociation to imide adspecies can be identified by the IR band of  $\delta(\text{NH})$  at  $1410\text{-}1460\text{ cm}^{-1}$ . Such a sequential  $\text{NH}_3$  dissociation

(hydrogen abstraction) is considered to be the mechanistic route to N<sub>2</sub>, NO and N<sub>2</sub>O formation in SCO reaction [13, 15, 23, 25]. The presence of Au seems to enhance H-abstraction from NH<sub>3</sub>.

Although the FTIR analysis could not identify the mechanistic route to N<sub>2</sub>, and NO<sub>x</sub> selectivity, it is clear that the SCO selectivity of the gold-based catalysts strongly depends on the type of MO<sub>x</sub> additive and is determined by a certain metal-support interaction. In addition, the product distribution depends on the ratio N/O on the surface and, as was already shown, the formation of N<sub>2</sub>O/NO is strongly related to the O<sub>2</sub> concentration. It is possible that at low temperature the reaction mechanism includes hydrogen abstraction from NH<sub>3,ads</sub> via mainly OH groups (reactions 7.1-7.2). The main product would be N<sub>2</sub>. This is supported by the FTIR findings (amide and imide species). At higher temperature the oxygen is readily activated and thus the reaction may proceed via a HNO (nitroxyl) intermediate (reactions 7.3-7.7), according to the following scheme:



A more detailed study is necessary in order to prove all the steps of the above-mentioned mechanism and a study of the reaction between NH<sub>3</sub> and NO could be a very useful step.

## 7.7 Conclusions

The addition of MO<sub>x</sub> to Au/Al<sub>2</sub>O<sub>3</sub> improves the catalytic activity in low-temperature oxidation of NH<sub>3</sub> for different reactant ratios. The catalytic activity of various gold-based catalysts does not depend strongly on the average gold particle size, but is strongly influenced by the nature of the additive. Also the selectivity towards different products (N<sub>2</sub>, N<sub>2</sub>O and NO) is greatly influenced by the additive. Besides a structural role of the additives towards stabilization of gold particles, some of them are active participants in the reaction process (CuO and FeO<sub>x</sub>).

FTIR analysis of adsorbed species carried out on some selected Au/MO<sub>x</sub>/Al<sub>2</sub>O<sub>3</sub> catalysts and their supports reveal the presence of NH<sub>4</sub><sup>+</sup> on Brønsted acid sites, NH<sub>3</sub> on Lewis acid sites, amide (or hydrazine), and imide. The assignment to hydrazine is hard to prove because some of its absorption bands fall in the range of NH<sub>3</sub> absorption. It was found that the addition of Au significantly enhances the intensity of an absorption band at 1460 cm<sup>-1</sup>, which is tentatively assigned to surface imido-species. Therefore, the enhanced catalytic activity by addition of Au is attributed to the increased surface concentration of this imido-species. It is suggested that possible reaction steps include a direct participation of OH groups at low

temperatures, whereas in the higher temperature range the formation of HNO as an intermediate may be relevant. Finally, N<sub>2</sub>O and/or NO are formed at higher temperatures.

## 7.8 References

- [1] S. D. Lin, A. C. Gluhoi, B. E. Nieuwenhuys, *Catal. Today* 90 (2004) 3.
- [2] A. C. Gluhoi, S. D. Lin, B. E. Nieuwenhuys, *Catal. Today* 90 (2004) 175.
- [3] A. C. Gluhoi, M. A. P. Dekkers, B. E. Nieuwenhuys, *J. Catal.* 219 (2003) 197.
- [4] A. C. Gluhoi, N. Bogdanchikova, B. E. Nieuwenhuys, *J. Catal.* 232 (2005) 96.
- [5] L. Gang, B. G. Anderson, J. van Grondelle, R. A. van Santen, W. J. H. van Gennip, J. W. Niemantsverdriet, P. J. Kooyman, A. Knoester, H. H. Brongersma, *J. Catal.* 206 (2002) 60.
- [6] J. A. Rodriguez, *Catal. Today* 85 (2003) 177.
- [7] R. W. Mayer, M. Havecker, A. Knop-Gericke, R. Schlögl, *Catal. Lett.* 74 (2001) 115.
- [8] T. Curtin, F. O' Regan, C. Deconinck, N. Knuttel, B. K. Hodnett, *Catal. Today* 55 (2000) 189.
- [9] A. A. Ivanov, V. S. Chernyavsky, M. J. Gross, A. S. Kharitonov, A. K. Uriarte, G. I. Panov, *Appl. Catal. A* 249 (2003) 327.
- [10] H. Orita, H. Kondoh, H. Nozoye, *J. Catal.* 177 (1998) 217.
- [11] G. Olofsson, L. R. Wallenberg, A. Andersson, *J. Catal.* 230 (2005) 1.
- [12] G. C. Bond, D. T. Thompson, *Catal. Rev. Sci. Eng.* 41 (1999) 319.
- [13] A. A. Davydov, *Infrared spectroscopy of adsorbed species on the surface of transition metal oxides*, Wiley 1990.
- [14] G. Busca, *J. Mol. Catal.* 43 (1987) 225.
- [15] G. Ramis, L. Yi, G. Busca, M. Turco, E. Kotur, R. J. Willey, *J. Catal.* 157 (1995) 523.
- [16] M. A. Larrubia, G. Ramis, G. Busca, *Appl. Catal. B* 30 (2001) 101.
- [17] G. Ramis, M. A. Larrubia, G. Busca, *Top. Catal.* 11/12 (2000) 161.
- [18] G. Ramis, L. Yi, G. Busca, *Catal. Today* 28 (1996) 373.
- [19] J. M. G. Amores, V. S. Escibano, G. Ramis, G. Busca, *Appl. Catal. B* 13 (1997) 45.
- [20] G. Bagnasco, G. Peluso, G. Russo, M. Turco, G. Busca, G. Ramis, *3rd World Congress on Oxidation Catalysis*, *Stud. Surf. Sci. Catal.* 110, pp. 643 (1997).
- [21] H. Zou, J. Shen, *Therm. Acta* 351 (2000) 165.
- [22] J. B. Peri, *J. Phys. Chem.* 69 (1965) 231.
- [23] S. Kagami, T. Onishi, K. Tamatu, *J. Chem. Soc. Farad. Trans. I* 80 (1984) 29.
- [24] A. A. Tsyganenko, D. V. Pozdnyakov, V. N. Filimonov, *J. Mol. Struct.* 29 (1975) 299.
- [25] M. Amblard, R. Burch, B. W. L. Southward, *Catal. Today* 59 (2000) 365.
- [26] N. I. Il'chenko, G. I. Golodet, *J. Catal.* 39 (1975) 57.
- [27] F. Cavani, F. Trifiro, *Catal. Today* 4 (1989) 253.
- [28] A. Wollner, F. Lange, *Appl. Catal. A* 94 (1993) 181.
- [29] L. Gang, B. G. Anderson, J. van Grondelle, R. A. van Santen, *Catal. Today* 61 (2000) 179.
- [30] R. Q. Long, R. T. Yang, *J. Catal.* 207 (2002) 158.
- [31] Y. Li, J. N. Armor, *Appl. Catal. B* 13 (1997) 131.
- [32] R. Q. Long, R. T. Yang, *Catal. Lett.* 78 (2002) 353.
- [33] M. Amblard, R. Burch, B. W. L. Southward, *Appl. Catal. B* 22 (1999) L159.
- [34] R. Q. Long, R. T. Yang, *Chem. Commun.* 1651 (2000).
- [35] M. Haruta, N. Yamada, T. Kobayashi, S. Iijima, *J. Catal.* 115 (1989) 301.
- [36] C.-M. Pradier, A. Adamski, C. Methivier, I. Louise-Rose, *J. Mol. Catal. A* 186 (2002) 193.
- [37] X.-C. Guo, R. J. Madix, *Surf. Sci.* 367 (1996) L95.
- [38] L. Gang, J. van Grondelle, B. G. Anderson, R. A. van Santen, *J. Catal.* 186 (1999) 100.





# Chapter 8

## Reduction reactions involving nitrogen oxides (NO and N<sub>2</sub>O) over gold-based catalysts

*The reduction of nitrogen oxides by hydrogen was studied over various gold-based catalysts, including Au/Al<sub>2</sub>O<sub>3</sub>, Au/MO<sub>x</sub>/Al<sub>2</sub>O<sub>3</sub> and Au/M<sup>I</sup>O<sub>x</sub>/M<sup>II</sup>O<sub>x</sub>/Al<sub>2</sub>O<sub>3</sub> (M, M<sup>I</sup>, M<sup>II</sup>: Li, Rb, Mg, Ba, Co, Fe, Zr, and Ce). It is found that supported gold catalysts convert nitric oxide in the presence of hydrogen (NO/H<sub>2</sub>=1 or 0.4) to the following products: N<sub>2</sub>O (at low temperature), N<sub>2</sub> (at intermediate temperature) and NH<sub>3</sub> (at high temperature). The catalytic performance and the product distribution strongly depend on the reaction temperature, the nature of the additive and the reactant ratio. It is suggested that hydrogen assists in NO decomposition. Based on the product distribution and other reported results, it is suggested that at low temperature NO partly decomposes to N<sub>2</sub>O and O<sub>ads</sub>. At higher temperatures, the amount of NO dissociatively adsorbed on the surface will increase and as a result, more N<sub>2</sub> will be produced via N combination. The atomic nitrogen might be hydrogenated in the presence of hydrogen to NH<sub>x</sub> species and NH<sub>3</sub> is formed. The selectivity will then depend on the relative concentrations of adsorbed species on the surface, i.e. NO, N and NH<sub>x</sub>. The oxidic additives might create new sites for dissociative adsorption of NO.*

*Regarding the reduction of N<sub>2</sub>O, the only N-containing product is N<sub>2</sub>. All the MO<sub>x</sub> (M: Li, Rb, Mg, Ba, Ti, Co, Ce, and Mn) additives were found to enhance the catalytic activity of Au/Al<sub>2</sub>O<sub>3</sub>.*

## 8.1 Outline

This chapter describes the catalytic activity of Au/Al<sub>2</sub>O<sub>3</sub>, Au/MO<sub>x</sub>/Al<sub>2</sub>O<sub>3</sub> and Au/M<sup>I</sup>O<sub>x</sub>/M<sup>II</sup>O<sub>x</sub>/Al<sub>2</sub>O<sub>3</sub> (M, M<sup>I</sup> and M<sup>II</sup>: Li, Rb, Mg, Ba, Fe, Co, Zr and Ce) in NO and N<sub>2</sub>O reduction by hydrogen. Section 8.2 discusses some experimental details concerning the preparation of the samples and the experimental set-up. Section 8.3 illustrates the catalytic performance (activity and selectivity) of the as-prepared supported gold catalysts in NO reduction by hydrogen (NO/H<sub>2</sub> = 1 and 0.4). Section 8.4 presents the catalytic activity results of various gold-based catalysts in N<sub>2</sub>O reduction by hydrogen (N<sub>2</sub>O/H<sub>2</sub> = 0.5), and section 8.5 presents a general discussion. The most important conclusions are summarized in section 8.6.

## 8.2 Experimental

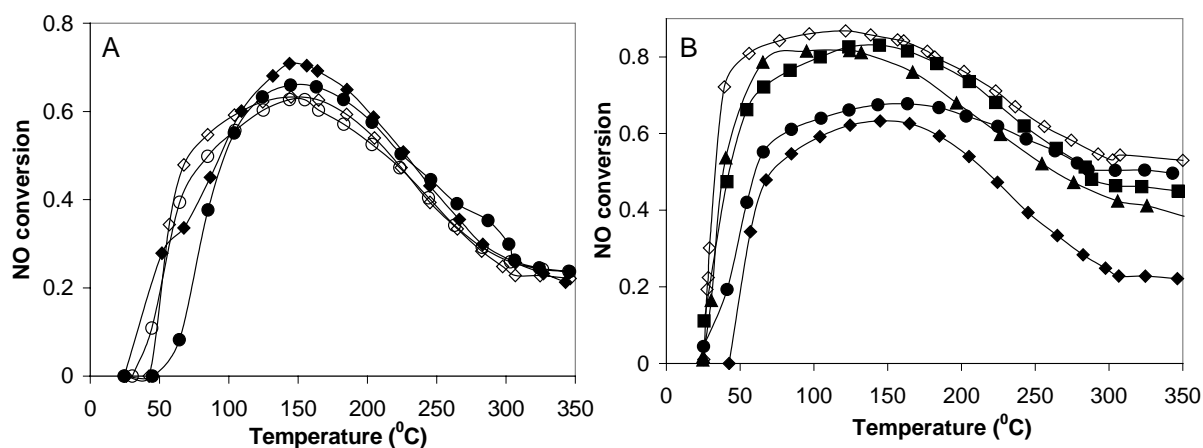
The same preparation method as described before (*Chapter 3* and thereafter) was used to prepare the unpromoted and promoted gold-based catalysts (HDP with urea). The experimental set-up used for catalytic activity measurements is described in *Chapter 3*. Since previously reported results [1] suggest that a reductive pretreatment is more efficient than an oxidative one, all the catalysts tested were solely subjected to a H<sub>2</sub> pretreatment (300<sup>0</sup>C). The gases employed were 4 vol %/He, with a total flow of 30 ml min<sup>-1</sup>. To reduce NO, two different reactant ratios have been used: NO/H<sub>2</sub> = 1 (the stoichiometry needed to produce N<sub>2</sub>) and NO/H<sub>2</sub> = 0.4, i.e. excess of hydrogen (the stoichiometry of NH<sub>3</sub> production). Regarding N<sub>2</sub>O reduction by hydrogen, the only reactant ratio used was N<sub>2</sub>O/H<sub>2</sub> = 0.5. The outlet gas stream was analysed by MS and the monitored mass signals included 2, 14, 16, 17, 18, 28, 30, 32, 44, and 46. Where required, the MS signal was corrected for the fragmentation peaks of other molecules. The comparison of various gold-based catalysts is made on the basis of the conversion achieved during the first cooling sequence. However, there is no significant difference between this branch and other heating/cooling cycles. The supports (either Al<sub>2</sub>O<sub>3</sub>, or MO<sub>x</sub>/Al<sub>2</sub>O<sub>3</sub>) have also been tested and found negligibly active under these reaction conditions. Following the catalytic test, the samples were analysed again by XRD.

## 8.3 Catalytic performance in NO reduction by H<sub>2</sub>

### Reactant ratio NO/H<sub>2</sub> = 1 – Catalytic activity

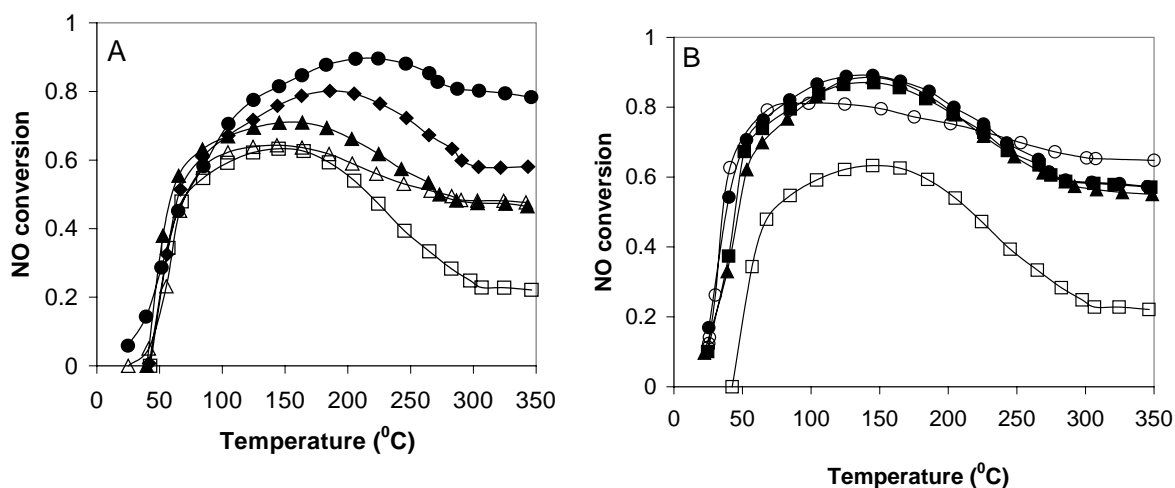
The catalytic conversion of Au/Al<sub>2</sub>O<sub>3</sub> versus temperature during two heating-cooling cycles is depicted in Fig. 8.1A. The NO conversion is initiated by increasing the reaction temperature. A maximum of 70% NO conversion is reached around 150<sup>0</sup>C. If the temperature is further increased, the NO conversion drops to a level of 22%, attained at 350<sup>0</sup>C. On the other hand, the catalyst deactivation is not strong after the first catalytic run, because the difference between different catalytic runs is rather small.

Fig. 8.1B presents a comparison of the catalytic performance versus temperature of various alkali (earth) metal oxides-promoted Au/Al<sub>2</sub>O<sub>3</sub>. Figs. 8.2A-B show the catalytic conversion versus temperature of various gold-based catalysts combined with TMO or ceria (Fig. 8.2A), or with two different metal oxides (Fig. 8.2B).



**Figure 8.1:** NO conversion vs. temperature over Au/Al<sub>2</sub>O<sub>3</sub> (A) and alkali (earth) metal oxides-promoted Au/Al<sub>2</sub>O<sub>3</sub> (B). The symbols in (A) correspond to: heating #1 (◆), cooling #1 (◇), heating #2 (●), cooling #2 (○); the symbols in (B) correspond to: Au/Al<sub>2</sub>O<sub>3</sub> (◆), Au/MgO/Al<sub>2</sub>O<sub>3</sub> (●), Au/Li<sub>2</sub>O/Al<sub>2</sub>O<sub>3</sub> (■), Au/Rb<sub>2</sub>O/Al<sub>2</sub>O<sub>3</sub> (▲), Au/BaO/Al<sub>2</sub>O<sub>3</sub> (◇). NO/H<sub>2</sub> = 1.

A summary of the maximum NO conversion,  $X^M$ , with the corresponding temperature, the maximum  $S_{N_2}$  with the corresponding temperature, the specific reaction rate,  $r$ , at 105°C (moles of NO converted per moles of Au and second), the mean diameter of gold particles before the reaction (fresh catalyst) and after reaction (used) is presented in Table 8.1.



**Figure 8.2:** NO conversion vs. temperature over: unpromoted (□) and CeO<sub>x</sub> (△), ZrO<sub>x</sub> (▲), CoO<sub>x</sub> (◆), FeO<sub>x</sub> (●) promoted Au/Al<sub>2</sub>O<sub>3</sub> (A); unpromoted (□), Rb<sub>2</sub>O/CeO<sub>x</sub> (▲), CeO<sub>x</sub>/ZrO<sub>x</sub> (■), Li<sub>2</sub>O/CeO<sub>x</sub> (●), BaO/CeO<sub>x</sub> (○) promoted Au/Al<sub>2</sub>O<sub>3</sub> (B). NO/H<sub>2</sub> = 1.

Clearly, all the additives positively influence the catalytic activity of Au/Al<sub>2</sub>O<sub>3</sub>. Previous studies, although scarce, were devoted to gold deposited on Al<sub>2</sub>O<sub>3</sub>, MgO, TiO<sub>2</sub> or SiO<sub>2</sub> [1-4], NaY [5] and Au/MO<sub>x</sub>/Al<sub>2</sub>O<sub>3</sub> (M = Co, Ce, La) [1]. The best promoting effect is obtained with BaO, which is able to sustain a high conversion (86%) over a relatively large temperature

region (between 90-145<sup>0</sup>C). Important promoting effects are also observed for the samples containing Rb<sub>2</sub>O and Li<sub>2</sub>O. The maximum NO conversion over Au/Rb<sub>2</sub>O/Al<sub>2</sub>O<sub>3</sub> (81%) appears slightly shifted to lower temperatures (73-110<sup>0</sup>C), as compared with the Li<sub>2</sub>O-containing catalyst (83%, 123-145<sup>0</sup>C). The least promoting effect is found with MgO, with a maximum NO conversion of 68% reached at 143<sup>0</sup>C. All the gold-based catalysts displayed a decrease of NO conversion by increasing temperature. The smallest drop in NO conversion was recorded for Au/BaO/Al<sub>2</sub>O<sub>3</sub> (53%), and the largest one was recorded for Au/Rb<sub>2</sub>O/Al<sub>2</sub>O<sub>3</sub> (41%). The good performance of the BaO-containing catalyst may be related to the well-known interaction between BaO and NO<sub>x</sub> [6-11].

The stability of the gold particles during the catalytic test is proven by the very small increase of  $d_{Au}^a$ . A similar trend in the variation of the catalytic activity is observed if the values of  $r$  are considered. For example, the presence of BaO causes an increase of the specific reaction rate by a factor of 2, compared with unpromoted Au/Al<sub>2</sub>O<sub>3</sub>.

**Table 8.1:** The maximum NO conversion ( $X^M$ ) with the corresponding temperature, the maximum selectivity to N<sub>2</sub> ( $S_{N_2}$ ) with the corresponding temperature, the specific reaction rate,  $r$ , the average gold particle size for fresh ( $d_{Au}^a$ ) and used ( $d_{Au}^b$ ) gold-based catalysts (XRD). NO/H<sub>2</sub> = 1.

Catalyst	$X^M/T$ ( <sup>0</sup> C)	$S_{N_2}/T$ ( <sup>0</sup> C)	$r \times 10^3$ (moles NO moles Au <sup>-1</sup> s <sup>-1</sup> )	$d_{Au}^a$ (nm)	$d_{Au}^b$ (nm)
Au/Al <sub>2</sub> O <sub>3</sub>	63/144	74/184	6.4±0.1	4.3±0.1	4.5±0.3
Au/Li <sub>2</sub> O/Al <sub>2</sub> O <sub>3</sub>	83/124	74/184	8.8±0.1	3.2±0.1	3.7±0.2
Au/Rb <sub>2</sub> O/Al <sub>2</sub> O <sub>3</sub>	81/72	75/183	10.3±0.2	<3.0	3.4±0.1
Au/MgO/Al <sub>2</sub> O <sub>3</sub>	68/145	78/184	6.7±0.1	4.0±0.1	4.5±0.2
Au/BaO/Al <sub>2</sub> O <sub>3</sub>	86/94	84/156	10.6±0.2	< 3.0	3.1±0.2
Au/CoO <sub>x</sub> /Al <sub>2</sub> O <sub>3</sub>	80/186	77/225	6.9±0.1	5.0±0.1	5.2±0.3
Au/FeO <sub>x</sub> /Al <sub>2</sub> O <sub>3</sub>	90/205	78/271	8.2±0.2	<3.0	3.5±0.1
Au/ZrO <sub>x</sub> /Al <sub>2</sub> O <sub>3</sub>	72/146	72/185	9.3±0.1	3.1±0.3	3.7±0.2
Au/CeO <sub>x</sub> /Al <sub>2</sub> O <sub>3</sub>	64/124	74/184	6.1±0.1	<3.0	3.4±0.2
Au/CeO <sub>x</sub> /ZrO <sub>x</sub> /Al <sub>2</sub> O <sub>3</sub>	87/146	76/146	11.6±0.2	<3.0	3.1±0.1
Au/Li <sub>2</sub> O/CeO <sub>x</sub> /Al <sub>2</sub> O <sub>3</sub>	89/125	78/145	8.3±0.1	<3.0	3.2±0.3
Au/Rb <sub>2</sub> O/CeO <sub>x</sub> /Al <sub>2</sub> O <sub>3</sub>	89/144	75/143	8.2±0.2	<3.0	3.4±0.1
Au/BaO/CeO <sub>x</sub> /Al <sub>2</sub> O <sub>3</sub>	81/94	84/165	8.8±0.2	<3.0	3.1±0.1

As already discussed for the alkali (earth) metal oxides, the identity of the additives has a strong impact on the catalytic performance of Au/Al<sub>2</sub>O<sub>3</sub> in NO/H<sub>2</sub> reaction. Contrary to the earlier reports by Dekkers that CoO<sub>x</sub> has a slight beneficial effect on the catalytic performance of Au/Al<sub>2</sub>O<sub>3</sub>, LaO<sub>x</sub> has almost no effect and CeO<sub>x</sub> acts as a poison [1], the results presented here show that all these additives can act as promoters. The promoting effect strongly depends on the nature of the oxide, although in the low temperature regime, the effect is less pronounced. Thus, although Au/CeO<sub>x</sub>/Al<sub>2</sub>O<sub>3</sub> equals Au/Al<sub>2</sub>O<sub>3</sub> in the low temperature regime, the decrease of  $X_{NO}$  in the high temperature region is only 46% (350<sup>0</sup>C). The stabilizing effect of ceria towards Au particles (*Chapter 4*) becomes important in the high temperature range. The effect of zirconia is both on the maximum conversion (72%) as

well as on the conversion at higher temperature. The high activity of Au/CoO<sub>x</sub>/Al<sub>2</sub>O<sub>3</sub> has already been reported [1]. This catalyst shows a high conversion in a wider temperature range (80% at 185°C). The best catalytic performance is displayed by FeO<sub>x</sub>-containing Au/Al<sub>2</sub>O<sub>3</sub> catalyst, which is able to convert 90% of NO and it also has the smallest drop in NO conversion in the higher temperature range (78%). The stability of the gold particles during the catalytic tests has been confirmed for this set of catalysts. Moreover, the variation of  $r$  as a measure of the catalytic activity points out that the presence of zirconia causes a 1.5-fold increase of  $r$ , compared with unpromoted Au/Al<sub>2</sub>O<sub>3</sub>.

Regarding the promoting effect of applying two different types of metal oxides (Fig. 8.2B), all the multicomponent catalysts display higher catalytic performance, compared with the unpromoted Au/Al<sub>2</sub>O<sub>3</sub>, but no clear relationship between the catalytic performance and the identity of the oxides was found. However, Au/BaO/CeO<sub>x</sub>/Al<sub>2</sub>O<sub>3</sub> shows a different catalytic conversion shape, along with a maximum NO conversion of only 80%, but shifted to lower temperatures. In addition, this catalyst presents the least decrease in catalytic conversion in the high temperature region. The size of the gold particles is roughly preserved during the catalytic test.

### Reactant ratio NO/H<sub>2</sub> = 1 - Selectivity

In general, it was found that all the supported gold catalysts convert nitric oxide in the presence of hydrogen (NO/H<sub>2</sub> = 1) to the following products: N<sub>2</sub>O (at low temperature), N<sub>2</sub> (at intermediate temperature) and NH<sub>3</sub> (at high temperature). The product distribution for Au/Al<sub>2</sub>O<sub>3</sub> and Au/BaO/CeO<sub>x</sub>/Al<sub>2</sub>O<sub>3</sub> is shown in Figs. 8.3A-B. A summary of the maximum N<sub>2</sub> selectivity with the corresponding temperature is presented in Table 8.1.

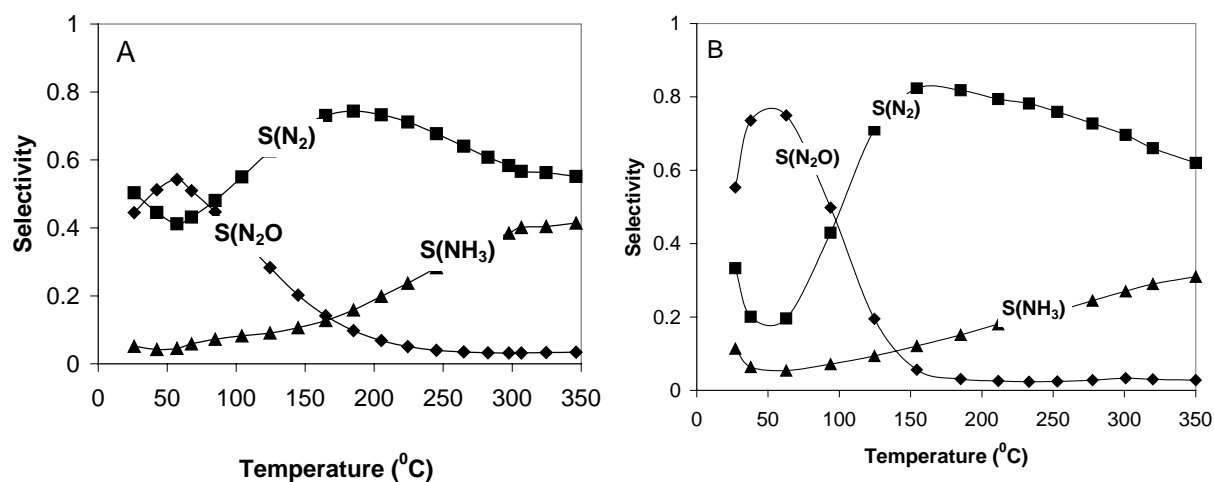


**Figure 8.3:** Product distribution vs. temperature over Au/Al<sub>2</sub>O<sub>3</sub> (A) and Au/BaO/CeO<sub>x</sub>/Al<sub>2</sub>O<sub>3</sub> (B). S<sub>N<sub>2</sub>O</sub> (◆), S<sub>N<sub>2</sub></sub> (■), S<sub>NH<sub>3</sub></sub> (▲). NO/H<sub>2</sub> = 1.

Over unpromoted Au/Al<sub>2</sub>O<sub>3</sub> the selectivity to N<sub>2</sub>O, being the main product in the low temperature range, reaches 54% at 57<sup>o</sup>C. By increasing the temperature, the selectivity to nitrous oxide drops and N<sub>2</sub> starts to be formed and at 184<sup>o</sup>C it reaches its maximum of 74%. A further increase in the reaction temperature causes a decrease of N<sub>2</sub> production and NH<sub>3</sub> formation is favoured. At the highest reaction temperature, the selectivity to NH<sub>3</sub> is 41%, whereas the S<sub>N<sub>2</sub></sub> is 55%. A similar reaction scheme is found for the all promoted gold-based catalysts, albeit the ratio between the products is directly related to the type of the additives.

The distribution of the products as presented in Figs 8.3A and 8.3B reveals that over unpromoted Au/Al<sub>2</sub>O<sub>3</sub>, a larger amount of ammonia is formed. On the other hand, the addition of BaO and CeO<sub>x</sub> appears to suppress to some extent the NH<sub>3</sub> formation. This trend is observed also for other catalysts (Table 8.1).

The alkali (earth) metal oxides appear to produce either a small increase of S<sub>N<sub>2</sub></sub>, without a visible influence on the temperature regime where this is formed (Au/MgO/Al<sub>2</sub>O<sub>3</sub>), or a strong one on both S<sub>N<sub>2</sub></sub> and temperature (Au/BaO/Al<sub>2</sub>O<sub>3</sub>). Concerning the effect of TMO/ceria, their positive effect is mainly related to the S<sub>N<sub>2</sub></sub>, with a shift towards higher temperatures. The synergy obtained by combining two different metal oxides is reflected on both the NO conversion and the selectivity towards various products.

#### Reactant ratio NO/H<sub>2</sub> = 0.4 – Catalytic activity

The catalytic conversion of NO versus temperature during two heating-cooling cycles over Au/Al<sub>2</sub>O<sub>3</sub> is depicted in Fig. 8.4A. As compared with the catalytic activity of the same catalyst under stoichiometric conditions (Fig 8.1A), if excess H<sub>2</sub> is used, the conversion of NO starts already at room temperature. Another striking difference between Figs. 8.1A and 8.4A and the next is that in excess of hydrogen, the conversion of NO continuously grows with increasing temperature, until the maximum temperature used. As observed before, the differences between consecutive heating-cooling cycles are relatively small.

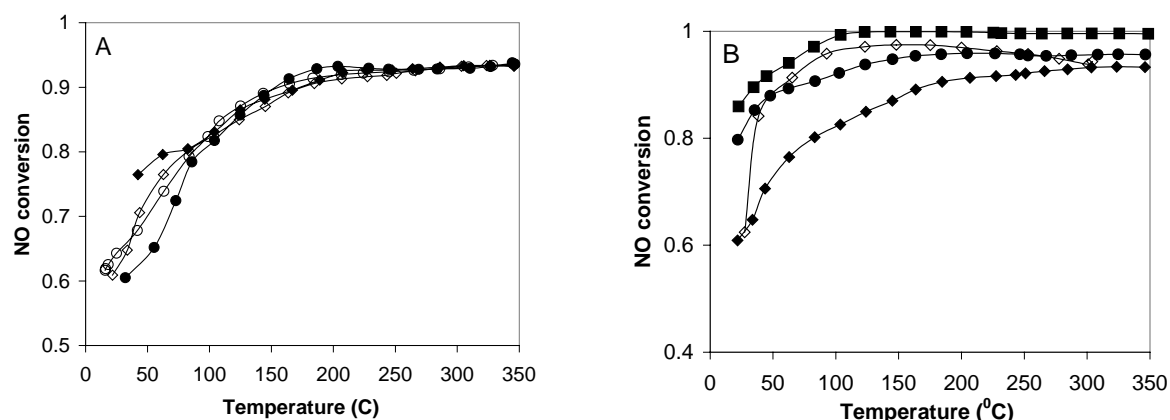


**Figure 8.4:** NO conversion vs. temperature over Au/Al<sub>2</sub>O<sub>3</sub> (A) and alkali (earth) metal oxides-promoted Au/Al<sub>2</sub>O<sub>3</sub> (B). The symbols in (A) correspond to: heating #1 (◆), cooling #1 (◇), heating #2 (●), cooling #2 (○); the symbols in (B) correspond to: Au/Al<sub>2</sub>O<sub>3</sub> (◆), Au/MgO/Al<sub>2</sub>O<sub>3</sub> (●), Au/Li<sub>2</sub>O/Al<sub>2</sub>O<sub>3</sub> (■), Au/BaO/Al<sub>2</sub>O<sub>3</sub> (◇). NO/H<sub>2</sub> = 0.4.

Fig. 8.4B shows the catalytic performance versus temperature for the reaction over various alkali (earth) metal oxides-promoted Au/Al<sub>2</sub>O<sub>3</sub>, while Figs. 8.5A-B show the catalytic conversion versus temperature of various gold-based catalysts combined with TMO or ceria (Fig. 8.5A), or with two different metal oxides (Fig. 8.5B). Table 8.2 summarizes the maximum S<sub>N<sub>2</sub></sub> with the corresponding temperature, the specific reaction rate at 105<sup>0</sup>C and the mean diameter of gold particles after reaction (used).

The positive effect of the additives on the catalytic activity of Au/Al<sub>2</sub>O<sub>3</sub> is clearly depicted in these figures. From the series of the alkali (earth) metal oxides, the most beneficial effect is found for Li<sub>2</sub>O. However, in terms of the specific reaction rate, *r*, the values obtained in excess hydrogen at the same reaction temperature are slightly lower than when the reaction was carried out under stoichiometric conditions. The difference may be due to the fact that under reactant ratio NO/H<sub>2</sub> = 1, almost full NO conversion is already attained at 105<sup>0</sup>C. In the case of excess H<sub>2</sub>, the conversion at 105<sup>0</sup>C is relatively far from the maximum possible conversion. Presumably, for a qualitative comparison of the reaction rates, the evaluation should be carried out at similar conversions.

**Table 8.2:** The maximum selectivity to N<sub>2</sub> (S<sub>N<sub>2</sub></sub>) with the corresponding temperature, the specific reaction rate, *r*, and the average gold particle size for used (d<sub>Au</sub><sup>b</sup>) gold-based catalysts (XRD). NO/H<sub>2</sub> = 0.4.

Catalyst	S <sub>N<sub>2</sub></sub> /T (°C)	r x 10 <sup>3</sup> (moles NO moles Au <sup>-1</sup> s <sup>-1</sup> )	d <sub>Au</sub> <sup>b</sup> (nm)
Au/Al <sub>2</sub> O <sub>3</sub>	54/145	5.1±0.1	4.6±0.1
Au/Li <sub>2</sub> O/Al <sub>2</sub> O <sub>3</sub>	77/104	6.2±0.1	3.6±0.3
Au/MgO/Al <sub>2</sub> O <sub>3</sub>	68/145	5.5±0.1	4.6±0.1
Au/BaO/Al <sub>2</sub> O <sub>3</sub>	85/98	6.7±0.2	3.0±0.3
Au/CoO <sub>x</sub> /Al <sub>2</sub> O <sub>3</sub>	66/144	5.5±0.1	5.3±0.1
Au/FeO <sub>x</sub> /Al <sub>2</sub> O <sub>3</sub>	73/188	6.1±0.1	3.6±0.2
Au/ZrO <sub>x</sub> /Al <sub>2</sub> O <sub>3</sub>	72/185	7.3±0.2	3.8±0.2
Au/CeO <sub>x</sub> /Al <sub>2</sub> O <sub>3</sub>	62/144	5.1±0.1	3.3±0.1
Au/CeO <sub>x</sub> /ZrO <sub>x</sub> /Al <sub>2</sub> O <sub>3</sub>	75/104	7.8±0.2	3.3±0.1
Au/Li <sub>2</sub> O/CeO <sub>x</sub> /Al <sub>2</sub> O <sub>3</sub>	79/101	5.5±0.1	3.1±0.1
Au/Rb <sub>2</sub> O/CeO <sub>x</sub> /Al <sub>2</sub> O <sub>3</sub>	75/101	5.6±0.1	3.1±0.3
Au/BaO/CeO <sub>x</sub> /Al <sub>2</sub> O <sub>3</sub>	82/126	4.8±0.1	3.2±0.2

In the series of the TMO/ceria additives, the effect of CoO<sub>x</sub> appears to be the most significant, although the difference between this catalyst and the catalysts containing ZrO<sub>x</sub> or FeO<sub>x</sub> is relatively small (Fig. 8.5A). On the other hand, a minor beneficial effect was found in the presence of ceria. In terms of *r* variation, zirconia appears the most efficient oxide. Regarding the stability of the gold particles during the catalytic test, sintering is prevented, presumably because of the additives.



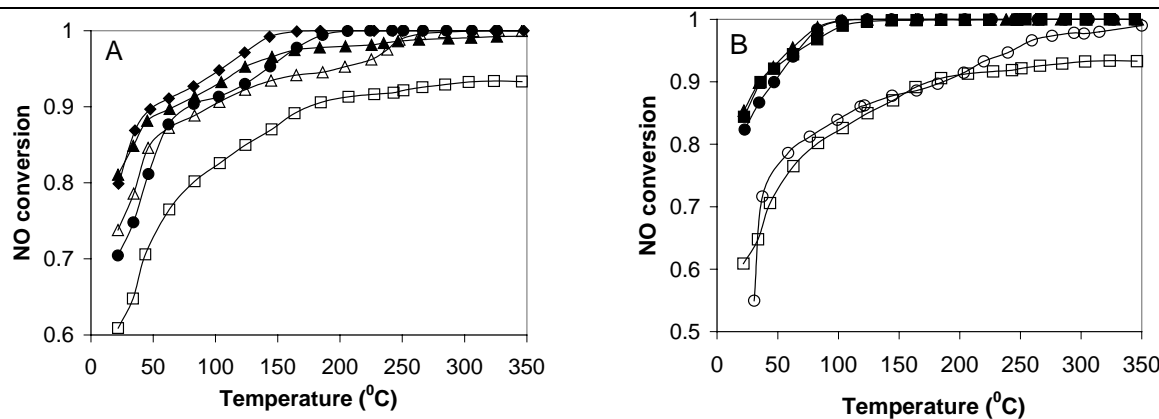


**Figure 8.5:** NO conversion vs. temperature over un-promoted (□) and CeO<sub>x</sub> (Δ), ZrO<sub>x</sub> (▲), CoO<sub>x</sub> (◆), FeO<sub>x</sub> (●) promoted Au/Al<sub>2</sub>O<sub>3</sub> (A); un-promoted (□), and Rb<sub>2</sub>O/CeO<sub>x</sub> (▲), CeO<sub>x</sub>/ZrO<sub>x</sub> (■), Li<sub>2</sub>O/CeO<sub>x</sub> (●), BaO/CeO<sub>x</sub> (○) promoted Au/Al<sub>2</sub>O<sub>3</sub> (B). NO/H<sub>2</sub> = 0.4.

Concerning the combined effect of the two metal oxides (Fig. 8.5B), although the difference among the samples is not significant, the catalyst with BaO+CeO<sub>x</sub> performs slightly different than the other catalysts and the variation of  $r$  at 105°C is relatively small, compared with the un-promoted Au/Al<sub>2</sub>O<sub>3</sub>. In terms of  $r$  variation, just like for the reactant ratio NO/H<sub>2</sub> = 1, the best performance is achieved by the combination CeO<sub>x</sub>+ZrO<sub>x</sub>.

### Reactant ratio NO/H<sub>2</sub> = 0.4 – Selectivity

The same sequence of the product distribution as already described for the reactant ratio NO/H<sub>2</sub> = 1 was found in excess hydrogen. However, as expected, the product distribution is affected by the presence of excess H<sub>2</sub> in the gas stream. Figs.8.6A shows the product distribution for Au/Al<sub>2</sub>O<sub>3</sub>. In Fig. 8.6B is presented a comparison of the product distribution for Au/Li<sub>2</sub>O/CeO<sub>x</sub>/Al<sub>2</sub>O<sub>3</sub> and Au/BaO/CeO<sub>x</sub>/Al<sub>2</sub>O<sub>3</sub>. Although these catalysts contain ceria as the common additive and the second additive belongs to the same class (alkali (earth) metal oxide), the product distribution differs significantly.

For Au/Al<sub>2</sub>O<sub>3</sub> and NO/H<sub>2</sub> = 0.4, the formation of N<sub>2</sub>O is observed in a broader temperature region, compared to NO/H<sub>2</sub> = 1. The production of N<sub>2</sub>O decreases at higher temperature, i.e. 90°C and 60°C, for NO/H<sub>2</sub> = 1. Another important difference resides in the maximum selectivity to N<sub>2</sub> (Table 8.2), which is strongly affected by the higher hydrogen concentration in the feed (decrease). On the other hand, a strong increase in the selectivity to NH<sub>3</sub> is observed, as expected.

As already mentioned, the identity of the additives has a great influence on the conversion and selectivity. With BaO as additive, the production of N<sub>2</sub>O and N<sub>2</sub> increases. On the other hand, the production of NH<sub>3</sub> is effectively suppressed, compared with Li<sub>2</sub>O-containing Au/CeO<sub>x</sub>/Al<sub>2</sub>O<sub>3</sub>. However, from a pragmatic point of view it is always a trade-off between conversion and selectivity, because the X<sub>NO</sub> is slightly inferior to what can be achieved by using Au/Li<sub>2</sub>O/CeO<sub>x</sub>/Al<sub>2</sub>O<sub>3</sub> (Fig. 8.5B). The combination with BaO proves to be extremely interesting for this reaction, more than with other alkali (earth) metal oxides.

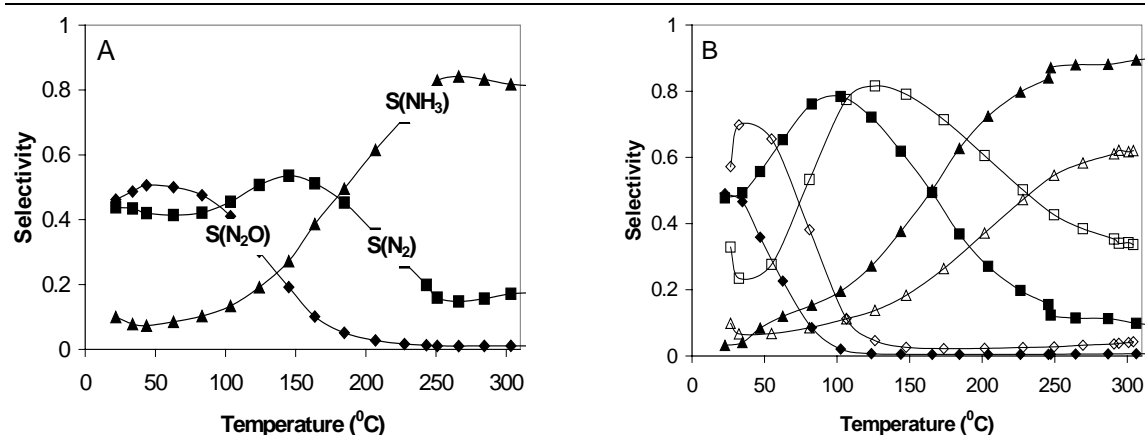


**Figure 8.6:** Product distribution vs. temperature over Au/Al<sub>2</sub>O<sub>3</sub> (A) and Au/Li<sub>2</sub>O/CeO<sub>x</sub>/Al<sub>2</sub>O<sub>3</sub> (filled symbols) and Au/BaO/CeO<sub>x</sub>/Al<sub>2</sub>O<sub>3</sub> (open symbols) (B). S<sub>N<sub>2</sub>O</sub> (◆), S<sub>N<sub>2</sub></sub> (■), S<sub>NH<sub>3</sub></sub> (▲). NO/H<sub>2</sub> = 0.4.

Regarding the selectivity to N<sub>2</sub> over the other gold-based catalysts, this is improved in all cases studied when one or two additives are present (Table 8.2). However, it was noticed that the temperature where S<sub>N<sub>2</sub></sub> reaches a maximum is greatly affected by the additives.

#### 8.4 Catalytic performance in N<sub>2</sub>O reduction by H<sub>2</sub>

The reduction of N<sub>2</sub>O with hydrogen has been carried out using a reactant ratio N<sub>2</sub>O/H<sub>2</sub> = 0.5 (excess hydrogen). No other products than N<sub>2</sub> and H<sub>2</sub>O are formed. The catalytic performance versus temperature of unpromoted- and alkali (earth) metal oxides-promoted Au/Al<sub>2</sub>O<sub>3</sub> is depicted in Figs. 8.7A. Similar to NO reduction, the first cooling cycle is considered for the purpose of comparison. The support-only was also tested and found negligibly active under these reaction conditions. Fig. 8.7B presents the effect of TMO/ceria addition on the catalytic activity of Au/Al<sub>2</sub>O<sub>3</sub> in nitrous oxide reduction. The combined effect of two different metal oxides acting as promoters for Au/Al<sub>2</sub>O<sub>3</sub> is depicted in Fig. 8.7C.

Table 8.3 summarizes the temperature needed to reach 50% N<sub>2</sub>O conversion, the specific reaction rate, *r*, at 100 °C expressed as moles of N<sub>2</sub>O transformed per mole of Au per second and the average size of the gold particles for the used (after reaction) catalysts.

The results presented in Figs. 8.7A-C and in Table 8.3 point to a very clear promoting effect of all the additives on the catalytic performance of Au/Al<sub>2</sub>O<sub>3</sub>. The presence of the additives shifts the conversion of N<sub>2</sub>O towards lower temperatures. For example, the effect of Li<sub>2</sub>O and Rb<sub>2</sub>O is roughly the same regarding T<sub>50%</sub> and superior to that of MgO. However, in terms of *r* variation, Rb<sub>2</sub>O performs slightly better. Based on the variation of *r*, the best catalysts in N<sub>2</sub>O conversion contain an alkali or an alkali-earth metal oxide in combination with ceria. Comparing the variation of *r* for NO/H<sub>2</sub> (0.4) and N<sub>2</sub>O/H<sub>2</sub>, the differences are relatively small and nearly the same order in the catalytic activity is found for both reduction reactions. This is not unexpected, since N<sub>2</sub>O is an intermediate in NO reduction that is observed only at relatively low temperatures.

As a final remark, the sintering of the gold particles is not significant.

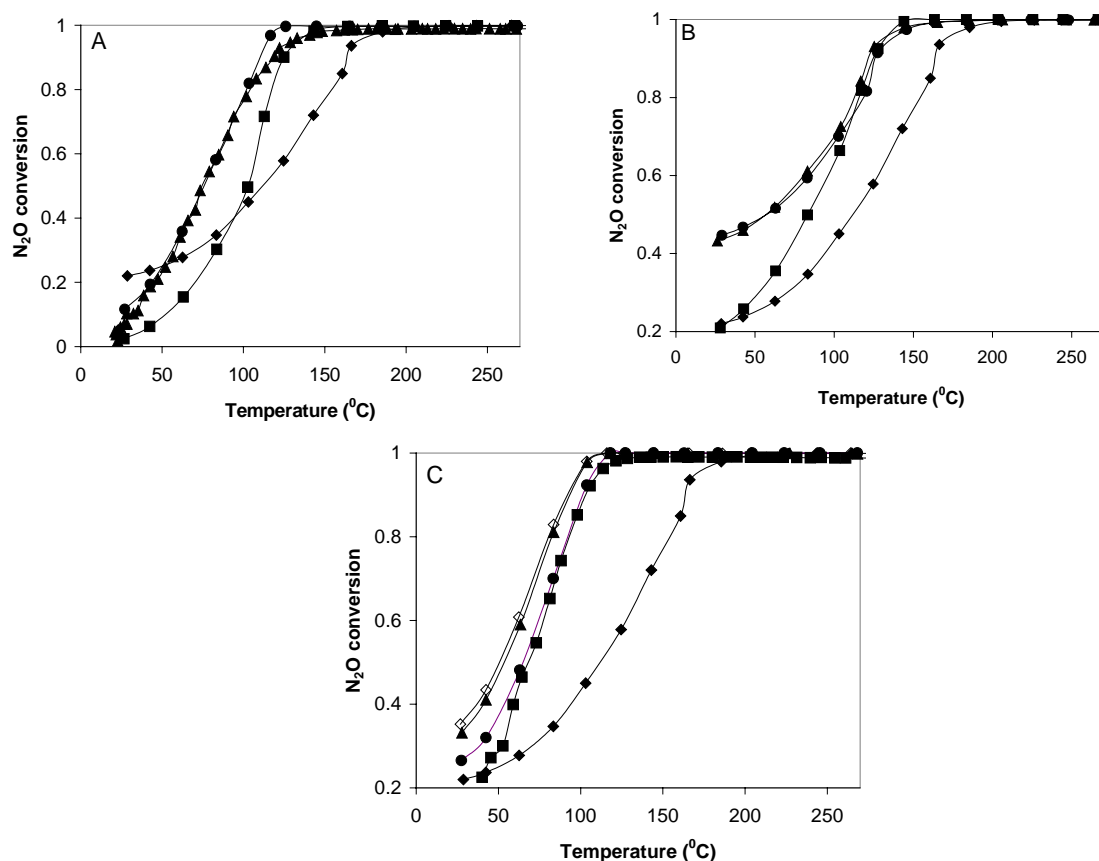


**Figure 8.7:**  $\text{N}_2\text{O}$  conversion vs. temperature over  $\text{Au}/\text{Al}_2\text{O}_3$  ( $\blacklozenge$ ),  $\text{Au}/\text{MgO}/\text{Al}_2\text{O}_3$  ( $\blacksquare$ ),  $\text{Au}/\text{Li}_2\text{O}/\text{Al}_2\text{O}_3$  ( $\bullet$ ),  $\text{Au}/\text{Rb}_2\text{O}/\text{Al}_2\text{O}_3$  ( $\blacktriangle$ ) (A);  $\text{Au}/\text{TiO}_x/\text{Al}_2\text{O}_3$  ( $\blacksquare$ ),  $\text{Au}/\text{CoO}_x/\text{Al}_2\text{O}_3$  ( $\blacktriangle$ ),  $\text{Au}/\text{CeO}_x/\text{Al}_2\text{O}_3$  ( $\bullet$ ) (B);  $\text{Au}/\text{BaO}/\text{CeO}_x/\text{Al}_2\text{O}_3$  ( $\blacksquare$ ),  $\text{Au}/\text{Li}_2\text{O}/\text{CeO}_x/\text{Al}_2\text{O}_3$  ( $\blacktriangle$ ),  $\text{Au}/\text{CoO}_x/\text{Li}_2\text{O}/\text{Al}_2\text{O}_3$  ( $\bullet$ ),  $\text{Au}/\text{Rb}_2\text{O}/\text{CeO}_x/\text{Al}_2\text{O}_3$  ( $\blacklozenge$ ) (C).  $\text{N}_2\text{O}/\text{H}_2 = 0.5$ .

**Table 8.3:**  $T_{50\%}$ , the specific reaction rate,  $r$ , and  $d_{\text{Au}}^b$  (nm), XRD.  $\text{N}_2\text{O}/\text{H}_2 = 0.5$ .

Catalyst	$T_{50\%}$ ( $^{\circ}\text{C}$ )	$r \times 10^3$ (moles $\text{N}_2\text{O}$ moles $\text{Au}^{-1} \text{s}^{-1}$ )	$d_{\text{Au}}^b$ (nm)
$\text{Au}/\text{Al}_2\text{O}_3$	111	$3.2 \pm 0.1$	$4.9 \pm 0.1$
$\text{Au}/\text{Li}_2\text{O}/\text{Al}_2\text{O}_3$	75	$6.0 \pm 0.2$	$3.9 \pm 0.3$
$\text{Au}/\text{Rb}_2\text{O}/\text{Al}_2\text{O}_3$	73	$6.5 \pm 0.1$	$5.0 \pm 0.1$
$\text{Au}/\text{MgO}/\text{Al}_2\text{O}_3$	103	$3.5 \pm 0.1$	$5.5 \pm 0.3$
$\text{Au}/\text{CoO}_x/\text{Al}_2\text{O}_3$	57	$5.0 \pm 0.1$	$6.1 \pm 0.1$
$\text{Au}/\text{CeO}_x/\text{Al}_2\text{O}_3$	56	$4.5 \pm 0.1$	$4.4 \pm 0.1$
$\text{Au}/\text{TiO}_x/\text{Al}_2\text{O}_3$	82	$4.1 \pm 0.2$	$5.1 \pm 0.1$
$\text{Au}/\text{CoO}_x/\text{Li}_2\text{O}/\text{Al}_2\text{O}_3$	64	$5.8 \pm 0.1$	$3.0 \pm 0.1$
$\text{Au}/\text{Li}_2\text{O}/\text{CeO}_x/\text{Al}_2\text{O}_3$	52	$6.2 \pm 0.2$	$4.5 \pm 0.1$
$\text{Au}/\text{Rb}_2\text{O}/\text{CeO}_x/\text{Al}_2\text{O}_3$	50	$6.4 \pm 0.1$	$4.8 \pm 0.3$
$\text{Au}/\text{BaO}/\text{CeO}_x/\text{Al}_2\text{O}_3$	68	$6.1 \pm 0.1$	$3.9 \pm 0.2$
$\text{Au}/\text{MnO}_x/\text{MgO}/\text{Al}_2\text{O}_3$	69	$5.5 \pm 0.1$	$4.5 \pm 0.4$

## 8.5 Discussion

### 8.5.1 NO reduction by H<sub>2</sub>

#### Active sites. The effect of MO<sub>x</sub> addition on the overall catalytic activity

The reduction of NO by hydrogen may proceed via the following reactions:



To obtain N<sub>2</sub> as the main reaction product, a reactant mixture NO/H<sub>2</sub> = 1 would be necessary. On the other hand, for NH<sub>3</sub> production, excess of hydrogen is required (NO/H<sub>2</sub> = 0.4).

It is believed that Au is a poor hydrogenation catalyst because of its very weak interaction with hydrogen. However, although this is true, results reported recently proved the contrary. It was reported that gold-based catalysts can have some catalytic activity in hydrogenation of acrolein [12, 13], NO reduction [1, 14] and even in the H/D isotopic exchange reaction at room temperature [15]. The present data give more evidence that even over unpromoted Au/Al<sub>2</sub>O<sub>3</sub> the reduction of NO by hydrogen proceeds at relatively low temperatures. Three different products were obtained, as a function of the reaction temperature: N<sub>2</sub>O, N<sub>2</sub> and NH<sub>3</sub>. Excess of the H<sub>2</sub> has a positive influence on the conversion of NO. In addition, the product distribution is also greatly influenced by the amount of H<sub>2</sub> in the gas stream. Contrary to earlier findings [1], all the metal oxides added to Au/Al<sub>2</sub>O<sub>3</sub> significantly shift the conversion of NO towards lower temperatures. The product distribution is also drastically affected by the nature of the additives.

It is well known that small gold particles are very efficient for various reactions such as CO oxidation [16-19], N<sub>2</sub>O reduction [20], C<sub>3</sub>H<sub>6</sub> oxidation [21, 22], etc. There are different explanations connected to this: either the presence of a large total Au/support interface [23-26], or the presence of special sites such as coordinatively unsaturated gold surface atoms [27, 28]. The number of low coordinated atoms is related to the size of the Au particles [28]. Smaller Au particles are considered to have an increased number of low coordinated atoms, highly active towards molecule activation. The characterization results discussed in *Chapter 4* point to the presence of very small gold particles, especially when two different metal oxides are present (XRD, HRTEM), or if BaO is present. In addition, the samples with very small gold particles are highly dispersed and have a larger metallic surface area than the samples with bigger gold particles. Further, all the results indicate that the state of gold is metallic.

The variation of the temperature needed for 50% conversion with the mean diameter of the gold particles is shown in Fig. 8.8 for various gold-based catalysts for NO/H<sub>2</sub> = 1. These data reveal that the catalytic performance of the gold-based catalysts is directly related to the size of the gold particles. However, this conclusion does not apply for all the catalytic systems studied. For instance, the CeO<sub>x</sub> promoted Au/Al<sub>2</sub>O<sub>3</sub> exhibits small gold particles, but

the catalytic activity, at least in the low temperature range, equals that of the larger particles of the Au/Al<sub>2</sub>O<sub>3</sub>.

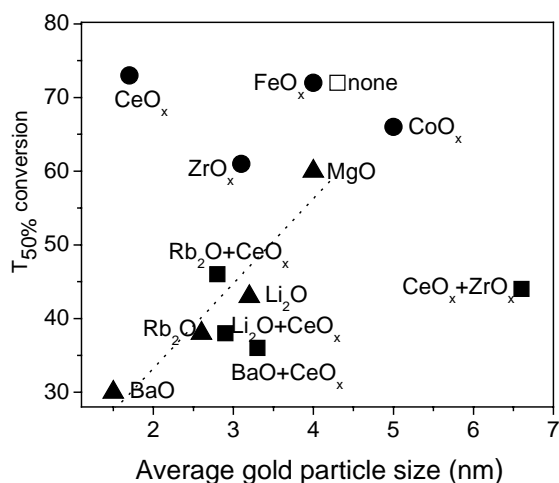


**Figure 8.8:** The temperature needed for 50% NO conversion vs. the average gold particle size of unpromoted and promoted Au/Al<sub>2</sub>O<sub>3</sub>. NO/H<sub>2</sub> = 1.

The conclusion is that the main driving force for this reaction is, indeed, the size of the gold particles, especially when non-reducible oxides are used as additives. The results presented in Fig. 8.8 show that only for the alkali (earth) metal oxides as additives, the data fall on a straight line. However, if easily reducible metal oxides are present, the situation may change. Similar results have already been reported for propene oxidation over some multicomponent gold-based catalysts [21]. However, as already mentioned, the identity of the additives has a large influence on the product distribution as well. It is possible that the binding of NO is facilitated in the presence of certain types of additives. For example it has been reported that CoO<sub>x</sub> added to Pt/SiO<sub>2</sub> enhances the dissociation of NO and finally improves the conversion of NO to N<sub>2</sub> [29]. Another aspect which may influence the overall catalytic activity and the product distribution is the acid-base characteristics of the mixed supports, as was already discussed in *Chapter 7* (NH<sub>3</sub> oxidation). This factor was reported to influence the catalytic activity of several gold-based catalysts in N<sub>2</sub>O reduction by H<sub>2</sub> [20].

### Selectivity. The influence of excess H<sub>2</sub>

As mentioned before, both the conversion of NO and the selectivity to different products are greatly influenced by the hydrogen concentration in the feed. This influence is clearly illustrated in Figs. 8.9A-B, where the change in the selectivity of Au/Al<sub>2</sub>O<sub>3</sub> (Fig. 8.9A) and Au/Li<sub>2</sub>O/CeO<sub>x</sub>/Al<sub>2</sub>O<sub>3</sub> (Fig. 8.9B) are shown for two different gas compositions. The filled symbols correspond to a reactant ratio NO/H<sub>2</sub> = 1, and the open symbols to a reactant ratio NO/H<sub>2</sub> = 0.4.

The N<sub>2</sub>O production does not appear to be strongly affected by the change in the reactant ratio in the case of Au/Al<sub>2</sub>O<sub>3</sub>. However, if excess of hydrogen is applied, N<sub>2</sub>O vanishes at lower temperature over Au/Li<sub>2</sub>O/CeO<sub>x</sub>/Al<sub>2</sub>O<sub>3</sub>. The selectivity towards N<sub>2</sub> and NH<sub>3</sub> are strongly affected by the H<sub>2</sub> concentration for both catalysts. Yet, differences between the catalysts exist: over Au/Al<sub>2</sub>O<sub>3</sub> less N<sub>2</sub> is produced in excess H<sub>2</sub>, although its maximum is shifted towards lower temperature. Over Au/Li<sub>2</sub>O/CeO<sub>x</sub>/Al<sub>2</sub>O<sub>3</sub> an excess of H<sub>2</sub> results in larger amounts of both N<sub>2</sub> and NH<sub>3</sub>. This difference is most likely related to the presence of the additives CeO<sub>x</sub> and Li<sub>2</sub>O that promotes the formation of N<sub>2</sub>.

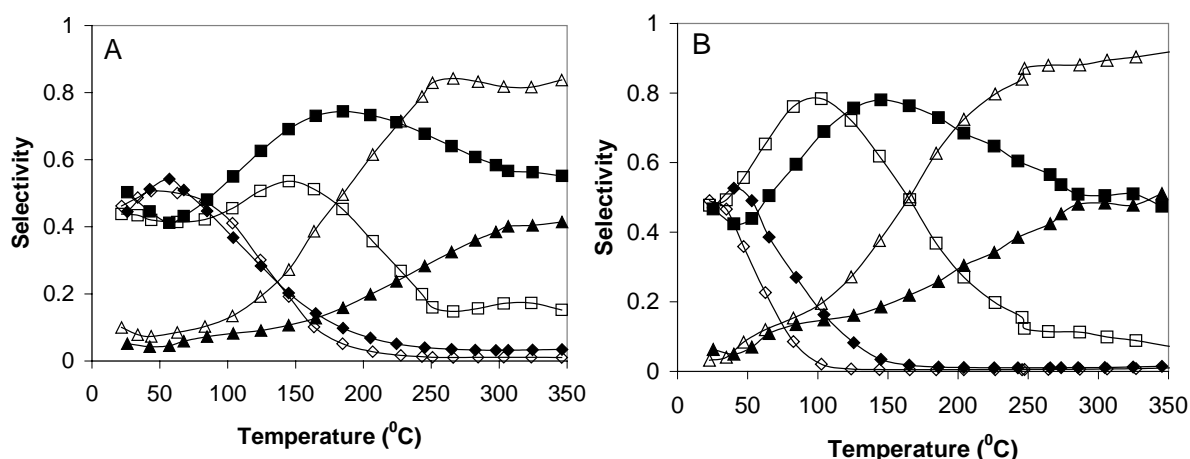


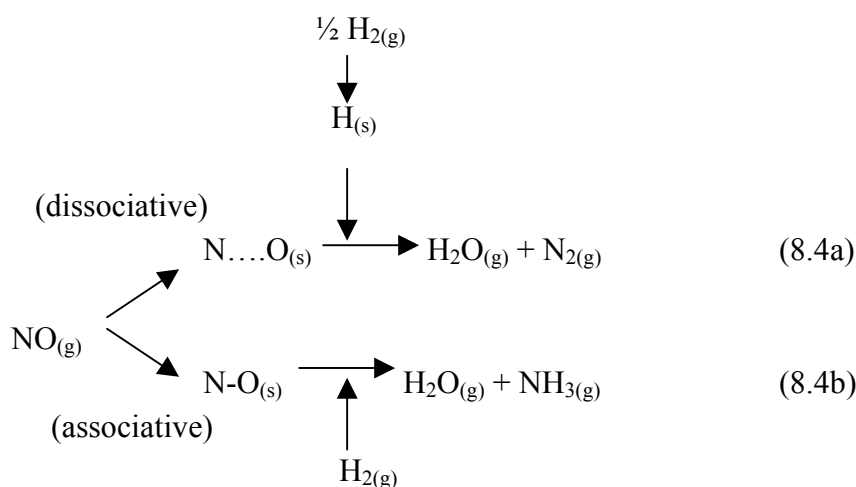
**Figure 8.9:** Product distribution vs. temperature over Au/Al<sub>2</sub>O<sub>3</sub> (A) and Au/Li<sub>2</sub>O/CeO<sub>x</sub>/Al<sub>2</sub>O<sub>3</sub> (B). Filled symbols: NO/H<sub>2</sub> = 1, open symbols: NO/H<sub>2</sub> = 0.4. S<sub>N<sub>2</sub>O</sub> (◆), S<sub>N<sub>2</sub></sub> (■), S<sub>NH<sub>3</sub></sub> (▲).

An excess of hydrogen influences the NO conversion as well. It was shown that by using a reactant ratio NO/H<sub>2</sub> = 1, the conversion of NO never reached 100%. On the other hand, if excess H<sub>2</sub> was present, full NO conversion could be attained at higher temperatures. The main product is N<sub>2</sub>O for a reactant ratio NO/H<sub>2</sub> = 1, in the low temperature regime. According to (8.1), the amount of hydrogen present is enough to convert all the NO. At intermediate temperatures when N<sub>2</sub> is the main product, there is still enough hydrogen to react with NO. However, when the reaction temperature increases, NH<sub>3</sub> is the main product, and because more H<sub>2</sub> is required to convert NO, the conversion of NO will drop because there is not enough H<sub>2</sub>. When excess of H<sub>2</sub> is supplied, NO will be totally converted because the amount of hydrogen is sufficient in the whole temperature range.

### Reaction mechanism

Studies of NO reduction over gold-based catalysts are scarce and the results are confusing. Various mechanisms have been proposed, but no general agreement seems to have been reached yet. Early as 1978 Galvagno and Paravano [2] have studied the reduction of NO by hydrogen over Au/SiO<sub>2</sub>, Au/MgO and Au/Al<sub>2</sub>O<sub>3</sub> at 350 °C and they found that, depending

on the support, more  $N_2$  or more  $NH_3$  is formed. They considered that the amount of  $N_2$  formed strongly depends on the size of the gold particles as well as on the Au-support interaction. They proposed a reaction mechanism, which consists of two different paths, via equation 8.4a or 8.4b, depending on the support identity. The associative path, which gives rise to more ammonia, was considered to be valid for Au/SiO<sub>2</sub>. The dissociative path, which results in more  $N_2$ , would be valid for Au/Al<sub>2</sub>O<sub>3</sub> and Au/MgO. Unfortunately, no direct evidence for NO adsorption and/or dissociation was presented. However, all catalysts used in this research showed similar product distributions, so we cannot differentiate between associative and dissociative pathways.



Later, in an infrared spectroscopic study carried out on Au/SiO<sub>2</sub> and Au/MgO, Lee and Schwank [3] claimed that NO does not adsorb on either catalyst. Moreover, they detected N<sub>2</sub>O formation at very low temperature (338K), which is probably an intermediate, along with HNO, as another reaction intermediate. Finally they assumed that the reduction of NO by hydrogen proceeds via associative adsorption of NO. A very weak or even absent NO adsorption was also reported by Dekkers on supported gold catalysts [1, 14] and more recently by McClure on Au(111) [30]. It was also reported that nitric oxide decomposition/desorption does not proceed on gold-based catalysts [1, 14]. On the other hand, recent theoretical studies have shown that NO can adsorb on cationic, anionic and neutral Au<sub>n</sub> clusters (n = 1-6) [31], or on Au(3111) [32].

Regarding the possible intermediates that are likely to be formed during NO reduction, HNO [3] and NO<sub>2</sub> were suggested [33]. However, it is clear that there is no general consensus regarding this reaction.

The data presented here do not contain any direct evidence to support any of the above presented mechanisms. However, although it was generally accepted that gold cannot activate hydrogen at relatively low temperature, recent studies proved that this is possible, especially if small gold particles are involved, with an increased number of edges, steps and kinks [15]. Moreover, it appears that NO and H<sub>2</sub> do not compete for the same adsorption sites, since

under excess of hydrogen the conversion of NO increased significantly. It is more probable that hydrogen assists the adsorption/dissociation of NO. In this way of thinking the formation of NH<sub>3</sub> is related to NO dissociation. Very recently, it was found that during NO adsorption at 300K on Au 3D hemispherical crystals (“field emitter tips”), (NO)<sub>2</sub> and N<sub>2</sub>O are formed [34]. The dimer (NO)<sub>2</sub> is proposed as the intermediate in N<sub>2</sub>O formation. On the contrary, other authors claim that the dimer formation is unlikely on Au(311) [32]. Moreover, the authors propose that NO decomposes even at 80K and forms N<sub>2</sub>O<sub>ads</sub> and O<sub>ads</sub> on the surface.

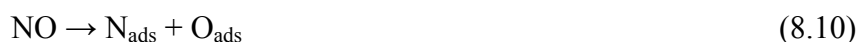
The following reaction mechanism is suggested based on the experimental data and the distribution of the products. At low temperature NO adsorbs associatively on gold and the gold-support interface. The dimer formation is a possible path in the production of N<sub>2</sub>O (reaction 8.6). Alternatively, however, N<sub>2</sub>O may be formed via a reaction between two NO<sub>ads</sub> (reaction 8.7). Calculations using density functional theory (DFT) have shown that over Pt catalyst the activation barrier for reaction (8.7) is considerably lower than that for reaction (8.8) [35].



At higher temperature, above 50<sup>0</sup>C, N<sub>2</sub>O may dissociate according to (8.9) – this is also supported by the fact that N<sub>2</sub>O is very reactive, at already around 100<sup>0</sup>C it is not found anymore.



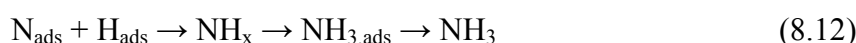
However, due to the higher temperature, NO dissociation may also occur, via reaction (8.10):



N<sub>2</sub> will be formed via recombination of two N<sub>ads</sub> atoms (reaction 8.11):



By further increasing the temperature, ammonia will be formed by recombination of N<sub>ads</sub> and H<sub>ads</sub>, via reaction (8.12):



The mechanism proposed for N<sub>2</sub> and NH<sub>3</sub> formation is similar to the mechanism established for the Pt-group metals [23]. The additives may create new sites for NO dissociation.



### 8.5.2 N<sub>2</sub>O reduction by H<sub>2</sub>

#### Active sites

The reduction of N<sub>2</sub>O with H<sub>2</sub> proceeds via the following reaction:



This reduction reaction is another example demonstrating that gold is a very active catalyst in hydrogenation reactions. As previously discussed, hydrogen may be activated on gold nanoparticles, especially if their size is well below 5 nm. That also may hold for N<sub>2</sub>O. In order to confirm the gold particle size effect on the catalytic performance of various gold-based catalysts, the T<sub>50%</sub> is plotted versus the average size of the gold particles and is shown in Fig. 8.10.

Similar to other oxidation and reduction reactions, the T<sub>50%</sub> varies in line with the variation of the gold particle size of various catalysts. However, there are situations when larger particles are still able to give an active catalyst (CoO<sub>x</sub>), whereas the presence of relatively small particles is not a guarantee for an active catalyst (MgO). Thus, in addition to the particle size effect, other factors may also control the catalytic performance.

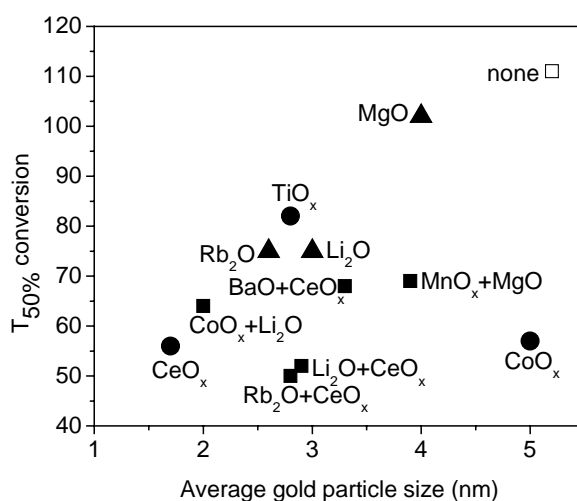


**Figure 8.10:** The temperature needed for 50% N<sub>2</sub>O conversion vs. the average gold particle size of unpromoted and promoted Au/Al<sub>2</sub>O<sub>3</sub>. N<sub>2</sub>O/H<sub>2</sub> = 0.5.

#### Reaction mechanism

N<sub>2</sub>O is a thermodynamically unstable molecule. However, the thermal decomposition reaction under homogeneous conditions does occur only above 600<sup>0</sup>C. It has been reported that on Au/Al<sub>2</sub>O<sub>3</sub> and Au/TiO<sub>2</sub> N<sub>2</sub>O decomposition in absence of H<sub>2</sub> does not occur [1, 20]. Possible reasons may include build-up of oxygen atoms on the surface that inhibit the reaction [36, 37], or the absence of a promoting effect of H<sub>2</sub> on the dissociation of N<sub>2</sub>O. The Au-N<sub>2</sub>O bond is very weak and desorption proceeds rapidly.

The N-N bond (474 kJ mol<sup>-1</sup>) in the N<sub>2</sub>O molecule is much stronger than its N-O bond (161 kJ mol<sup>-1</sup>). Therefore, if a N<sub>2</sub>O molecule dissociates, a reasonable assumption is that it will break through its N-O bond (8.14), rather than dissociation to NO<sub>ads</sub> and N<sub>ads</sub> (8.15):



Reduction of N<sub>2</sub>O with hydrogen occurs already at room temperature. Since only N<sub>2</sub> is formed as a nitrogen-containing product, the reduction of N<sub>2</sub>O with hydrogen may include a Langmuir-Hinshelwood mechanism, between O<sub>ads</sub> formed as a result of N<sub>2</sub>O dissociation and H<sub>ads</sub> on gold:



The adsorbed oxygen then reacts with hydrogen to form water. The experimental results obtained for the H<sub>2</sub>/O<sub>2</sub> reaction support this mechanism [1, 20]. Since the decomposition of N<sub>2</sub>O in the absence of H<sub>2</sub> did not reveal any product formation, it is proposed that the presence of hydrogen enhances the decomposition of nitrous oxide.

The mechanism of the beneficial effects of the additives (TMO, ceria or alkali metal oxides) is still under debate. Many researchers agree that the gold-TMO interface may play a significant role [23, 38, 39]. These results prove that reduction of N<sub>2</sub>O to N<sub>2</sub> and O<sub>ads</sub> is enhanced in the presence of a TMO or ceria, or, more general, oxides with a high capability to store and release oxygen (Fig. 8.7B-C). The presence of CeO<sub>x</sub> or a TMO might create new sites for N<sub>2</sub>O dissociation at the gold/ceria or TMO interface. A striking result is that by addition of both an alkali metal oxide (Li<sub>2</sub>O or Rb<sub>2</sub>O) and CeO<sub>x</sub> or a TMO, a dramatic increase in the catalyst performance is obtained. This can be explained by taking into consideration the already discussed effect of ceria on the catalytic activity, in combination with the beneficial effect of an (earth) alkali metal oxide on the performance of gold catalysts. The basicity of the alkali metal oxide increases from Li<sub>2</sub>O to Rb<sub>2</sub>O. The effect of alkali or alkali-earth metal oxide on Pt/Al<sub>2</sub>O<sub>3</sub> was extensively studied by Yentekakis and co-workers [40-42] for NO reduction by propene in presence of oxygen. In case of Pt/Al<sub>2</sub>O<sub>3</sub>, the promoting effect of Rb<sub>2</sub>O is the largest one. The effect of basicity on the catalytic activity was also observed in hydrogen/water isotopic exchange reaction on nickel-based catalysts [43]. For gold supported catalysts, the combined actions of Rb<sub>2</sub>O (Li<sub>2</sub>O) and CeO<sub>x</sub> are very efficient: sintering of gold particles is prevented by the presence of the promoter Rb<sub>2</sub>O (Li<sub>2</sub>O) and the intrinsic catalytic activity is enhanced by the presence of the CeO<sub>x</sub>.

## 8.6 Conclusions

Gold-based catalysts are efficient catalysts for the low temperature conversion of NO and N<sub>2</sub>O. Nitric oxide is converted in the presence of hydrogen (NO/H<sub>2</sub>=1 or 0.4) to the following products: N<sub>2</sub>O (at low temperature), N<sub>2</sub> (at intermediate temperature) and NH<sub>3</sub> (at high temperature). The catalytic performance as well as the product distribution strongly depends on the reaction temperature, nature of the additive and reactant ratio. It is suggested that hydrogen assists in NO decomposition. Based on the product distribution and other reported results, it is suggested that at low temperature NO partly decomposes to N<sub>2</sub>O and O<sub>ads</sub>, in agreement with recent papers [32]. At higher temperatures, the amount of NO dissociatively adsorbed on the surface will increase and as a result, more N<sub>2</sub> will be produced via N combination. The atomic nitrogen might be hydrogenated in the presence of hydrogen to NH<sub>x</sub> species and NH<sub>3</sub> is formed. The selectivity will then depend on the relative concentrations of adsorbed species on the surface, i.e. NO, N and NH<sub>x</sub>. The oxidic additives might create new sites for dissociative adsorption of NO.

The nature of the additives is also highly important in reduction of nitrous oxide with hydrogen. During N<sub>2</sub>O reduction with H<sub>2</sub> the only products obtained are N<sub>2</sub> and H<sub>2</sub>O. Most probably the role of the partly reducible metal oxide additive is to contribute to the formation of new active sites and increase N<sub>2</sub>O dissociation.

## 8.7 References

- [1] M. A. P. Dekkers, *Supported gold catalysts for automotive catalysis reactions*, PhD thesis, Leiden University (2000).
- [2] S. Galvagno, G. Parravano, *J. Catal.* 55 (1978) 178.
- [3] J. Y. Lee, J. Schwank, *J. Catal.* 102 (1986) 207.
- [4] A. Ueda, M. Haruta, *Gold Bull.* 32 (1999) 3.
- [5] T. M. Salama, R. Ohnishi, M. Ichikawa, *J. Chem. Soc. Farad. Trans.* 92 (1996) 301.
- [6] J. Szanyi, J. H. Kwak, J. Hanson, C. M. Wang, T. Szailer, C. H. F. Peden, *J. Phys. Chem. B* 109 (2005) 7339.
- [7] J. Szanyi, J. H. Kwak, D. H. Kim, S. D. Burton, C. H. F. Peden, *J. Phys. Chem. B* 109 (2005) 27.
- [8] J. Dawody, M. Skoglundh, S. Wall, E. Fridell, *J. Mol. Catal. A* 225 (2005) 259.
- [9] K. S. Kabin, R. L. Muncrief, M. P. Harold, Y. J. Li, *Chem. Eng. Sci.* 59 (2004) 5319.
- [10] Y. Su, M. D. Amiridis, *Catal. Today* 96 (2004) 31.
- [11] P. Broqvist, H. Gronbeck, E. Fridell, I. Panas, *Catal. Today* 96 (2004) 71.
- [12] P. Claus, A. Bruckner, C. Mohr, H. Hofmeister, *J. Am. Chem. Soc.* 122 (2000) 11430 and refs. therein.
- [13] S. Schimpf, M. Lucas, C. Mohr, U. Rodemerck, A. Bruckner, J. Radnik, H. Hofmeister, P. Claus, *Catal. Today* 72 (2002) 63.
- [14] M. A. P. Dekkers, M. J. Lippits, B. E. Nieuwenhuys, *Catal. Today* 54 (1999) 381.
- [15] A. C. Gluhoi, H. S. Vreeburg, J. W. Bakker, B. E. Nieuwenhuys, *Appl. Catal. A* 291 (2005) 145.
- [16] M. Haruta, S. Tsubota, T. Kobayashi, H. Kageyama, M. J. Genet, B. Delmon, *J. Catal.* 144 (1993) 175.
- [17] M. Valden, S. Pak, X. Lai, D. W. Goodman, *Catal. Lett.* 56 (1998) 7.
- [18] S. Tsubota, T. Nakamura, K. Tanaka, M. Haruta, *Catal. Lett.* 56 (1998) 7.
- [19] R. J. H. Grisel, C. J. Weststrate, A. C. Gluhoi, B. E. Nieuwenhuys, *Gold Bull.* 35 (2002) 39.
- [20] A. C. Gluhoi, M. A. P. Dekkers, B. E. Nieuwenhuys, *J. Catal.* 219 (2003) 197.
- [21] A. C. Gluhoi, N. Bogdanchikova, B. E. Nieuwenhuys, *J. Catal.* 229 (2005) 154.
- [22] A. C. Gluhoi, N. Bogdanchikova, B. E. Nieuwenhuys, *J. Catal.* 232 (2005) 96.
- [23] B. E. Nieuwenhuys, *Elementary reaction steps in heterogeneous catalysis*, R.W. Joyner, R.A. van Santen (eds.), Kluwer 1993.
- [24] G. R. Bamwenda, S. Tsubota, T. Nakamura, M. Haruta, *Catal. Lett.* 44 (1997) 83.
- [25] D. A. H. Cunningham, S. Tsubota, N. Kamijo, M. Haruta, *Res. Chem. Intermed.* 19 (1993) 1.
- [26] B. E. Nieuwenhuys, *Adv. Catal., Vol. 44* 1999.
- [27] F. Boccuzzi, G. Cerrato, F. Pinna, G. Strukul, *J. Phys. Chem. B* 102 (1998) 5733.

- [28] N. Lopez, J. K. Norskov, T. V. W. Janssens, A. Carlsson, A. Puig-Molina, B. S. Clausen, J. D. Grunwaldt, *J. Catal.* 225 (2004) 86.
- [29] Y. Mergler, A. van Aalst, J. van Delft, B. E. Nieuwenhuys, *Stud. Surf. Sci. Catal.* 96 (1995) 163.
- [30] S. M. McClure, T. S. Kim, J. D. Stiehl, P. L. Tanaka, C. B. Mullins, *J. Phys. Chem. B* 108 (2004) 17952.
- [31] X. Ding, Z. Li, J. Yang, K. G. Hou, Q. Zhu, *J. Chem. Phys.* 121 (2004) 2558.
- [32] C. P. Vinod, J. W. Niemantsverdriet, B. E. Nieuwenhuys, *Appl. Catal. A* 291 (2005) 93.
- [33] T. M. Salama, R. Ohnishi, M. Ichikawa, *Chem. Commun.* (1997) 105.
- [34] T.-D. Chau, T. Visart de Bocarme, N. Kruse, *Catal. Lett.* 98 (2004) 85.
- [35] R. Burch, S. T. Daniells, P. Hu, *J. Chem. Phys.* 117 (2002) 2902.
- [36] S. A. C. Carabineiro, B. E. Nieuwenhuys, *Surf. Sci.* 495 (2001) 1.
- [37] J. Ma, N. M. Rodriguez, M. A. Vannice, R. T. B. Bakker, *Top. Catal.* 10 (2000) 27.
- [38] M. Haruta, *Catal. Surv. Jpn.* 1 (1997) 61.
- [39] R. J. H. Grisel, B. E. Nieuwenhuys, *Catal. Today* 64 (2001) 69.
- [40] I. V. Yentekakis, M. Konsolakis, R. M. Lambert, N. Macleod, L. Nalbantian, *Appl. Catal. B* 22 (1999) 123.
- [41] M. Konsolakis, I. V. Yentekakis, *J. Catal.* 198 (2001) 142.
- [42] M. Konsolakis, I. V. Yentekakis, *Appl. Catal. B* 29 (2001) 103.
- [43] A. C. Gluhoi, P. Marginean, D. Lupu, E. Indrea, A. R. Biris, *Appl. Catal. A* 232 (2002) 121.



# Chapter 9

## CO oxidation in the presence (*PROX*) and absence of hydrogen over Au-based catalysts

*Supported gold catalysts are very active in CO oxidation at low temperatures. Fundamental studies were carried out to get more insight into the role of the active species (metallic/ionic Au) and the reaction mechanism. Pretreatment at mild temperatures, viz. 200°C, results in the highest catalytic performance of Au/Al<sub>2</sub>O<sub>3</sub> in low-temperature CO oxidation. The results also indicate a particle size effect, next to the pre-requisite for the presence of Au<sup>0</sup>. Alkali (earth) metal oxide additives are most probably structural promoters. Moreover, the results indicate a direct relationship between the loading of this type of additives and the catalytic performance of Au/Al<sub>2</sub>O<sub>3</sub>. The high catalytic performance of certain catalysts such as Au/CeO<sub>x</sub>/Al<sub>2</sub>O<sub>3</sub> and Au/MO<sub>x</sub>/CeO<sub>x</sub>/Al<sub>2</sub>O<sub>3</sub> (M: Ba, Mg, Li, Rb) is partly due to the ability of ceria to provide active oxygen during the reaction.*

*The selective oxidation of CO in the presence of hydrogen has been studied on some selected Au-based catalysts since it has been reported that Au-based catalysts are promising catalysts to selectively oxidize CO in the presence of hydrogen (*PROX*), especially in the low temperature range. Regarding the catalytic performance of the unpromoted Au/Al<sub>2</sub>O<sub>3</sub>, the results were similar to the findings concerning CO oxidation in the absence of hydrogen. However, the effect of the presence of hydrogen affects the ranking of the promoted-Au/Al<sub>2</sub>O<sub>3</sub> catalysts.*

## 9.1 Outline

This chapter describes the catalytic performance of unpromoted- and promoted- Au/Al<sub>2</sub>O<sub>3</sub> in low-temperature CO oxidation in the absence or presence of hydrogen (also known as “preferential oxidation of CO” - *PROX*). Due to the well-known ability of Au to act as a better catalyst for CO oxidation than for H<sub>2</sub> oxidation [1], the *PROX* reaction is particularly interesting for hydrogen purification needed for fuel cell applications. Specific details concerning the experimental procedures are described in Section 9.2. Section 9.3 presents the experimental results obtained during CO oxidation and *PROX*. A detailed discussion concerning the effect of the thermal/gas treatment, types of additives and active sites is provided in Section 9.4. The conclusions are summarized in Section 9.5.

## 9.2 Experimental

The unpromoted gold-based catalysts (5 wt-% Au) were prepared via HDP with urea (*Chapter 3*). The freshly prepared Au/Al<sub>2</sub>O<sub>3</sub> catalysts (i.e. after drying) were subjected to different thermal treatments. The samples were treated in either O<sub>2</sub> (i.e. the usual procedure), or H<sub>2</sub>, at 150, 200, 300 and 500°C. The effect of various treatments on the structure of Au/Al<sub>2</sub>O<sub>3</sub> was followed using XRD. The next step - the final step in the treatment of the samples prior to the catalytic reaction - was also varied: *in-situ* heating in H<sub>2</sub> (i.e. usual procedure), O<sub>2</sub> or He.

The mixed supports in the form of either MO<sub>x</sub>/Al<sub>2</sub>O<sub>3</sub>, or M<sup>I</sup>O<sub>x</sub>/M<sup>II</sup>O<sub>x</sub>/Al<sub>2</sub>O<sub>3</sub> (M: Rb, Li, Ba, Mg, Cu, Ce) were obtained by pore volume impregnation of alumina with a solution of the corresponding nitrates. A detailed description of the experimental procedure is found in *Chapter 3*. The physico-chemical properties of the above-mentioned catalysts have been discussed in *Chapter 4*. For some of the catalysts the preparation procedure was slightly changed. For example, LiNO<sub>3</sub> was added to Au/Al<sub>2</sub>O<sub>3</sub> via pore volume impregnation, followed by drying and calcination in an oxygen flow at 300°C. The atomic ratio Li:Al was 1/15. This catalyst will be designated as Li<sub>2</sub>O/Au/Al<sub>2</sub>O<sub>3</sub>. Other catalysts prepared by changing the usual recipe include Au/Li<sub>2</sub>O/Al<sub>2</sub>O<sub>3</sub> with different ratios Li:Al, i.e. 1/1, 1/5 and 1/30. Ag/Al<sub>2</sub>O<sub>3</sub> was prepared by pore volume impregnation of  $\gamma$ -Al<sub>2</sub>O<sub>3</sub> with the corresponding AgNO<sub>3</sub> solution, such that the atomic ratio Ag:Al = 1:10. This ratio corresponds to 17 wt-% Ag. Au/Ag/Al<sub>2</sub>O<sub>3</sub> was prepared by depositing Au on Ag/Al<sub>2</sub>O<sub>3</sub> (5 wt-% Au, Ag:Al = 1:10-atomic ratio), via HDP with urea. Au/Ag/CuO/Al<sub>2</sub>O<sub>3</sub> was prepared in a similar manner (5 wt-% Au, Ag:Cu:Al = 1:1:10-atomic ratio).

A description of the lab-scale flow system used for CO oxidation and *PROX* experiments can be found in *Chapter 3*. A deficient detection of hydrogen made a direct quantification of the hydrogen consumption impossible. CO oxidation was carried out under a reactant mixture of CO:O<sub>2</sub> = 2:1. The total flow gas that passed over the catalyst bed was set to 40 ml min<sup>-1</sup>, which corresponds to a GHSV ~ 2500 h<sup>-1</sup>.

The *PROX* reaction was performed under hydrogen rich conditions, in a mixture of H<sub>2</sub> (70 vol%) and CO+O<sub>2</sub> (1.2 vol%) in helium (~29 vol%). The amount of oxygen with respect to the minimum amount of oxygen required for CO oxidation to CO<sub>2</sub> in the absence of side reactions is characterized by the process parameter  $\lambda$  (equation 9.1). For practical applications

the value of  $\lambda$  in the PROX process should be as close as possible to 1 (i.e. stoichiometric), since hydrogen oxidation is not desired. This is also the ratio used in this study (CO:O<sub>2</sub> molar ratio of 2:1).

$$\lambda = \frac{C_{O_2,i}}{2 \cdot C_{CO,i}} \quad (9.1)$$

The selectivity to CO<sub>2</sub> was evaluated according to the formula (3.16) described in *Chapter 3*:

$$S_{CO_2,T} = \frac{C_{CO_2,T}}{2 \cdot (C_{O_2,i} - C_{O_2,T})} \quad (9.2)$$

The reactant mixture was stabilized for at least 30 min at RT. Afterwards at least two consecutive heating-cooling reaction cycles were performed. To compare the catalytic performance, the results of the second heating cycle are considered. The specific reaction rate,  $r$ , expressed as the number of CO (moles) transformed over the amount of Au (moles) per second was determined for both CO oxidation and PROX.

After performing the test reaction, the catalysts were again analysed by XRD.

### 9.3 Catalytic activity measurements

#### 9.3.1 Low-temperature carbon monoxide oxidation

##### *Unpromoted Au/Al<sub>2</sub>O<sub>3</sub>*

In 1987 striking results showing an exceptionally high activity of gold-based catalysts for low-temperature CO oxidation were published [2]. Compared with highly dispersed supported Pt catalysts, Au-based catalysts can be an order of a magnitude more active [3]. A large variation in the observed catalytic activity is found through the papers dealing with gold catalysis. Among them, the results regarding the catalytic performance of the most simple Au catalyst, Au/Al<sub>2</sub>O<sub>3</sub>, show perhaps the widest variety. Hence, Au/Al<sub>2</sub>O<sub>3</sub> was reported to be either very inactive [4, 5], or being comparable to or even better than Au/TiO<sub>2</sub> [6, 7]. Also the results obtained as a function of various calcination procedures vary among the papers. It was reported that for Au/TiO<sub>2</sub> [8, 9], Au/Fe<sub>2</sub>O<sub>3</sub> [9-11], and Au/MnO<sub>x</sub> [12] catalysts, calcination at mild temperatures (100-200<sup>0</sup>C) results in more active catalysts than calcination at higher temperatures. There are also reports that uncalcined Au/Al<sub>2</sub>O<sub>3</sub> [7] or Au/Y [13] can be very active. In addition, a higher calcination temperature may cause a severe sintering of the gold crystallites [14, 15]. On the other hand, it has been reported that a higher calcination temperature may positively influence the catalytic activity of Au/TiO<sub>2</sub> in the sense that a stronger Au-support interaction is created and this phenomenon leads to a higher catalytic efficiency, even though some sintering of the gold particles was observed [14]. Regarding the effect of the pretreatment, i.e. heating in either a hydrogen or an oxygen atmosphere, Dekkers found that a reductive pretreatment of Au/Al<sub>2</sub>O<sub>3</sub> gives better results than an oxidative one, at 300<sup>0</sup>C [16]. Later on, the studies of Grisel confirmed this result [15]. In addition he found, in



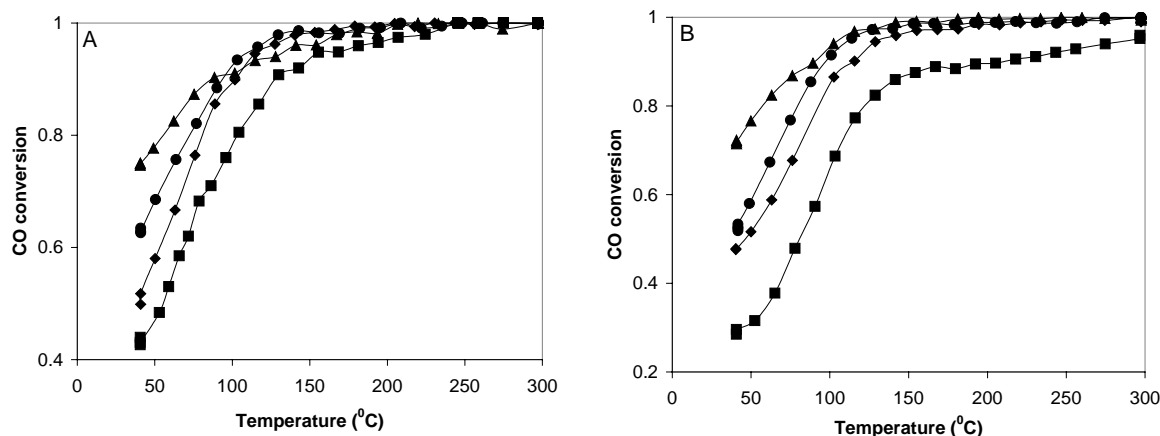
line with previous results [14], that larger Au particles ( $\sim 10$  nm), easily obtained by calcination at  $400^{\circ}\text{C}$ , are less active than smaller gold particles, obtained by calcination at  $300^{\circ}\text{C}$  [15].

Figure 9.1A shows the catalytic behaviour of Au/Al<sub>2</sub>O<sub>3</sub> that was subjected to calcination (i.e. the usual procedure) at different temperatures (150, 200, 300 or  $500^{\circ}\text{C}$ ). The second thermal treatment of the catalysts, carried out *in-situ*, was performed at the same temperature as used during the first treatment. Clearly, all the catalysts are highly active in CO oxidation and at around  $140^{\circ}\text{C}$  complete CO conversion is obtained. Moreover, the thermal treatment influences the catalytic performance of Au/Al<sub>2</sub>O<sub>3</sub>. Thus, the best procedure consists of calcination at  $200^{\circ}\text{C}$  without any additional treatment. Less active catalysts are obtained as a result of either calcination at  $500^{\circ}\text{C}$  (due to some sintering), or at  $150^{\circ}\text{C}$  (most likely due to incomplete reduction of Au<sup>3+</sup> to Au<sup>0</sup>). This is supported by the TPR (Chapter 4) that shows that the complete reduction of Au<sup>3+</sup> to Au<sup>0</sup> proceeds around  $163^{\circ}\text{C}$ . However, it should be mentioned that after calcination at  $150^{\circ}\text{C}$  the colour of the catalyst changed from yellow to purple, indicating that the decomposition of oxidic gold to Au<sup>0</sup> proceeded, but full reduction probably needs higher temperatures. It should be mentioned that the conversion of CO over bare alumina is not significant up to  $300^{\circ}\text{C}$ .

A similar trend in the catalytic performance of Au/Al<sub>2</sub>O<sub>3</sub> is obtained if O<sub>2</sub> is replaced by H<sub>2</sub>. The results are presented in Fig. 9.1B. The most active sample is obtained after H<sub>2</sub> treatment at  $200^{\circ}\text{C}$ . Just like the results presented in Fig. 9.1A, the effect of some sintering eventually prevails over the effect of incomplete Au<sup>3+</sup> reduction.

All the data concerning the catalytic performance of Au/Al<sub>2</sub>O<sub>3</sub> catalysts are presented in Table 9.1. The data include the temperature required for 95% CO conversion, the CO conversion at  $70^{\circ}\text{C}$  ( $X_{70}$ ), the specific reaction rate  $r$  calculated at  $70^{\circ}\text{C}$  and the average gold particle size before ( $d_{\text{Au}}^{\text{a}}$ ) and after ( $d_{\text{Au}}^{\text{b}}$ ) reaction (XRD). The Au loading varies between 3.8 wt-% Au and 4.8 wt-% Au.

Among all the samples, the specific reaction rate  $r$  shows the largest value for the calcined Au/Al<sub>2</sub>O<sub>3</sub> without any *in-situ* post-treatment. There is a difference between the values of  $r$  for the samples treated at  $150^{\circ}$  in O<sub>2</sub> or H<sub>2</sub>: the former being more active. Possibly, at  $150^{\circ}\text{C}$ , contaminants are easier removed in O<sub>2</sub>. These differences are not due to a particle size effect since the average size of the gold particles is nearly the same for all samples except for treatment at  $500^{\circ}\text{C}$  (Table 9.1). Thus, the differences observed in the catalytic performance are probably due to the chemical state of gold, which depends on the thermal treatment. However, as a secondary effect, the particle size effect may play a role as well: after heating in oxygen at  $150^{\circ}\text{C}$  some of gold is still in the oxidic state. *In-situ* studies of the chemical state of the gold during different treatments, eventually combined with XPS, may clarify these aspects.



**Figure 9.1:** CO conversion vs. temperature over calcined (A) and reduced (B) Au/Al<sub>2</sub>O<sub>3</sub>. The symbol in (A) corresponds to: 200/no pretreatment (▲), 300/H<sub>2</sub>/300 (●), 500/H<sub>2</sub>/300 (◆), 150/He/150 (■). The symbols in (B) correspond to 200/He/200 (▲), 300/He/300 (●), 500/He/300 (◆), 150/He/150 (■). Reactant ratio: CO:O<sub>2</sub> = 2:1.

**Table 9.1:** T<sub>95%</sub>, the conversion at 70°C (X<sub>70</sub>), the specific reaction rate, *r*, the average size of the gold particles for the fresh (d<sub>Au</sub><sup>a</sup>) and used (d<sub>Au</sub><sup>b</sup>) Au-based catalysts (XRD).

Treatment	d <sub>Au</sub> <sup>a</sup> (nm)	d <sub>Au</sub> <sup>b</sup> (nm)	T <sub>95%</sub> (°C)	X <sub>70</sub>	<i>r</i> x 10 <sup>3</sup> (moles CO moles <sup>-1</sup> Au s <sup>-1</sup> )
O <sub>2</sub> /150/He	<3.0	3.0±0.1	168	0.61	5.5±0.1
O <sub>2</sub> /200/He	3.0±0.2	3.0±0.3	117	0.81	6.3±0.1
O <sub>2</sub> /200/no treatment	3.0±0.1	3.0±0.2	135	0.85	6.7±0.1
O <sub>2</sub> /200/H <sub>2</sub>	3.0±0.1	3.0±0.2	128	0.79	6.2±0.2
O <sub>2</sub> /300/H <sub>2</sub>	3.0±0.3	3.0±0.2	112	0.78	5.5±0.1
O <sub>2</sub> /300/no treatment	3.0±0.2	3.0±0.1	162	0.79	5.5±0.1
O <sub>2</sub> /500/H <sub>2</sub>	4.3±0.3	4.5±0.4	114	0.71	5.4±0.1
H <sub>2</sub> /150/He	<3.0	3.3±0.3	290	0.41	3.3±0.1
H <sub>2</sub> /200/He	<3.0	<3.0	107	0.84	6.6±0.1
H <sub>2</sub> /200/H <sub>2</sub>	<3.0	<3.0	84	0.95	6.4±0.1
H <sub>2</sub> /300/He	3.3±0.2	3.4±0.1	113	0.74	5.3±0.1
H <sub>2</sub> /500/He	4.8±0.1	4.6±0.2	133	0.63	5.4±0.1

### Alkali (earth) metal oxides as additives

Previous studies showed that Au supported on Mg(OH)<sub>2</sub> or Be(OH)<sub>2</sub> display high catalytic activity in CO oxidation, especially if the average size of the Au particles is around 2 nm [17]. Chapters 5-8 describe beneficial effects of addition of various alkali (earth) metal oxides, such as Li<sub>2</sub>O, Rb<sub>2</sub>O, MgO and BaO to Au/Al<sub>2</sub>O<sub>3</sub> for various oxidation and reduction reactions. Fig. 9.2A shows the conversion of CO versus temperature over alkali (earth) metal oxide-promoted Au/Al<sub>2</sub>O<sub>3</sub> (second heating) and Li<sub>2</sub>O/Al<sub>2</sub>O<sub>3</sub> support. The influence of the Li<sub>2</sub>O concentration on the catalytic performance of Au/Al<sub>2</sub>O<sub>3</sub> is presented in Fig. 9.2B.

The best performance is obtained if Au is combined with BaO and full CO conversion is reached at RT. The catalytic activity of Au/Al<sub>2</sub>O<sub>3</sub> is also enhanced in the presence of Rb<sub>2</sub>O and Li<sub>2</sub>O. The addition of Li<sub>2</sub>O after Au deposition onto the support produces a decrease in

the catalytic performance compared with the other alkali (earth)-promoted Au/Al<sub>2</sub>O<sub>3</sub> catalysts. Concerning the effect of Li<sub>2</sub>O, the order of addition significantly influences the catalytic performance (see Table 9.2). Most likely, the interaction between Au and the support, crucial for high catalytic activity, is stronger if Li<sub>2</sub>O is first added to alumina.

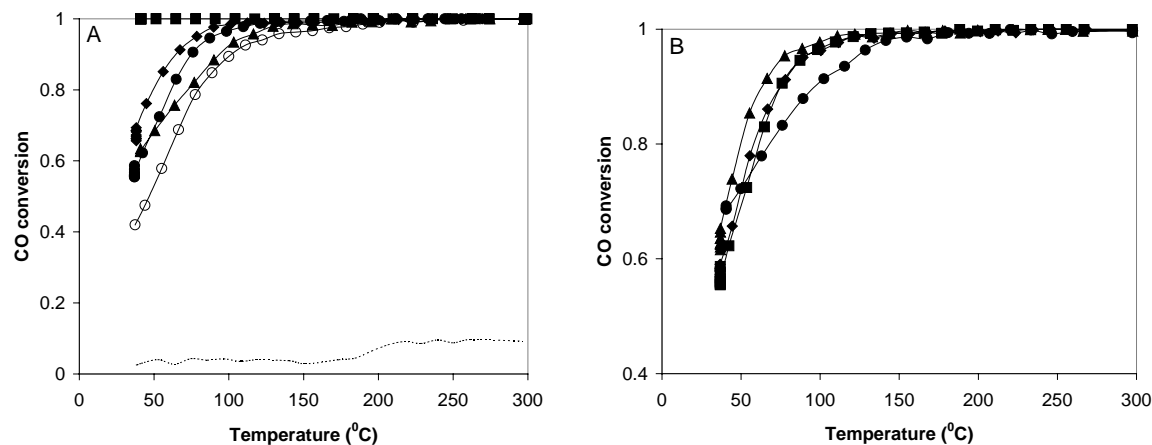


**Figure 9.2:** CO conversion vs. temperature over Au/BaO/Al<sub>2</sub>O<sub>3</sub> (■), Au/Rb<sub>2</sub>O/Al<sub>2</sub>O<sub>3</sub> (◆), Au/Li<sub>2</sub>O/Al<sub>2</sub>O<sub>3</sub> (●), Au/Al<sub>2</sub>O<sub>3</sub> (O<sub>2</sub>/300/H<sub>2</sub>) (▲), Li<sub>2</sub>O/Au/Al<sub>2</sub>O<sub>3</sub> (○), Li<sub>2</sub>O/Al<sub>2</sub>O<sub>3</sub> (--) (A); Au/Li<sub>2</sub>O/Al<sub>2</sub>O<sub>3</sub> (Li:Al = 1:30) (▲), Au/Li<sub>2</sub>O/Al<sub>2</sub>O<sub>3</sub> (Li:Al = 1:5) (◆), Au/Li<sub>2</sub>O/Al<sub>2</sub>O<sub>3</sub> (Li:Al = 1:15) (■), Au/Li<sub>2</sub>O/Al<sub>2</sub>O<sub>3</sub> (Li:Al = 1:1) (●) (B).

**Table 9.2:** T<sub>95%</sub>, the conversion at 70<sup>0</sup>C (X<sub>70</sub>), the specific reaction rate, *r*, the average size of the gold particles for the fresh (d<sub>Au</sub><sup>a</sup>) and used (d<sub>Au</sub><sup>b</sup>) Au-based catalysts (XRD).

Catalyst	d <sub>Au</sub> <sup>a</sup> (nm)	d <sub>Au</sub> <sup>b</sup> (nm)	T <sub>95%</sub> ( <sup>0</sup> C)	X <sub>70</sub>	<i>r</i> x 10 <sup>3</sup> (moles CO moles <sup>-1</sup> Au s <sup>-1</sup> )
Au/Al <sub>2</sub> O <sub>3</sub>	3.0±0.3	3.0±0.2	112	0.78	5.5±0.1
Au/Li <sub>2</sub> O/Al <sub>2</sub> O <sub>3</sub> (Li:Al=1:15)	3.4±0.1	3.2±0.1	89	0.87	6.9±0.1
Au/Li <sub>2</sub> O/Al <sub>2</sub> O <sub>3</sub> (Li:Al=1:30)	<3.0	3.0±0.1	77	0.93	7.4±0.1
Au/Li <sub>2</sub> O/Al <sub>2</sub> O <sub>3</sub> (Li:Al=1:5)	4.3±0.2	4.7±0.3	90	0.88	7.2±0.2
Au/Li <sub>2</sub> O/Al <sub>2</sub> O <sub>3</sub> (Li:Al=1:1)	<3.0	3.1±0.3	123	0.8	4.9±0.1
Li <sub>2</sub> O/Au/Al <sub>2</sub> O <sub>3</sub> (Li:Al=1:15)	3.8±0.1	3.6±0.2	127	0.71	5.9±0.1
Au/Rb <sub>2</sub> O/Al <sub>2</sub> O <sub>3</sub>	<3.0	<3.0	78	0.92	8.9±0.1
Au/BaO/Al <sub>2</sub> O <sub>3</sub>	<3.0	<3.0	<25	1	7.6±0.1*

\* this value corresponds to 100% CO conversion.

The loading of Li<sub>2</sub>O does not have a significant influence on the size of the Au particles (see Table 9.2). The best result is obtained for an atomic ratio Li:Al = 1:30 (1 wt% Li<sub>2</sub>O). A larger amount of Li<sub>2</sub>O (22 wt-%, atomic ratio Li:Al = 1:1) causes only a small increase in the catalytic performance. In fact, the catalyst with the highest Li<sub>2</sub>O concentration shows a lower

$r$  compared with the unpromoted Au/Al<sub>2</sub>O<sub>3</sub>. A summary of all the data concerning the promoting effect of various alkali (earth) metal oxides on the catalytic performance of Au/Al<sub>2</sub>O<sub>3</sub> is presented in Table 9.2.

In spite of its slightly lower  $r$ -value Au/BaO/Al<sub>2</sub>O<sub>3</sub> shows the lowest T<sub>95%</sub>. Au sintering was not observed using XRD.

### Multicomponent Au-based catalysts

Reports concerning the catalytic performance of Au/Al<sub>2</sub>O<sub>3</sub> promoted with various metal oxides for CO oxidation are rather scarce. However, it was reported that TMO such as MnO<sub>x</sub> and FeO<sub>x</sub> are efficient promoters for Au/Al<sub>2</sub>O<sub>3</sub> [15, 18]. Most of the papers discuss the catalytic activity of Au-based catalysts as a function of various supports such as TiO<sub>2</sub>, MgO, CO<sub>3</sub>O<sub>4</sub>, MnO<sub>x</sub>, Fe<sub>2</sub>O<sub>3</sub>, ZrO<sub>2</sub> [18-20].

Figs. 9.3A-B show the catalytic performance of various Au-based catalysts in terms of CO conversion versus temperature. The bare supports showed extremely low catalytic activity under these reaction conditions.

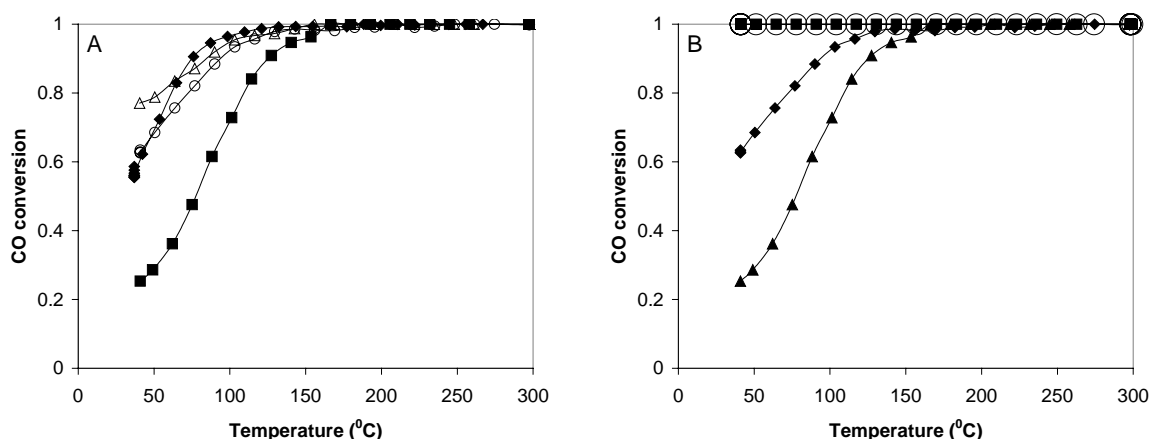


**Figure 9.3:** CO conversion vs. temperature over Au/Al<sub>2</sub>O<sub>3</sub> (○), Au/CeO<sub>x</sub>/Al<sub>2</sub>O<sub>3</sub> (■), Au/Li<sub>2</sub>O/CeO<sub>x</sub>/Al<sub>2</sub>O<sub>3</sub> (Δ), Au/Li<sub>2</sub>O/Al<sub>2</sub>O<sub>3</sub> (◇) (A); Au/BaO/CeO<sub>x</sub>/Al<sub>2</sub>O<sub>3</sub> (■), Au/BaO/Al<sub>2</sub>O<sub>3</sub> (○), Au/Al<sub>2</sub>O<sub>3</sub> (◇), Au/CeO<sub>x</sub>/Al<sub>2</sub>O<sub>3</sub> (▲) (B).

The results presented in Fig. 9.3A and Table 9.3 illustrate the large synergistic effects obtained if Li<sub>2</sub>O and CeO<sub>x</sub> are both added to Au/Al<sub>2</sub>O<sub>3</sub>. The multicomponent Au/Li<sub>2</sub>O/CeO<sub>x</sub>/Al<sub>2</sub>O<sub>3</sub> is particularly active in the low temperature range. According to the results displayed in Fig. 9.3B and Table 9.3, the most active catalysts contain BaO, either alone or in combination with ceria and full conversion of CO is reached already at RT. A large synergistic effect is also obtained if CeO<sub>x</sub> is combined with MgO.

A summary of the T<sub>95%</sub>, X<sub>70</sub>, the specific reaction rate,  $r$ , (70<sup>0</sup>C) and the variation in the Au particle size before ( $d_{Au}^a$ ) and after reaction ( $d_{Au}^b$ ) is presented in Table 9.3.

**Table 9.3:**  $T_{95\%}$ , the conversion at 70°C,  $X_{70}$ , the specific reaction rate,  $r$ , the average size of the gold particles for the fresh ( $d_{Au}^a$ ) and used ( $d_{Au}^b$ ) multicomponent Au-based catalysts (XRD).

Catalyst	$d_{Au}^a$ (nm)	$d_{Au}^b$ (nm)	$T_{95\%}$ (°C)	$X_{70}$	$r \times 10^3$ (moles CO moles <sup>-1</sup> Au s <sup>-1</sup> )
Au/Al <sub>2</sub> O <sub>3</sub>	3.0±0.3	3.0±0.2	112	0.78	5.5±0.1
Au/BaO/CeO <sub>x</sub> /Al <sub>2</sub> O <sub>3</sub>	<3.0	<3.0	<25	1	8.1±0.2 <sup>c</sup>
Au/Li <sub>2</sub> O/O/CeO <sub>x</sub> /Al <sub>2</sub> O <sub>3</sub>	<3.0	<3.0	100	0.85	8.0±0.1
Au/Rb <sub>2</sub> O/O/CeO <sub>x</sub> /Al <sub>2</sub> O <sub>3</sub>	3.1±0.2	3.3±0.1	152	0.63	5.7±0.1
Au/MgO/CeO <sub>x</sub> /Al <sub>2</sub> O <sub>3</sub>	<3.0	<3.0	<25	1	10.8±0.1
Li <sub>2</sub> O/CeO <sub>x</sub> /Au/Al <sub>2</sub> O <sub>3</sub>	3.9±0.1	4.8±0.2	141	0.54	5.5±0.1
Au/CuO/CeO <sub>x</sub> /Al <sub>2</sub> O <sub>3</sub>	16.8±0.1	18.1±0.1	128	0.58	3.3±0.1
Au/CeO <sub>x</sub> /Al <sub>2</sub> O <sub>3</sub>	3.4±0.3	3.5±0.2	145	0.43	5.0±0.2

<sup>c</sup> this value corresponds to 100% CO conversion

If Li<sub>2</sub>O and CeO<sub>x</sub> are added after Au is deposited on Al<sub>2</sub>O<sub>3</sub>, the catalytic performance is decreased, compared with the catalytic activity of Au/Li<sub>2</sub>O/CeO<sub>x</sub>/Al<sub>2</sub>O<sub>3</sub>. The average gold particle size for Li<sub>2</sub>O/CeO<sub>x</sub>/Au/Al<sub>2</sub>O<sub>3</sub> is around 3.8 nm (XRD), most probably because the small Au crystallites were weakly attached to the bare alumina. Moreover, subsequent addition of Li<sub>2</sub>O and CeO<sub>x</sub> probably blocks some of the Au active sites. Similar results were obtained when Li<sub>2</sub>O was added prior or after Au deposition on Al<sub>2</sub>O<sub>3</sub> (Table 9.2).

#### Variation of the catalytic performance within Group IB (Cu, Ag, Au)

Copper oxide is known as an active catalyst for oxidation reactions ([21-23] and Chapters 5-7). For CO oxidation, relatively high temperatures, above 200°C, are required for CuO-based catalysts [24, 25]. Regarding the ability of Ag as a catalyst in oxidation reactions, its unique property to transform ethylene to ethylene oxide is well known. On the other hand there are only a few papers dealing with CO oxidation over Ag (e.g. [26, 27]). However, it was reported that the catalytic performance of Au powder in CO oxidation is drastically affected by the presence of Ag [28].

The performance in CO oxidation of Ag-, CuO-, Au- or combinations of them is presented in Fig. 9.4. The most realistic comparison of the catalytic performance of these samples is based on the variation of the specific reaction rate  $r$ . The XRD results indicate that Ag is mainly in its metallic form, whereas Cu is present as CuO. The corresponding results are summarized in Table 9.4.

The most active catalyst, according to the results presented in Fig. 9.4 and Table 9.4 is Au/Al<sub>2</sub>O<sub>3</sub> (●). Although the concentration of Ag in Ag/Al<sub>2</sub>O<sub>3</sub> (◆) is 4 times larger than the corresponding Au loading in Au/Al<sub>2</sub>O<sub>3</sub>, the former is less active. The same holds for CuO/Al<sub>2</sub>O<sub>3</sub> (▲), which shows a CO conversion that is shifted to even higher temperatures, compared with Au/Al<sub>2</sub>O<sub>3</sub> or Ag/Al<sub>2</sub>O<sub>3</sub>.

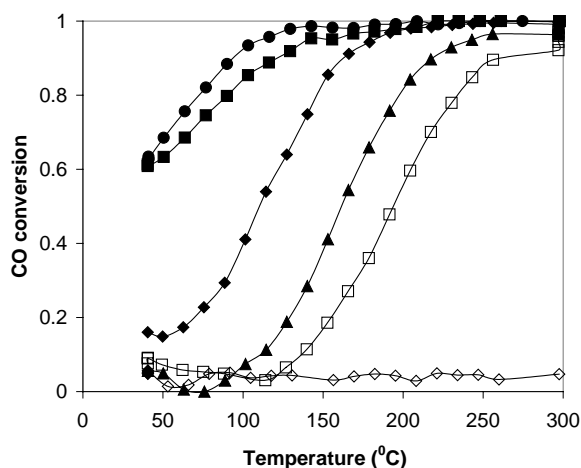


**Figure 9.4:** CO conversion vs. temperature over Au/Al<sub>2</sub>O<sub>3</sub> (●), Au/CuO/Al<sub>2</sub>O<sub>3</sub> (■), Ag/Al<sub>2</sub>O<sub>3</sub> (◆), CuO/Al<sub>2</sub>O<sub>3</sub> (▲), Au/Ag/CuO/Al<sub>2</sub>O<sub>3</sub> (□), Au/Ag/Al<sub>2</sub>O<sub>3</sub> (◇).

**Table 9.4:** T<sub>95%</sub>, the conversion at 70°C, the specific reaction rate, *r*, the average size of Au or Ag particles for the fresh (d<sub>M</sub><sup>a</sup>) and used (d<sub>M</sub><sup>b</sup>) catalysts (XRD).

Catalyst	d <sub>M</sub> <sup>a</sup> (nm)	d <sub>M</sub> <sup>b</sup> (nm)	T <sub>95%</sub> (°C)	X <sub>70</sub>	<i>r</i> × 10 <sup>3</sup> (moles CO moles <sup>-1</sup> M <sub>1</sub> s <sup>-1</sup> )
Au/Al <sub>2</sub> O <sub>3</sub>	3.0±0.3	3.0±0.2	112	0.78	5.5±0.1
Ag/Al <sub>2</sub> O <sub>3</sub>	<3.0	<3.0	181	0.2	0.5±0.1
CuO/Al <sub>2</sub> O <sub>3</sub>	–	–	245	0.01	~0
Au/CuO/Al <sub>2</sub> O <sub>3</sub>	<3.0	<3.0	143	0.72	1.3±0.1
Au/Ag/Al <sub>2</sub> O <sub>3</sub>	25.2±1.5	29.9±1.5	>300	0.02	~0
Au/Ag/CuO/Al <sub>2</sub> O <sub>3</sub>	26.7±0.4	28.3±0.5	300	0.05	0.4±0.1

M = Au, Ag; M<sub>1</sub>: Au, Ag, Cu.

Au/CuO/Al<sub>2</sub>O<sub>3</sub> and CuO/Al<sub>2</sub>O<sub>3</sub> were studied in more detail and the results are presented in Fig. 9.5A-B.

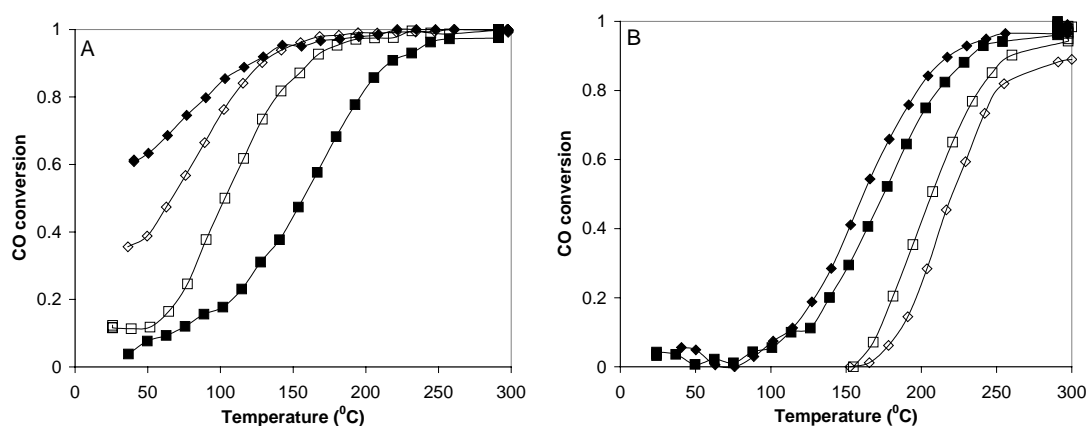


**Figure 9.5:** CO conversion vs. temperature over Au/CuO/Al<sub>2</sub>O<sub>3</sub>: #h1/H<sub>2</sub> (■), #h2/H<sub>2</sub> (◆), #h1/O<sub>2</sub> (□), #h2/O<sub>2</sub> (◇) (A); CuO/Al<sub>2</sub>O<sub>3</sub>: #h1/H<sub>2</sub> (■), #h2/H<sub>2</sub> (◆), #h1/O<sub>2</sub> (□), #h2/O<sub>2</sub> (◇) (B).

As illustrated in Fig. 9.5A, a large difference exists between the first heating branch and the second one. The difference is larger if the catalyst was first treated in hydrogen, prior to the reaction, than under  $O_2$ . The second heating branch is always shifted to significantly lower temperatures.  $CuO/Al_2O_3$  shows slightly different behaviour. Reductive pretreatment increases the performance, but the difference between different cycles is smaller compared with  $Au/CuO/Al_2O_3$ . In addition, some deactivation of  $CuO/Al_2O_3$  is found after the first heating branch if the catalyst was treated in oxygen prior the reaction test.  $Au/CuO/Al_2O_3$  is activated after the first heating run and this makes the second heating more active.

### 9.3.2 Low-temperature CO oxidation in the presence of hydrogen (PROX)

#### Unpromoted $Au/Al_2O_3$

Fig. 9.6 shows the conversion of CO and  $O_2$  and the selectivity to  $CO_2$  (second heating) over  $Au/Al_2O_3$  during selective oxidation of CO in the presence of  $H_2$  by using a ratio  $CO:O_2 = 2:1$  ( $\lambda = 1$ ) and a hydrogen rich feed (70 vol%  $H_2$ ). The catalyst was calcined in  $O_2$  at  $200^\circ C$  followed by an *in-situ* reductive treatment at the same temperature.

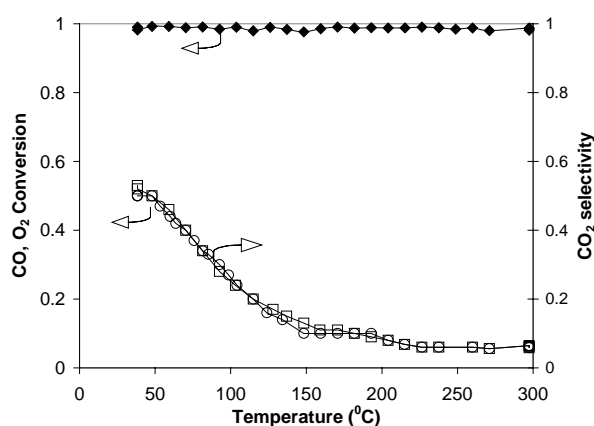


**Figure 9.6:**  $CO$  (□) and  $O_2$  (◆) conversion and  $CO_2$  selectivity (○) over  $Au/Al_2O_3$   $O_2/200/H_2/200$ . Reaction conditions: 70 vol%  $H_2$ ,  $\lambda = 1$ .

Similar patterns of conversion and selectivity have been found for the other pretreatments of the  $Au/Al_2O_3$  catalyst. Under these reaction conditions the consumption of  $O_2$  is (nearly) 100%, whereas the maximum CO conversion is around 52%. The conversion reached its maximum in the low temperature range; a further increase in the reaction temperature results in a drop in CO conversion. Around  $150^\circ C$  the conversion of CO is around 11% and it remains at this level in the higher temperature range. Full  $O_2$  conversion in the whole temperature range implies that the rate of  $H_2$  oxidation is rather significant even in the low-temperature range and above  $150^\circ C$  it becomes the main reaction. However, for practical applications the conversion of CO should be close to 100%, even at the sacrifice of some  $H_2$ , and that may be obtained by using more  $O_2$  in the gas stream (i.e.  $\lambda > 1$ ). The measurements presented in this chapter were focused on examining the effect of various types of additives on PROX and only results obtained for  $\lambda = 1$  will be discussed. Regarding the selectivity to

CO<sub>2</sub>, this is nearly the CO conversion divided by  $\lambda$  [15]. For  $\lambda = 1$ , the CO conversion and the selectivity to CO<sub>2</sub> are equal. This is also illustrated in the Fig. 9.6.

Similar experiments as those performed for CO oxidation were carried out for the PROX reaction. Fig. 9.7A shows the catalytic behaviour of Au/Al<sub>2</sub>O<sub>3</sub> subjected to calcination at different temperatures (150, 200, 300 or 500°C), followed by a treatment in H<sub>2</sub> or He. The results shown in Fig. 9.7B correspond to Au/Al<sub>2</sub>O<sub>3</sub> subjected to a H<sub>2</sub> treatment at different temperatures, followed by various *in-situ* treatments. A summary of all relevant data is presented in Table 9.5.

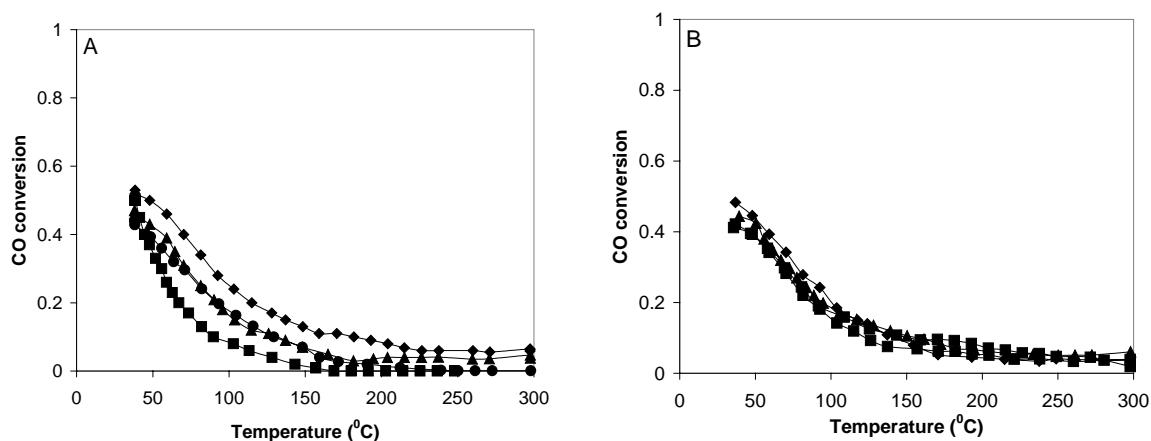


**Figure 9.7:** CO conversion vs. temperature over calcined (A) and reduced (B) Au/Al<sub>2</sub>O<sub>3</sub>. 200/H<sub>2</sub>/200 (◆), 300/H<sub>2</sub>/300 (▲), 500/H<sub>2</sub>/300 (●), 150/He/150 (■) (A); 200/He/200 (◆), 300/He/300 (▲), 500/He/300 (●), 150/H<sub>2</sub>/150 (■) (B). Reactant ratio: 70 vol% H<sub>2</sub>,  $\lambda = 1$ .

**Table 9.5:** The CO conversion at 70°C, X<sub>70</sub>, the specific reaction rate,  $r$ , (70°C), the average size of the gold particles for the fresh ( $d_{Au}^a$ ) and used ( $d_{Au}^b$ ) Au/Al<sub>2</sub>O<sub>3</sub> (XRD).

Treatment	$d_{Au}^a$ (nm)	$d_{Au}^b$ (nm)	X <sub>70</sub>	$r \times 10^3$ (moles CO moles <sup>-1</sup> Au s <sup>-1</sup> )
O <sub>2</sub> /150/H <sub>2</sub>	<3.0	3.2±0.1	0.21	1.1±0.1
O <sub>2</sub> /200/H <sub>2</sub>	3.0±0.2	3.1±0.2	0.4	2.1±0.1
O <sub>2</sub> /300/H <sub>2</sub>	3.0±0.3	3.2±0.1	0.31	1.5±0.1
O <sub>2</sub> /500/H <sub>2</sub>	4.3±0.3	4.6±0.5	0.28	1.5±0.1
H <sub>2</sub> /150/He	<3.0	3.2±0.4	0.29	1.6±0.1
H <sub>2</sub> /200/H <sub>2</sub>	<3.0	<3.0	0.42	2.3±0.2
H <sub>2</sub> /200/He	<3.0	<3.0	0.34	1.8±0.1
H <sub>2</sub> /300/He	3.3±0.2	3.3±0.2	0.30	1.5±0.1
H <sub>2</sub> /500/He	4.8±0.1	4.9±0.3	0.28	1.7±0.1

Among the samples subjected to a treatment in oxygen, the best result is obtained using a thermal treatment that does not exceed 200°C. The next best catalytic performance is obtained after a treatment at 300, followed by 500 and 150°C. This sequence is roughly the same as found for CO oxidation in the absence of hydrogen (section 9.3.1). The differences



between all the catalysts first treated in H<sub>2</sub> are very small, the most active catalyst being obtained using a H<sub>2</sub> treatment at 200°C followed by post-treatment in H<sub>2</sub>. If the overall effect of O<sub>2</sub> versus H<sub>2</sub> treatment is compared, H<sub>2</sub> produces catalysts slightly more active than heating in O<sub>2</sub>, although the differences are small. Compared with CO oxidation, the differences between different thermal treatments are much smaller for PROX.

### *Alkali (earth) metal oxides as additives*

Previously reported results show that Au/MgO/Al<sub>2</sub>O<sub>3</sub> is able to convert, under similar reaction conditions, 32% of CO to CO<sub>2</sub> (70°C) [15]. The results presented in the previous section demonstrated that the addition of alkali (earth) metal oxides to Au/Al<sub>2</sub>O<sub>3</sub> is truly beneficial for CO oxidation. The effect of various alkali (earth) metal oxides on the catalytic activity in the second heating stage of Au/Al<sub>2</sub>O<sub>3</sub> in PROX is presented in Fig. 9.8A. Subsequent heating-cooling cycles resemble the behaviour shown for the second heating branch (#h2). The influence of the Li<sub>2</sub>O loading on the catalytic performance of the unpromoted Au/Al<sub>2</sub>O<sub>3</sub> is shown in Fig. 9.8B. The catalytic activity of the supports was found negligible under the reaction conditions used in this study.

Similar to the results shown in Figs. 9.7A-B, the maximum CO conversion is reached at low temperatures and by increasing the temperature, the CO conversion drops. A summary of the CO conversion at 70°C, X<sub>70</sub>, the specific reaction rate, *r*, calculated at 70°C and the Au particle size before (d<sub>Au</sub><sup>a</sup>) and after (d<sub>Au</sub><sup>b</sup>) the PROX reaction is presented in Table 9.6.

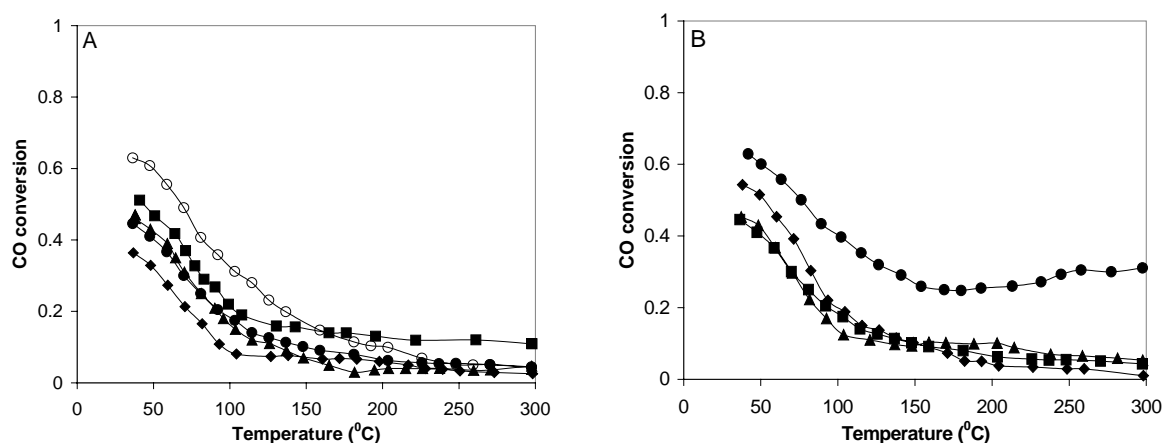


**Figure 9.8:** CO conversion vs. temperature over Au/BaO/Al<sub>2</sub>O<sub>3</sub> (■), Au/Rb<sub>2</sub>O/Al<sub>2</sub>O<sub>3</sub> (◆), Au/Li<sub>2</sub>O/Al<sub>2</sub>O<sub>3</sub> (●), Au/Al<sub>2</sub>O<sub>3</sub> (▲), Li<sub>2</sub>O/Au/Al<sub>2</sub>O<sub>3</sub> (○) (A); Au/Li<sub>2</sub>O/Al<sub>2</sub>O<sub>3</sub> (Li:Al = 1:30) (▲), Au/Li<sub>2</sub>O/Al<sub>2</sub>O<sub>3</sub> (Li:Al = 1:5) (◆), Au/Li<sub>2</sub>O/Al<sub>2</sub>O<sub>3</sub> (Li:Al = 1:15) (■), Au/Li<sub>2</sub>O/Al<sub>2</sub>O<sub>3</sub> (Li:Al = 1:1) (●) (B). Reactant ratio: 70 vol% H<sub>2</sub>, λ = 1.

The most active catalyst in CO oxidation in the absence of H<sub>2</sub> (section 9.3.1) was Au/BaO/Al<sub>2</sub>O<sub>3</sub>, and the lowest activity was found for Li<sub>2</sub>O/Au/Al<sub>2</sub>O<sub>3</sub>. Among the catalysts with different Li<sub>2</sub>O loading, the best catalyst contains the least Li<sub>2</sub>O concentration. However, this catalyst was inferior to Au/BaO/Al<sub>2</sub>O<sub>3</sub> or Au/Rb<sub>2</sub>O/Al<sub>2</sub>O<sub>3</sub>. For the PROX reaction, the results are quite different. First of all, Li<sub>2</sub>O/Au/Al<sub>2</sub>O<sub>3</sub> shows the best performance among the

Au-based catalyst containing various alkali (earth) metal oxides as additives and M/Al = 1/15 (atomic ratio). The conversion of CO at RT is around 63%. The largest specific reaction rate values among the samples with different Li<sub>2</sub>O concentrations are obtained for an atomic ratio Li/Al of 1/5 and 1/1. Opposite to the results obtained for CO oxidation, Li<sub>2</sub>O/Au/Al<sub>2</sub>O<sub>3</sub> is the best catalyst among *all* alkali (earth) metal oxide-containing Au-based catalysts.

**Table 9.6:** The CO conversion at 70<sup>0</sup>C, X<sub>70</sub>, the specific reaction rate, *r*, the average size of the gold particles for the fresh (*d*<sub>Au</sub><sup>a</sup>) and used (*d*<sub>Au</sub><sup>b</sup>) Au-based catalysts (XRD).

Catalyst	<i>d</i> <sub>Au</sub> <sup>a</sup> (nm)	<i>d</i> <sub>Au</sub> <sup>b</sup> (nm)	X <sub>70</sub>	<i>r</i> x 10 <sup>3</sup> (moles CO moles <sup>-1</sup> Au s <sup>-1</sup> )
Au/Al <sub>2</sub> O <sub>3</sub>	3.0±0.3	3.2±0.1	0.31	1.5±0.1
Au/Li <sub>2</sub> O/Al <sub>2</sub> O <sub>3</sub> (Li:Al=1:15)	3.4±0.1	3.4±0.2	0.30	1.6±0.1
Au/Li <sub>2</sub> O/Al <sub>2</sub> O <sub>3</sub> (Li:Al=1:30)	<3.0	3.1±0.2	0.29	1.6±0.1
Au/Li <sub>2</sub> O/Al <sub>2</sub> O <sub>3</sub> (Li:Al=1:5)	4.3±0.2	4.6±0.1	0.39	2.3±0.2
Au/Li <sub>2</sub> O/Al <sub>2</sub> O <sub>3</sub> (Li:Al=1:1)	<3.0	3.3±0.1	0.53	2.3±0.1
Li <sub>2</sub> O/Au/Al <sub>2</sub> O <sub>3</sub> (Li:Al=1:15)	3.8±0.1	3.7±0.3	0.49	2.7±0.2
Au/Rb <sub>2</sub> O/Al <sub>2</sub> O <sub>3</sub>	<3.0	3.1±0.3	0.21	1.4±0.1
Au/BaO/Al <sub>2</sub> O <sub>3</sub>	<3.0	3.2±0.2	0.37	2.0±0.2

As previously observed for CO oxidation, the gold particles show a good stability during more than 8 hours in the reactor and sintering is not significant.

### Multicomponent Au-based catalysts

There are not many studies regarding the effect of different additives on the catalytic activity of Au/Al<sub>2</sub>O<sub>3</sub> in the PROX reaction. Most of the studies were focused on the catalytic performance of Au/Al<sub>2</sub>O<sub>3</sub>, Au/Co<sub>3</sub>O<sub>4</sub>, Au/TiO<sub>2</sub>, Au/CeO<sub>2</sub> and Au/Fe<sub>2</sub>O<sub>3</sub> [4, 29-33]. Although the results are not easy to compare due to the very different reaction conditions used, it appears that one of the most active catalysts is Au/Fe<sub>2</sub>O<sub>3</sub>, with a specific reaction rate of 3.09 x 10<sup>-5</sup> mol<sub>CO</sub> (mol<sub>Au</sub> s)<sup>-1</sup> (the reaction was carried out under hydrogen rich conditions, 75% H<sub>2</sub>, and *r* was calculated at 80<sup>0</sup>C) [4]. Regarding the effect of two different additives, it was reported that, under H<sub>2</sub>-rich conditions and λ = 1, MnO<sub>x</sub>/Au/MgO/Al<sub>2</sub>O<sub>3</sub> converted 61% of CO at 70<sup>0</sup>C [15].

The effect of the addition of two different metal oxides on the catalytic activity of Au/Al<sub>2</sub>O<sub>3</sub> in PROX is shown in Fig. 9.9. A summary of all the relevant data such as X<sub>70</sub>, *r* (70<sup>0</sup>C) and the variation of the Au particle size during the catalytic test is shown in Table 9.7.

The most active catalysts are Au/BaO/CeO<sub>x</sub>/Al<sub>2</sub>O<sub>3</sub> and Au/MgO/CeO<sub>x</sub>/Al<sub>2</sub>O<sub>3</sub>. It is interesting to note the behaviour at higher temperatures. Au/BaO/CeO<sub>x</sub>/Al<sub>2</sub>O<sub>3</sub> is able to maintain a rather high CO conversion (30%) even at 300<sup>0</sup>C. Au/MgO/CeO<sub>x</sub>/Al<sub>2</sub>O<sub>3</sub> and Li<sub>2</sub>O/CeO<sub>x</sub>/Au/Al<sub>2</sub>O<sub>3</sub> are the most active samples according to *r*. The addition of an alkali metal oxide *after* gold has been deposited on the carrier creates a highly active catalyst in PROX. The explanation may be related to either intrinsic H<sub>2</sub> oxidation activity, or to other aspects, for example carbonaceous deposition. A study of H<sub>2</sub> oxidation over these catalysts may clarify at least one of these hypotheses.

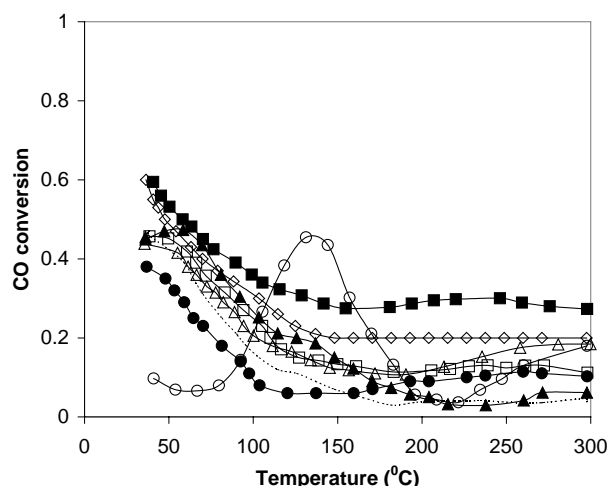


**Figure 9.9:** CO conversion vs. temperature over Au/BaO/CeO<sub>x</sub>/Al<sub>2</sub>O<sub>3</sub> (■), Au/MgO/CeO<sub>x</sub>/Al<sub>2</sub>O<sub>3</sub> (◇), Au/Li<sub>2</sub>O/CeO<sub>x</sub>/Al<sub>2</sub>O<sub>3</sub> (Δ), Au/Al<sub>2</sub>O<sub>3</sub> (---), Au/Rb<sub>2</sub>O/CeO<sub>x</sub>/Al<sub>2</sub>O<sub>3</sub> (●), Li<sub>2</sub>O/CeO<sub>x</sub>/Au/Al<sub>2</sub>O<sub>3</sub> (▲), Au/CuO/CeO<sub>x</sub>/Al<sub>2</sub>O<sub>3</sub> (○), Au/CeO<sub>x</sub>/Al<sub>2</sub>O<sub>3</sub> (□). Reactant ratio: 70 vol% H<sub>2</sub>, λ = 1.

In addition, it should be mentioned that for PROX, Au/CeO<sub>x</sub>/Al<sub>2</sub>O<sub>3</sub> is a rather active catalyst, in line with previous reports [4, 30, 31]. It was also found that at 300<sup>o</sup>, the mixed support CeO<sub>x</sub>/Al<sub>2</sub>O<sub>3</sub> itself is able to convert 50% of CO to CO<sub>2</sub>. However, for the PROX reaction the low-temperature region is of interest, where CeO<sub>x</sub>/Al<sub>2</sub>O<sub>3</sub> is completely inactive.

**Table 9.7:** CO conversion at 70<sup>o</sup>C, X<sub>70</sub>, the specific reaction rate, *r*, estimated at 70<sup>o</sup>C, the average size of the gold particles for the fresh (*d*<sub>Au</sub><sup>a</sup>) and used (*d*<sub>Au</sub><sup>b</sup>) Au-based catalysts (XRD).

Catalyst	<i>d</i> <sub>Au</sub> <sup>a</sup> (nm)	<i>d</i> <sub>Au</sub> <sup>b</sup> (nm)	X <sub>70</sub>	<i>r</i> × 10 <sup>3</sup> (moles CO moles <sup>-1</sup> Au s <sup>-1</sup> )
Au/Al <sub>2</sub> O <sub>3</sub>	3.0±0.3	3.2±0.1	0.31	1.5±0.1
Au/BaO/CeO <sub>x</sub> /Al <sub>2</sub> O <sub>3</sub>	<3.0	<3.0	0.45	2.5±0.1
Au/Li <sub>2</sub> O/O/CeO <sub>x</sub> /Al <sub>2</sub> O <sub>3</sub>	<3.0	<3.0	0.34	2.3±0.1
Au/Rb <sub>2</sub> O/O/CeO <sub>x</sub> /Al <sub>2</sub> O <sub>3</sub>	3.1±0.2	3.2±0.2	0.23	1.5±0.1
Au/MgO/CeO <sub>x</sub> /Al <sub>2</sub> O <sub>3</sub>	<3.0	<3.0	0.4	3.0±0.2
Li <sub>2</sub> O/CeO <sub>x</sub> /Au/Al <sub>2</sub> O <sub>3</sub>	3.9±0.1	4.8±0.2	0.43	3.0±0.1
Au/CuO/CeO <sub>x</sub> /Al <sub>2</sub> O <sub>3</sub>	16.8±0.1	17.5±0.4	0.07	~0
Au/CeO <sub>x</sub> /Al <sub>2</sub> O <sub>3</sub>	3.4±0.3	3.6±0.3	0.36	2.9±0.1

Among all the catalysts presented in Table 9.7, Au/CuO/CeO<sub>x</sub>/Al<sub>2</sub>O<sub>3</sub> shows a very different behaviour, compared with the other Au-based catalysts. This catalyst is inactive at low temperatures, but, by increasing the temperature, the CO conversion reaches 45% (131<sup>o</sup>C). A further increase of the T results in a lower CO conversion until a level of ~ 4%, but above 220<sup>o</sup>C, the CO conversion increases again. This unusual behaviour is most likely due to the presence of CuO, because Au/CeO<sub>x</sub>/Al<sub>2</sub>O<sub>3</sub> displays the typical behaviour of an Au-based catalyst. The activity of CuO-containing catalysts will be discussed below. Such a catalytic activity profile as that found for Au/CuO/CeO<sub>x</sub>/Al<sub>2</sub>O<sub>3</sub> was earlier reported for

Pt/Al<sub>2</sub>O<sub>3</sub> [34], Ag/Al<sub>2</sub>O<sub>3</sub> [34, 35], and CuO-CeO<sub>x</sub> catalysts [36-38]. Earlier reports showed that a CuO-CeO<sub>x</sub> catalyst is inferior to the Au-based catalysts described in this chapter [36, 38]. The reported selectivity to CO<sub>2</sub> was slightly larger than the results presented here, but under different reaction conditions ( $\lambda = 2$ ).

Sintering of the gold particles during the PROX process did not appear to be significant.

### Variation of the catalytic performance within Group IB (Cu, Ag, Au)

Fig. 9.10 compares the catalytic performance among the elements of the Group IB metals in terms of CO conversion versus temperature corresponding to the second heating branch. Table 9.8 collects all the relevant data such as  $X_{70}$ ,  $r$  (70°C) and the variation of the Au particle size during the catalytic test.

The results obtained for the PROX reaction differ rather significantly, compared with the corresponding results presented in Fig. 9.4 and Table 9.4. In CO oxidation Au/Al<sub>2</sub>O<sub>3</sub> showed the best performance, followed by Au/CuO/Al<sub>2</sub>O<sub>3</sub>, Ag/Al<sub>2</sub>O<sub>3</sub>, CuO/Al<sub>2</sub>O<sub>3</sub>, Au/Ag/CuO/Al<sub>2</sub>O<sub>3</sub> and Au/Ag/Al<sub>2</sub>O<sub>3</sub>.

In the PROX reaction, Au/Al<sub>2</sub>O<sub>3</sub> remains the best catalyst in the low-temperature range, similar to the results obtained for CO oxidation. If the reaction temperature increases, the CO conversion/CO<sub>2</sub> selectivity decreases. Ag/Al<sub>2</sub>O<sub>3</sub> shows a similar behaviour as Au/Al<sub>2</sub>O<sub>3</sub>. Its catalytic activity is rather high in the low-temperature range, but it drops upon increasing the temperature. However, the maximum CO conversion of Ag/Al<sub>2</sub>O<sub>3</sub> is shifted to higher temperatures, compared with Au/Al<sub>2</sub>O<sub>3</sub>.

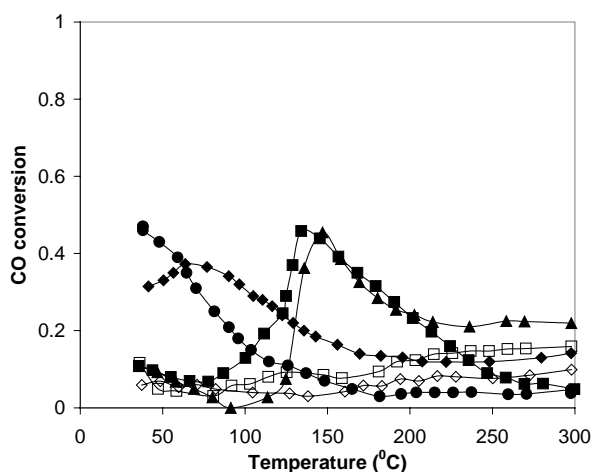


**Figure 9.10:** CO conversion vs. temperature over Au/Al<sub>2</sub>O<sub>3</sub> (●), Au/CuO/Al<sub>2</sub>O<sub>3</sub> (■), Ag/Al<sub>2</sub>O<sub>3</sub> (◆), CuO/Al<sub>2</sub>O<sub>3</sub> (▲), Au/Ag/CuO/Al<sub>2</sub>O<sub>3</sub> (□), Au/Ag/Al<sub>2</sub>O<sub>3</sub> (◇). 70 vol% H<sub>2</sub>,  $\lambda = 1$ .

A completely different behaviour is found for Au/CuO/Al<sub>2</sub>O<sub>3</sub> and CuO/Al<sub>2</sub>O<sub>3</sub> catalysts. These samples show a similar dependence of CO conversion on the temperature, as that already described for Au/CuO/CeO<sub>x</sub>/Al<sub>2</sub>O<sub>3</sub>. The CO conversion reaches its maximum at 134°C (46%) over Au/CuO/Al<sub>2</sub>O<sub>3</sub> and at 145°C (45%) over CuO/Al<sub>2</sub>O<sub>3</sub>. It is clear that all these samples strongly retain the behaviour of CuO and the presence of Au does not influence

either the general behaviour, or the temperature of maximum CO conversion. Moreover, combining Au with Ag and CuO does not create an active catalyst for the PROX process, and the same holds for Au/Ag/Al<sub>2</sub>O<sub>3</sub>. It is possible that the particle size effect is the main factor, because the samples with large Au particles (Table 9.8) are hardly active in PROX reaction.

**Table 9.8:** The CO conversion at 70<sup>0</sup>C, X<sub>70</sub>, the specific reaction rate, *r*, estimated at 70<sup>0</sup>C, the average size of the Au and Ag particles for the fresh (d<sub>M</sub><sup>a</sup>) and used (d<sub>M</sub><sup>b</sup>) catalysts (XRD).

Catalyst	d <sub>M</sub> <sup>a</sup> (nm)	d <sub>M</sub> <sup>b</sup> (nm)	X <sub>70</sub>	r x 10 <sup>3</sup> (moles CO moles <sup>-1</sup> M <sub>1</sub> s <sup>-1</sup> )
Au/Al <sub>2</sub> O <sub>3</sub>	3.0±0.3	3.2±0.1	0.31	1.5±0.1
Ag/Al <sub>2</sub> O <sub>3</sub>	<3.0	3.2±0.2	0.37	~0
CuO/Al <sub>2</sub> O <sub>3</sub>	–	–	0.05	~0
Au/CuO/Al <sub>2</sub> O <sub>3</sub>	<3.0	3.2±0.3	0.07	~0
Au/Ag/Al <sub>2</sub> O <sub>3</sub>	25.2±1.5	28.6±1.1	0.06	~0
Au/Ag/CuO/Al <sub>2</sub> O <sub>3</sub>	26.7±0.4	27.9±0.1	0.04	~0

M = Au, Ag; M<sub>1</sub>: Au, Ag, Cu.

## 9.4 Discussion

### *Catalyst activation*

The influence of the thermal treatment and the nature of the employed gas (O<sub>2</sub>, H<sub>2</sub>, or He) were studied for unpromoted Au/Al<sub>2</sub>O<sub>3</sub> catalysts for CO oxidation both in the absence and the presence of H<sub>2</sub>. It was found that the best results are obtained if the as-prepared (i.e. dried) catalyst is subjected to an O<sub>2</sub> treatment at 200<sup>0</sup>C. After a treatment in H<sub>2</sub> or O<sub>2</sub> at 200<sup>0</sup>C, presumably all the gold is transformed into Au<sup>0</sup> (TPR results support this model). Most probably, metallic Au is the species for both reactions involving CO. The next thermal treatment does not significantly influence the catalytic performance. The fact that “no pretreatment” proved to be a better choice than any other possible treatment may be connected with the presence of some adsorbed water on the surface of the catalyst. However, this is unlikely since we have shown the results corresponding to the second heating cycle, and, presumably, the amount of adsorbed water after one heating-cooling cycle is relatively small. It should be mentioned that during the first heating cycle all the samples performed slightly better than during the second one, but with no noticeable difference in CO conversion. Regarding the overall effect of the thermal treatment of the dried samples, the variation of the catalytic activity correlates to some extent with the average size of the Au particles, although not completely. Even a treatment at 500<sup>0</sup>C did not produce a severe sintering of the gold particles.

In conclusion, the metallic gold is the (major) active species during both direct and preferential CO oxidation. Unpromoted Au/Al<sub>2</sub>O<sub>3</sub> showed that, similar to Au/TiO<sub>2</sub> and Au/Co<sub>3</sub>O<sub>4</sub> [7], the optimum temperature that should be applied in order to obtain an active Au-based catalyst is 200<sup>0</sup>C.

**The effect of  $MO_x$  on the catalytic activity of Au/ $Al_2O_3$ . The active sites**

The results presented throughout this chapter show that the catalytic performance of Au/ $Al_2O_3$  is improved by using certain types of additives. The improvement was observed for both CO oxidation and PROX reactions, although the trends were different. The high catalytic performance at RT made it impossible to acquire kinetic data for the catalytic systems tested in these reactions. It follows that Au is the main active species, especially in the low temperature range. Most probably the beneficial effect of the additives can be attributed to a change of the morphology and size of the Au particles due to the addition of certain  $MO_x$  to  $Al_2O_3$ .

*Particle size effect*

An overview of the variation of  $r$  with the average Au particle size of the samples with various additives is depicted in Fig. 9.11A for CO oxidation and Fig. 9.11B for the PROX reaction.

Some differences between the behaviour of the Au-based catalysts in the two reactions are observed. Although the size of the Au particles is very important, it is not the only factor that controls the catalytic performance. The specific reaction rate varies also with the identity of the  $MO_x$ . For CO oxidation, the most efficient additives are the alkali (earth) metal oxides. For the PROX process, ceria is also efficient. It was previously reported that the presence of a  $M^{n+}$  cation that can easily change its valency is important, but that its identity is not that important for low-temperature activity [15].

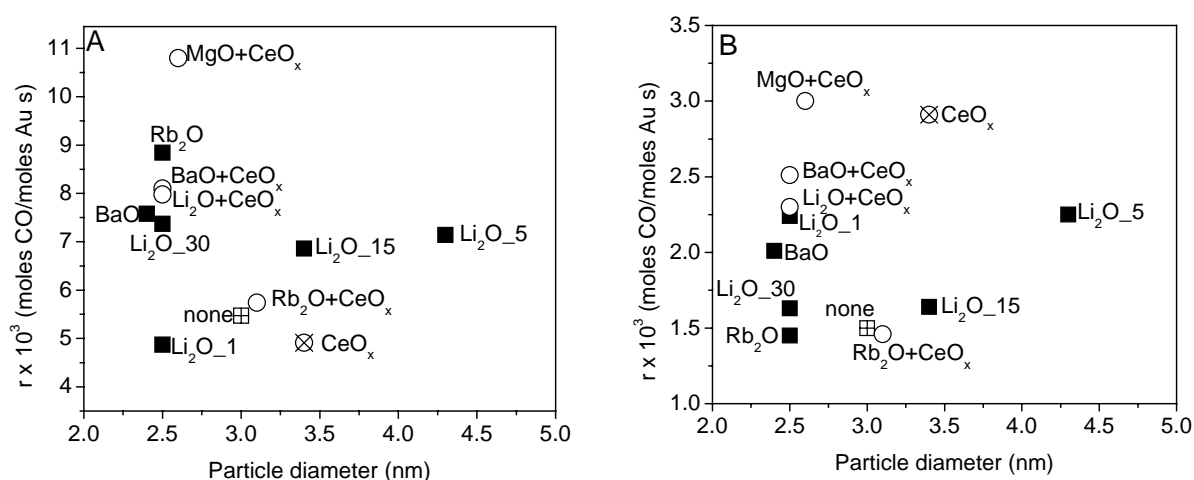


**Figure 9.11:** The variation of the specific reaction rate vs. the average Au particle size for CO+O<sub>2</sub> (A) and PROX (B) reactions.

Higher catalytic performance is obtained when BaO and Rb<sub>2</sub>O are used, compared with CuO. Ceria, for example, has a more pronounced promoter effect in the PROX reaction. Whereas the promoting effect of ceria or CuO can be explained on the basis of the redox properties of this kind of oxides (see also below), different models may rationalize the catalytic performance of the alkali (earth) metal oxides-promoting Au/ $Al_2O_3$  catalysts.

## Non-reducible metal oxides

It was already shown (*Chapter 4* and thereafter) that the main role of the alkali (earth) metal oxides is to stabilize the small gold particles during preparation and catalytic reaction (structural promoters). The data presented in this chapter indicate that there is a clear particle size effect for both reactions. This is also illustrated in Fig. 9.12A that shows how the conversion of CO (second heating cycle, CO + O<sub>2</sub>) is affected by the average Au particle size of the same catalyst composition. The results are depicted for two different Au/Rb<sub>2</sub>O/Al<sub>2</sub>O<sub>3</sub> ( $d_{\text{Au}} < 3.0$  nm and  $d_{\text{Au}} = 5.9$  nm) and Au/Rb<sub>2</sub>O/CeO<sub>x</sub>/Al<sub>2</sub>O<sub>3</sub> ( $d_{\text{Au}} = 3.4$  nm and  $d_{\text{Au}} = 7.9$  nm) catalysts. Au-based catalysts with larger Au particles are definitely less active than catalysts with smaller Au particles.

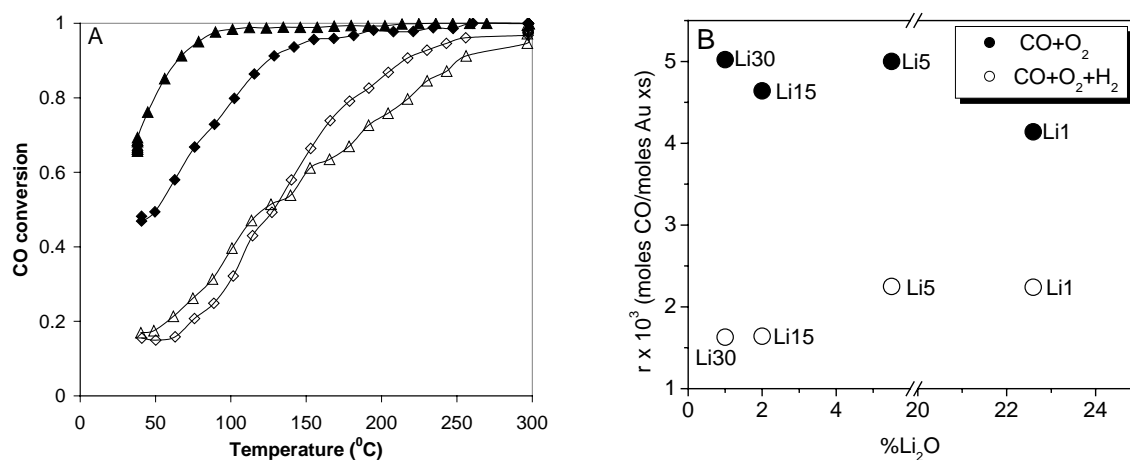


**Figure 9.12:** CO conversion vs. temperature over Au/Rb<sub>2</sub>O/Al<sub>2</sub>O<sub>3</sub>:  $d_{\text{Au}} < 3.0$  nm ( $\blacktriangle$ ),  $d_{\text{Au}} = 5.9$  nm ( $\triangle$ ), Au/Rb<sub>2</sub>O/CeO<sub>x</sub>/Al<sub>2</sub>O<sub>3</sub>:  $d_{\text{Au}} = 3.4$  nm ( $\blacklozenge$ ),  $d_{\text{Au}} = 7.9$  nm ( $\lozenge$ ), CO/O<sub>2</sub> = 2:1 (A). The specific reaction rate,  $r$ , vs. Li<sub>2</sub>O loading in CO+O<sub>2</sub> (full symbols) and CO+O<sub>2</sub>+H<sub>2</sub> (open symbols) (B).

The detailed study concerning the promoter effect of Li<sub>2</sub>O revealed that the concentration of Li<sub>2</sub>O also influences the catalytic performance of Au-based catalysts in both CO oxidation and PROX reaction. The differences in the catalytic performance are then not only related to the size of the Au particles, but also to the *concentration* of these additives and the *order* of their addition to Au/Al<sub>2</sub>O<sub>3</sub> (Figs. 9.2A and 9.8A). The variation of  $r$  with the concentration of Li<sub>2</sub>O is shown in Fig. 9.12B, for CO oxidation (filled symbols) and PROX reaction (open symbols), respectively. The results show that more Li<sub>2</sub>O is beneficial in PROX reaction, whereas in CO oxidation there is no direct correlation between  $r$  and Li<sub>2</sub>O loading.

The exact role of the alkali (earth) metal oxides on the activity of Au/Al<sub>2</sub>O<sub>3</sub> is not clear yet, although this topic has attracted a lot of research interest in the past years. It was suggested that their role would be mostly directed towards stabilization of the Au nanoparticles [15, 39, 40]. This is further connected with a relatively high abundance of low-coordinated Au sites that may be responsible for the high activity [41, 42]. Based on theoretical studies it has been suggested that in the case of Au/Mg(100), the role of MgO is

twofold. First it may provide excess electrons to the Au clusters, forming ionic bonds to the peroxy part of the proposed  $\text{CO}\cdot\text{O}_2$  reaction intermediate [43, 44]. Second, the authors suggest the interface boundary Au-MgO as most important for the reaction to proceed, and that is directly related to the Au nanoparticles. The mechanism for the catalytic reaction would then be an Eley-Rideal type [43, 44]. An earlier study showed that the presence of some alkali (Li, Na, K) metal oxides is beneficial for the catalytic activity of Au/MnO<sub>x</sub> and it was hypothesized that this promotion might be connected with the suppression of CO<sub>2</sub> retention [45]. The results presented in this chapter but also in *Chapter 5* (propene oxidation) clearly point to a structural role of these additives. In propene oxidation the results did not show any evidence that these additives interact with propene (i.e. chemical promoter-like behaviour), and, probably, the same holds for CO. Using FTIR it was found that when MO<sub>x</sub> (M: Mg, Mn, and Fe) is added to Au/Al<sub>2</sub>O<sub>3</sub>, both the C-O stretching frequency and the CO adsorption capacity are significantly affected (decreased) [15]. MgO induced the smallest effect on the adsorption capacity of Au/Al<sub>2</sub>O<sub>3</sub>, compared with MnO<sub>x</sub> and FeO<sub>x</sub>. If H<sub>2</sub> was first admitted, followed by CO and O<sub>2</sub>, such that the final reactant ratio was H<sub>2</sub>:CO:O<sub>2</sub> = 4:2:1, the CO peak positions after either oxidative or reductive pretreatment were nearly identical to those obtained for CO without H<sub>2</sub> (at RT) [15]. Thus, FTIR showed that the nature of MO<sub>x</sub> influences the adsorption of CO, and that at room temperature, H<sub>2</sub> does not appear to significantly influence the activation of CO.

On the other hand, Au-based catalysts either deposited on non-reducible metal oxides such as Al<sub>2</sub>O<sub>3</sub> (this chapter) or MgO, or doped with alkali (earth) metal oxides (this chapter) are very active in low-temperature CO oxidation. This could be due to lowering of the reaction barrier of O<sub>2</sub> adsorption by these additives. It is widely accepted that O<sub>2</sub> activation during CO oxidation is the most difficult step and the inertness of gold bulk surfaces is understood from the poor affinity toward molecular oxygen [46-49]. It was also suggested that the support material induces strain in the gold particles due to the mismatch of the lattice at the interface, an effect that is more pronounced in small gold particles than in larger ones [50]. However, this effect is more connected with the role of Au in the reaction and will be discussed in more detail below.

#### *Easily reducible metal oxides*

Opposite to the results described in previous chapters, ceria does not significantly promote the catalytic activity of Au/Al<sub>2</sub>O<sub>3</sub> for CO oxidation. Previously reported results showed that from the class of easily reducible metal oxides, FeO<sub>x</sub>, CuO and CoO<sub>x</sub> do not promote the catalytic performance of Au/Al<sub>2</sub>O<sub>3</sub>, whereas MnO<sub>x</sub> does promote it [15]. No simple correlation regarding the identity of the additives and the catalytic performance of Au-based catalysts in CO oxidation is observed. In literature different effects of ceria have been reported. Ceria has been reported not to be a suitable support for gold-based catalyst in CO oxidation at low temperature [1, 51]. On the other hand, a compound such as Au<sub>0.05</sub>[Ce(La)]<sub>0.95</sub>O<sub>x</sub> has been reported to achieve 100% CO conversion at 26<sup>0</sup>C, under excess of oxygen [24]. More recently it has been reported that nanocrystalline CeO<sub>2</sub> increases the activity of Au for CO oxidation, achieving 100% CO conversion at 10<sup>0</sup>C under excess of



oxygen [52]. Apparently, the ratio CO:O<sub>2</sub> is an important factor, since all the results that reported Au/CeO<sub>2</sub> being active are based on measurements in a large excess of oxygen in the gas stream. In line with these results Dekkers found some promoting effect of CeO<sub>2</sub> on the catalytic performance of Au/Al<sub>2</sub>O<sub>3</sub>, for a reactant ratio of CO/O<sub>2</sub> = 1 [16]. Moreover, it was reported that the catalytic performance of such a catalyst is greatly influenced by the average size of ceria particles. Their role may even be more relevant than the widely accepted role of the Au particle size [52]. It was suggested that the active oxygen may originate from ceria, rather than from the gas phase, and smaller ceria crystallites supply more active O than larger crystallites. The average size of the ceria crystallites for the Au/CeO<sub>x</sub>/Al<sub>2</sub>O<sub>3</sub> presented in Fig. 9.3A is around 9 nm (XRD) and increases to 10 nm after CO oxidation. Hence, the size of ceria particles is much larger than those used in [52], i.e. 3.3 nm. This may explain the lower activity of this catalyst.

The oxygen defects, which either improve O<sub>2</sub> trapping by the support [8, 53], or change the charge on the Au nanoparticles [54] have also been discussed in literature in connection with the active role played by the easily reducible metal oxides. It has been argued that more reactive supports may function as oxygen reservoirs [29, 55]. The dominant reaction pathway then involves the adsorption of a mobile, molecular oxygen species on the support, dissociation at the interface, and reaction on the gold particles and/or at the interface with CO adsorbed on the Au [29]. It was already demonstrated in *Chapter 5* and [56] that CeO<sub>x</sub>- and MnO<sub>x</sub>- containing Au/Al<sub>2</sub>O<sub>3</sub> catalysts are able to convert C<sub>3</sub>H<sub>6</sub> to CO<sub>2</sub> in the absence of O<sub>2</sub> in the gas stream. Most probably the reaction mechanism is of the Mars and van Krevelen type.

A similar type of experiment has been performed with CO [57]. A reactant mixture of CO (8.6 ml min<sup>-1</sup> 4 vol%CO/He) and Ar was passed over Au/Al<sub>2</sub>O<sub>3</sub>, Au/CeO<sub>x</sub>/Al<sub>2</sub>O<sub>3</sub> and their corresponding supports. The results are depicted in Fig. 9.13A in terms of CO conversion versus temperature. Au/Al<sub>2</sub>O<sub>3</sub> and  $\gamma$ -Al<sub>2</sub>O<sub>3</sub> did not show any CO conversion, as expected, since there is no available oxygen, at least at temperatures below 300<sup>0</sup>C. However, ceria-containing Au/Al<sub>2</sub>O<sub>3</sub> is able to oxidize CO molecules even in the absence of O<sub>2</sub> in the feed, with a maximum CO conversion of 40% at 300<sup>0</sup>C. The corresponding support gave only 8% conversion at 300<sup>0</sup>C.

By XRD on the fresh and used Au/CeO<sub>x</sub>/Al<sub>2</sub>O<sub>3</sub> catalysts (Fig. 9.13B) no significant change could be observed in the structure of both Au and ceria. For comparison the same figure displays the XRD results for the samples after CO oxidation. As was mentioned in *Chapter 4* and thereafter, the structure of ceria for the fresh samples corresponds to CeO<sub>2</sub> (Ce<sup>4+</sup>) and the same structure was found for the used samples. Thus, although during CO+Ar experiments, CO<sub>2</sub> is formed over all ceria-containing samples, no noticeable reduction of Ce<sup>4+</sup> to Ce<sup>3+</sup> due to the presence of CO was noticed. Similar findings were reported if CO was replaced by C<sub>3</sub>H<sub>6</sub> [58]. It is suggested that only the near surface oxygen atoms, known as highly mobile species, play an active role in the CO oxidation and the temperature and reaction conditions used were not sufficiently high to convert CeO<sub>2</sub> into Ce<sub>2</sub>O<sub>3</sub>.

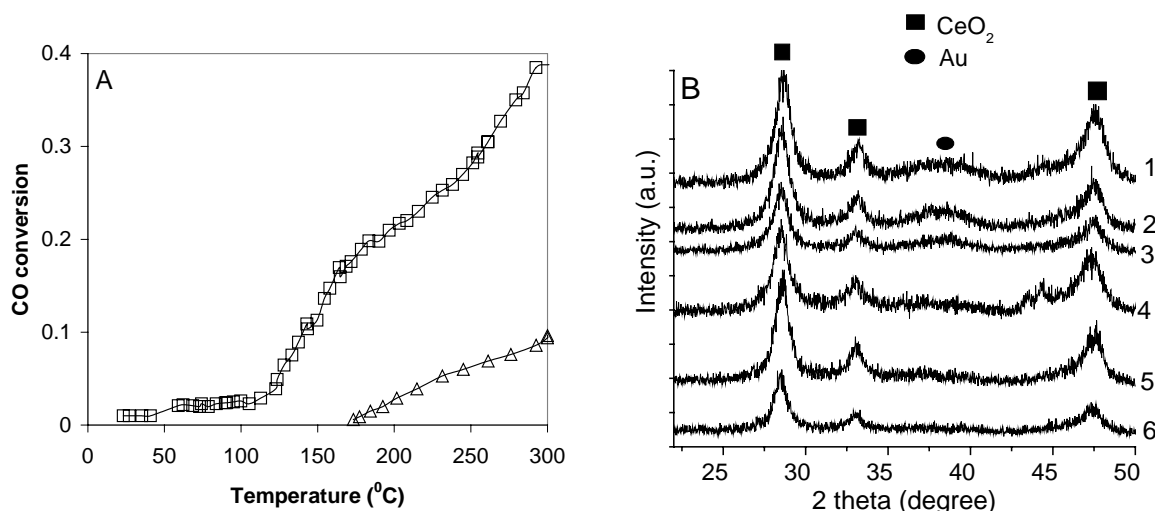


**Figure 9.13:** CO oxidation in the absence of O<sub>2</sub> over Au/CeO<sub>x</sub>/Al<sub>2</sub>O<sub>3</sub> (□) and CeO<sub>x</sub>/Al<sub>2</sub>O<sub>3</sub> (Δ) during co-feeding of 30 ml min<sup>-1</sup> CO+Ar (A). XRD patterns of Au/CeO<sub>x</sub>/Al<sub>2</sub>O<sub>3</sub> fresh (1) and used (2) (CO+O<sub>2</sub>), (CO+Ar) (3), CeO<sub>x</sub>/Al<sub>2</sub>O<sub>3</sub> fresh (4), and used (CO+O<sub>2</sub>) (5), (6) (CO+Ar) (B). The square symbols correspond to CeO<sub>2</sub> and the circle symbols correspond to Au.

Thus, CO is oxidized on Au/CeO<sub>x</sub>/Al<sub>2</sub>O<sub>3</sub> by the highly mobile oxygen of ceria. However, ceria alone is not able to oxidize CO to an important extent. Hence, gold and ceria are both needed for high activity. Au is most probably involved in CO activation, although it may also influence the amount of available oxygen during reaction. The concentration of low coordinated gold atoms, reported to adsorb CO and O<sub>2</sub> much better than Au(111) [59], depends on both the size and the shape of the particles [41]. On the other hand, a stronger Au-ceria interaction, enhanced by the oxygen vacancies of CeO<sub>2</sub>, improves the catalytic activity in CO oxidation. These results show that the reaction mechanism involves the active participation of the oxygen of ceria through a Mars and van Krevelen type of mechanism and that Au is required to activate CO.

#### *Variation of the catalytic activity within Group IB*

The results presented in this chapter showed that a relatively large difference in the catalytic behaviour exists among Group IB metals. Based on the available results (i.e. Figs. 9.4 and 9.5A-B), several conclusions can be drawn:

a) Apparently there is a particle size effect involved among the following samples: Au/Al<sub>2</sub>O<sub>3</sub>, Ag/Al<sub>2</sub>O<sub>3</sub>, Au/Ag/Al<sub>2</sub>O<sub>3</sub> and Au/Ag/CuO/Al<sub>2</sub>O<sub>3</sub>. Catalysts with smaller particles (Au or Ag) are more active than those with larger particles. However, the differences found upon addition of, for example, Au to Ag/Al<sub>2</sub>O<sub>3</sub>, or Au to Ag/CuO/Al<sub>2</sub>O<sub>3</sub> might not only be connected to a particle size effect; other factors may contribute to the catalytic performance as well. For example, it is possible that some intermetallic compound between Au and Ag and/or CuO is formed during the preparation steps. A more detailed study of the structure of these Au-Ag-CuO- containing catalysts may help to understand the differences in the catalytic behaviour.

b) The variation of the specific reaction rate,  $r$ , calculated at 70<sup>0</sup>C, suggests that CuO/Al<sub>2</sub>O<sub>3</sub> is the least active sample, followed by Ag/Al<sub>2</sub>O<sub>3</sub> and Au/Al<sub>2</sub>O<sub>3</sub>.

c) Although Ag/Al<sub>2</sub>O<sub>3</sub> shows some activity in CO oxidation, its catalytic performance is inferior to Au/Al<sub>2</sub>O<sub>3</sub>. Moreover, these results show that Au/Ag/Al<sub>2</sub>O<sub>3</sub> is completely inactive. This might partly be due to the very large Au particles formed during the preparation. Nevertheless, these results prove that the catalytic activity of Au/Al<sub>2</sub>O<sub>3</sub> comes *only* from Au and that Ag (as impurity or as additive), does not contribute to the observed catalytic activity of Au.

The differences observed in the catalytic performance of Au/CuO/Al<sub>2</sub>O<sub>3</sub> and CuO/Al<sub>2</sub>O<sub>3</sub> as a result of reductive or oxidative pretreatment (Figs. 9.5A-B) may be rationalized if it is considered that partly reduced “CuO” catalyst may be more active than CuO or Cu<sup>2+</sup>. H<sub>2</sub> is a stronger reductant than a mixture of CO and O<sub>2</sub>. After H<sub>2</sub>-treatment the catalyst is most probably in a fully reduced state, as is also shown from TPR results presented in *Chapter 4*. This implies that during the first heating cycle, the surface of Au/CuO/Al<sub>2</sub>O<sub>3</sub> is less involved in converting CO to CO<sub>2</sub> and the Cu catalyst becomes oxidized. Most likely this process takes place only at the near-surface layers. This is further supported by the results obtained for the preoxidized Au/CuO/Al<sub>2</sub>O<sub>3</sub>, which shows the same sequence, but a slightly lower activity, compared with a catalyst following a reductive pretreatment. These data may suggest that partly oxidized Cu, possibly in the form of Cu<sup>+</sup> is more active than either Cu<sup>0</sup> or Cu<sup>2+</sup>. This conclusion is in line with previously reported results [25].

The slightly different behaviour found for CuO/Al<sub>2</sub>O<sub>3</sub> that was subjected to an oxidative pretreatment may be due to a redispersion of copper surface atoms. As a result, the catalyst performed slightly better during heating #1. However, an oxidative treatment prior to the reaction is less efficient, compared with a reductive one. The “redispersion” phenomenon may result in the formation of a surface-spinel, viz. CuAl<sub>2</sub>O<sub>4</sub>, and it is probably hindered in the presence of Au. It is known that the reactivity of this spinel is lower than that of CuO/Al<sub>2</sub>O<sub>3</sub> [25], but direct evidence for this assumption is missing at this point. These results indicate that (i) the pretreatment may have a great influence on the catalytic activity of CuO-containing Au/Al<sub>2</sub>O<sub>3</sub>, (ii) that Cu<sup>δ+</sup> (1 ≤ δ < 2) may be more efficient than Cu<sup>2+</sup> or Cu<sup>0</sup> and, (iii) the presence of Au is crucial to obtain good activity.

Another important issue is the effect of moisture on the catalytic activity in CO oxidation. The effect of water was reported to be either beneficial [2, 18] or detrimental [60, 61]. Haruta and co-workers [62] and Kung and co-workers [6, 63] have reasoned that CO oxidation by water-derived species such as hydroxyl is a more competitive mechanism based on the often observed beneficial effect of moisture on reaction rates. The gases employed in the current study were used without any further purification and it is possible that some traces (*ppm* range) of water are still present.

## **Reaction mechanism**

### **CO oxidation**

As already pointed out, CO oxidation is currently studied by many researchers and many models have been suggested to explain the unexpected behaviour of various Au-based catalysts. This section is not aimed to review all the existing published results. A detailed description of all these aspects can be found in *Chapters 1-2* and also in [1, 15, 64, 65]. However, it is generally accepted that CO adsorption takes place on Au [66, 67] or at the Au-support interface [68, 69]. Moreover, based on DFT calculations, it was reported that the availability of many low-coordinated Au atoms, with an increased number of steps and kinks, accommodated by the defects of the support, is most important to obtain an active Au-based catalyst [41, 42, 50].

The main issue remains the activation of oxygen. Recently, DFT calculations showed that O<sub>2</sub> can adsorb at the Au-support interface, but the dissociation of O<sub>2</sub> cannot occur at low temperatures [70]. It was proposed that the reaction occurs on Au steps via a two-step mechanism involving reaction between CO adsorbed on Au defects and O<sub>2</sub> accommodated at the Au-support interface [70].

Other mechanisms have also been discussed in literature, but based on all relevant data reported and on the results presented in this chapter, it is concluded that CO is adsorbed on Au or at the Au-support interface and reacts with the oxygen, most probably at the interface. This mechanism would be valid mainly for Au/Al<sub>2</sub>O<sub>3</sub> and alkali (earth) metal oxide promoted-Au/Al<sub>2</sub>O<sub>3</sub>. If a reducible metal oxide is used as additive, the activation of O<sub>2</sub> is facilitated. In addition, it is possible that various pathways are active simultaneously, eventually in direct relationship with reaction temperature and/or experimental factors such as H<sub>2</sub>O, flow rate, etc.

### **PROX**

The differences found in the catalytic activity for the CO oxidation and the PROX reaction are certainly related to the absence/presence of hydrogen in the gas stream. A detailed study of H<sub>2</sub> oxidation over these catalysts should clarify these differences.

It was reported that in the presence of hydrogen (under hydrogen-rich conditions and at  $\lambda = 2$ ), a boost in CO conversion is observed on model catalysts such as Au/Al<sub>2</sub>O<sub>3</sub>, Au/ZrO<sub>2</sub> and Au/TiO<sub>2</sub> [71]. The extent of this boost depends on the nature of the support. However, the results reported in this chapter do not point to any boost in CO conversion after H<sub>2</sub> addition. In fact the effect is negative. This opposite behaviour is probably caused by the different reaction conditions. However, a large difference was noticed in the catalytic activity of the Au-based catalysts described in this chapter and those reported in [71] (the former are more active). It has been reported that under very different reaction conditions the presence of H<sub>2</sub> in the reactant flow has a considerably positive effect on the CO oxidation activity over Au/MgO/Al<sub>2</sub>O<sub>3</sub> (H<sub>2</sub>:CO:O<sub>2</sub> = 4:2:1) [72].

The selectivity to CO<sub>2</sub> is a very important issue in PROX. DFT calculations performed on Au(111), Cu(111) and Pt(111) have demonstrated that the barrier for CO oxidation on Au is 0.18 eV; the corresponding barrier for OH formation is much higher, 0.9 eV (at low

temperatures) [73]. Similarly, Cu(111) shows a lower barrier for CO oxidation (0.82 eV) than for H<sub>2</sub> oxidation (1.28 eV), whereas Pt(111) shows a higher barrier for CO oxidation (0.96 eV) than for H<sub>2</sub> oxidation (0.83 eV). These calculations explain why Au and Cu are more selective than Pt in the PROX reaction at low temperature and agree with other experimental reports [38].

Next to the nature of the catalyst, the reactant ratio contributes to the CO<sub>2</sub> selectivity in PROX. It was reported that at higher H<sub>2</sub> pressure but similar  $\lambda$ , the selectivity to CO<sub>2</sub> drops, compared with lower H<sub>2</sub> partial pressure [15]. However, if these catalysts are aimed to be used in H<sub>2</sub>-fueled polymer electrolyte membrane fuel cells (H<sub>2</sub>-PEMFCs), a typical composition of the gas stream would be: 45-75 vol% H<sub>2</sub>, 15-25 vol% CO<sub>2</sub>, 0.5-2 vol% CO, a few vol% H<sub>2</sub>O and N<sub>2</sub> [38]. It is then important that the selectivity to CO<sub>2</sub> is high at temperatures below 100<sup>0</sup>C and under H<sub>2</sub>-rich atmospheres.

DFT calculations have shown that on Au(111) and 150<sup>0</sup>C,  $\theta_{\text{CO}}/\theta_{\text{H}} = 1.17 \times 10^{-3}$  and changes to  $\theta_{\text{CO}}/\theta_{\text{H}} = 2.66 \times 10^{-6}$  at 550<sup>0</sup>C [73]. This implies that at low temperature CO oxidation is the main reaction, whereas upon increasing temperature H<sub>2</sub> oxidation starts, at the expense of CO oxidation. This reaction sequence will obviously affect the selectivity to CO<sub>2</sub>. Oxidation of H<sub>2</sub> was reported to depend to a lesser extent on the size of the Au particles [74] than CO, but direct evidence for the variation of H<sub>2</sub> oxidation over the Au-based catalysts presented in this chapter does not yet exist.

Based on the results presented above and on literature data, the following mechanism is proposed. CO in PROX, similar to the sequence of CO oxidation in the absence of hydrogen, is adsorbed on small Au crystallites, including the Au-support interface. Although it has been shown both by theoretical calculations [75] and experiments [76] that Au is the most inactive metal towards H<sub>2</sub> dissociation, some recent results demonstrated that a thin Au film grown on Ir (111) is able to dissociatively adsorb H<sub>2</sub> (D<sub>2</sub>) at temperatures as low as -173<sup>0</sup>C [77]. In addition, a FTIR study revealed dissociation of H<sub>2</sub> at room temperature on Au/TiO<sub>2</sub> and Au/Fe<sub>2</sub>O<sub>3</sub> [78]. More recently it was reported that Au/Al<sub>2</sub>O<sub>3</sub> is active in the H<sub>2</sub>/D<sub>2</sub> isotopic exchange reaction even at room temperature [57]. However, H<sub>2</sub> activation over Au at low temperatures proceeds to a lesser extent than CO activation. At low temperatures the predominant reaction is CO oxidation. By increasing the temperature, desorption of CO increases and more H<sub>2</sub> will be activated and subsequently oxidized. Oxygen might be activated due to the presence of certain additives (i.e. alkali (earth) metal oxides). Alternatively, if the additive is an easily reducible metal oxide, the near-surface or even the lattice oxygen is actively involved in the reaction.

## 9.5 Conclusions

Unpromoted Au/Al<sub>2</sub>O<sub>3</sub> catalysts are highly active in both CO oxidation and PROX. It is found that a thermal treatment at 200<sup>0</sup>C in oxygen applied on the as-prepared (dried) samples is more efficient than a thermal treatment at 150, 300 or 500<sup>0</sup>C. It is concluded that the active form of gold is mainly metallic.

Important promoting effects are obtained by using different types of additives. Their role is primarily related to stabilizing the very small gold particles, which are highly active

towards activation of molecules. The catalytic activity can be further improved upon addition of ceria to BaO or MgO. For PROX, this combination leads to a higher CO<sub>2</sub> selectivity in the whole temperature range (up to 300<sup>0</sup>C). Various concentrations of Li<sub>2</sub>O directly influence the catalytic performance in both CO oxidation and PROX. More Li<sub>2</sub>O is beneficial in PROX reaction, whereas in CO oxidation there is no direct correlation between *r* and Li<sub>2</sub>O loading.

Among the Group IB metals, Au shows the best performance in both CO oxidation and PROX. The catalytic activity of Au/Al<sub>2</sub>O<sub>3</sub> is not improved if CuO or Ag is added to Au/Al<sub>2</sub>O<sub>3</sub>.

It is proposed that CO is activated on Au or the Au-support interface and the active oxygen originates from the lattice of MO<sub>x</sub> or is activated due to the presence of certain types of additives. Regarding PROX, the same reaction mechanism may proceed, with additionally H<sub>2</sub> in the gas stream that competes with CO on the gold or at gold-support interface. The selectivity to CO<sub>2</sub> in PROX decreases with increasing temperature and hydrogen partial pressure.

## 9.6 References

- [1] G. C. Bond, D. T. Thompson, *Catal. Rev. Sci. Eng.* 41 (1999) 319.
- [2] M. Haruta, T. Kobayashi, N. Yamada, *Chem. Lett.* 2 (1987) 405.
- [3] M. Haruta, *Stud. Surf. Sci. Catal.* 110 (1997) 123.
- [4] M. M. Schubert, V. Plzak, J. Garche, R. J. Behm, *Catal. Lett.* 76 (2001) 143.
- [5] M. Okumura, S. Nakamura, S. Tsubota, T. Nakamura, M. Azuma, M. Haruta, *Catal. Lett.* 51 (1998) 53.
- [6] C. K. Costello, M. C. Kung, S.-O. Oh, Y. Wang, H. H. Kung, *Appl. Catal. A* 232 (2002) 159.
- [7] A. Wolf, F. Schuth, *Appl. Catal. A* 226 (2002) 1.
- [8] F. Boccuzzi, A. Chiorino, M. Manzoli, P. Lu, T. Akita, S. Ichikawa, M. Haruta, *J. Catal.* 202 (2001) 256.
- [9] E. D. Park, J. S. Lee, *J. Catal.* 186 (1999) 1.
- [10] N. A. Hodge, C. J. Kiely, R. Whyman, M. R. H. Siddiqui, G. J. Hutchings, Q. A. Pankhurst, F. E. Wagner, R. R. Rajaram, S. E. Golunski, *Catal. Today* 72 (2002) 133.
- [11] S. Minico, S. Scire, C. Crisafulli, S. Galvagno, *Appl. Catal. B* 34 (2001) 277.
- [12] S.-J. Lee, A. Gavrilidis, Q. A. Pankhurst, A. Kyek, F. E. Wagner, P. C. L. Wong, K. L. Yeung, *J. Catal.* 200 (2001) 298.
- [13] J.-N. Lin, J.-H. Chen, C.-Y. Hsiao, Y.-M. Kang, B.-Z. Wan, *Appl. Catal. B* 36 (2002) 19.
- [14] S. Tsubota, T. Nakamura, K. Tanaka, M. Haruta, *Catal. Lett.* 56 (1998) 131.
- [15] R. J. H. Grisel, *Supported gold catalysts for environmental applications*, PhD thesis, Leiden University (2002).
- [16] M. A. P. Dekkers, *Supported gold catalysts for automotive catalysis reactions*, PhD thesis, Leiden University (2000).
- [17] S. Tsubota, M. Haruta, T. Kobayashi, A. Ueda, Y. Nakahara, in "*Preparation of Catalysts V*", Elsevier 1991, 695.
- [18] M. Haruta, S. Tsubota, T. Kobayashi, H. Kageyama, M. J. Genet, B. Delmon, *J. Catal.* 144 (1993) 175.
- [19] S. D. Gardner, G. B. Hoflund, B. T. Upchurch, D. R. Schryer, E. J. Kielin, *J. Catal.* 129 (1991) 114.
- [20] A. Knell, P. Barnickel, A. Baiker, A. Wokaun, *J. Catal.* 137 (1992) 306.
- [21] M. C. Marion, E. Garbowski, M. Primet, *J. Chem. Soc.-Farad. Trans.* 86 (1990) 3027.
- [22] M. C. Marion, E. Garbowski, M. Primet, *J. Chem. Soc.-Farad. Trans* 87 (1991) 1795.
- [23] E. Finocchio, R. J. Willey, G. Busca, V. Lorenzelli, *J. Chem. Soc.-Farad. Trans.* 93 (1997) 175.
- [24] W. Liu, M. Flytzani-Stephanopoulos, *J. Catal.* 153 (1995) 304.
- [25] C. C. Chien, W. P. Chuang, T. J. Huang, *Appl. Catal. A* 131 (1995) 73.
- [26] Z. P. Ou, M. J. Cheng, W. X. Huang, X. H. Bao, *J. Catal.* 229 (2005) 446.
- [27] E. F. Iliopoulou, E. A. Efthimiadis, I. A. Vasalos, *Ind. Eng. Chem. Res.* 43 (2004) 1388.
- [28] Y. Iizuka, A. Kawamoto, K. Akita, M. Date, S. Tsubota, M. Okumura, M. Haruta, *Catal. Lett.* 97 (2004) 203.

- [29] M. M. Schubert, S. Hackenberg, A. C. van Veen, M. Muhler, V. Plzak, R. J. Behm, *J. Catal.* 197 (2001) 113.
- [30] W.-S. Shin, C.-R. Jung, J. Han, S.-W. Nam, T.-H. Lim, S.-A. Hong, H.-I. Lee, *J. Ind. Eng. Chem.* 10 (2004) 302.
- [31] A. Luengnaruemitchai, S. Osuwan, E. Gulari, *Int. J. Hydrogen Energy* 29 (2004) 429.
- [32] B. Schumacher, Y. Denkwitz, V. Plzaak, M. Kinne, R. J. Behm, *J. Catal.* 224 (2004) 449.
- [33] M. J. Kahlich, H. A. Gasteiger, R. J. Behm, *J. Catal.* 182 (1999) 430.
- [34] A. Wootsch, C. Descorme, D. Duprez, *J. Catal.* 225 (2004) 259.
- [35] S. H. Oh, R. Sinkevitch, *J. Catal.* 142 (1993) 254.
- [36] G. Avgouropoulos, T. Ioanides, H. K. Matralis, J. Batista, S. Hocevar, *Catal. Lett.* 73 (2001) 33.
- [37] D. H. Kim, J. E. Cha, *Catal. Lett.* 86 (2003) 107.
- [38] G. Avgouropoulos, T. Ioanides, C. Papadopoulou, J. Batista, S. Hocevar, H. K. Matralis, *Catal. Today* 75 (2002) 157.
- [39] A. C. Gluhoi, M. A. P. Dekkers, B. E. Nieuwenhuys, *J. Catal.* 219 (2003) 197.
- [40] A. C. Gluhoi, S. D. Lin, B. E. Nieuwenhuys, *Catal. Today* 90 (2004) 175.
- [41] N. Lopez, J. K. Norskov, T. V. W. Janssens, A. Carlsson, A. Puig-Molina, B. S. Clausen, J. D. Grunwaldt, *J. Catal.* 225 (2004) 86.
- [42] N. Lopez, T. V. W. Janssens, B. S. Clausen, Y. Xu, M. Mavrikakis, T. Bligaard, J. K. Norskov, *J. Catal.* 223 (2004) 232.
- [43] L. M. Molina, B. Hammer, *Phys. Rev. B* 69 (2004) 155424.
- [44] L. M. Molina, B. Hammer, *Phys. Rev. Lett.* 90 (2003) 206102.
- [45] G. B. Hoflund, S. D. Gardner, D. R. Schryer, B. T. Upchurch, E. J. Kielin, *Appl. Catal. B* 6 (1995) 117.
- [46] D. A. Outka, R. J. Madix, *Surf. Sci.* 179 (1987) 351.
- [47] D. H. Parker, B. E. Koel, *J. Vac. Sci. Technol. A* 8 (1990) 2585.
- [48] Y. Xu, M. Mavrikakis, *J. Phys. Chem. B* 107 (2003) 9298.
- [49] G. Mills, M. S. Gordon, H. Metiu, *J. Chem. Phys.* 118 (2003) 4198.
- [50] M. Mavrikakis, P. Stoltze, J. K. Norskov, *Catal. Lett.* 64 (2000) 101.
- [51] P. Bera, M. S. Hegde, *Catal. Lett.* 79 (2002) 75.
- [52] S. Carrettin, P. Concepcion, A. Corma, J. M. Lopez Nieto, V. F. Puentes, *Angew. Chem. Int. Ed.* (2004) 2538.
- [53] M. Manzoli, A. Chiorino, F. Boccuzzi, *Surf. Sci.* 532 (2003) 377.
- [54] G. C. Bond, D. T. Thompson, *Gold Bull.* 33 (2001) 41.
- [55] J. D. Grunwaldt, A. Baiker, *J. Phys. Chem. B* 103 (1999) 1002.
- [56] A. C. Gluhoi, N. Bogdanchikova, B. E. Nieuwenhuys, *J. Catal.* 229 (2005) 154.
- [57] A. C. Gluhoi, H. S. Vreeburg, J. W. Bakker, B. E. Nieuwenhuys, *Appl. Catal. A* 291 (2005) 145.
- [58] A. C. Gluhoi, N. Bogdanchikova, B. E. Nieuwenhuys, *J. Catal.*, submitted.
- [59] N. Lopez, J. K. Norskov, *J. Am. Chem. Soc.* 124 (2002) 11262.
- [60] G. B. Hoflund, S. D. Gardner, D. R. Schryer, B. T. Upchurch, E. J. Kielin, *Langmuir* 11 (1995) 3431.
- [61] M. Bollinger, M. A. Vannice, *Appl. Catal. B* 8 (1996) 417.
- [62] M. Date, M. Haruta, *J. Catal.* 201 (2001) 221.
- [63] S.-O. Oh, C. K. Costello, C. Cheung, H. H. Kung, M. C. Kung, *Stud. Surf. Sci. Catal.* 139 (2001) 375.
- [64] G. C. Bond, D. T. Thompson, *Gold Bull.* 33 (2000) 41.
- [65] M. Haruta, *Gold Bull.* 37 (2004) 27.
- [66] F. Boccuzzi, A. Chiorino, S. Tsubota, M. Haruta, *Catal. Lett.* 29 (1994) 225.
- [67] I. N. Remediakis, N. Lopez, J. K. Norskov, *Angew. Chem. Int. Ed.* 44 (2005) 1824.
- [68] G. R. Bamwenda, S. Tsubota, T. Nakamura, M. Haruta, *Catal. Lett.* 44 (1997) 83.
- [69] F. Boccuzzi, A. Chiorino, S. Tsubota, M. Haruta, *J. Phys. Chem. B* 100 (1996) 3625.
- [70] Z.-P. Liu, P. Hu, A. Alavi, *J. Am. Chem. Soc.* 124 (2002) 14770.
- [71] C. Rossignol, S. Arrii, F. Morfin, L. Piccolo, V. Caps, J.-L. Rousset, *J. Catal.* 230 (2005) 476.
- [72] R. J. H. Grisel, C. J. Weststrate, A. Goossens, M. W. J. Craje, A. M. van der Kraan, B. E. Nieuwenhuys, *Catal. Today* 72 (2002) 123.
- [73] S. Kandoi, A. A. Gokhale, L. C. Grabow, J. A. Dumesic, M. Mavrikakis, *Catal. Lett.* 93 (2004) 93.
- [74] M. Haruta, *Catal. Today* 36 (1997) 153.
- [75] B. Hammer, J. K. Norskov, *Nature* 376 (1995) 238.
- [76] A. G. Sault, R. J. Madix, C. T. Cambell, *Surf. Sci.* 169 (1986) 347.
- [77] M. Okada, M. Nakamura, K. Moritani, T. Kasai, *Surf. Sci.* 523 (2003) 218.
- [78] F. Boccuzzi, A. Chiorino, M. Manzoli, D. Andreeva, T. Tabakova, *J. Catal.* 188 (1999) 176.

# Chapter 10

## General discussion

*This chapter provides a general discussion of all the results presented throughout this thesis. In addition, future prospects and research recommendations are outlined.*



## 10.1 Introduction

Although gold is the most inert of all metals, it has some interesting properties as a heterogeneous catalyst. It becomes active, however, *only* if the size of the gold particles is in the nanometer range. There is a number of exciting aspects of gold catalysts that are currently attracting the interest of both academia and industry. This thesis assessed a number of different aspects related to Au catalysts and a summary of the most important findings is presented below.

## 10.2 Unpromoted Au/Al<sub>2</sub>O<sub>3</sub>. Preparation, activation and working state

Since Haruta claimed that nano-Au particles are surprisingly active if prepared and deposited on suitable carriers [1], it is now generally accepted that the special property of catalytically active gold is mainly connected to its particle size which must be in a very narrow range, between 2 and 3 nm [2, 3], or 3 to 5 nm [4-6]. However, an optimum range of 7 to 8 nm for some reactions has also been claimed [7] and activity has even been reported for particles in the 30 to 50 nm range [8, 9]. Nevertheless, most of the reports agree that for reactions involving CO, hydrocarbons, NO<sub>x</sub> and NH<sub>3</sub> molecules, the size of the Au particles should be below 5 nm.

The results presented in this thesis are in line with earlier reported results, i.e. that the average size for active Au particles should be below 5 nm. This is true for all the reactions studied: the oxidation of saturated (methane and propane) and unsaturated (propene) hydrocarbons, the reduction of NO<sub>x</sub>, the oxidation of ammonia and of CO.

As described in *Chapter 1*, the fraction of surface atoms increases and also the length of the periphery per unit mass of Au rises with decreasing **size of the Au particles**. Theoretical calculations showed that the availability of low-coordinated Au atoms on the small particles makes Au an active catalyst [10]. Another related effect is thought to be the strain due to the mismatch at the Au-support interface [11]. Of course these assumptions are difficult to prove with the “real” Au-based catalysts, but *Chapter 4* showed that for an average Au particle size of about 4.3 nm (XRD), the Au surface area is around 2.4 m<sup>2</sup>g<sup>-1</sup>, with a corresponding dispersion of ~ 12%. These values are superior to the corresponding characteristics of, for example, Au/CoO<sub>x</sub>/Al<sub>2</sub>O<sub>3</sub>. Nevertheless, the catalytic performance of Au/CoO<sub>x</sub>/Al<sub>2</sub>O<sub>3</sub> is significantly higher, compared with the unpromoted Au/Al<sub>2</sub>O<sub>3</sub> for all the reactions studied, pointing to secondary effects that also contribute to the high catalytic performance of the Au-based catalysts.

In addition, it was proposed that Au particles with other **shapes** than spherical are beneficial for a high catalytic activity [1]. Icosahedra of a nominal Au<sub>13</sub> stoichiometry are reported to be the active particles in Au/MgO. For Au/TiO<sub>2</sub> hemispherical fcc cuboctahedral particles seem to do the work [12]. Moreover, it has been shown that 2 nm diameter clusters consisting of two layers of about 50 Au atoms each are active for CO oxidation [3]. Such a structure is too thin to have fcc (the bulk form of gold) structure and is basically two-dimensional. All the preparation techniques of “real” Au-based catalysts result in a rather broad particle size distribution and it is not clear how many Au particles are responsible for the catalytic activity (maybe only a few). It is clear that there is not yet a consensus regarding

some particular shape of the Au particles that makes the catalysis. The HRTEM measurements shown in *Chapter 4* revealed shapes such as hemispherical (majority), but also other shapes, such as truncated, but no correlation between the existence of a particular morphology of the Au particles and the catalytic performance could be found.

The **thermal treatment** of the catalyst precursor has also been reported to have a great influence on the final catalytic properties of Au. There are reports that show that uncalcined Au/Al<sub>2</sub>O<sub>3</sub> can be very active [13]. For catalysts supported on other carriers than alumina, it was reported that calcination at mild temperature (100-200<sup>0</sup>C) results in more active catalysts than calcination at higher temperatures [14-18]. Regarding the effect of the treatment prior to the reaction, Dekkers found that for Au/Al<sub>2</sub>O<sub>3</sub> a reductive pretreatment gives better results than an oxidative one (300<sup>0</sup>C) [19]. These findings were later confirmed by Grisel [20]. The effect of temperature and gas phase composition is discussed in *Chapter 9*. Of the temperatures selected (i.e. 150, 200, 300 and 500<sup>0</sup>C), and different gases (i.e. O<sub>2</sub> and H<sub>2</sub>), calcination at 200<sup>0</sup>C gives the best results in both CO oxidation and PROX. In addition, it was concluded that after pretreatment at 200<sup>0</sup>C the chemical state of Au is already metallic (TPR and DR/UV-Vis, *Chapter 4*) and represents the active state of Au. Of course we cannot rule out the existence of some traces of ionic gold, but its role in the catalytic processes is believed to be minor.

Because the reproducibility of various **preparation methods** for active gold catalysts is not always very good, the recipes to prepare active Au catalysts sometimes appear a bit mysterious. Although the general idea is that impregnation is not suitable for Au-based catalysts, due to the low degree of Au-support interaction, and the presence of large amounts of poisonous Cl<sup>-</sup> ions, recent results indicate that this idea might change [21]. Overall, however, deposition-precipitation and coprecipitation are accepted as appropriate methods for preparing active and rather reproducible Au-based catalysts, although the recipes differ regarding the basic media used to deposit Au onto the support (i.e. Na<sub>2</sub>CO<sub>3</sub>, urea, etc). Previously reported results have demonstrated that using urea is more advantageous than Na<sub>2</sub>CO<sub>3</sub> (higher gold loading and superior Au dispersion) [20, 22]. This preparation method proved to be fairly reproducible and finely dispersed Au nanoparticles were obtained, especially when additional metal oxides were added to  $\gamma$ -Al<sub>2</sub>O<sub>3</sub> prior Au deposition (see below).

Finally, the **stability** of the nanometer Au particles is an important issue in gold catalysis. By decreasing the size of the Au particles, their mobility increases, such that sintering becomes a very important issue if the reaction temperature exceeds 400<sup>0</sup>C. The present results showed that the Au particles were rather stable during various thermal treatments, if mild temperatures were used ( $\leq$  500<sup>0</sup>C). However, relative severe sintering of the Au-based catalysts was observed during *methane oxidation* (*Chapter 6*), when the maximum reaction temperature reached 740<sup>0</sup>. The sintering might be retarded when Au is held on the carrier surface by a stronger interaction, i.e. when various additives are added to  $\gamma$ -Al<sub>2</sub>O<sub>3</sub> (see below).

### 10.3 Multicomponent Au-based catalysts. Promoter vs. cocatalyst

There are different ways to rationalize the influence of promoters on the catalytic activity of Au catalysts. One model suggests that, in the case of nonreducible supports such as alumina or silica, or if additives such as MgO, Li<sub>2</sub>O, Rb<sub>2</sub>O or BaO are present, the unique role of these oxides is to stabilize small gold particles during the preparation and further thermal treatments [20, 23, 24].

Various types of metal oxides have been tested as possible additives, aiming to improve the catalytic performance of the reference-Au/Al<sub>2</sub>O<sub>3</sub>. The results presented throughout this thesis showed that *all* metal oxides used improve the catalytic performance of Au/Al<sub>2</sub>O<sub>3</sub>. Moreover, the beneficial role of these metal oxides strongly depends on their identity. By their role, these additives can be broadly divided into (structural) promoters and cocatalysts.

#### *Structural promoters*

This class of additives includes those metal oxides that increase the catalytic performance of Au/Al<sub>2</sub>O<sub>3</sub> mainly by modifying the structure/morphology/size of the gold particles, without being catalytically active by any means. Based on the results presented in *Chapter 4* and thereafter, the additives of the alkali (earth) metal oxide type may be included in this category. XRD and HRTEM results showed that the role of this kind of MO<sub>x</sub> is to stabilize finely dispersed Au particles onto the support. For example, if BaO was added to Al<sub>2</sub>O<sub>3</sub> prior Au deposition, the final Au dispersion was around 55 % (HRTEM); the calculated Au surface area was significantly affected as well. Moreover, for the Au-containing catalysts with alkali (earth) metal oxide additives, a clear relationship was observed between the Au particle size/dispersion and the catalytic performance in various reactions. The formation of very small gold particles also affects their shape. HRTEM showed that for some of the catalysts the shape was not hemispherical. However, as already mentioned, no direct correlation could be established between this factor and a high catalytic performance.

For ammonia synthesis, the role of alkali metal oxides (K<sub>2</sub>O, Cs<sub>2</sub>O) on Fe- and Ru-based catalysts is well established and they are considered to act as chemical promoters by lowering the N<sub>2</sub> dissociation barrier [25-28]. Although in the presence of certain alkali (earth) metal oxides a more than six-fold increase in the specific reaction rate was observed (C<sub>3</sub>H<sub>6</sub> total oxidation), the apparent activation energy showed an insignificant difference between  $E_a$  for the unpromoted Au/Al<sub>2</sub>O<sub>3</sub> and that for the alkali (earth) metal oxide-promoted Au/Al<sub>2</sub>O<sub>3</sub> [24]. Similar results have been obtained for methane and propane total oxidation (*Chapter 6*). It was concluded, based on these results, that the role of alkali (earth) metal oxides is rather to increase the concentration of the Au active sites, without creating new reaction pathways. These additives appear to act as structural promoters [24].

The stability of the finely dispersed Au nano-particles increases in the presence of these structural promoters and their sintering is prevented. These structural promoters are actively involved in the stabilization of Au nano-particles in several ways. It is possible that the presence of MO<sub>x</sub> creates more defects on the surface of alumina during various preparation steps. A defect-rich surface is certainly more active in both anchoring of Au nanoparticles and molecule activation. If the anchoring/interaction of Au is enhanced in the presence of this

kind of promoters, then it is likely that the mobility of small Au nanoparticles diminishes. In this way also the tendency of Au nanoparticles to cluster/agglomerate during the reaction cycles is affected (decreased). The affinity of Au to the  $\text{MO}_x$ -modified alumina support is most probably directly related to the identity of the  $\text{MO}_x$  used as promoter. As a result, the catalytic performance of Au-based catalysts promoted with various alkali (earth) metal oxides differs. Finally, it is possible that due to the stronger Au-support interaction obtained in the presence of the promoters, a small part of Au species is still in ionic form. These ionic Au species would act as a "glue" between  $\text{Au}^0$  and the modified support and possibly play a role in the catalytic cycle. However, these ionic Au species are below the detection limit of any of the techniques used in this thesis.

The very high temperatures needed for methane oxidation result in sintering of the Au particles, independent of the identity of the additives.

### *Cocatalysts*

A cocatalyst has an active role in the catalytic action and acts along with the main catalyst.

Theoretical calculations showed that the requirement of a support rich in defects is crucial for an efficient adhesion of Au, and it influences both the size and the shape of the Au particles [29]. Although this is not necessarily connected with the anion vacancy, it is believed that the reducible supports have a larger number of oxygen vacancies, useful for Au anchoring. The concept of strong metal support interaction, valid for Ni and Pt deposited on  $\text{TiO}_2$  appears to be valid for Au as well [30, 31]. Moreover, it was suggested that for this type of easily reducible metal oxides, an additional reaction path might be valid, i.e. the metal oxide is the supplier of the active oxygen during the reaction [32, 33].

The results presented in this thesis concerning the role of metal oxides other than the alkali (earth) metal oxides (i.e. TMO, ceria, copper oxide or ZnO) support the conclusion that all these additives act as cocatalysts. For this class of promoted Au-based catalysts the average gold particle size varies rather significantly, from very small Au particles, below the detection limit of the XRD technique (i.e.  $\text{Au/CeO}_x/\text{Al}_2\text{O}_3$ ) to medium sized (i.e.  $\text{Au/MnO}_x/\text{Al}_2\text{O}_3$ ), or to very large particles ( $\text{Au/CuO/CeO}_x/\text{Al}_2\text{O}_3$ ) – see *Chapters 4-9*. Although this directly influences the Au dispersion and the metallic surface area values, the catalytic performance did not follow the same trend. A particular case is CuO, which is by itself an active catalyst in oxidation reactions. Experimental evidence supports the conclusion that these additives act as cocatalysts, via a Mars and van Krevelen mechanism. According to this mechanism, the reactant is activated on gold or on the gold-support interface and the active oxygen is provided by the lattice of the metal oxide. The structure of the metal oxide is important and it affects both the anchoring of gold particles, and the supply of the active oxygen. In this light, the average size of  $\text{MO}_x$  is important as well. One of the most active catalysts comprises Au and  $\text{CeO}_x$ , both in the nanometer range.

For similar reasons the selectivity in ammonia oxidation or NO reduction is strongly related to the identity of the additives. Thus, it was observed that in ammonia oxidation, a

readily reducible metal oxide helps the production of oxygenated N-compounds (NO or N<sub>2</sub>O).

#### 10.4 Mechanistic considerations

The results presented in this thesis could not explicitly identify the place where the oxidation and reduction reactions proceed: on the Au particles, or at the Au-support interface. While it is clear that bulk gold is inactive, it is still undecided whether the Au particle perimeter is more active than its surface. It is possible that for the same reaction various reaction mechanisms may operate depending on the catalyst composition and the operating temperature.

However, the results suggest that the activation of oxygen may proceed differently, depending on the identity of the support/additive. If nonreducible metal oxides are involved, the activation of O<sub>2</sub> probably takes place at the interface Au-MO<sub>x</sub>, or directly on gold. Generally, this requires higher temperatures. If easily reducible metal oxides are present, the oxygen from the lattice of MO<sub>x</sub>, highly mobile, may facilitate the oxidation reaction.

Concerning the activation of hydrogen, although Au was regarded as a poor hydrogenation catalyst because of its very weak interaction with hydrogen, recent results proved the contrary [19, 34-37]. It was reported that even on unpromoted Au/Al<sub>2</sub>O<sub>3</sub> the isotopic H<sub>2</sub>-D<sub>2</sub> exchange reaction proceeds [37]. The activation of hydrogen most probably takes place at the Au-support interface and a defect-rich gold surface facilitates this activation.

The activation of other molecules such as hydrocarbons, NH<sub>3</sub>, NO and N<sub>2</sub>O is directly related to the presence of Au. This model is supported by the steep decrease of  $E_a$  for various reactions after Au addition to alumina. However, besides a direct involvement of the Au nanoparticles in the activation of these molecules, most probably the Au-support interface is also required.

#### 10.5 Future prospects and recommendations

Although gold is a *relatively* new catalyst, it has already been demonstrated that it is the best catalyst for low-temperature CO removal. Au may also be a suitable catalyst for: fuel cell development (cold start stage), hydrochlorination of ethyne to vinyl chloride monomer, the production of vinyl acetate monomer from acetic acid, ethylene and oxygen, and low-temperature NO production from NH<sub>3</sub> oxidation. However, there are still fundamental/theoretical aspects to be solved. Among them, the following may help in developing new directions in Au catalysis:

(i) A more detailed study of the structure of the additives, since it was proved that not only the size of the Au particles is important, but also that of the additives. Since ceria appears to be one of the best additives for Au, efforts should be driven to stabilize both Au and CeO<sub>x</sub> particles during the reaction;

(ii) The use of *in-situ* techniques in order to follow the structural and chemical changes of the catalyst in real time, aiming for fundamental understanding of various processes;

(iii) A more detailed study of the Ce-Zr mixed oxide structure. Throughout this thesis it was shown that Au/CeO<sub>x</sub>/ZrO<sub>x</sub>/Al<sub>2</sub>O<sub>3</sub> is a very efficient catalyst for many reactions. Optimising the structure of (Ce-Zr)O<sub>x</sub> may help in developing a new class of supports, with high surface area and *redox* properties;

(iv) Optimising the role of the additives by tuning the effect of their loading on the catalytic performance of Au/Al<sub>2</sub>O<sub>3</sub>;

(v) FTIR studies of various molecules interacting with promoted-Au/Al<sub>2</sub>O<sub>3</sub> catalysts for a better understanding of the role of these promoters and also for mechanistic purposes;

(vi) A more detailed study of Au/hopcalite (MnO<sub>x</sub>-CuO<sub>y</sub>), in order to implement new stable and more active catalysts needed for CO sensors and gas masks;

(vii) Study of low-temperature CO oxidation under acidic environment. This reaction is important in relation to the polymer electrolyte fuel cell. The anode should also be active for electrochemical oxidation of CO and the Pt electrode is quickly deactivated by CO.

## 10.6 References

- [1] M. Haruta, T. Kobayashi, N. Yamada, Chem. Lett. 2 (1987) 405.
- [2] D. T. Thompson, Gold Bull. 32 (1999) 12.
- [3] M. Valden, X. Lai, D. W. Goodman, Science 281 (1998) 1647.
- [4] G. C. Bond, Gold Bull. 34 (2001) 117.
- [5] B. E. Salisbury, W. T. Wallace, R. L. Whetten, Chem. Phys. 262 (2000) 131.
- [6] D. T. Thompson, Gold Bull. 31 (1998) 111.
- [7] L. Prati, G. Martra, Gold Bull. 32 (1999) 96.
- [8] Y. Yuan, A. Kozlova, H. Asakura, H. Wan, K. Tsai, Y. Isawa, J. Catal. 170 (1997) 191.
- [9] H. S. Oh, J. H. Yang, C. K. Costello, Y. M. Wang, S. R. Bare, H. H. Kung, M. C. Kung, J. Catal. 210 (2002) 375.
- [10] N. Lopez, T. V. W. Janssens, B. S. Clausen, Y. Xu, M. Mavrikakis, T. Bligaard, J. K. Norskov, J. Catal. 223 (2004) 232.
- [11] M. Mavrikakis, P. Stoltze, J. K. Norskov, Catal. Lett. 64 (2000) 101.
- [12] D. A. H. Cunningham, W. Vogel, R. M. Torres Sanchez, K. Tanaka, M. Haruta, J. Catal. 183 (1999) 24.
- [13] A. Wolf, F. Schuth, Appl. Catal. A 226 (2002) 1.
- [14] F. Boccuzzi, A. Chiorino, M. Manzoli, P. Lu, T. Akita, S. Ichikawa, M. Haruta, J. Catal. 202 (2001) 256.
- [15] E. D. Park, J. S. Lee, J. Catal. 186 (1999) 1.
- [16] N. A. Hodge, C. J. Kiely, R. Whyman, M. R. H. Siddiqui, G. J. Hutchings, Q. A. Pankhurst, F. E. Wagner, R. R. Rajaram, S. E. Golunski, Catal. Today 72 (2002) 133.
- [17] S. Minico, S. Scire, C. Crisafulli, S. Galvagno, Appl. Catal. B 34 (2001) 277.
- [18] S.-J. Lee, A. Gavriilidis, Q. A. Pankhurst, A. Kyek, F. E. Wagner, P. C. L. Wong, K. L. Yeung, J. Catal. 200 (2001) 298.
- [19] M. A. P. Dekkers, *Supported gold catalysts for automotive catalysis reactions*, PhD thesis, Leiden University (2000).
- [20] R. J. H. Grisel, *Supported gold catalysts for environmental applications*, PhD thesis, Leiden University (2002).

- [21] Q. Xu, K. C. C. Kharas, A. K. Datye, *Catal. Lett.* 85 (2003) 229.
- [22] R. J. H. Grisel, P. J. Kooyman, B. E. Nieuwenhuys, *J. Catal.* 191 (2000) 430.
- [23] R. J. H. Grisel, B. E. Nieuwenhuys, *J. Catal.* 199 (2001) 48.
- [24] A. C. Gluhoi, N. Bogdanchikova, B. E. Nieuwenhuys, *J. Catal.* 232 (2005) 96.
- [25] Z. Kowalczyk, J. Sentek, S. Jodzis, M. Muhler, O. Hinrichsen, *J. Catal.* 169 (1997) 407.
- [26] Z. Kowalczyk, M. Krukowski, W. Rarog-Pilecka, D. Szmigiel, J. Zielinski, *Appl. Catal. A* 248 (2003) 67.
- [27] D. Szmigiel, H. Bielawa, M. Kurtz, O. Hinrichsen, M. Muhler, W. Rarog, S. Jodzis, Z. Kowalczyk, L. Znak, J. Zielinski, *J. Catal.* 205 (2002) 205.
- [28] R. A. van Santen, J. W. Niemantsverdriet, *Chemical Kinetics and Catalysis*, Plenum Press, New York 1995.
- [29] N. Lopez, J. K. Norskov, T. V. W. Janssens, A. Carlsson, A. Puig-Molina, B. S. Clausen, J. D. Grunwaldt, *J. Catal.* 225 (2004) 86.
- [30] S. D. Lin, M. Bollinger, M. A. Vannice, *Catal. Lett.* 17 (1993) 245.
- [31] D. W. Goodman, *Catal. Lett.* 99 (2005) 1.
- [32] M. M. Schubert, S. Hackenberg, A. C. van Veen, M. Muhler, V. Plzak, R. J. Behm, *J. Catal.* 197 (2001) 113.
- [33] A. C. Gluhoi, N. Bogdanchikova, B. E. Nieuwenhuys, *J. Catal.* 229 (2005) 154.
- [34] M. Okada, M. Nakamura, K. Moritani, T. Kasai, *Surf. Sci.* 523 (2003) 218.
- [35] P. Claus, A. Bruckner, C. Mohr, H. Hofmeister, *J. Am. Chem. Soc.* 122 (2000) 11430 and refs. therein.
- [36] S. Schimpf, M. Lucas, C. Mohr, U. Rodemerck, A. Bruckner, J. Radnik, H. Hofmeister, P. Claus, *Catal. Today* 72 (2002) 63.
- [37] A. C. Gluhoi, H. S. Vreeburg, J. W. Bakker, B. E. Nieuwenhuys, *Appl. Catal. A* 291 (2005) 145.

## Summary

### *Fundamental studies focused on understanding of gold catalysis*

Although the catalytic properties of Pt were already discovered by Faraday in 1835, and soon after those of transition metal (oxides), it has been widely believed until recently that Au is too inert to catalyse chemical reactions. Recently, it was found that its nobility disappears for Au particles in the nanometer range.

The aim of this thesis was to study the catalytic properties of unpromoted, singly ( $\text{MO}_x$ ) and doubly ( $\text{M}^{\text{I}}\text{O}_x/\text{M}^{\text{II}}\text{O}_x$ ) promoted Au-based catalysts (M: alkali (earth), transition metals (TM), Cu, rare earth) for reactions relevant to air pollution control. The reactions include total oxidation of (un)saturated hydrocarbons, CO oxidation in the presence and absence of hydrogen,  $\text{NH}_3$  oxidation and  $\text{NO}_x$  reduction. The influence of various kinds of additives on the size/shape of the Au particles was investigated using XRD, HRTEM and SEM. Further, the possible effect of the presence of additives on the chemical state of Au and on the active sites was examined (DR/UV-Vis, TPR and XPS). The final aim was to investigate possible correlations between the size/shape of Au particles, the identity/role of the additives and the catalytic performance.

Deposition precipitation with urea proved to be a reproducible preparation method and finely dispersed Au nanoparticles were obtained (*Chapter 4*). A thermal treatment of the as-prepared Au/ $\text{Al}_2\text{O}_3$  in  $\text{H}_2$  or  $\text{O}_2$  at  $150^\circ\text{C}$  causes gold reduction from  $\text{Au}^{3+}$  to  $\text{Au}^0$  (DR/UV-Vis, TPR). The degree of reduction increases with increasing temperature. A thermal treatment of Au/ $\text{Al}_2\text{O}_3$  up to  $500^\circ\text{C}$  did not cause a significant sintering of the Au particles. Various  $\text{MO}_x$  additives modify the structure/morphology/size of the gold particles (XRD, HRTEM). There was no experimental evidence that the presence of  $\text{MO}_x$  alters the chemical state of gold. However, the existence of traces of ionic gold, below the detection limit of the various techniques employed (DR/UV-Vis, TPR, XPS), cannot be excluded. The catalytic performance for various reactions is directly related to the dispersion/Au surface area of the promoted Au/ $\text{Al}_2\text{O}_3$  catalysts. On the other hand, no direct correlation could be established between a particular morphology of the Au particles and the catalytic performance. The concentration of low coordinated gold atoms, responsible for stronger Au-support interaction and molecule activation, is considered to increase by using the promoters, due to a decrease of the size of the Au particles.

A detailed and comparative study of the catalytic performance of unpromoted, singly and doubly  $\text{MO}_x$  promoted Au/ $\text{Al}_2\text{O}_3$  (M: alkali (earth), TM, Cu, rare earth) for propene oxidation is presented in *Chapter 5*. The variation of  $T_{50\%}$  and  $r$  clearly indicate an Au particle size effect on the activity for the alkali (earth)-promoted Au/ $\text{Al}_2\text{O}_3$  catalysts. Moreover, the values of the apparent activation energy,  $E_a$ , for Au/ $\text{Al}_2\text{O}_3$  and Au/ $\text{MO}_x/\text{Al}_2\text{O}_3$  (M: alkali (earth))



reveal that the additives are not directly responsible for the higher catalytic activity. These additives also prevent the agglomeration of Au nanoparticles during catalytic reaction. Thus, it is concluded that this kind of additives increases the concentration of the Au active sites, by acting as structural promoters. The best promoting effect is obtained with BaO. The variation of the  $T_{50\%}$  and  $r$  does not directly correlate with the average size of the Au particles if the additives are TM/Cu/rare earth oxides. The role of these additives is twofold: they are directly involved in stabilization of the gold particles against sintering and also act as cocatalysts. The oxidation of propene proceeds via a Mars and van Krevelen type of mechanism: the reactant (propene) is activated on gold or the gold-support interface and active oxygen comes from the lattice of the metal oxide. The anchoring of gold particles and the supply of the active oxygen are directly related to the structure of  $MO_x$ . A key additive in obtaining a highly active catalyst is ceria.

Total oxidation of saturated hydrocarbons (methane and propane) over Au-based catalysts is presented in *Chapter 6*. The significant decrease of  $T_{50\%}$  and  $E_a$  accompanied by an increase in  $r$  after addition of Au to  $MO_x/Al_2O_3$  confirm that Au is active in total oxidation of methane and propane. A direct relationship exists between the catalytic performance and the average size of the Au particles, especially if alkali (earth) metal oxides are used as additives. Similar to the results presented in *Chapter 5*, the role of these additives is that of a structural promoter. On the other hand, TMO, CuO and ceria act as a cocatalyst, i.e. as supplier of oxygen. The results also suggest that oxides with a basic character may be beneficial for high catalytic activity, compared with those with an acidic character. For both reactions the presence of the additives prevents the sintering of Au nanoparticles during reaction. However, the temperatures needed to activate  $CH_4$  are rather high and some sintering of Au particles is observed.

Ammonia oxidation over gold-based catalysts is presented in *Chapter 7*. It is found that the addition of  $MO_x$  to Au/ $Al_2O_3$  improves the catalytic activity in ammonia oxidation. The size of the Au particles is important for high activity. However, the catalytic activity of the various gold-based catalysts is also strongly influenced by the nature of the additive. The same holds for the selectivity towards different products ( $N_2$ ,  $N_2O$  and NO), which can be steered as a function of  $MO_x$  identity. Similar to the results found for total oxidation of (un)saturated hydrocarbons, the role of the additives is twofold: that of a structural promoter and that of a cocatalyst. FTIR measurements reveal the presence of  $NH_4^+$  on Brønsted acid sites,  $NH_3$  on Lewis acid sites, amide (or hydrazine), and imide. The addition of Au to  $MO_x/Al_2O_3$  significantly enhances the intensity of the absorption band assigned to surface imido-species, proposed to be a reaction intermediate.

Gold-based catalysts are also efficient catalysts for the low temperature conversion of NO and  $N_2O$  (*Chapter 8*). Nitric oxide is converted in the presence of hydrogen ( $NO/H_2 = 1$  or 0.4) to the following products:  $N_2O$  (at low temperature),  $N_2$  (at intermediate temperature) and  $NH_3$  (at high temperature). The catalytic performance as well as the product distribution

strongly depends on the reaction temperature, nature of the additive and reactant ratio. The catalytic performance of the gold-based catalysts is directly related to the size of the gold particles, especially when non-reducible oxides (i.e. alkali (earth) metal oxides) are used as additives. The results suggest that hydrogen assists in NO decomposition. At low temperature NO partly decomposes to  $N_2O$  and  $O_{ads}$ ; at higher temperatures, the amount of NO dissociatively adsorbed on the surface increases and as a result, more  $N_2$  is produced via N combination.  $NH_x$  species are the precursors for  $NH_3$  formation. The selectivity depends on the relative concentrations of adsorbed species on the surface, i.e. NO, N and  $NH_x$ . The oxidic additives might create new sites for dissociative adsorption of NO. The nature of the additives is also very important in reduction of nitrous oxide with hydrogen. During  $N_2O$  reduction with  $H_2$ , the only products obtained are  $N_2$  and  $H_2O$ . Most probably, the role of the non-reducible metal oxides is to stabilize the finely dispersed Au nanoparticles, whereas the partly reducible metal oxide additives are involved in creating new active sites and increasing  $N_2O$  dissociation.

As expected, gold-based catalysts are highly active in low-temperature CO oxidation and PROX (*Chapter 9*). The highest efficiency of the unpromoted Au/ $Al_2O_3$  is achieved following a thermal treatment at  $200^{\circ}C$  in oxygen. Alkali (earth) metal oxides (i.e.  $Li_2O$ ,  $Rb_2O$ ,  $BaO$ ) function as structural promoters. Moreover, the loading of  $Li_2O$  directly influence the catalytic performance in both CO oxidation and PROX. More  $Li_2O$  is beneficial in PROX reaction, whereas in CO oxidation there is no direct correlation between  $r$  and  $Li_2O$  loading. The easily reducible metal oxides can supply active oxygen via a Mars and van Krevelen type of mechanism. Thus, it is proposed that CO is activated on Au or the Au-support interface and the active oxygen originates from the lattice of  $MO_x$  or is activated due to the presence of certain types of additives. Regarding PROX, the same reaction mechanism may proceed, with additionally  $H_2$  in the gas stream that competes with CO on the gold or at the gold-support interface. The selectivity to  $CO_2$  in PROX decreases with increasing temperature and hydrogen partial pressure.



## Samenvatting

### *Fundamenteel onderzoek gericht op het begrijpen van goud katalyse*

Hoewel de katalytische eigenschappen van Pt al in 1835 door Faraday zijn ontdekt (en snel daarna ook die van de overgangsmetalen en oxiden), werd tot voor kort aangenomen dat Au te edel is om chemische reacties te katalyseren. Enige jaren geleden werd echter gevonden dat Au in de vorm van kleine gouddeeltjes (diameter  $\sim 2$  nm) heel reactief is.

Het doel van dit proefschrift was de bestudering van de katalytische eigenschappen van niet-gepromoteerde, enkel gepromoteerde ( $\text{MO}_x$ ) en dubbel gepromoteerde ( $\text{M}^{\text{I}}\text{O}_x/\text{M}^{\text{II}}\text{O}_x$ ) Au-gebaseerde katalysatoren (M: (aard) alkalimetalen, overgangsmetalen (TM), Cu, zeldzame aardmetalen), in reacties die belangrijk zijn voor luchtzuiveringsprocessen. De bestudeerde reacties zijn: volledige oxidatie van (on)verzadigde koolwaterstoffen, CO oxidatie in aan- en afwezigheid van  $\text{H}_2$ ,  $\text{NH}_3$  oxidatie en  $\text{NO}_x$  reductie. De invloed van verschillende additieven op de grootte/vorm van de Au deeltjes is bestudeerd met XRD, HRTEM en SEM. Ook is het mogelijke effect van de additieven op de chemische toestand van het Au en op het actieve centrum bestudeerd (DR/UV-Vis, TPR en XPS). Het uiteindelijke doel was om mogelijke correlaties tussen grootte/vorm van de Au deeltjes, de identiteit/rol van de additieven en de katalytische activiteit te vinden.

Depositie precipitatie met ureum bleek een reproduceerbare preparatietechniek, waarmee fijn verdeelde Au-deeltjes verkregen konden worden (*hoofdstuk 4*). Een thermische behandeling van de verse katalysator Au/ $\text{Al}_2\text{O}_3$  in  $\text{H}_2$  of  $\text{O}_2$  bij  $150^\circ\text{C}$  resulteert in reductie van  $\text{Au}^{3+}$  naar  $\text{Au}^0$  (DR/UV-Vis, TPR), waarbij de gereduceerde fractie toeneemt met de temperatuur. Verwarmen tot  $500^\circ\text{C}$  resulteerde niet in het sinteren van de Au deeltjes. Verscheidene  $\text{MO}_x$  additieven veranderen de structuur/morfologie/grootte van de Au deeltjes (XRD, HRTEM). Er is geen experimenteel bewijs gevonden dat erop wijst dat de aanwezigheid van  $\text{MO}_x$  de chemische toestand van het Au beïnvloedt. De aanwezigheid van minieme hoeveelheden Au ionen, beneden de detectielimiet van de gebruikte technieken (DR/UV-Vis, TPR, XPS) kan echter niet worden uitgesloten. De katalytische activiteit gevonden voor de verschillende reacties kan direct gerelateerd worden aan de dispersie en de grootte van het Au oppervlak van de diverse gepromoteerde Au/ $\text{Al}_2\text{O}_3$  katalysatoren. Aan de andere kant kan er geen direct verband worden gelegd tussen een specifieke morfologie van de Au deeltjes en de katalytische activiteit. De concentratie Au atomen met een laag coördinatiegetal, die verantwoordelijk worden gehouden voor sterke Au-drager interacties en activering van geadsorbeerde moleculen, neemt toe bij gebruik van promoterende materialen, aangezien de Au deeltjes kleiner zijn in aanwezigheid van deze promotoren.

*Hoofdstuk 5* bevat een gedetailleerde vergelijkende studie over de katalytische activiteit van niet-gepromoteerd, enkelvoudig gepromoteerd en dubbel gepromoteerd Au/ $\text{MO}_x/\text{Al}_2\text{O}_3$  (M:

(aard) alkalimetalen, TM, Cu, zeldzame aardmetalen). De variatie van  $T_{50\%}$  en  $r$  laten een duidelijk effect zien van de Au-deeltjesgrootte bij de (aard) alkali gepromoteerde Au/Al<sub>2</sub>O<sub>3</sub> katalysatoren. Bovendien laten de waarden van de schijnbare activeringsenergie,  $E_a$ , voor Au/Al<sub>2</sub>O<sub>3</sub> en Au/MO<sub>x</sub>/Al<sub>2</sub>O<sub>3</sub> (M: (aard) alkalimetaal) zien, dat de toevoegingen zelf niet direct verantwoordelijk zijn voor de verhoogde katalytische activiteit. Deze additieven voorkomen ook activiteitsverlies van de Au deeltjes tijdens een katalytische reactie. Daarom wordt geconcludeerd dat dit type toevoegingen ((aard) alkalimetaaloxiden) de concentratie van de actieve centra op de Au deeltjes verhoogt, door als structurele promotor op te treden. Het beste promoterende effect wordt verkregen na toevoeging van BaO. De variatie van  $T_{50\%}$  en  $r$  is niet direct gerelateerd aan de gemiddelde Au deeltjesgrootte als TM/Cu/zeldzame aardoxiden worden gebruikt. De rol van deze oxiden is tweevoudig: ze zijn direct betrokken bij de stabilisatie van de Au deeltjes (zodat sinteren wordt voorkomen) en daarnaast treden ze ook op als co-katalysator. De oxidatie van bijvoorbeeld propaan verloopt via een Mars van Krevelen type mechanisme: de reactant (propaan) wordt geactiveerd op het Au oppervlak of op het Au-drager grensvlak en de actieve zuurstof wordt geleverd door het metaaloxide rooster. De hechting van de Au deeltjes en de toevoer van de actieve zuurstof zijn direct gerelateerd aan de structuur van het metaaloxide. Een belangrijke toevoeging voor het verkrijgen van actieve katalysatoren is CeO<sub>x</sub>.

In *hoofdstuk 6* wordt de volledige oxidatie van verzadigde koolwaterstoffen (methaan en propaan) over Au-gebaseerde katalysatoren behandeld. De significante afname van  $T_{50\%}$  en  $E_a$  en de toename van  $r$ , die wordt waargenomen na toevoeging van Au aan MO<sub>x</sub>/Al<sub>2</sub>O<sub>3</sub> bevestigen dat Au een actieve katalysator is voor de volledige oxidatie van methaan en propaan. Er bestaat een directe relatie tussen de katalytische activiteit en de gemiddelde Au deeltjesgrootte, in het bijzonder als (aard) alkali-oxiden worden toegevoegd. Vergelijkbaar met de resultaten gepresenteerd in *hoofdstuk 5*, spelen deze additieven ((aard)alkali-oxiden) een rol als structurele promotoren. TMO, CuO en CeO<sub>x</sub> aan de andere kant, fungeren als co-katalysator, als leverancier van actieve zuurstof. De resultaten suggereren ook dat oxiden met basische eigenschappen bevorderlijk zijn voor een hogere katalytische activiteit, vergeleken met oxiden met zure eigenschappen. Voor beide reacties (methaan en propaan oxidatie) is gevonden dat de additieven voorkomen dat de Au deeltjes sinteren tijdens de reactie. Door de hoge temperaturen die nodig zijn om methaan te activeren werd sintering van de Au deeltjes toch waargenomen.

In *hoofdstuk 7* wordt de ammonia oxidatie over Au-gebaseerde katalysatoren besproken. Er werd gevonden dat de toevoeging van MO<sub>x</sub> aan Au/Al<sub>2</sub>O<sub>3</sub> de katalytische activiteit voor ammonia oxidatie verhoogt. De grootte van de Au deeltjes is een belangrijke variabele voor een hoge activiteit. De katalytische activiteit van de diverse goud-gebaseerde katalysatoren wordt echter ook sterk beïnvloed door de eigenschappen van het additief. Hetzelfde geldt voor de selectiviteit voor verschillende producten (N<sub>2</sub>, N<sub>2</sub>O en NO), die beïnvloed kan worden door het additief te variëren. De toegevoegde oxiden vervullen, evenals gevonden werd voor volledige oxidatie van (on)verzadigde koolwaterstoffen, een dubbele rol:

structurele promotor en co-katalysator. Met behulp van FTIR werden  $\text{NH}_4^+$  (op zure Brønsted sites),  $\text{NH}_3$  (op zure Lewis sites) amide (of hydrazine) en imide gedetecteerd. De toevoeging van Au aan  $\text{MO}_x/\text{Al}_2\text{O}_3$  resulteert in een significante toename van de intensiteit van de absorptieband toegeschreven aan imido-species, een voorgesteld reactie intermediair.

Au gebaseerde katalysatoren zijn ook goede katalysatoren voor de conversie van NO en  $\text{N}_2\text{O}$  bij lage temperatuur (*hoofdstuk 8*). Stikstofmono-oxide wordt in aanwezigheid van waterstof ( $\text{NO}/\text{H}_2 = 1$  of 0.4) omgezet in de volgende producten:  $\text{N}_2\text{O}$  (lage temperatuur),  $\text{N}_2$  (hogere temperatuur) en  $\text{NH}_3$  (hoge temperatuur). De katalytische activiteit en de selectiviteit hangen sterk af van de reactietemperatuur, het toegevoegde oxide en de verhouding van de reactanten. De katalytische activiteit hangt ook sterk af van de grootte van de gouddeeltjes, in het bijzonder als niet-reduceerbare oxiden ((aard) alkali metaaloxiden) worden toegevoegd. De resultaten suggereren dat  $\text{H}_2$  een actieve rol vervult in de NO decompositiestap. Bij lage temperatuur dissocieert een deel van het aanwezige NO, waarbij  $\text{N}_2\text{O}$  en  $\text{O}_{\text{ads}}$  gevormd wordt; bij hogere temperatuur is de fractie van NO die dissocieert hoger en dit resulteert in de vorming van  $\text{N}_2$  via  $\text{N}_{\text{ads}}$  combinatie.  $\text{NH}_x$  species zijn intermediairen voor  $\text{NH}_3$  vorming. De selectiviteit wordt bepaald door de relatieve concentraties van de geadsorbeerde species, NO, N en  $\text{NH}_x$ . De toegevoegde oxiden zouden nieuwe sites kunnen creëren voor dissociatieve adsorptie van NO. Het gebruikte oxide is ook van groot belang voor de reductie van distikstofmono-oxide (lachgas) met  $\text{H}_2$ .  $\text{N}_2$  en  $\text{H}_2\text{O}$  zijn de enige producten die werden waargenomen tijdens de reductie van  $\text{N}_2\text{O}$  met  $\text{H}_2$ . Waarschijnlijk zijn de niet-reduceerbare metaaloxiden verantwoordelijk voor stabilisatie van de fijnverdeelde Au nanodeeltjes, terwijl de reduceerbare metaaloxiden betrokken zijn bij de vorming van nieuwe actieve sites en de  $\text{N}_2\text{O}$  dissociatie.

Au-gebaseerde katalysatoren zijn, zoals verwacht, heel actief voor lage temperatuur CO oxidatie en PROX (*hoofdstuk 9*). De hoogste efficiency van de niet-gepromoteerde Au/ $\text{Al}_2\text{O}_3$  katalysator wordt verkregen na een thermische behandeling bij  $200^\circ\text{C}$  in zuurstof. (Aard) alkali metaaloxiden ( $\text{Li}_2\text{O}$ ,  $\text{Rb}_2\text{O}$ ,  $\text{BaO}$ ) fungeren als structurele promotors. Voor  $\text{Li}_2\text{O}$  werd gevonden dat de hoeveelheid  $\text{Li}_2\text{O}$  de katalytische activiteit direct beïnvloedt, beide voor CO oxidatie en PROX. Meer  $\text{Li}_2\text{O}$  bevordert de PROX reactie, terwijl er voor CO oxidatie geen direct verband gevonden is tussen  $r$  en de hoeveelheid  $\text{Li}_2\text{O}$ . De makkelijk reduceerbare metaaloxiden kunnen actief zuurstof leveren via een Mars en van Krevelen-type mechanisme. Het volgende mechanisme wordt voorgesteld: CO wordt geactiveerd op het Au of het Au-dragers grensvlak, en de actieve zuurstof wordt geleverd door het rooster van het metaaloxide, of wordt geactiveerd door sommige van de gebruikte additieven. Tijdens de PROX reactie kan hetzelfde mechanisme actief zijn. Naast CO is er in dat geval ook  $\text{H}_2$  aanwezig, dat met CO concurreert voor adsorptie sites. De selectiviteit naar  $\text{CO}_2$  in PROX neemt af met toenemende temperatuur en toenemende  $\text{H}_2$  partiële druk.



## ***Acknowledgments***

Although it should be relatively simple, this part is not the easiest part of my thesis. All the work presented here would not have been possible without the help, the collaboration and encouragement of many people to whom I am very grateful. After finishing the above thesis, I might forget to mention a few people...but certainly they are not forgotten and they are in my mind and memories.

I am grateful to Mischa Bonn for offering me the opportunity to come to The Netherlands. I am most grateful to all my colleagues for the friendly and enjoyable atmosphere within our group: Kees-Jan Weststrate, Emile Rienks, Sònia Carabineiro, François Devred, Roman Tsybukh, Jacques Aarts, Ellen Backus, Wim Roeterdink, Otto Berg, Sylvie Roke, Ludo Juurlink, Euan Hendry, Meindert Lippits, Huib Vreeburg, Reindt Boer-Iwema, Wiebke Ludwig, Mattijs Koeberg, Ruud Grisel. I will certainly not forget Johan Bakker, Rob van Schie, Peter Schakel and Wessel Nagel who always helped me to solve my “never-ending problems” with the set-up, PC or whatever came up. Many thanks also for my students Taihei Kaneto and Michelle (Xiaohua) Tang who did a very good job and contributed with their measurements and discussions to this work. Further, I would also like to mention some people from *Kamerlingh-Onnes Laboratory* for their special friendship: Cor Snel and Ton Gortmulder.

During my years as a PhD student I had the opportunity to meet wonderful people also outside the Gorlaeus Laboratories and to build up not only scientific collaborations, but also nice personal relationships. I'm grateful to Shawn Lin (*Taiwan*) and Vladimir Gorodetskii (*Russia*). My thanks go also to the whole team from CCMC-UNAM (*Mexico*): Nina Bogdanchikova, Miguel Avalos-Borja, Inga Tuzovskaya, José Cuauhtémoc Samaniego-Reyna, Mario Farias, Vitalii Petranovskii, Eric Flores, Fernando Ruiz Medina, Israel Gradilla Martinez for making my stay in Ensenada a very pleasant one. It also contributed a lot to the scientific content of this thesis. *Muchas gracias por todo!*

For the financial support in carrying out this research and participation at national and international conferences, NWO is gratefully acknowledged (project #700.399.037).

The list would not be complete without mentioning my former colleagues from Romania. I'm most indebted to Petru Marginean. *Dragă Sefule*, without your support, help and encouragements, the completion of this thesis would not have been possible. Nelu Gudea, Undina Stanescu, Dan Lupu, Diana Lazar, Valer Almasan, Nicu Aldea are also not forgotten.

I would also like to thank to Guido Janssen and Netherlands Institute for Metals Research (NIMR) for allowing me to combine the work on the new research project with the completion of my thesis.



I would certainly not be able to mention all my friends from Romania and elsewhere, but I thank them all for their unconditional friendship and support. They were always next to me when needed: Mihaela, Stefi, Teodora and Mitel, Monica, Irina and Stelian, Dani and Cami with their families. My friends and relatives from Cugir are also not forgotten! I was fortunate to have a few good friends in The Netherlands as well: Stefania, Dana, Gabi, Ildi and Gerold, Mihai and Stefania, Diana and Marius, Cati. Thank you all for the nice moments we spent together.

The last words are dedicated to my parents! You were always there for me, loving me and encouraging me all the time. Without you in my life I could not have accomplished it. Words are too poor to express all my love for and gratitude to you!

*Ar fi trebuit să incep "mulțumirile" cu voi, dragii mei părinți! Dragostea și suportul vostru necondiționat au făcut posibilă realizarea acestei teze! Vouă vă datorez totul și uneori cuvintele sunt mult prea sărace să exprime tot ceea ce aș vrea să vă spun acum...Vă mulțumesc!*

Thank you all!  
Andreea

Delft, October 19, 2005

**List of Publications and Patents Related to this Thesis:**

1. **A.C. Gluhoi**, B. E. Nieuwenhuys, *Patent application* 2004
2. **A.C. Gluhoi**, N. Bogdanchikova, B.E. Nieuwenhuys, “*The effect of different types of additives on the catalytic activity of Au/Al<sub>2</sub>O<sub>3</sub> in propene total oxidation: Transition metal oxides and ceria*”, **J. Catal.** 229 (2005) 159 (Chapter 5)
3. **A.C. Gluhoi**, N. Bogdanchikova, B.E. Nieuwenhuys, “*Alkali (earth)-doped Au/Al<sub>2</sub>O<sub>3</sub> catalysts for total oxidation of propene*”, **J. Catal.** 232 (2005) 96 (Chapter 5)
4. **A.C. Gluhoi**, N. Bogdanchikova, B.E. Nieuwenhuys, “*Total oxidation of propene and propane over gold-copper oxide on alumina catalysts. Comparison with Pt/Al<sub>2</sub>O<sub>3</sub>*”, **Catal. Today**, submitted (Chapter 5, 6)
5. R. Grisel, K.J. Weststrate, **A.C. Gluhoi**, B.E. Nieuwenhuys, “*Catalysis by gold nanoparticles*” **Gold Bull.** 35/2 (2002) 59 (Chapter 5)
6. **A.C. Gluhoi**, S. D. Lin, B. E. Nieuwenhuys, “*The beneficial effect of the addition of base metal oxides to gold catalysts on reactions relevant to air pollution abatement*”, **Catal. Today** 90 (2004) 175 (Chapter 5, 7)
7. B.E. Nieuwenhuys, **A.C. Gluhoi**, E.D.L. Rienks, C.J. Weststrate, C.P. Vinod, “*Chaos, oscillations and the golden future of catalysis*”, **Catal. Today**, 100 (2005) 49 (Chapter 5, 7)
8. S. D. Lin, **A. C. Gluhoi**, B. E. Nieuwenhuys, “*Ammonia Oxidation over Au/MO<sub>x</sub>/γ-Al<sub>2</sub>O<sub>3</sub> - Activity, Selectivity and FTIR Measurements*”, **Catal. Today** 90 (2004) 3 (Chapter 7)
9. **A.C. Gluhoi**, M.A.P. Dekkers, B. E. Nieuwenhuys, “*Comparative studies of the N<sub>2</sub>O/H<sub>2</sub>, N<sub>2</sub>O/CO, H<sub>2</sub>/O<sub>2</sub> and CO/O<sub>2</sub> reactions on supported gold catalysts: effect of the addition of different oxides*” **J. Catal.** 219 (2003) 197 (Chapter 8)
10. **A.C. Gluhoi**, H. S. Vreeburg, J. W. Bakker, B. E. Nieuwenhuys, “*Activation of CO, O<sub>2</sub> and H<sub>2</sub> on gold-based catalysts*”, **Appl. Catal. A** 291 (2005) 145 (Chapter 9)
11. **A.C. Gluhoi**, B.E. Nieuweunhuys, “*Catalytic oxidation of saturated hydrocarbons on multicomponent Au/Al<sub>2</sub>O<sub>3</sub>. Effect of various promoters*”, **Catal. Today**, submitted (Chapter 6)

12. **A.C. Gluhoi**, X. Tang, P. Marginean, B.E. Nieuwenhuys, “*In-depth characterization and catalytic activity of unpromoted and alkali-promoted Au/Al<sub>2</sub>O<sub>3</sub> catalysts for low-temperature CO oxidation*”, **Topics in Catalysis**, submitted (Chapter 9)

#### ***Presentations at (Inter)National Conferences***

- **A.C. Gluhoi**, S. D. Lin, B. E. Nieuwenhuys, “*Reactions of N-containing molecules catalyzed by gold-based catalyst*”, **Gold 2003**, Vancouver, 28<sup>th</sup> September - 1<sup>st</sup> October 2003, oral [http://www.gold.org/discover/sci\\_indu/gold2003/pdf/s36a1314p938.pdf](http://www.gold.org/discover/sci_indu/gold2003/pdf/s36a1314p938.pdf)
- **A.C. Gluhoi**, N. Bogdanchikova, B. E. Nieuwenhuys, “*Hydrocarbon oxidation catalysis by gold nanoparticles*”, **Gold 2003**, Vancouver, 28<sup>th</sup> September - 1<sup>st</sup> October 2003, poster [http://www.gold.org/discover/sci\\_indu/gold2003/pdf/s36a1314p939.pdf](http://www.gold.org/discover/sci_indu/gold2003/pdf/s36a1314p939.pdf)
- **A.C. Gluhoi**, S. D. Lin, B. E. Nieuwenhuys, “*The prominent part of base metal oxides in the performance of Au/Al<sub>2</sub>O<sub>3</sub> catalysts in reactions of N-containing molecules*”, **13<sup>th</sup> International Congress on Catalysis**, Paris, 11<sup>th</sup> -16<sup>th</sup> July 2004, oral, awarded with “*Young Scientist Prize*”
- **A.C. Gluhoi**, N. Bogdanchikova, B. E. Nieuwenhuys, “*Gold as a catalyst for hydrocarbon oxidation reactions*”, **13<sup>th</sup> International Congress on Catalysis**, Paris, 11<sup>th</sup> -16<sup>th</sup> July 2004, poster
- **A.C. Gluhoi**, B.E. Nieuwenhuys, “*Supported gold catalysts for total oxidation of propene*”, **Netherlands Catalysis and Chemistry Conference**, Noordwijkerhout, 2002, poster
- **A.C. Gluhoi**, S.D. Lin, B.E. Nieuwenhuys, “*Oxidation and reduction reactions on gold-based catalysts*”, **Netherlands Catalysis and Chemistry Conference**, Noordwijkerhout, 2003, poster
- **A.C. Gluhoi**, B.E. Nieuwenhuys, “*The beneficial effect of addition of base metal oxides to gold catalysts on reactions relevant to air pollution abatement*”, **Netherlands Catalysis and Chemistry Conference**, Noordwijkerhout, 2004, poster
- **A.C. Gluhoi**, N. Bogdanchikova, B.E. Nieuwenhuys, “*A different approach of gold catalysts: support assisted reactions?*”, **Netherlands Catalysis and Chemistry Conference**, Noordwijkerhout, 2005, oral



## CURRICULUM VITAE

### ANDREEA CATALINA GLUHOI

Born in Cugir, ROMANIA, 16<sup>th</sup> December 1973

- 1988-1992      *Theoretical Lyceum, Cugir, Romania*
- 1992-1997      *Faculty of Chemistry and Chemical Engineering, University Babes-Bolyai, Cluj-Napoca, Romania, with thesis “Synthesis and characterization of *Leonetia clerckella*, specific pheromone of peach muscle”*  
Supervisor: Prof. Dr. M. Vlassa
- 1997-2000      *Researcher at National Institute for Research and Development of Isotopic and Molecular Technologies, Cluj-Napoca, Romania*  
Dept. of Heterogeneous Catalysis  
Supervisor: Prof. Dr. P. Marginean  
Topics of research: physico-chemical characterization and catalytic studies of nickel and platinum-based catalysts
- 2000-2005      *PhD studies at Leiden Institute of Chemistry, Leiden University, The Netherlands*  
Dept. of Heterogeneous Catalysis and Surface Chemistry  
Supervisor: Prof. Dr. B.E. Nieuwenhuys  
Topics of research: development of new gold-based catalysts with applicability to environmental pollution control. This research has been sponsored by NWO, project #700.99.037, title: “*A golden future for catalysts based on gold? Fundamental research focused on understanding of the catalytic behaviour of gold* “.  
One month stage (2003) at *Centro de Ciencias de la Materia Condensada (CCMC)*, UNAM, Mexico, under supervision of Dr. N. Bogdanchikova. Scientific objective: in-depth physico-chemical characterization of gold-based catalysts.
- 2005-present      *Postdoctoral research fellow at NIMR, Delft, The Netherlands*  
Dept. of Materials Science and Technology  
Supervisor: Prof. Dr. G.C.A.M. Janssen

## STELLINGEN

behorende bij het proefschrift

### FUNDAMENTAL STUDIES FOCUSED ON UNDERSTANDING OF GOLD CATALYSIS

1. The Mars and van Krevelen type of mechanism proposed for the catalytic combustion of some volatile organic compounds (VOCs) (2-propanol, methanol and toluene) over Au/CeO<sub>2</sub> catalysts appears to have an important contribution to total oxidation reactions over catalysts containing gold and ceria or a transition metal oxide.

S. Scire, S. Minico, C. Crisafulli, C. Satriano, A. Pistone, Appl. Catal. B 40 (2003) 43.  
*Chapter 5 of this thesis.*

2. The conclusion of Haruta that Au/Co<sub>3</sub>O<sub>4</sub> (10 wt-% Au) is more active than Pt/Al<sub>2</sub>O<sub>3</sub> (1 wt-% Pt) and Pd/Al<sub>2</sub>O<sub>3</sub> (1 wt-% Pd) for the total combustion of CH<sub>4</sub> and C<sub>3</sub>H<sub>8</sub> is not right. It is not correct to compare the catalytic performance of different catalysts only on the basis of differences in the temperature of 50% hydrocarbon conversion, without considering the loading of the noble metal, especially when there are large differences in loading of the active components.

M. Haruta, Catal. Today 36 (1997) 153.  
*Chapter 6 of this thesis.*

3. The mechanism proposed by Schubert *et al.* for Au supported on active materials (Fe<sub>2</sub>O<sub>3</sub>, TiO<sub>2</sub>, NiO<sub>x</sub>, CoO<sub>x</sub>) in CO oxidation that the dominant reaction pathway involves the facile supply of reactive oxygen via the support, also applies for Au/CeO<sub>x</sub>/Al<sub>2</sub>O<sub>3</sub>.

M.M. Schubert, S. Hackenberg, A.C. van Veen, M. Muhler, V. Plzak, R.J. Behm, J. Catal. 197 (2001) 113.  
*Chapter 9 of this thesis.*

4. The published activation energy for CO oxidation over Au/CeO<sub>x</sub> of 106 kJ mol<sup>-1</sup> indicates that the reaction was carried out under mass transfer limitation conditions. Typically, Au-based catalysts have a very low activation energy in CO oxidation.

P. Bera, H.S. Hedge, Catal. Lett. 79 (2002) 75.

5. Based on DFT calculations Broqvist *et al.* concluded that Na promotes the catalytic activity of Au/MgO in CO oxidation by enhancing both the O<sub>2</sub> binding and CO·O<sub>2</sub> formation, via electron

donation from Na to Au. However, this conclusion is not relevant for real catalysts, since Na is present as ionic Na, thus it loses its ability to donate electrons.

P. Broqvist, L. M. Molina, H. Gronbeck, B. Hammer, *J. Catal.* 227 (2004) 217.

6. Pt/CuO/Al<sub>2</sub>O<sub>3</sub> is an efficient catalyst for NH<sub>3</sub> oxidation, but since both Pt/Al<sub>2</sub>O<sub>3</sub> and CuO/Al<sub>2</sub>O<sub>3</sub> are active, any discussion on the role of Pt, without mentioning the effect of CuO leads to incomplete conclusions.

G. Olofsson, L. R. Wallenberg, A. Andersson, *J. Catal.* 230 (2005) 1.

7. The term “calcination at 200K” used by B. Qiao *et al.* is a “contradictio in terminis” because the “calcination” is a temperature-related process which requires that the temperature is higher than room temperature.

B. Qiao, Y. Deng, *Chem. Comm.* (2003) 2192.

8. An oxygen off-stoichiometry in REMnO<sub>3</sub> compounds enhances/hides two types of behaviour: the magnetic behaviour detected at low temperatures (T~100K) and also the electric behaviour which is detected at high temperatures (T~1000K).

T. Lonkai, D.G. Tomuta, U. Amann, J. Ihringer, R.W.A. Hendrikx, D.M. Tobbens, J.A. Mydosh, *Phys. Rev. B* 69 (2004) 134108.

9. The rapid development of computer power and computational methods will result in the replacement of many experimental measurements by computer simulations. However, reliable computer “experiments” require reliable computational methods. For the development of a computational method experimental information is still required.
10. Cyclists can suffer from RSI (Repetitive Strain Injury) as a result of using badly surfaced cycle paths.